Fenomenología de Mezcla de Sabor en Modelos Supersimétricos

Muhammad Rehman

Instituto de Física de Cantabria,
Universidad de Cantabria

Flavor Mixing Phenomenology in Supersymmetric Models

Muhammad Rehman

Instituto de Física de Cantabria,
Universidad de Cantabria

Instituto de Física de Cantabria
Universidad de Cantabría

Fenomenología de Mezcla de Sabor en Modelos Supersimétricos

Memoria de Tesis Doctoral realizada por

Muhammad Rehman

presentada en el Instituto de Física de Cantabria,
Universidad de Cantabría

Trabajo dirigido por el
Dr. Sven Heinemeyer,
Investigador científico del Instituto de Física de Cantabría IFCA (CSIC-UC)

y por el
Dr. Mario E. Gómez,
Investigador científico del Departamento de Física Aplicada, Universidad de Huelva

Santander, Diciembre de 2015

Instituto de Física de Cantabria
Universidad de Cantabria

Flavor Mixing Phenomenology in Supersymmetric Models

A dissertation submitted in partial fulfillment of the requirements
for the degree of Doctor of Philosophy in Physics by

Muhammad Rehman

Presented to Instituto de Física de Cantabria,
Universidad de Cantabria

Work done under the supervision of
Dr. Sven Heinemeyer,
Scientific Investigator, Instituto de Física de Cantabria IFCA (CSIC-UC)

and
Dr. Mario E. Gómez,
Scientific Investigator, Departamento de Física Aplicada, Universidad de Huelva

Santander, December 2015

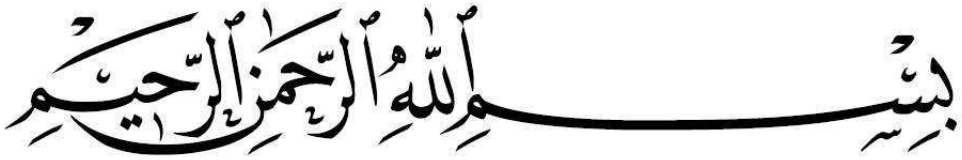

In the Name of Allāh, the Most Gracious, the Most Merciful

MY SUCCESS CAN ONLY COME FROM ALLAH.
IN HIM I TRUST AND UNTO HIM I LOOK.

(Al Quran 11:88)

TO

THE GUIDING LIGHT PROPHET MUHAMMAD (P.B.U.H) &
MY FATHER MR. NAZIR HUSSAIN

Contents

Acknowledgement

I find no words to praise Allah, who is the sole owner of the treasures of knowledge. He, who inspired all the prophets and sent revelation to enable them to guide the humanity to the path of virtue, also inspired me, enlightened my mind, blessed me with sufficient wisdom and laid bare before me the hidden treasures of knowledge. He guided me through all the labyrinths of life and brought me to this stage that I have succeeded in doing something worthwhile. Whenever, I try to think that what I could do without His mercy, my faith in His benevolence, strengthens.

Infinite salutations be upon the Holy Prophet Muhammad (P.B.U.H) who brought Man out of the depth of ignorance and introduced him to the light of knowledge. In his sayings he laid great stress on acquiring knowledge and aroused deep love for it in his Ummah. His teachings encouraged me and proved to be a torch in the exploration of new realities.

Although on the cover page of this thesis only my name is mentioned but I acknowledge the services of so many people whose names may not all be enumerated. Their contributions and sincere motivations are gratefully acknowledged. I beg pardon to all those whose names I did not mention. But there are some names which I can never forget due to their relentless efforts.

Bundles of thanks to my reverend supervisor Sven Heinemeyer who allowed me to share his vast knowledge and get maximum experience from his lifelong experience. I could not have imagined having a better advisor and mentor for my Ph.D study. During the whole research he guided me beyond my expectations. Without his exemplary supervision, I could not do whatever I have done. He showed an attitude and substance of a genius; he continually and convincingly conveyed a spirit of adventure in regard to research. I do not remember a single moment during the whole course of my study, when I found him non-cooperative or reluctant to help. I wish that one day I would become as good an advisor to my students as he has been to me.

Special thanks to my co-supervisor Mario E Gomez, who provided me valuable information and sagacious suggestions during the entire course of my research. I am greatly indebted to him not only for his dynamic guidance and encouragement but also for his positive and constructive criticism. His lively remarks and encouragement refreshed my mind and gave me new energy to complete this cumbrous work. Without his persistent help this dissertation would not have been possible.

I am deeply thankful to Multidark mangement specially Susana Hernandez (Manager Multidark) and Carlos Muñoz (Cooridinator Multidark) for their help and support dur-

ing my Ph.D. I would like to pay my gratitude to Thomas Hahn, who provided me with every possible help whenever it was needed. This work would not have been possible without his help in the implimentation of new Feynman rules in `FeynArts`, `FormCalc` and `FeynHiggs`. I also would like to thank Barbara Chazin for her help in writing the Spanish part of the thesis. I also cannot forget the earnest cooperation of my friends Federico van der Pahlen and Leo Galeta, who proved very helpful to me during my entire PhD.

Sincere thanks to my brother Muhammad Qamar, sisters, nephews and nieces whose love and friendly gossips lessened my worries, refreshed my mind and encouraged me to complete my work. Although I lived far from my relatives but communication with them provided emotional atmosphere and concentration that was needed for this cumbersome work.

I would like to pledge my gratitude and deepest emotion to my wife, Ayesha Rehman for her moral support and cheerful inspiration which did not let me down whenever I found my task tiresome and unaccomplished. I will never forget the time when she presented a cup of hot tea and tasty snacks in the middle of the night, keeping a lively smile on her face. I also would like to mention the names of my cute little daughters Ayerah Rehman and Ayezah Rehman whose innocent smile and lively antics provided a soothing and balmy effect on my burdened mind.

I bow my head in honor of my father Nazir Hussain (late) and my mother Hameeda Begum, who always loved me, blessed me with their noble advice, prayed for my success and bestowed upon me sufficient material resources. They spent many sleepless nights while praying for my success and worrying about my health. They always prayed to see the bud of their wishes bloom into a flower. It is all due to them whatever I have achieved today. It is heart wrenching for me to think that when I will return to my country my father will not be there to hug me and appreciate my efforts. After his death, I feel as if I have lost a source of great motivation and strong support.

I also express my deepest and immeasurable appreciations to my dear homeland i.e. Pakistan whose holy soil gave birth to so many talented people. Its serene environment and cheerful people prompted me to do something worthwhile that can add to its glory.

Last but not least I would like to acknowledge Spanish Government for providing me financial support through the Spanish MICINN's Consolider-Ingenio 2010 Programme under grant MultiDark CSD2009-00064. I also express my sincere gratitude to the Instituto de Fisica de Cantabria and Universidad de Cantabria for letting my dreams of being a student there be fulfilled. They generously provided me all sufficient means necessary for my research requirements.

Finally, I would like to say that, apart from me, this research will be immensely important for those who are interested to know about this subject. I hope they will find it valuable. I have tried heart and soul to gather all relevant documents regarding this subject. I do not know how far I am able to do that. Furthermore I do not claim that all the information included in this thesis is described perfectly. There may be shortcomings, factual errors and mistakes which I confess entirely to be mine. I humbly invite positive criticism for future guidance.

List of Publications

This thesis is based on the following puplications.

- M.E. Gómez, S. Heinemeyer and M. Rehman, *The Quark Flavor Violating Higgs Decay $\boldsymbol{h \to \bar{b}s + b\bar{s}}$ in the MSSM*, `arXiv:1511.04342 [hep-ph]`.
- M. Gómez, S. Heinemeyer and M. Rehman, *Effects of Sfermion Mixing induced by RGE Running in the Minimal Flavor Violating CMSSM*, *Eur. Phys. J.* **C** (2015) 9, 434 `arXiv:1501.02258 [hep-ph]`.
- M. Gómez, T. Hahn, S. Heinemeyer, M. Rehman, *Higgs masses and Electroweak Precision Observables in Lepton Flavor Violating MSSM*, *Phys. Rev.* **D 90** (2014) 074016 `arXiv:1408.0663 [hep-ph]`.

List of Tables

List of Figures

Introducción

El Modelo Estándar (ME) de la física de partículas [1–3], fruto de un inmenso esfuerzo tanto teórico como experimental, muestra la naturaleza de los ingredientes que forman nuestro universo y cómo interactúan entre sí. Según el ME, nuestro universo se compone de fermiones (partículas de spin 1/2), de los que seis son leptones y otros seis quarks, contenidos en tres familias. A cada fermión le corresponde una anti-partícula con números cuánticos opuestos. Las partículas asociadas con los campos de interacción son bosones (partículas de spin 1); los fotones (γ) y los bosones l ($W^{\pm}$ y Z) se asocian a la interacción electrodébil, los gluones (g) a la fuerte. La gravedad no es parte del ME. Las simetrías y los principios de invariancia determinan la forma de estas fuerzas, el ME se basa en el grupo gauge $SU(3)_{\rm C} \times SU(2)_{\rm L} \times U(1)_{\rm Y}$. La renormalizabilidad e invariancia gauge exigen que la simetría $SU(2)_{\rm L} \times U(1)_{\rm Y}$ se rompa espontáneamente mediante el llamado mecanismo de Higgs. Todas las predicciones establecidas por ME se han confirmado experimentalmente. El descubrimiento de la última pieza que faltaba por conocer, el bosón de Higgs, se anunció el 4 de julio de 2012 en el gran Colisionador de Hadrones (LHC) del Conseil Européen pour la Recherche Nucleaire (CERN) [4, 5]. De este modo, el ME es la teoría más precisa y elegante en la actualidad. Sin embargo, a pesar su éxito, hay buenas razones tanto teóricas como experimentales que nos llevan más allá del ME. De modo que puede pensarse que ME es un caso límite de una teoría más general.

El primer problema no explicado por el ME está relacionado con el sector de los neutrinos, considerados sin masa en el ME. En varios experimentos se ha observado la desaparición del neutrinos electrónico o muónico. Esto ha aportado la evidencia suficiente para aceptar su oscilación de sabor [6]. Esta observación ha confirmado que los neutrinos tienen masas diferentes y que los tres sabores de neutrinos ν_e, ν_μ y ν_τ se mezclan entre a sí para formar tres estados propios de masa. Esto implica la no conservación del sabor leptónico, por lo tanto, la predicción de procesos de violacion de sabor de leptones cagados (cLFV), como ocurre en el sector de los quarks.

La extensión más simple del ME para acomodar las masas de los neutrinos consiste en introducir tres singletes fermiónicos $SU(3)_{\rm C} \times SU(2)_{\rm L} \times U(1)_{\rm Y}$ y acoplarlos a neutrinos mediante interacciones Yukawa, las masas de los neutrinos se generarían a través de ruptura de simetría electrodébil (EWSB). Sin embargo esta extensión del ME requiere accoplamientos de Yukawa extremadamente pequeños y violar el número leptónico a baja energía. Como ni los neutrinos dextrógiros ni la violación del número leptónico se han observado a esa escala, es preciso buscar un mecanismo que explique las masas

de los neutrinos respetando ambas evidencias. Una de las soluciones al problema es incluir en la teoría un mecanismo "see-saw" (mecanismo de balancín) [7] para generar las masas de los neutrinos, el cual no sólo permite los acoplamientos de Yukawa, sino que además explica porque los neutrinos levógiros son más ligeros que los otros fermiones de ME. Estos mecanismos asumen la existencia de neutrinos my pesados del tipo de Majorana, los cuales se acoplan a los del ME mediante interacciones Yukawa. Las masas de los neutrinos son generadas por un operador efectivo de dimension 5. Esto da lugar a estados físicos de neutrinos que mezclan el sabor y en consecuencia predicen violación del sabor leptones (LFV).

Por otro lado ME tampoco explica suficientemente el sector de Higgs. Aunque el ME es renormalizable, se cree que es válido sólo hasta cierta escala de energía, la cual está realcionada con la aparición de física desconocida. Si esta escala se asocia con la integración de la gravedad en teoría, debería estar en torno a la masa de Planck (10^{19} GeV). De este modo, las correcciones a la masa del Higgs M_H debidas a los fermiones serían:

$$\delta M_H^2(f) = -\frac{|\lambda_f|^2}{8\pi^2}[\Lambda^2 + ...], \tag{1}$$

donde λ_f representa el acoplamiento del fermión f al campo de Higgs y Λ es el corte ultravioleta utilizado para regular el integral. Si éste se reemplaza por la masa de Planck se obtiene $\delta M_H^2 \approx 10^{30}$ GeV^2. Esta enorme corrección se podría cancelar con una masa original del mismo orden y signo opuesto. Sin embargo, estas dos contribuciones se deberían cancelar entre sí con una precisión de una parte en 10^{26} para explicar la masa del Higgs observada experimentalmete. Este es el llamado "problema de la jerarquía".

El tercer problema que el ME no explica es el de la materia oscura (MO). Las primeras especulaciones sobre la existencia de MO se debieron al astrónomo Zwicky. En 1933, observó que la masa total de la materia luminosa procedente del cúmulo de Coma es mucho menor que la masa total podemos suponer por movimiento de las galaxias que lo integran [8]. En la actualidad hay diversas muestras de la presencia de MO en nuestro universo. El efecto de lente gravitatoria y las curvas de rotación de las galaxias espirales son observaciones que apuntan a la existencia de la llamada "masa perdida" en el universo. Resultados recientes de los expeimentos WMAP [9] y Planck [10] proporcionan un valor preciso de la masa del universo y la forma en que se divide entre los diferentes tipos de materia y energía. No hay ninguna partícula del ME que pueda servir como candidato MO.

Por las razones anteriores hay que encontrar teorías renormalizables que puedan eliminar divergencias cuadráticas en la masa del bosón de Higgs, proporcionar un candidato a MO y explicar el la violación del sabor leptónico. Una de éstas, la extensión supersimétrica del ME, cuya versión más simple es el *Minimal Supersymmetric Standard Model (MSSM)* [11], puede hacer frente a los problemas mencionados. El MSSM predice la existencia de una pareja para cada una de las partículas fundamentales de la ME a las que se atribuye un espín que se diferencia en media unidad de sus compañeros del ME. La presencia de las super-partículas contribuye a cancelar las divergencias cuadráticas en el bosón masa de Higgs. También la partícula supersimétrica más ligera (LSP) puede ser un candidato a MO. Sin embargo, el MSSM, como el ME, asumen neutrinos sin masa,

por lo que el MSSM tiene que ser ampliado para que sea consistente con las observaciones de las mezclas de sabor de éstos [6].

Gran parte del esfuerzo del LHC se ha dedicado a descubrir la supersimetría (SUSY), pero hasta el momento ninguna partícula SUSY se ha observado [12, 13]. Otro enfoque para descubrir SUSY procede del estudio de los efectos indirectos de las partículas SUSY en otros observables [14]. Las mezclas de sabor ofrecen una perspectiva única en este sentido, ya que la mayor parte de los efectos indirectos de las partículas SUSY proceden de observaciones en los que éstas se producen. La primera de ellas, es el proceso de cambio de sabor en el sector de los quarks en corrientes neutras (FCNC). En ME, los procesos del tipo FCNC están ausentes a nivel de árbol y sólo pueden ocurrir en nivel de un bucle. La única fuente de FCNC de en el ME es la matriz de Cabibbo, Kobayashi y Maskawa (CKM), sin embargo no es significativa debido a la cancelación entre las diversas contribuciones (mecanismo GIM). Por otro lado, en el MSSM, la posible desalineación entre las matrices de masa de los quarks y sus parejas supersiméticas (squarks) es otra fuente de violación de sabor, capaz de superar a la contribución ME en varios órdenes de magnitud. Cualquier posible desviación experimental de la predicción de ME para la FCNS sería una evidencia clara de nueva física y, posiblemente, un indicio del MSSM. Del mismo modo, las predicciones del MSSM para cLFV son cero. Incluso las extensiones del tipo "see-saw" del ME no predicen tasas considerables para estos procesos. Las tasas cLFV en esta extensión del ME son casi 40 órdenes de magnitud menor que las actuales límites experimentales y, por consiguiente sin posibilidad de ser observadas. En cambio, la extensión "see-saw" del MSSM, predice valores más altos, cercanos a los límites de observación actuales. Por otro lado, tras el descubrimiento del bosón de Higgs con una masa en torno a los 125 GeV, es preciso incorporar correcciones radiativas grandes para su explicación. Una masa superior a 1 TeV de la pareja supersimétrica del top, el s-top, podría dar respuesta al problema, pero a costa de reintroducir un ajuste innatural de los parámetros. Sin embargo, esta inconveniencia puede evitarse con una mezcla fuerte entre las compontes quirales del stop o mediante una mezcla de sabor ente los s-quarks.

La forma más general de introducir mezcla de sabor en el MSSM es a través de los parámetros que rompen la supersimetría. Estos parámetros, dotan de masas moderamente grandes a las partículas supersimétricas. De este modo, no es posible con una única rotación en el espacio del sabor diagonalizar simultáneamente las masas de los fermiones y las de sus correspondientes parejas supersimétricas. Esta desalineación puede producirse por varias causas; un ejemplo son las ecuaciones de renormalización (RGE): Aun partiendo de masas supersimétricas sin violación de sabor a una alta energía, las RGE pueden inducirla debido a que contienen acoplamientos Yukawa no diagonales. Este tipo de enfoque es conocido en la literatura como la violación de sabor mínima (MFV) [15, 16], donde se supone que el sabor y la violación de la simetría CP en el sector de quarks se describe en su totalidad por la matriz CKM.

Los escenerios del tipo MFV están bien motivados por el hecho de que no introducen nuevas fuentes de violación de sabor y de CP. Los cuales entrarían en conflicto con los límites experimentales en los sectores de los kaones y B_d, descritos por el ME con una

precisión del% 10 [17]. Para la primera y segunda generación squarks, sensibles a los datos de $K^0 - \bar{K}^0$ y $D^0 - \bar{D}^0$, las restricciones son muy fuertes. Sin embargo, sistemas con la tercera generación están menos limitados, ya que los datos de la mezcla $B^0 - \bar{B}^0$ aún dejan lugar para nuevas fuentes de violación sabor. Esto abre la posibilidad para scenerios más generales como los de violación no mínima de sabor (NMFV), aparte de los de MFV.

En esta tesis, se presenta un estudio sistemático y simultáneo de los efectos de la mezcla de sabor en diferentes observables utilizando el MFV y el NMFV. Como un primer paso estudiaremos las mezclas de squarks y sleptones en el MSSM a baja energía, sin utilizar un modelo específico (MI). Para el enfoque MI, introducimos arbitrariamente los parámetros de mezcla de sabor en las matrices de masa de los sfermiones, sin tener en cuenta el origen de estos parámetros. Estudiamos los efectos de la mezcla de los squark en los observables de la interacción electrodébiles medidos con gran precisión (EWPO), la física del quark b (BPO) y las desintegraciones del bosón de Higgs que violan el sabor. Para la mezcla del sabor leptónico, estudiamos también los efectos sobre EWPO, la masa del los bosones de Higgs y las desintegraciones de éstos que violan el sabor leptónico (LFVHD). En segundo lugar, extendemos nuestro análisis a la fuente de la mezcla de sabor. Para ello analizamos la mezcla de sabor inducida por las RGE en la evoulción de los parámetros desde las escalas GUT y electrodébil. En este estudio trabajamos con la hipótesis de MFV tanto para squarks como para sleptones. Por consiguiente, vamos a investigar dos modelos (en los siguientes capítulos se introduciran más definiciones y citas):

(i) El modelo supersimétrico mínimo con rotura de la supersimetría mediante parámetros universales (CMSSM). En este caso solo hay violación de sabor en los squarks.

(ii) El modelo CMSSM ampliado mediante un mecanismo "see-saw" de tipo I [7], llamado "CMSSM-seesaw I"

En muchos análisis del CMSSM o sus extensiones como el NUHM1 o NUHM2 (véase la Ref. [18] y las referencias en él), se ha utilizado la hipótesis de MFV , asumiendo que contribuciones procedentes de MFV son insignificantes tanto para procesos FCNC como para otros observables como EWPO y la masa del bosón de Higgs masas (ver por ejemplo [19]). En este trabajo vamos a analizar si esta suposición está justificada, y si la inclusión de los efectos MFV podrían conducir a restricciones adicionales del espacio de parámetros del CMSSM. En este sentido, vamos a evaluar en el CMSSM y en el CMSSMI el siguiente conjunto de observables: BPO, en particular, BR($B \to X_s\gamma$), BR($B_s \to \mu^+\mu^-$) y ΔM_{B_s}; EWPO, en particular, M_W y el ángulo de Weinberg efectivo, $\sin^2\theta_{\rm eff}$; la masas de los bosones de Higgs neutros y cargados en el MSSM, así como cLFV y LFVHD.

La disposición de la tesis es la siguiente. El capítulo 1 contiene una introducción al ME. En el capítulo 2 presentamos MSSM y sus extensiones "see-saw". El capítulo 3 está dedicado a la base de cálculo de los observables considerados en este trabajo. En el capítulo 4 presentaremos los resultados en el caso de la mezcla de sabor squark en el

enfoque MI y el estudio sus efectos para los observables BPO, EWPO y QFVHD. En el capítulo 5, de estudian los efectos de la mezcla de los sleptones en EWPO, las correciones a las masas de los Higgs y LFVHD en el contexto MI. El capítulo 6 se centrará en el análisis del CMSSM y CMSSMI, para los que presentamos los efectos de mezcla del sabor en los observabels EWPO, BPO, las predicciones de masas del bosón de Higgs, QFVHD, cLFV mezcla y LFVHD. El capítulo 7 se reserva para las conclusiones.

Introduction

The Standard Model (SM) of the fundamental interactions [1–3], the results of immense experimental and theoretical effort, elucidates the ingredients forming our universe and how do they interact. SM asserts that our universe is made up of fermions (spin 1/2 particles) interacting through fields of which they are the sources. Among the fermions, there are six leptons and six quarks categorized in three families and have their respective anti particles with opposite quantum numbers. The particles associated with the interaction fields are bosons (spin 1 particles) namely photon (γ), weak vector boson ($W^{\pm}$, Z) and gluons (g) and a scalar particle Higgs (H). The gauge bosons act as force carriers of electromagnetic, weak and strong interactions. Gravity is not part of SM. Symmetries and invariance principles determine the form of these forces. SM is based on the gauge group $SU(3)_{\rm C} \times SU(2)_{\rm L} \times U(1)_{\rm Y}$. The renormalizability and gauge invariance demands the $SU(2)_{\rm L} \times U(1)_{\rm Y}$ symmetry to be spontaneously broken through Higgs mechanism. All the predictions laid down by SM have been experimentally confirmed. The discovery of the last missing piece namely the Higgs boson at large hadron collider (LHC) was announced on 4th July 2012 at Conseil Europeen pour la Recherche Nucleaire (CERN) [4, 5], proving SM the most accurate and elegant theory at present. In spite of all its successes SM is believed to be a limiting case of a more general theory. There are well motivated theoretical as well as experimental reasons which coerce us to go beyond the SM.

The first problem of the SM is related to the neutrino sector. Neutrinos are strictly massless in the SM. Several key experiments with solar, atmospheric, reactor and accelerator neutrinos observed the disappearance of electron or muon neutrinos, the evidence enough for scientists to acquiesce neutrino oscillation [6]. This observation has confirmed that neutrinos have distinct masses and that 3 neutrino flavors ν_e, ν_μ and ν_τ mix among themselves to form 3 mass eigenstates. The fact that neutrinos are massive and mix implies non-conservation of lepton flavor, hence charged lepton flavor violating processes (cLFV) are expected in lepton sector just as quark flavor violating processes arise in quark sector.

The trivial extension to SM to accomodate neutrino masses is to introduce three fermionic $SU(3)_{\rm C} \times SU(2)_{\rm L} \times U(1)_{\rm Y}$ singlets (missing right handed neutrinos) and write down the neutrino Yukawa couplings which generates neutrino masses via electroweak symmetry breaking (EWSB). However this extension of SM requires extremely small Yukawa couplings and violate lepton number at low energy scale. As right handed neutrinos and lepton number violation has not been observed at low energy, one should look

for a mechanism that can generate masses for left handed neutrinos at low energy and also respect the non observation of right handed neutrinos and lepton number violation. One of the solutions to overcome this problem is the so called "seesaw mechanism" [7] which can be used to generate neutrino masses which not only allow large neutrino Yukawa couplings but also explain why left handed neutrinos are lighter compared to other SM fermions. These mechanisms assume the nature of neutrinos to be Majorana and existance of very massive particle that couple to the neutrinos in Yukawa analogue. The neutrino masses are then generated by an effective dimension 5 operator. This gives rise to neutrino physical states which are not flavor diagonal and consequently generate lepton flavor violation (LFV).

On the other hand SM also lack sufficient explaination in Higgs sector. For example SM is renormalizable, yet it is believed that SM is valid only up to some cut-off energy scale. This cut-off can be related to the scale where new physics appear, for example the Planck scale (10^{19} GeV) where quantum gravity becomes important. One-loop corrections to the Higgs mass M_H due to a fermion f in the loop are given by

$$\delta M_H^2(f) = -\frac{|\lambda_f|^2}{8\pi^2}[\Lambda^2 + ...], \tag{2}$$

where λ_f represents the fermion coupling to the Higgs field and Λ is the ultraviolet cutoff used to regulate the loop integral. If one replace the cutoff by the Planck mass one obtains $\delta M_H^2 \approx 10^{30}$ GeV^2. One could cancel these large correction with a bare mass of the same order and opposite sign. However, these two contributions should cancel with a precision of one part in 10^{26} to provide the observed Higgs mass. This is the so-called "hierarchy problem".

Third and equally important issue is the Dark Matter (DM). First speculation about the DM was due to astronomer Zwicky. In 1933, he observed that the mass from the luminous matter coming from COMA cluster is much smaller than the total mass we can derivate from the motion of the cluster member galaxies [8]. There are now several pieces of observational evidence for DM in our universe. Gravitational lensing and the unexpected rotational curves of spiral galaxies are among these observations that point to there being so-called "missing mass" throughout the universe. Recent results from WMAP [9] and PLANCK [10] give us our most accurate value for the total mass in the universe and how it is divided among different types of matter and energy. There is no SM particle that can serve as a DM candidate.

Due to all these reasons one needs to find renormalizable theories that can remove quadratic divergences in the Higgs boson mass, a theory that can provide us with a DM candidate and can explain LFV. Supersymmetric extension of the SM namely Minimal Supersymmetric Standard Model (MSSM) [11], is technically well equipped to deal with above mentioned discrepancies. The MSSM predicts the existence of a super-partner for each of the fundamental degree of freedom of the SM with spin differing by half unit. The presence of super-partners called sparticles in the loop cancels the quadratic divergences in the Higgs boson mass. Also the lightest supersymmetric particle (LSP) can be a DM candidate. However, the MSSM, like SM, assume neutrinos to be massless

so simple version of MSSM has to be extended with a mechanism like the seesaw to make it consistent with experimental observation of neutrino masses and mixing [6].

Much of the effort has been devoted at the LHC to discover supersymmetry (SUSY). But as of yet no SUSY particle has been observed at the colliders [12, 13]. Another approach to discover SUSY could be to study the indirect effects of the SUSY particles on other observables [14]. Flavor mixing offer a unique prospective in this regard since most of the indirect effects of the SUSY particles involve the flavor mixing observables. First among these are the Flavor Changing Neutral Current (FCNC) processes in the quark sector. In SM, FCNC processes are absent at tree level and can only occur at one-loop level. The only source of FCNC's in the SM is the Cabibbi Kobayashi Maskawa (CKM) matrix. However these processes are highly supressed due to GIM cancellations. On the other hand, in the MSSM, possible misalignment between the quark and squark mass matrices is another source of flavor violation that can dominate the SM contribution by several orders of magnitude. Any possible experimental deviation from the SM prediction for FCNS's would be a clear evidence of new physics and possibly a hint for MSSM. Similarly, SM predictions for cLFV are zero. Even seesaw extensions of the SM do not predict sizable rates for these processes, the cLFV rates in SM seesaw models are almost 40 orders of magnitude smaller than the present experimental bounds and consequently beyond the experimental reach. On the other hand seesaw extensions of MSSM are well capable of explaining the higher rates (touching the present experimental bounds) for these processes if observed. Also after the discovery of the Higgs boson with mass $M_h \approx 125$ GeV, one needs large radiative corrections. One obvious choice would be to choose scalar top mass heavier ≥ 1 TeV. However this could go into the direction of (re-)introducing tuning. One can avoid this problem by choosing large left-right or flavor mixing (instead of assuming heavy scalar top mass). Consequently the issue of flavor mixing in SUSY needs to be explored in detail, which precisely is the aim of the thesis in hand.

Within the MSSM, the possible presence of soft SUSY-breaking (SSB) parameters in the squark and slepton sector, which are off-diagonal in flavor space (mass parameters as well as trilinear couplings) are the most general way to introduce flavor mixing within the MSSM. For example in MSSM, the off-diagonality in the sfermion mass matrix reflects the misalignment (in flavor space) between fermions and sfermions mass matrices, that cannot be diagonalized simultaneously. This misalignment can be produced from various origins. For instance, off-diagonal sfermion mass matrix entries can be generated by Renormalization Group Equations (RGE) running. Going from a high energy scale, where no flavor violation is assumed, down to the electroweak (EW) scale can generate such entries due to presence of non diagonal Yukawa matrices in RGE's. This kind of approach in the literature is known as the Minimal Flavor Violation (MFV) [15, 16], where flavor and $\mathcal{CP}$-violation in quark sector is assumed to be entirely described by the CKM matrix, even in theories beyond the SM.

MFV scenerios are well motivated due to the fact that they do not introduce new sources of flavor and $\mathcal{CP}$-violation, which can potentially lead to large non-standard effects in flavor processes, in conflict with experimental bounds particularly from the

kaon and B_d sectors which are well described by the SM upto an accuracy of the $\sim 10\%$ level [17]. For the first and second generation squarks which are sensitive to the data on $K^0 - \bar{K}^0$ and $D^0 - \bar{D}^0$ the constraints are very tight. However the third generation system is, in principle, less constrained, since present data on $B^0 - \bar{B}^0$ mixing still leaves some room for new sources of flavor violation. This opens the prospect for the more general scenerios, namely the Non Minimal Flavor Violation (NMFV) scenerios, other then the MFV ones.

In this thesis we will present a systematic and simultanous study of the effects of flavor mixing on different observables in MFV as well as the NMFV scenerios. As a first step we will study squark and slepton mixing in the MSSM at low energy in Model-Independent (MI) way. For MI approach, we introduce flavor mixing parameters into the sfermion mass matrices by hand and do not consider the possible origin of these parameters. For the squark mixing we will be presenting the effects to electroweak precision observables (EWPO), B-Physics Observables (BPO) and quark flavor violating higgs decays (QFVHD). For slepton mixing we will study the effects to EWPO, higgs boson mass predictions and lepton flavor violating higgs decays (LFVHD).

In the second step we will extend our analysis to the source of flavor mixing and will analyze the flavor mixing induced by RGE running from GUT to EW scale. In this study we will work within the MFV hypothesis for squarks as well as sleptons. Consequently, we will investigate two models (more detailed definitions and citations will follow in the next chapters):

(i) the Constrained Minimal Supersymmetric Standard Model (CMSSM), where only flavor violation in the squark sector is present.

(ii) the CMSSM augmented by the seesaw type I mechanism [7], called "CMSSM-seesaw I" below.

In many analyses of the CMSSM, or extensions such as the NUHM1 or NUHM2 (see Ref. [18] and references therein), the hypothesis of MFV has been used, and it has been assumed that the contributions coming from MFV are negligible not only for FCNC processes but for other observables like EWPO and Higgs masses as well, see, e.g., Ref. [19]. We will analyze whether this assumption is justified, and whether including these MFV effects could lead to additional constraints on the CMSSM parameter space. In this respect we will evaluate in the CMSSM and in the CMSSM-seesaw I the following set of observables: BPO, in particular BR($B \to X_s\gamma$), BR($B_s \to \mu^+\mu^-$) and ΔM_{B_s}; EWPO, in particular M_W and the effective weak leptonic mixing angle, $\sin^2\theta_{\rm eff}$; the masses of the neutral and charged Higgs bosons in the MSSM, as well as cLFV and LFVHD.

The layout of the thesis is as follows. Chapter 1 contains the introduction to SM. In chapter 2 we introduce MSSM and its seesaw extensions. Chapter 3 is devoted to the calculational basis of the observables considered in this work. In chapter 4 we will be presenting our results in the case of squark flavor mixing in MI approach and study the effects to the BPO, EWPO and QFVHD. In chapter 5 slepton mixing effects to EWPO, Higgs mass predictions and LFVHD in MI approach will be presented. Chapter

6 will be focusing on our analysis in CMSSM and CMSSM-seesaw I where we present the flavor mixing effects to EWPO, BPO, Higgs boson mass predictions, QFVHD, cLFV and LFVHD. Chapter 7 is devoted to the summary and conclusions.

Chapter 1

The Standard Model

Symmetries play an important role in physics. Their presence in a particular problem often simplifies the problem. Particle physicists, using the concept of gauge symmetries, are able to build SM, which is a very successful model to explain the fundamental particles and their interactions. The theory has been formulated by writing the Lagrangian of the fundamental particles. The Lagrangian has been written by using the concept of internal symmetries and gauge invariance. All these aspects are discussed in detail hereafter and subsequent discussion follows closely Refs. [20, 21].

1.1 Fundamental particles and forces

Quarks and leptons (collectively called fermions, spin 1/2 particles) are (assumed to be) elementary particles of nature. There are six types (flavors) of leptons and quarks placed in three families. Fermions are chiral particles which connotes that left and right handed fields transform differently. The left handed components are placed in EW $SU(2)$ doublets and right handed components are placed in EW singlets

$$\begin{aligned} L &= \begin{pmatrix}\nu_e \\ e\end{pmatrix}_L, \quad \begin{pmatrix}\nu_\mu \\ \mu\end{pmatrix}_L, \quad \begin{pmatrix}\nu_\tau \\ \mu\end{pmatrix}_L, \\ & \quad e_R, \quad \mu_R, \quad \tau_R, \end{aligned} \tag{1.1}$$

$$\begin{aligned} Q &= \begin{pmatrix}u \\ d\end{pmatrix}_L, \quad \begin{pmatrix}c \\ s\end{pmatrix}_L, \quad \begin{pmatrix}t \\ b\end{pmatrix}_L, \\ & \quad u_R, \quad d_R, \quad c_R, \quad s_R, \quad t_R, \quad b_R \end{aligned} \tag{1.2}$$

L on the left represents lepton and in the subscript on the right it means left-handed. Neutrinos being left handed are absent in the EW singlets. For the quarks another index is required to describe how the quarks transform under $SU(3)$ transformation.

$$Q_\alpha = \begin{pmatrix}u_\alpha \\ d_\alpha\end{pmatrix}_L \tag{1.3}$$

Quarks and leptons interact through unified EW and strong forces. These forces are transmitted by the exchange of particles, called gauge bosons (γ , $W^{\pm}$ and Z). These are the mediators of the unified EW force and gluons are the mediators of strong force. There is an additional particle called Higgs boson predicted by the SM, which has implications with regard to the origin of mass. It was discovered recently at LHC CERN [4, 5].

1.2 Gauge transformation and invariance

All particles appear to have three kind of gauge invariances, ($U(1)$, $SU(2)$, $SU(3)$). The $U(1)$ is related to the electromagnetic charge, the $SU(2)$ corresponds to the non-abelian weak isospin and $SU(3)$ is associated with the non-abelian strong (color) charge. In 1961 Glashow [1] proposed $SU(2)_{\mathrm{L}} \times U(1)_{\mathrm{Y}}$ structure of the SM. Weinberg and Salam [2, 3] extended his idea and employed the hypothesis of spontaneous symmetry breaking in their gauge theory models to generate masses of gauge boson and fermions. Later on the Glashow, Weinberg and Salam model achieved the theoretical status when 't Hooft [22] demonstrated that the form of symmetry breaking would not spoil the renormalizability possessed by the massless theory.

1.3 The SM Lagrangian

The complete Lagrangian for the SM can be written as

$$\mathcal{L} = \mathcal{L}_{\mathrm{fermion}} + \mathcal{L}_{\mathrm{gauge}} + \mathcal{L}_{\mathrm{Higgs}} \tag{1.4}$$

$\mathcal{L}_{\mathrm{fermion}}$ is given by the relation

$$\mathcal{L}_{\mathrm{fermion}} = \sum_{f=L,Q} \bar{f} \iota \gamma^{\mu} D_{\mu} f, \tag{1.5}$$

where L and Q are given in Eq. (1.1) and Eq. (1.2) and D_{μ} is a covariant derivative given by

$$D_{\mu} = \partial_{\mu} - \iota g_1 \frac{Y}{2} B_{\mu} - \iota g_2 \frac{\sigma^i}{2} W_{\mu}^i - \iota g_3 \frac{\lambda^{\alpha}}{2} G_{\mu}^{\alpha}. \tag{1.6}$$

It is to be noted that whenever the terms in D_{μ} act on a fermionic state of different matrix form, they give zero, by definition. The second term represents the $U(1)$ symmetry. B_{μ} is spin 1 field needed to maintain gauge invariance and Y is the generator of $U(1)$ transformations, that is also called hypercharge. The g_1 is the $U(1)$ gauge coupling, the third and the fourth term represents $SU(2)$ and $SU(3)$ symmetries respectively, three W_{μ}^i for $SU(2)$ and eight G_{μ}^{α} for $SU(3)$, one for each generator $(\sigma^i, \lambda^{\alpha})$ of transformation whereas g_2 and g_3 are the $SU(2)$ and $SU(3)$ gauge couplings respectively.

The Lagrangian for the $SU(2)_{\mathrm{L}} \times U(1)_{\mathrm{Y}}$ gauge sector of the theory is

$$\mathcal{L}_{\mathrm{gauge}} = -\frac{1}{4} W_{\mu\nu}^i W_i^{\mu\nu} - \frac{1}{4} F_{\mu\nu} F^{\mu\nu}, \tag{1.7}$$

where $F_{\mu\nu}$ is the field strength tensor for $U(1)$ gauge boson B_μ and is given by

$$F_{\mu\nu} = \partial_\mu B_\nu - \partial_\nu B_\mu \tag{1.8}$$

and

$$W^i_{\mu\nu} = \partial_\mu W^i_\nu - \partial_\nu W^i_\mu + g_2 \varepsilon_{ijk} W^j_\mu W^k_\nu \tag{1.9}$$

is the field strength tensor for the $SU(2)$ gauge boson, ε_{ijk} in the third term of Eq. (1.9) is structure constant and this term appears due to non-abelian nature of the $SU(2)$ group.

$\mathcal{L}$ does not contain any mass term. In order to generate masses for fermions and bosons, Higgs mechanism is introduced which will be discussed in Sect. 1.6.

1.4 Electroweak theory

By using Eq. (1.5), the $U(1)$ and $SU(2)$ terms for the Lagrangian of the first generation of leptons can be written as

$$\begin{aligned}
\mathcal{L}_{\text{lepton}} &= \frac{g_1}{2}[Y_L(\bar{\nu}_L\gamma^\mu\nu_L + \bar{e}_L\gamma^\mu e_L) + Y_R\bar{e}_R\gamma^\mu e_R)]B_\mu \\
&\quad -\frac{g_2}{2}[\bar{\nu}_L\gamma^\mu\nu_L W^o_\mu - \bar{e}_L\gamma^\mu e_L W^o_\mu - \sqrt{2}\bar{\nu}_L\gamma^\mu e_L W^+_\mu \\
&\quad -\sqrt{2}\bar{e}_L\gamma^\mu\nu_L W^-_\mu],
\end{aligned} \tag{1.10}$$

as neutrinos do not have electromagnetic interactions, the terms of the form $\frac{g_1}{2}Y_L\bar{\nu}_L\gamma^\mu\nu_L B_\mu$ must be avoided. To do so the coefficient $Z_\mu \propto g_1 Y_L B_\mu - g_2 W^0_\mu$ of the term $\bar{\nu}_L\gamma^\mu\nu_L$ is assumed to be orthogonal to the electromagnetic field A_μ. After diagonalization one gets

$$A_\mu = \frac{g_2 B_\mu - g_1 Y_L W^0_\mu}{\sqrt{g_2^2 + g_1^2 Y_L^2}}, \tag{1.11}$$

$$Z_\mu = \frac{g_1 Y_L B_\mu - g_2 W^0_\mu}{\sqrt{g_2^2 + g_1^2 Y_L^2}}. \tag{1.12}$$

Solving for B_μ and W^0_μ, one gets

$$B_\mu = \frac{g_2 A_\mu + g_1 Y_L Z_\mu}{\sqrt{g_2^2 + g_1^2 Y_L^2}}, \tag{1.13}$$

$$W^o_\mu = \frac{g_2 Z_\mu - g_1 Y_L A_\mu}{\sqrt{g_2^2 + g_1^2 Y_L^2}}. \tag{1.14}$$

With these definitions the neutral current interactions of the electrons in Eq. (1.10) are modified as

$$\begin{aligned}
&-A_\mu[\bar{e}_L\gamma^\mu e_L \frac{g_1 g_2 Y_L}{\sqrt{g_2^2 + g_1^2 Y_L^2}} + \bar{e}_R\gamma^\mu e_R \frac{g_1 g_2 Y_R}{2\sqrt{g_2^2 + g_1^2 Y_L^2}}], \\
&-Z_\mu[\bar{e}_L\gamma^\mu e_L \frac{g_1^2 Y_L^2 - g_2^2}{\sqrt{g_2^2 + g_1^2 Y_L^2}} + \bar{e}_R\gamma^\mu e_R \frac{g_1^2 Y_L Y_R}{2\sqrt{g_2^2 + g_1^2 Y_L^2}}].
\end{aligned} \tag{1.15}$$

This gives

$$e = \frac{-g_1 g_2 Y_L}{\sqrt{g_2^2 + g_1^2 Y_L^2}} \tag{1.16}$$

and

$$e = \frac{-g_1 g_2 Y_R}{2\sqrt{g_2^2 + g_1^2 Y_L^2}} \tag{1.17}$$

From Eq. (1.16) and Eq. (1.17) it follows that

$$2Y_L = Y_R \tag{1.18}$$

As g_1 can be redefined to absorb any change in Y_L, Y_L has been set to -1 and Eq. (1.16) is modified as

$$e = \frac{g_1 g_2}{\sqrt{g_2^2 + g_1^2}} \tag{1.19}$$

$$e = g_2 \sin\theta_W \tag{1.20}$$

where θ_W is EW mixing angle with $\sin^2\theta_W = (\frac{g_1}{\sqrt{g_2^2+g_1^2}})^2$.

1.5 Spontaneous symmetry breaking

The Lagrangian in Eq. (1.5) does not contain any mass term and mass terms can not be added explicitly by hand as it would break gauge invariance. Mass terms are included in SM Lagrangian by the Higgs mechanism, using the idea of spontaneous symmetry breaking. Consider the Lagrangian for a scalar field ϕ

$$\mathcal{L} = \frac{1}{2}\partial_\mu\phi\partial^\mu\phi - (\frac{1}{2}\mu^2\phi^2 + \frac{1}{4}\lambda\phi^4); \qquad \lambda > 0 \tag{1.21}$$

Here

$$V = \frac{1}{2}\mu^2\phi^2 + \frac{1}{4}\lambda\phi^4. \tag{1.22}$$

If $\mu^2 > 0$ then the vacuum corresponds to $\phi_0 = 0$ but if $\mu^2 < 0$ then the minimum of the potential is

$$\frac{\partial V}{\partial\phi} = 0$$

$$\phi_0(\mu^2 + \lambda\phi_0^2) = 0 \tag{1.23}$$

$$\phi_0 = \pm\sqrt{\frac{-\mu^2}{\lambda}} = v \tag{1.24}$$

where v is vacuum expectation value (VEV) of Higgs field ϕ. To determine the particle spectrum one must study the theory in the region of the minimum by putting $\phi = v+\eta(x)$ and expanding around $\eta = 0$. Using $\phi = v + \eta(x)$ and Eq. (1.24) in Eq. (1.21) yields

$$\mathcal{L} = \frac{1}{2}\partial_\mu\eta\partial^\mu\eta - (\lambda v\eta^2 + \lambda v\eta^3 + \frac{1}{4}\lambda\eta^4) + \text{const.} \tag{1.25}$$

The term in η^2 has the correct sign so it can be interpreted as mass square and the vacuum does not have the reflection symmetry of the original Lagrangian. This is called spontaneous symmetry breaking.

1.6 Higgs mechanism

The renormalizability and gauge invariance of the theory demands that the symmetry $SU(2)_{\mathrm{L}} \times U(1)_{\mathrm{Y}}$ be spontaneously broken through Higgs mechanism. For this purpose a complex weak doublet of Higgs scalar with hypercharge $Y = 1$,

$$\Phi(x) = \begin{pmatrix} \phi^+(x) \\ \phi^0(x) \end{pmatrix} \tag{1.26}$$

is introduced which is coupled to the gauge fields through

$$\mathcal{L}_{\mathrm{Higgs}} = (D_\mu \Phi)^\dagger (D_\mu \Phi) - V(\Phi). \tag{1.27}$$

In this case the covariant derivative is given by

$$D_\mu = \partial_\mu - \iota \frac{g_1}{2} B_\mu - \iota g_2 \frac{\sigma^i}{2} W_\mu^i. \tag{1.28}$$

The Higgs field self-interaction enters through the Higgs potential with constants μ^2 and λ,

$$V(\Phi) = -\mu^2 \Phi^\dagger \Phi + \frac{\lambda}{4} (\Phi^\dagger \Phi)^2. \tag{1.29}$$

In the ground state, the vacuum, the potential has a minimum. For μ^2, $\lambda > 0$, the minimum does not occur for $\Phi = 0$; instead, V is minimized by all non-vanishing field configurations with $\Phi^\dagger \Phi = 2\mu^2\, \lambda$. Selecting the one which is real and electrically neutral, one gets the VEV

$$\langle \Phi \rangle = \frac{1}{\sqrt{2}} \begin{pmatrix} 0 \\ v \end{pmatrix}. \tag{1.30}$$

Although the Lagrangian is symmetric under gauge transformations of the full $SU(2) \times U(1)$ group, the vacuum configuration $\langle \Phi \rangle$ does not have this symmetry: the symmetry has been spontaneously broken. $\langle \Phi \rangle$ is still symmetric under transformations of the electromagnetic subgroup $U(1)_{\mathrm{em}}$, which is generated by the charge Q, thus preserving the electromagnetic gauge symmetry.

The scalar feld in Eq. (1.26) can be written as

$$\Phi(x) = \begin{pmatrix} \phi^+(x) \\ \left(v + H(x) + \iota \chi(x)\right)/\sqrt{2} \end{pmatrix}, \tag{1.31}$$

where the components ϕ^+, H, χ have vacuum expectation values zero. Expanding the potential in Eq. (1.29) around the vacuum configuration in terms of the components yields a mass term for H, whereas ϕ^+ and χ are massless. Exploiting the invariance

of the Lagrangian, the components ϕ^+ and χ can be eliminated by a suitable gauge transformation; this means that they are unphysical degrees of freedom (called Higgs ghosts or would-be Goldstone bosons). Choosing this particular gauge where $\phi^+ = \chi = 0$, denoted as the unitary gauge, the Higgs doublet field has the simple form

$$\Phi(x) = \frac{1}{\sqrt{2}} \begin{pmatrix} 0 \\ v + H(x) \end{pmatrix}. \tag{1.32}$$

The real field $H(x)$ thus describes physical neutral scalar particles, the Higgs bosons, with mass

$$M_H = \sqrt{2}\mu = \sqrt{\lambda} v. \tag{1.33}$$

The gauge invariant Higgs–gauge field interaction in the kinetic part of Eq. (1.27) gives rise to mass terms for the vector bosons in the non-diagonal form

$$\frac{1}{2}\left(\frac{g_2}{2}v\right)^2 (W_1^2 + W_2^2) + \frac{1}{2}\left(\frac{v}{2}\right)^2 (W_\mu^3, B_\mu) \begin{pmatrix} g_2^2 & g_1 g_2 \\ g_1 g_2 & g_1^2 \end{pmatrix} \begin{pmatrix} W^{\mu,3} \\ B_\mu \end{pmatrix}. \tag{1.34}$$

The first term can be written as

$$\left(\frac{g_2}{2}v\right)^2 W_\mu^+ W^{-\mu}. \tag{1.35}$$

For the charged boson the expected mass term for the Lagrangian would be $m^2 W^+ W^-$, so we can conclude that the charged W boson has indeed acquired a mass

$$M_W = \frac{1}{2} g_2 v. \tag{1.36}$$

The second term in the Eq. (1.34) is not diagonal and we have to define new eigenvalues to find the particles with definite mass. In fact, we already have the answer in hand, because the combination of B and W^3 appearing in Eq. (1.34) is just the combination we have called Z_μ (see Eq. (1.12)). From Eq. (1.34) and normalization of Z in Eq. (1.12), we can conclude that the neutral gauge boson Z acquires mass

$$M_Z = \frac{v}{2}\sqrt{g_2^2 + g_1^2} = \frac{M_W}{\cos\theta_W}, \tag{1.37}$$

while the photon remains massless.

In SM, all quarks and charged fermions get their masses through the Yukawa couplings with the Higgs field Φ:

$$\mathcal{L}_{\text{Yukawa}} = (Y^u)_{ij} \bar{Q}_{L_i} \Phi^* u_{R_j} + (Y^d)_{ij} \bar{Q}_{L_i} \Phi d_{R_j} + (Y^e)_{ij} \bar{L}_{L_i} \Phi e_{R_j}, \tag{1.38}$$

where Y^u, Y^d and Y^e are up-quark down-quark and charged leptons Yukawa coupling, Q_L and L_L are left handed quark and lepton doublets, u_R, d_R and e_R are $SU(2)_L$ - singlet right-handed fields of up-type quarks, down-type quarks and charged leptons respectively and i, j are the generation indices. After the EW symmetry is broken by a nonzero VEV v of the Higgs field, the Yukawa terms in Eq. (1.38) yield the mass matrices of quarks and charged leptons

$$(m_u)_{ij} = (Y^u)_{ij} v,\ (m_d)_{ij} = (Y^d)_{ij} v,\ (m_e)_{ij} = (Y^e)_{ij} v \tag{1.39}$$

Neutrinos are massless in the SM. They cannot have Dirac masses because there are no $SU(2)_{\text{L}}$ - singlet ("sterile") right-handed neutrinos ν_R in the SM.

1.7 The CKM matrix

The quark doublets introduced in Eq. (1.2) can have up-down transitions of the form $u_i \to d_i$ mediated by the $W^{\pm}$, where u_i can be any up type quark and d_i represents any down type quark. These kind of interactions are absent among lepton doublets due to conservation of lepton flavor. The mixing among different generations indicated by rare kaon decay led Cabibbo [23] to introduce the mixing angle θ_c called cabibbo angle so that the quark doublet given in Eq. (1.2) is modified to

$$\begin{pmatrix} u \\ d' \end{pmatrix} = \begin{pmatrix} u \\ d\cos\theta_c + s\sin\theta_c \end{pmatrix}. \tag{1.40}$$

This means that the weak eigenstate d' is a linear combination of real mass eigenstates d and s. This concept was modified by S.L. Glashow, J. Iliopoulos and L. Maiani [24]. They were able to predict the existence of charm quark even before its discovery. This completed the two quark doublets. They explained the mixing with the help of 2×2 unitary matrix. As the concept of quark mixing was indicated through the rare kaon decays, there was also indication of $\mathcal{CP}$ violation in these decays. So it was believed that the $\mathcal{CP}$ violation has its origin in quark mixing. This idea was adopted by Kobayashi and Maskawa [25] to introduce the third quark doublet, as $\mathcal{CP}$ violation cannot be accommodated by two doublets, consequently, they proposed the 3×3 unitary matrix called CKM matrix given by

$$V_{\rm CKM} = \begin{pmatrix} V_{ud} & V_{us} & V_{ub} \\ V_{cd} & V_{cs} & V_{cb} \\ V_{td} & V_{ts} & V_{tb} \end{pmatrix}. \tag{1.41}$$

Thus the rotation from the $SU(2)$ interaction eigenstate basis, $q^{\rm int}_{L,R}$, to the physical mass eigenstate basis, $q^{\rm phys}_{L,R}$, is performed by the unitary transformations, $V^{u,d}_{L,R}$:

$$\begin{pmatrix} u^{\rm phys}_{L,R} \\ c^{\rm phys}_{L,R} \\ t^{\rm phys}_{L,R} \end{pmatrix} = V^{u}_{L,R} \begin{pmatrix} u^{\rm int}_{L,R} \\ c^{\rm int}_{L,R} \\ t^{\rm int}_{L,R} \end{pmatrix}, \qquad \begin{pmatrix} d^{\rm phys}_{L,R} \\ s^{\rm phys}_{L,R} \\ b^{\rm phys}_{L,R} \end{pmatrix} = V^{d}_{L,R} \begin{pmatrix} d^{\rm int}_{L,R} \\ s^{\rm int}_{L,R} \\ b^{\rm int}_{L,R} \end{pmatrix}, \tag{1.42}$$

such that the quark mass matrices in the physical basis are:

$$\frac{v}{\sqrt{2}} V^{u}_{L} Y^{u*} V^{u\dagger}_{R} = \mathrm{diag}\,(m_u, m_c, m_t)\,, \tag{1.43}$$

$$\frac{v}{\sqrt{2}} V^{d}_{L} Y^{d*} V^{d\dagger}_{R} = \mathrm{diag}\,(m_d, m_s, m_b)\,. \tag{1.44}$$

In short, the quark flavour mixing is encoded in the CKM matrix,

$$V_{\rm CKM} = V^{u}_{L} V^{d\dagger}_{L}. \tag{1.45}$$

There are nine parameters in the CKM matrix as shown in Eq. (1.41) which can be reduced to four in the standard parametrization [26]. The three Euler angles $\theta_{12},\ \theta_{13},\ \theta_{23}$

and one phase factor δ, which accounts for the $\mathcal{CP}$ violation. The CKM matrix in standard parameterization is given by

$$V_{\mathrm{CKM}} = \begin{pmatrix} c_{12}c_{13} & s_{12}c_{13} & s_{13}e^{-\iota\delta} \\ -s_{12}c_{23} - c_{12}s_{13}e^{\iota\delta} & c_{12}c_{23} - s_{12}s_{23}s_{13}e^{\iota\delta} & s_{23}c_{13} \\ s_{12}s_{23} - c_{12}c_{23}s_{13}e^{\iota\delta} & -c_{12}s_{23} - s_{12}c_{23}s_{13}e^{\iota\delta} & c_{13}c_{23} \end{pmatrix} \tag{1.46}$$

where $c_{ij} = \cos\theta_{ij}$ and $s_{ij} = \sin\theta_{ij}$ $(i, j = 1, 2, 3)$. The elements of the CKM matrix exhibit a pronounced hierarchy. While the diagonal elements are close to unity, the off-diagonal elements are small, such that e.g. $V_{ud} \gg V_{us} \gg V_{ub}$. In terms of the angles θ_{ij} we have $s_{12} \gg s_{23} \gg s_{13}$. This fact is usually expressed in terms of the Wolfenstein parameterization [27], which can be understood as an expansion in $\lambda = |V_{us}|$. This reads up to order λ^3

$$V_{\mathrm{CKM}} = \begin{pmatrix} 1 - \frac{\lambda^2}{2} & \lambda & A\lambda^3(\rho - \iota\eta) \\ -\lambda & 1 - \frac{\lambda^2}{2} & A\lambda^2 \\ A\lambda^3(1 - \rho - \iota\eta) & A\lambda^2 & 1 \end{pmatrix} \tag{1.47}$$

with parameters A, ρ and η are assumed to be of order 1. The current values of the CKM elements, obtained from a global fit using all the available measurements and imposing the SM constraints, are collected in the following matrix [28]:

$$V_{\mathrm{CKM}} = \begin{pmatrix} 0.97427 \pm 0.00014 & 0.22536 \pm 0.00061 & 0.00355 \pm 0.00015 \\ 0.22522 \pm 0.00061 & 0.97343 \pm 0.00015 & 0.0414 \pm 0.0012 \\ 0.00886^{+0.00033}_{-0.00032} & 0.0405^{+0.0011}_{-0.0012} & 0.99914 \pm 0.00005 \end{pmatrix}. \tag{1.48}$$

Chapter 2

Supersymmetry & Its Seesaw Extention

A SUSY transformation turns a bosonic state into a fermionic state, and vice versa. The operator Q that generates such transformations must be an anticommuting spinor, with

$$Q\left|\text{Boson}\right\rangle = \left|\text{Fermion}\right\rangle, \quad Q\left|\text{Fermion}\right\rangle = \left|\text{Boson}\right\rangle. \tag{2.1}$$

Spinors are intrinsically complex objects, so $Q^\dagger$ (the hermitian conjugate of Q) is also a symmetry generator. Because Q and $Q^\dagger$ are fermionic operators, they carry spin angular momentum 1/2, so it is clear that SUSY must be a spacetime symmetry. The No-go theorem [29] asserts that it is impossible to mix internal and Lorentz space time symmetries (when described by the commutators only) in a non-trivial way. If one wants to extend the space-time structure, one will be left with the only choice of SUSY with graded Lie algebra. The simplest realization is given by

$$\{Q_\alpha, Q^\dagger_{\dot\alpha}\} = 2\sigma^\mu_{\alpha\dot\alpha} P_\mu, \tag{2.2}$$

$$\{Q_\alpha, Q_\beta\} = \{Q_{\dot\alpha}, Q_{\dot\beta}\} = 0, \tag{2.3}$$

$$[Q_\alpha, P_\mu] = [Q_{\dot\alpha}, P_\mu] = 0, \tag{2.4}$$

where P^μ is the momentum generator of space-time translations and $\sigma^\mu = (1, \sigma^1, \sigma^2, \sigma^3)$. In the following sections, we will give some motivation for SUSY and review main aspacts of the SUSY, in particular the MSSM and its seesaw extension. The subsequent discussion follows closely Refs. [14, 30].

2.1 Motivation

SUSY can successfully explain some of the major deficiencies of SM, as discussed in the introduction, in a more natural way.

- **Hierarchy problem:** The simplest form of SUSY can solve the hierarchy problem mentioned in the introduction. Quadratic divergences appearing at one loop level in Higgs mass vanish due to cancellation between bosons and fermions. Consider for example coupling of the Higgs field H to a Dirac fermion f with a term in the Lagrangian $-\lambda_f H\bar{f}f$. The one-loop radiative corrections to the Higgs mass M_H will be of the form

$$\delta M_H^2(f) = -\frac{|\lambda_f|^2}{8\pi^2}[\Lambda^2 - 2m_f^2 \ln\frac{\Lambda}{m_f} + ...] \tag{2.5}$$

where m_f is the mass of the fermion in the loop. As can be seen from above equation Higgs boson mass is quadratically divergent. In the case of fermion (gauge boson), the chiral (gauge) symmetry constitutes the "natural barrier" preventing their masses to become arbitrarily large. In the case of Higgs boson, there is no symmetry that protects the scalar mass and in the limit $M_H \to 0$, the symmetry of the model is not increased. SUSY constitutes so far the most interesting answer to hierarchy problem. As we have mentioned in the introduction, SUSY associates a scalar particle with every fermionic degree of freedom in the theory with, in principle, identical masses and gauge quantum numbers. Therefore, in a supersymmetric theory we would have a new contribution to the Higgs mass at one loop given by

$$\delta M_H^2(\tilde{f}) = -\frac{\lambda_{\tilde{f}}}{8\pi^2}[\Lambda^2 - 2m_{\tilde{f}}^2 \ln\frac{\Lambda}{m_{\tilde{f}}} + ...], \tag{2.6}$$

where $\lambda_{\tilde{f}}$ is the SUSY particle coupling to the Higgs field, $m_{\tilde{f}}$ is the mass of the SUSY particle in the loop. If we compare Eq. (2.5) and Eq. (2.6) we see that with $|\lambda_f|^2 = -\lambda_{\tilde{f}}$ and $m_f = m_{\tilde{f}}$ we obtain a total correction $\delta M_H^2(f) + \delta M_H^2(\tilde{f}) = 0$, i.e. quadratic divergence cancels exactly. If SUSY was an exact symmetry of nature, particles and their superpartners would have the same mass, and therefore the superpartners should have been observed in collider experiments. However we have not found scalars exactly degenerate with the SM fermions. This means SUSY can not be an exact symmetry of nature, it must be a broken symmetry. By comparing Eq. (2.5) and Eq. (2.6), we can see that we must still require $|\lambda_f|^2 = -\lambda_{\tilde{f}}$ if we want to ensure the cancellation of quadratic divergences. SUSY can be broken only in couplings with positive mass dimension, as for instance the masses. This is called "soft SUSY-breaking" [31]. Now if we take $m_{\tilde{f}}^2 = m_f^2 + \delta^2$ we obtain a correction to the Higgs mass,

$$\delta M_H^2(f) + \delta M_H^2(\tilde{f}) = \frac{|\lambda_f|^2}{8\pi^2}\delta^2 \ln\frac{\Lambda}{m_{\tilde{f}}} + ..., \tag{2.7}$$

and this is only logarithmically divergent and proportional to mass difference between fermion and its scalar partner and is, therefor, under control.

- **Gauge coupling unification:** The idea of gauge unification gets simplified by the SUSY. The coupling constants α_1, α_2 and α_3 vary with energy and the rate of the variation of these coupling constants depends on the particle content of the theory. If these coupling constants are extrapolated to the higher energies using the particle content of the SM, these do not meet at the same point. However, when the same extrapolation is repeated using the particle contents of the SUSY, the three coupling constants meet at the same point [32–34]. The "exact" unification of the gauge couplings within the MSSM may or may not be an accident. But it provides enough reasons to consider supersymmetric models seriously as it links SUSY and grand unification in an inseparable manner [35].

- **Dark Matter candidate:** There is no particle in the SM that can serve as a DM candidate. However most of the SUSY models provide a particle which might explain missing mass in the universe. For example lightest neutralino could be a DM candidate in the MSSM (see details below).

- **Supergravity:** If SUSY is formulated as a local symmetry, a spin 2 particle corresponding to the graviton, the hypothetical particle that mediates gravity, is introduced. Then the supersymmetric models of gravity called supergravity have the elegant feature to link the SM fundamental interactions with gravity [36].

2.2 Superpotential

In this section we will describe the concept of superpotential. The aim is to arrive at a recipe that will allow to write down the allowed interaction terms of a general supersymmetric theory, so that later these results can be applied to the special case of the MSSM (see, e.g., the discussion in Ref. [30]).

The single-particle states of a supersymmetric theory fall into irreducible representations of the SUSY algebra, called supermultiplets. Each supermultiplet contains both fermion and boson states, which are commonly known as superpartners of each other. Each supermultiplet contains an equal number of fermionic and bosonic degrees of freedom.

The minimum fermion content of any theory in four dimensions consists of a single left-handed two-component Weyl fermion ψ. Since this is an intrinsically complex object, it seems sensible to choose as its superpartner a complex scalar field ϕ. This combination of a two-component Weyl fermion and a complex scalar field is called a chiral or matter or scalar supermultiplet.

The next-simplest possibility for a supermultiplet contains a spin-1 vector boson. If the theory is to be renormalizable, this must be a gauge boson that is massless, at least before the gauge symmetry is spontaneously broken. Its superpartner is therefore a massless spin-1/2 Weyl fermion, called gaugino. Such a combination of spin-1/2 gauginos and spin-1 gauge bosons is called a gauge or vector supermultiplet.

The simplest action one can write down for chiral supermultiplet just consists of

kinetic energy terms for scalar and fermionic fields.

$$S = \int d^4x(\mathcal{L}_{\text{scalar}} + \mathcal{L}_{\text{fermion}}) \tag{2.8}$$

with

$$\mathcal{L}_{\text{scalar}} = \partial^\mu \phi^* \partial_\mu \phi, \qquad \mathcal{L}_{\text{fermion}} = \iota \bar{\psi} \bar{\sigma}^\mu \partial_\mu \psi. \tag{2.9}$$

This is called the massless, non-interacting Wess-Zumino model. The number of fermionic degrees of freedom must be equal to the number of bosonic degrees of freedom. But scalar field contains one degree of freedom and one can add one more if a complex scalar field is introduced. However, a fermionic field carries at least four components. Two of these degrees of freedom can be fixed by Dirac equation. It means, the algebra of SUSY only closes on-shell in this formulation. This can be fixed by a trick. One can invent a new complex scalar field F, which does not have a kinetic term. Such fields are called auxiliary, and they are really just book-keeping devices that allow the SUSY algebra to close off-shell. Thus the free part of the Lagrangian is

$$\mathcal{L}_{\text{free}} = \partial^\mu \phi^{*i} \partial_\mu \phi_i + \iota \bar{\psi}^i \bar{\sigma}^\mu \partial_\mu \psi_i + F^{*i} F_i \ , \tag{2.10}$$

where it is summed over repeated indices i (not to be confused with the suppressed spinor indices). Now the most general set of renormalizable interactions for these fields that is consistent with SUSY must have dynamical field content with mass dimension $\leq$ 4. So, the candidate terms that are also SUSY invariant are:

$$\mathcal{L}_{\text{int}} = -\frac{1}{2} W^{ij} \psi_i \psi_j + W^i F_i + c.c. \tag{2.11}$$

A very useful object W called the superpotential is introduced.

$$W = \frac{1}{2} M^{ij} \phi_i \phi_j + \frac{1}{6} y^{ijk} \phi_i \phi_j \phi_k \tag{2.12}$$

where M^{ij} is a symmetric mass matrix for the fermion fields, and y^{ijk} is the Yukawa coupling of the scalar ϕ_k. One can write

$$W^{ij} = \frac{\partial^2}{\partial \phi_i \partial \phi_j} W, \quad W^i = \frac{\partial W}{\partial \phi_i}. \tag{2.13}$$

The auxiliary fields F_i and F^{*i} can be eliminated using their classical equations of motion. The part of $\mathcal{L}_{\text{free}} + \mathcal{L}_{\text{int}}$ that contains the auxiliary fields is $F_i F^{*i} + W^i F_i + W_i^* F^{*i}$, leading to the equations of motion

$$F_i = -W_i^*; \quad F^{*i} = -W^i. \tag{2.14}$$

After making the replacement Eq. (2.14) in $\mathcal{L}_{\text{free}} + \mathcal{L}_{\text{int}}$, one obtains the Lagrangian density

$$\mathcal{L} = \partial^\mu \phi^{*i} \partial_\mu \phi_i + \iota \bar{\psi}^i \bar{\sigma}^\mu \partial_\mu \psi_i - \frac{1}{2}(W^{ij} \psi_i \psi_j + W^*_{ij} \bar{\psi}^i \bar{\psi}^j) - W^i W_i^*. \tag{2.15}$$

In short, the most general non-gauge interactions for chiral supermultiplets are determined by a single analytic function of the complex scalar fields, the superpotential W.

Superfields	spin 0	spin 1/2	$(SU(3)_C,\ SU(2)_L,\ U(1)_Y)$
$\hat{Q}$	$(\widetilde{u}_L \quad \widetilde{d}_L)$	$(u_L \quad d_L)$	$(\mathbf{3},\ \mathbf{2}\ ,\ \frac{1}{6})$
$\hat{U}$	$\widetilde{u}_R^*$	$u_R^\dagger$	$(\overline{\mathbf{3}},\ \mathbf{1},\ -\frac{2}{3})$
$\hat{D}$	$\widetilde{d}_R^*$	$d_R^\dagger$	$(\overline{\mathbf{3}},\ \mathbf{1},\ \frac{1}{3})$
$\hat{L}$	$(\widetilde{\nu} \quad \widetilde{e}_L)$	$(\nu \quad e_L)$	$(\mathbf{1},\ \mathbf{2}\ ,\ -\frac{1}{2})$
$\hat{E}$	$\widetilde{e}_R^*$	$e_R^\dagger$	$(\mathbf{1},\ \mathbf{1},\ 1)$
$\hat{H}_2$	$(\mathcal{H}_2^+ \quad \mathcal{H}_2^0)$	$(\widetilde{\mathcal{H}}_2^+ \quad \widetilde{\mathcal{H}}_2^0)$	$(\mathbf{1},\ \mathbf{2}\ ,\ +\frac{1}{2})$
$\hat{H}_1$	$(\mathcal{H}_1^0 \quad \mathcal{H}_1^-)$	$(\widetilde{\mathcal{H}}_1^0 \quad \widetilde{\mathcal{H}}_1^-)$	$(\mathbf{1},\ \mathbf{2}\ ,\ -\frac{1}{2})$

Table 2.1: Chiral supermultiplets in the MSSM, their field content, and their representations in the gauge groups. Here $u = u, c, t$; $d = d, s, b$; $e = e, \mu, \tau$ and $\nu = \nu_e, \nu_\mu, \nu_\tau$.

Superfields	spin 1/2	spin 1	$(SU(3)_C,\ SU(2)_L,\ U(1)_Y)$
$\hat{G}^a$	$\widetilde{g}$	g	$(\mathbf{8},\ \mathbf{1}\ ,\ 0)$
$\hat{W}^i$	$\widetilde{W}^\pm \quad \widetilde{W}^0$	$W^\pm \quad W^0$	$(\mathbf{1},\ \mathbf{3}\ ,\ 0)$
$\hat{B}$	$\widetilde{B}^0$	B^0	$(\mathbf{1},\ \mathbf{1}\ ,\ 0)$

Table 2.2: Gauge supermultiplets in the MSSM, their field content, and their representations in the gauge groups.

2.3 The MSSM

The supersymmetric version of SM is called the MSSM with $N = 1$ generators, where N refer to the number of distinct copies of Q and $Q^\dagger$. According to the MSSM each of the fundamental particle of SM has a superpartner with spin differing by half unit. These particles are placed either in chiral or gauge supermultiplet as shown in Tab. 2.1 and Tab. 2.2.

In order to keep anomaly cancellation, contrary to the SM a second Higgs doublet is needed [37]. One Higgs doublet, $\mathcal{H}_1$, gives mass to the d-type fermions (with weak isospin -1/2), the other doublet, $\mathcal{H}_2$, gives mass to the u-type fermions (with weak isospin +1/2). All SM multiplets, including the two Higgs doublets, are extended to supersymmetric multiplets, resulting in scalar partners for quarks and leptons ("squarks" and "sleptons") and fermionic partners for the SM gauge boson and the Higgs bosons ("gauginos" and "gluinos") as shown in Tab. 2.1 and Tab. 2.2.

The mass eigenstates of the gauginos are linear combinations of these fields, denoted as "neutralinos" and "charginos". Also the left- and right-handed squarks (and sleptons) can mix, yielding the mass eigenstates (denoted by the indices $1, 2$ instead of L, R). The

EW interaction eigenstates and mass eigenstates of the MSSM particle spectrum are given in Tab. 2.3. Here mass eigenstates are written with the assumption of no flavor violation. If flavor violation is assumed, all six up- and down-type squarks and all six charged sleptons mix separately to give six mass eigenstates (see Sect. 2.3.6).

Particle	Electroweak eigenstate	Mass Eigenstate
squarks	$\tilde{u}_L$,$\tilde{u}_R$,$\tilde{d}_L$,$\tilde{d}_R$	$\tilde{u}_1$,$\tilde{u}_2$,$\tilde{d}_1$,$\tilde{d}_2$
	$\tilde{c}_L$,$\tilde{c}_R$, $\tilde{s}_L$,$\tilde{s}_R$	$\tilde{c}_1$,$\tilde{c}_2$,$\tilde{s}_1$,$\tilde{s}_2$
	$\tilde{t}_L$,$\tilde{t}_R$,$\tilde{b}_L$,$\tilde{b}_R$	$\tilde{t}_1$,$\tilde{t}_2$,$\tilde{b}_1$,$\tilde{b}_2$
sleptons	$\tilde{e}_L$,$\tilde{e}_R$,$\tilde{\nu}_e$	$\tilde{e}_1$,$\tilde{e}_2$,$\tilde{\nu}_e$
	$\tilde{\mu}_L$,$\tilde{\mu}_R$,$\tilde{\nu}_\mu$	$\tilde{\mu}_1$,$\tilde{\mu}_2$,$\tilde{\nu}_\mu$
	$\tilde{\tau}_L$,$\tilde{\tau}_R$,$\tilde{\nu}_\tau$	$\tilde{\tau}_1$,$\tilde{\tau}_2$,$\tilde{\nu}_\tau$
neutralinos	$\tilde{B}$,$\tilde{W}$,$\tilde{H}_u^0$,$\tilde{H}_d^0$	$\tilde{\chi}_1^0$,$\tilde{\chi}_2^0$,$\tilde{\chi}_3^0$,$\tilde{\chi}_4^0$
charginos	$\tilde{W}^\pm$,$\tilde{H}_u^+$,$\tilde{H}_d^-$	$\tilde{\chi}_1^\pm$,$\tilde{\chi}_2^\pm$
gauge boson	B,W^1,W^2,W^3	$W^\pm$,Z,γ
gluon and gluino	g,$\tilde{g}$	g,$\tilde{g}$

Table 2.3: The EW interaction eigenstates and mass eigenstates of the MSSM particles. No flavor mixing is assumed here.

At knowing the particle content of MSSM, one can write the most general $SU(3)_{\rm C} \times SU(2)_{\rm L} \times U(1)_{\rm Y}$ gauge invariant and renormalizable superpotential as [11]

$$W_{\rm MSSM} = \epsilon_{ab}[Y_{ij}^e \hat{H}_1^a \hat{L}_i^b \hat{E}_j^C + Y_{ij}^d \hat{H}_1^a \hat{Q}_i^b \hat{D}_j^C + Y_{ij}^u \hat{H}_2^a \hat{Q}_i^b \hat{U}_j^C - \mu \hat{H}_1^a \hat{H}_2^b] \tag{2.16}$$

where $\hat{L}$ represents the chiral multiplet of a $SU(2)_{\rm L}$ doublet lepton, $\hat{E}$ a $SU(2)_{\rm L}$ singlet charged lepton, $\hat{H}_1$ and $\hat{H}_2$ two Higgs multiplets with opposite hypercharge. Similarly $\hat{Q}$, $\hat{U}$ and $\hat{D}$ represent chiral multiplets of quarks of a $SU(2)_{\rm L}$ doublet and two singlets with different $U(1)_{\rm Y}$ charges whereas $i, j = 1, 2, 3$ are family indices and a, b are $SU(2)$ indices. The symbol ϵ_{ab} is an anti-symmetric tensor with $\epsilon_{12} = 1$.

As mentioned in Sect. 2.1, SUSY is not an exact symmetry of nature. It must be a

broken symmetry. The general set-up for the SSB parameters is given by [11]

$$\begin{aligned}
-\mathcal{L}_{\rm soft} &= (m^2_{\tilde{\mathcal{Q}}})^j_i \tilde{\mathcal{Q}}^{\dagger i}\tilde{\mathcal{Q}}_j + (m^2_{\tilde{\mathcal{U}}})^i_j \tilde{\mathcal{U}}^*_i \tilde{\mathcal{U}}^j + (m^2_{\tilde{\mathcal{D}}})^i_j \tilde{\mathcal{D}}^*_i \tilde{\mathcal{D}}^j \\
&+(m^2_{\tilde{\mathcal{L}}})^j_i \tilde{\mathcal{L}}^{\dagger i}\tilde{\mathcal{L}}_j + (m^2_{\tilde{\mathcal{E}}})^i_j \tilde{\mathcal{E}}^*_i \tilde{\mathcal{E}}^j \\
&+m^2_{H_1}\mathcal{H}_1^\dagger \mathcal{H}_1 + m^2_{H_2}\mathcal{H}_2^\dagger \mathcal{H}_2 + (B\mu \mathcal{H}_1\mathcal{H}_2 + \text{h.c.}) \\
&+((\bar{A}^d)_{ij}\mathcal{H}_1 \tilde{\mathcal{D}}^*_i \tilde{\mathcal{Q}}_j + (\bar{A}^u)_{ij}\mathcal{H}_2 \tilde{\mathcal{U}}^*_i \tilde{\mathcal{Q}}_j + (\bar{A}^e)_{ij}\mathcal{H}_1 \tilde{\mathcal{E}}^*_i \tilde{\mathcal{E}}_j \\
&+\frac{1}{2}M_1 \tilde{B}^0_L \tilde{B}^0_L + \frac{1}{2}M_2 \tilde{W}^a_L \tilde{W}^a_L + \frac{1}{2}M_3 \tilde{G}^a \tilde{G}^a + \text{h.c.}).
\end{aligned} \tag{2.17}$$

Here we have used calligraphic capital letters for the sfermion fields in the interaction basis with generation indices,

$$\begin{aligned}
\tilde{\mathcal{U}}_{1,2,3} &= \tilde{u}_R, \tilde{c}_R, \tilde{t}_R; \quad \tilde{\mathcal{D}}_{1,2,3} = \tilde{d}_R, \tilde{s}_R, \tilde{b}_R; \quad \tilde{\mathcal{Q}}_{1,2,3} = (\tilde{u}_L\, \tilde{d}_L)^T, (\tilde{c}_L\, \tilde{s}_L)^T, (\tilde{t}_L\, \tilde{b}_L)^T \\
\tilde{\mathcal{E}}_{1,2,3} &= \tilde{e}_R, \tilde{\mu}_R, \tilde{\tau}_R; \quad \tilde{\mathcal{L}}_{1,2,3} = (\tilde{\nu}_{eL}\, \tilde{e}_L)^T, (\tilde{\nu}_{\mu L}\, \tilde{\mu}_L)^T, (\tilde{\nu}_{\tau L}\, \tilde{\tau}_L)^T
\end{aligned} \tag{2.18}$$

and all the gauge indices have been omitted. Here $m^2_{\tilde{Q}}$ and $m^2_{\tilde{L}}$ are 3×3 matrices in family space (with i, j being the generation indeces) for the soft masses of the left handed squark $\tilde{\mathcal{Q}}$ and slepton $\tilde{\mathcal{L}}$ $SU(2)$ doublets, respectively. $m^2_{\tilde{U}}$, $m^2_{\tilde{D}}$ and $m^2_{\tilde{E}}$ contain the soft masses for right handed up-type squark $\tilde{\mathcal{U}}$, down-type squarks $\tilde{\mathcal{D}}$ and charged slepton $\tilde{\mathcal{E}}$ $SU(2)$ singlets, respectively. $\bar{A}^u$, $\bar{A}^d$ and $\bar{A}^e$ are the 3×3 matrices for the trilinear couplings for up-type squarks, down-type squarks and charged slepton, respectively. m_{H_1} and m_{H_2} contain the soft masses of the Higgs sector. In the last line M_1, M_2 and M_3 define the bino, wino and gluino mass terms, respectively.

It is noteworthy that the terms in Eq. (2.16) conserve lepton and baryon numbers, which is neither required by gauge invariance nor by renormalization. One can add the terms of the form

$$\epsilon_{ab}[\lambda_{ijk}\hat{L}^a_i \hat{L}^b_j \hat{E}^c_k + \lambda'_{ijk}\hat{L}^a_i \hat{Q}^b_j \hat{D}^c_k + \lambda''_{ijk}\hat{U}^c_i \hat{D}^c_j \hat{D}^c_k] \tag{2.19}$$

to Eq. (2.16) where λ_{ijk}, λ'_{ijk} and λ''_{ijk} are the R-parity violating couplings. However these terms violate either lepton or baryon number by one unit, and presence of these terms have dangerous impact on matter i.e. these terms lead to fast proton decay, which is in contradiction to experimental observations. So in order to avoid this situation we have to introduce ad-hoc symmetry, known as R-parity, defined as [38, 39]

$$R_p = (-1)^{3(B-L)+2s} \tag{2.20}$$

where B represents baryon number, L the lepton number and s the intrinsic spin of the particle. Invariance of Lagrangian under R-parity implies -1 phase for sparticle and $+1$ for SM particles. Under this condition the L and B number violating processes are prohibited, this prevents the proton from decaying rapidly.

Though R-parity is introduced by hand just to safe proton decay, but it has large impact on particle physics phenomenology. The conservation of R-parity demands that the sparticles are always produced in pairs. e.g. the LSP must be stable and is assumed

as the excellent candidate for DM. To detect a LSP, collider experiments search for missing transverse energy that would arise if one of these particles were created during a collision process and escaped undetected. For example, at the LHC, the major SUSY production processes are gluinos $\tilde{g}$ and squarks $\tilde{q}$ e.g., $p + p \to \tilde{g} + \tilde{q}$. These then decay into lighter SUSY particles. The final states involve two lightest neutralinos $\tilde{\chi}_1^0$ (giving rise to missing transverse energy E_T^{miss}), quarks (jets) and leptons. The signal is thus E_T^{miss}+ jets +leptons, which should be observable at the LHC detectors.

2.3.1 The scalar fermion sector

The squarks and charged sleptons mass term (sneutrinos being treated differently) of the MSSM Lagrangian is given by

$$\mathcal{L}_{m_{\tilde{f}}} = -\frac{1}{2}\left(\tilde{f}_L^\dagger, \tilde{f}_R^\dagger\right) \mathbf{M}_{\tilde{\mathbf{f}}} \begin{pmatrix} \tilde{f}_L \\ \tilde{f}_R \end{pmatrix} , \tag{2.21}$$

where

$$\mathbf{M}_{\tilde{\mathbf{f}}} = \begin{pmatrix} M_{\tilde{f}}^2 + M_Z^2 \cos 2\beta (I_3^f - Q_f s_{\text{w}}^2) + m_f^2 & m_f X_f \\ m_f X_f & M_{\tilde{f}'}^2 + M_Z^2 \cos 2\beta Q_f s_{\text{w}}^2 + m_f^2 \end{pmatrix} , \tag{2.22}$$

with $X_f = A_f - \mu\{\cot\beta; \tan\beta\}$ and $\tan\beta = v_2/v_1$, the ratio of the VEV's of the two Higgs doublets, corresponds to d-type squarks and charged sleptons whereas $\cot\beta$ corresponds to u-type squarks. The SSB term $M_{\tilde{f}'}$ represents right handed squarks and right handed charged sleptons. Sneutrino mass term is given by

$$M_{\tilde{\nu}}^2 = m_{\tilde{L}}^2 + \left(\frac{1}{2} M_Z^2 \cos 2\beta\right) \tag{2.23}$$

In order to diagonalize the sfermion mass matrix and to determine the physical mass eigenstates the following rotation has to be performed:

$$\begin{pmatrix} \tilde{f}_1 \\ \tilde{f}_2 \end{pmatrix} = \begin{pmatrix} \cos\theta_{\tilde{f}} & \sin\theta_{\tilde{f}} \\ -\sin\theta_{\tilde{f}} & \cos\theta_{\tilde{f}} \end{pmatrix} \begin{pmatrix} \tilde{f}_L \\ \tilde{f}_R \end{pmatrix} . \tag{2.24}$$

The mixing angle $\theta_{\tilde{f}}$ is given for $\tan\beta > 1$ by:

$$\cos\theta_{\tilde{f}} = \frac{\sqrt{M_{\tilde{f}}^2 + M_Z^2 \cos 2\beta (I_3^f - Q_f s_{\text{w}}^2) + m_f^2 - m_{\tilde{f}_2}^2}}{\sqrt{m_{\tilde{f}_1}^2 - m_{\tilde{f}_2}^2}} \tag{2.25}$$

$$\sin\theta_{\tilde{f}} = \frac{m_f X_f}{\sqrt{M_{\tilde{f}}^2 + M_Z^2 \cos 2\beta (I_3^f - Q_f s_{\text{w}}^2) + m_f^2 - m_{\tilde{f}_2}^2}\sqrt{m_{\tilde{f}_1}^2 - m_{\tilde{f}_2}^2}} . \tag{2.26}$$

The masses are given by the eigenvalues of the mass matrix:

$$m^2_{\tilde{f}_{1,2}} = m_f^2 + \frac{1}{2}\Big[M^2_{\tilde{f}} + M^2_{\tilde{f}'} + M_Z^2 \cos 2\beta I_3^f \tag{2.27}$$

$$\mp\sqrt{[M^2_{\tilde{f}} - M^2_{\tilde{f}'} + M_Z^2 \cos 2\beta (I_3^f - Q_f s_{\rm w}^2)]^2 + 4m_f^2 |X_f|^2}\ \Big]. \tag{2.28}$$

Since the non-diagonal entry of the mass matrix Eq. (2.22) is proportional to the fermion mass, mixing becomes particularly important for $\tilde{f} = \tilde{t}$, in the case of $\tan\beta \gg 1$ also for $\tilde{f} = \tilde{b}$.

2.3.2 The Higgs sector of the MSSM

The two Higgs doublets form the Higgs potential [40]

$$\begin{aligned} V &= (m_1^2 + |\mu|^2)|\mathcal{H}_1|^2 + (m_2^2 + |\mu|^2)|\mathcal{H}_2|^2 - m_{12}^2(\epsilon_{ab}\mathcal{H}_1^a\mathcal{H}_2^b + \text{h.c.}) \\ &\quad + \frac{1}{8}({g_1}^2 + {g_2}^2)\left[|\mathcal{H}_1|^2 - |\mathcal{H}_2|^2\right]^2 + \frac{1}{2}{g_2}^2|\mathcal{H}_1^\dagger \mathcal{H}_2|^2\ , \end{aligned} \tag{2.29}$$

which contains m_1, m_2, m_{12} as SSB parameters. The doublet fields $\mathcal{H}_1$ and $\mathcal{H}_2$ are decomposed in the following way:

$$\begin{aligned} \mathcal{H}_1 &= \begin{pmatrix} \mathcal{H}_1^0 \\ \mathcal{H}_1^- \end{pmatrix} = \begin{pmatrix} v_1 + \frac{1}{\sqrt{2}}(\phi_1^0 - i\chi_1^0) \\ -\phi_1^- \end{pmatrix} \\ \mathcal{H}_2 &= \begin{pmatrix} \mathcal{H}_2^+ \\ \mathcal{H}_2^0 \end{pmatrix} = \begin{pmatrix} \phi_2^+ \\ v_2 + \frac{1}{\sqrt{2}}(\phi_2^0 + i\chi_2^0) \end{pmatrix}\ . \end{aligned} \tag{2.30}$$

The potential (2.29) can be described with the help of two independent parameters (besides g_1 and g_2): $\tan\beta$ and $M_A^2 = -m_{12}^2(\tan\beta + \cot\beta)$, where M_A is the mass of the $\mathcal{CP}$-odd A boson.

The diagonalization of the bilinear part of the Higgs potential, i.e. the Higgs mass matrices, is performed via the orthogonal transformations

$$\begin{pmatrix} H^0 \\ h^0 \end{pmatrix} = \begin{pmatrix} \cos\alpha & \sin\alpha \\ -\sin\alpha & \cos\alpha \end{pmatrix} \begin{pmatrix} \phi_1^0 \\ \phi_2^0 \end{pmatrix} \tag{2.31}$$

$$\begin{pmatrix} G^0 \\ A^0 \end{pmatrix} = \begin{pmatrix} \cos\beta & \sin\beta \\ -\sin\beta & \cos\beta \end{pmatrix} \begin{pmatrix} \chi_1^0 \\ \chi_2^0 \end{pmatrix} \tag{2.32}$$

$$\begin{pmatrix} G^\pm \\ H^\pm \end{pmatrix} = \begin{pmatrix} \cos\beta & \sin\beta \\ -\sin\beta & \cos\beta \end{pmatrix} \begin{pmatrix} \phi_1^\pm \\ \phi_2^\pm \end{pmatrix}\ . \tag{2.33}$$

The mixing angle α is determined through

$$\tan 2\alpha = \tan 2\beta \, \frac{M_A^2 + M_Z^2}{M_A^2 - M_Z^2}; \qquad -\frac{\pi}{2} < \alpha < 0 \; . \tag{2.34}$$

One gets the following Higgs spectrum:

$$\begin{aligned} \text{2 neutral bosons, } \mathcal{CP} = +1 \quad &: \quad h^0, H^0 \\ \text{1 neutral boson, } \mathcal{CP} = -1 \quad &: \quad A^0 \\ \text{2 charged bosons} \quad &: \quad H^+, H^- \\ \text{3 unphysical Goldstone bosons} \quad &: \quad G^0, G^+, G^- . \end{aligned} \tag{2.35}$$

The masses of the gauge bosons are given in analogy to the SM:

$$M_W^2 = \frac{1}{2} g_2^2 (v_1^2 + v_2^2); \qquad M_Z^2 = \frac{1}{2}(g_1^2 + g_2^2)(v_1^2 + v_2^2); \qquad M_\gamma = 0. \tag{2.36}$$

At tree level the mass matrix of the neutral $\mathcal{CP}$-even Higgs bosons is given in the ϕ_1-ϕ_2-basis in terms of M_Z, M_A, and $\tan\beta$ by

$$\begin{aligned} M_{\text{Higgs}}^{2,\text{tree}} &= \begin{pmatrix} m_{\phi_1}^2 & m_{\phi_1\phi_2}^2 \\ m_{\phi_1\phi_2}^2 & m_{\phi_2}^2 \end{pmatrix} \\ &= \begin{pmatrix} M_A^2 \sin^2\beta + M_Z^2 \cos^2\beta & -(M_A^2 + M_Z^2)\sin\beta\cos\beta \\ -(M_A^2 + M_Z^2)\sin\beta\cos\beta & M_A^2 \cos^2\beta + M_Z^2 \sin^2\beta \end{pmatrix}, \end{aligned} \tag{2.37}$$

which by diagonalization according to Eq. (2.31) yields the tree-level Higgs boson masses

$$M_{\text{Higgs}}^{2,\text{tree}} \xrightarrow{\alpha} \begin{pmatrix} m_{H,\text{tree}}^2 & 0 \\ 0 & m_{h,\text{tree}}^2 \end{pmatrix} . \tag{2.38}$$

The mixing angle α satisfies

$$\tan 2\alpha = \tan 2\beta \frac{M_A^2 + M_Z^2}{M_A^2 - M_Z^2}, \quad -\frac{\pi}{2} < \alpha < 0. \tag{2.39}$$

Since we treat all MSSM parameters as real there is no mixing between $\mathcal{CP}$-even and $\mathcal{CP}$-odd Higgs bosons.

The tree-level results for the neutral $\mathcal{CP}$-even Higgs-boson masses of the MSSM read

$$m_{(H,h),\text{tree}}^2 = \frac{1}{2}\left[M_A^2 + M_Z^2 \pm \sqrt{(M_A^2 + M_Z^2)^2 - 4 M_Z^2 M_A^2 \cos^2 2\beta} \right] . \tag{2.40}$$

This implies an upper bound of $m_{h,\text{tree}} \leq M_Z$ for the light $\mathcal{CP}$-even Higgs-boson mass of the MSSM. The direct prediction of an upper bound for the mass of the light $\mathcal{CP}$-even Higgs-boson mass is one of the most striking phenomenological predictions of the MSSM. The existence of such a bound, which does not occur in the case of the SM Higgs boson, can be related to the fact that the quartic term in the Higgs potential of the MSSM is given in terms of the gauge couplings, while the quartic coupling is a free parameter in the SM.

2.3.3 Charginos

The charginos $\tilde{\chi}_i^+$ $(i = 1, 2)$ are four component Dirac fermions. The mass eigenstates are obtained from the winos $\tilde{W}^\pm$ and the charged higgsinos $\tilde{H}_1^-$, $\tilde{H}_2^+$:

$$\tilde{W}^+ = \begin{pmatrix} -i\lambda^+ \\ i\bar{\lambda}^- \end{pmatrix} \quad ; \quad \tilde{W}^- = \begin{pmatrix} -i\lambda^- \\ i\bar{\lambda}^+ \end{pmatrix} \quad ; \quad \tilde{H}_2^+ = \begin{pmatrix} \psi_{H_2}^+ \\ \bar{\psi}_{H_1}^- \end{pmatrix} \quad ; \quad \tilde{H}_1^- = \begin{pmatrix} \psi_{H_1}^- \\ \bar{\psi}_{H_2}^+ \end{pmatrix} . \tag{2.41}$$

The chargino masses are defined as mass eigenvalues of the diagonalized mass matrix,

$$\mathcal{L}_{\tilde{\chi}^+,\text{mass}} = -\frac{1}{2} \left(\psi^+, \psi^-\right) \begin{pmatrix} 0 & \mathbf{X}^T \\ \mathbf{X} & 0 \end{pmatrix} \begin{pmatrix} \psi^+ \\ \psi^- \end{pmatrix} + \text{h.c.} \ , \tag{2.42}$$

or given in terms of two-component fields

$$\begin{aligned} \psi^+ &= (-i\lambda^+, \psi_{H_2}^+) \\ \psi^- &= (-i\lambda^-, \psi_{H_1}^-) \end{aligned} \ , \tag{2.43}$$

where $\mathbf{X}$ is given by

$$\mathbf{X} = \begin{pmatrix} M_2 & \sqrt{2}\, M_W \, \sin\beta \\ \sqrt{2}\, M_W \, \cos\beta & \mu \end{pmatrix} . \tag{2.44}$$

The physical (two-component) mass eigenstates are obtained via unitary (2×2) matrices $\mathbf{U}$ and $\mathbf{V}$:

$$\begin{aligned} \chi_i^+ &= V_{ij}\, \psi_j^+ \\ \chi_i^- &= U_{ij}\, \psi_j^- \end{aligned} \qquad i, j = 1, 2 \ . \tag{2.45}$$

This results in a four-component Dirac spinor

$$\tilde{\chi}_i^+ = \begin{pmatrix} \chi_i^+ \\ \bar{\chi}_i^- \end{pmatrix} \qquad i = 1, 2 \ , \tag{2.46}$$

where $\mathbf{U}$ and $\mathbf{V}$ are given by

$$\mathbf{U} = \mathbf{O}_- \qquad ; \qquad \mathbf{V} = \begin{cases} \mathbf{O}_+ & \det \mathbf{X} > 0 \\ \sigma_3\, \mathbf{O}_+ & \det \mathbf{X} < 0 \end{cases} \tag{2.47}$$

with

$$\mathbf{O}_\pm = \begin{pmatrix} \cos\phi_\pm & \sin\phi_\pm \\ -\sin\phi_\pm & \cos\phi_\pm \end{pmatrix} \; ; \tag{2.48}$$

$\cos\phi_\pm$ and $\sin\phi_\pm$ are given by ($\epsilon = \mathrm{sgn}[\det \mathbf{X}]$)

$$\begin{aligned} \tan\phi_+ &= \frac{\sqrt{2}\, M_W(\sin\beta m_{\tilde{\chi}_1^+} + \epsilon\, \cos\beta m_{\tilde{\chi}_2^+})}{(M_2\, m_{\tilde{\chi}_1^+} + \epsilon\, \mu\, m_{\tilde{\chi}_2^+})} \\ \tan\phi_- &= \frac{-\mu\, m_{\tilde{\chi}_1^+} - \epsilon\, M_2\, m_{\tilde{\chi}_2^+}}{\sqrt{2}\, M_W(\sin\beta m_{\tilde{\chi}_1^+} + \epsilon\, \cos\beta m_{\tilde{\chi}_2^+})} \; . \end{aligned} \tag{2.49}$$

(If $\phi_+ < 0$ it has to be replaced by $\phi_+ + \pi$.) $m_{\tilde{\chi}_1^+}$ and $m_{\tilde{\chi}_2^+}$ are the eigenvalues of the diagonalized matrix

$$\begin{aligned} \mathbf{M}^2_{\mathrm{diag},\tilde{\chi}^+} &= \mathbf{V}\,\mathbf{X}^\dagger\,\mathbf{X}\,\mathbf{V}^{-1} \;=\; \mathbf{U}^*\,\mathbf{X}\,\mathbf{X}^\dagger\,(\mathbf{U}^*)^{-1} \\ \mathbf{M}_{\mathrm{diag},\tilde{\chi}^+} &= \mathbf{U}^*\,\mathbf{X}\,\mathbf{V}^{-1} \;=\; \begin{pmatrix} m_{\tilde{\chi}_1^+} & 0 \\ 0 & m_{\tilde{\chi}_2^+} \end{pmatrix} . \end{aligned} \tag{2.50}$$

They are given by

$$\begin{aligned} m^2_{\tilde{\chi}^+_{1,2}} \;=\; \frac{1}{2}\Big\{ & M_2^2 + \mu^2 + 2M_W^2 \mp \Big[(M_2^2 - \mu^2)^2 \\ & + 4M_W^4 \cos^2 2\beta + 4M_W^2(M_2^2 + \mu^2 + 2\,\mu\, M_2\, \sin 2\beta)\Big]^{\frac{1}{2}} \Big\} \; . \end{aligned} \tag{2.51}$$

2.3.4 Neutralinos

Neutralinos $\tilde{\chi}_i^0$ ($i = 1, 2, 3, 4$) are four-component Majorana fermions. They are the mass eigenstates of the photino, $\tilde{\gamma}$, the zino, $\tilde{Z}$, and the neutral higgsinos, $\tilde{H}_1^0$ and $\tilde{H}_2^0$, with

$$\tilde{\gamma} = \begin{pmatrix} -i\lambda_\gamma \\ i\bar{\lambda}_\gamma \end{pmatrix} \quad ; \quad \tilde{Z} = \begin{pmatrix} -i\lambda_Z \\ i\bar{\lambda}_Z \end{pmatrix} \quad ; \quad \tilde{H}_1^0 = \begin{pmatrix} \psi^0_{H_1} \\ \bar{\psi}^0_{H_1} \end{pmatrix} \quad ; \quad \tilde{H}_2^0 = \begin{pmatrix} \psi^0_{H_2} \\ \bar{\psi}^0_{H_2} \end{pmatrix} \; . \tag{2.52}$$

Analogously to the SM, the photino and zino are mixed states from the bino, $\tilde{B}$, and the wino, $\tilde{W}$,

$$\tilde{B} = \begin{pmatrix} -i\lambda' \\ i\bar{\lambda}' \end{pmatrix} \qquad ; \qquad \tilde{W}^3 = \begin{pmatrix} -i\lambda^3 \\ i\bar{\lambda}^3 \end{pmatrix} \; , \tag{2.53}$$

with

$$\begin{aligned} \tilde{\gamma} &= \tilde{W}^3\, s_\mathrm{w} + \tilde{B}\, c_\mathrm{w} \\ \tilde{Z} &= \tilde{W}^3\, c_\mathrm{w} - \tilde{B}\, s_\mathrm{w} \; . \end{aligned} \tag{2.54}$$

The mass term in the Lagrange density is given by

$$\mathcal{L}_{\tilde{\chi}^0,\text{mass}} = -\frac{1}{2}(\psi^0)^T \, \mathbf{Y} \, \psi^0 + \text{h.c.} \; , \tag{2.55}$$

with the two-component fermion fields

$$(\psi^0)^T = (-i\lambda', -i\lambda^3, \psi^0_{H_1}, \psi^0_{H_2}) \; . \tag{2.56}$$

The mass matrix $\mathbf{Y}$ is given by

$$\mathbf{Y} = \begin{pmatrix} M_1 & 0 & -M_Z s_\text{w} \cos\beta & M_Z s_\text{w} \sin\beta \\ 0 & M_2 & M_Z c_\text{w} \cos\beta & -M_Z c_\text{w} \sin\beta \\ -M_Z s_\text{w} \cos\beta & M_Z c_\text{w} \cos\beta & 0 & -\mu \\ M_Z s_\text{w} \sin\beta & -M_Z c_\text{w} \sin\beta & -\mu & 0 \end{pmatrix} \; . \tag{2.57}$$

The physical neutralino mass eigenstates are obtained with the unitary transformation matrix $\mathbf{N}$:

$$\chi^0_i = N_{ij} \, \psi^0_j \qquad i,j = 1,\ldots,4, \tag{2.58}$$

resulting in the four-component spinor (representing the mass eigenstate)

$$\tilde{\chi}^0_i = \begin{pmatrix} \chi^0_i \\ \\ \bar{\chi}^0_i \end{pmatrix} \qquad i = 1,\ldots,4 \; . \tag{2.59}$$

The diagonal mass matrix is then given by

$$\mathbf{M}_{\text{diag},\tilde{\chi}^0} = \mathbf{N}^* \, \mathbf{Y} \, \mathbf{N}^{-1} \; . \tag{2.60}$$

2.3.5 Gluinos

The gluino, $\tilde{g}$, is the spin 1/2 superpartner (Majorana fermion) of the gluon. According to the 8 generators of $SU(3)_C$ (colour octet), there are 8 gluinos, all having the same Majorana mass

$$m_{\tilde{g}} = |M_3| \; . \tag{2.61}$$

In SUSY GUTs M_1, M_2 and M_3 are not independent but connected via

$$m_{\tilde{g}} = M_3 = \frac{g_3^2}{g_2^2} \, M_2 \; = \; \frac{\alpha_s}{\alpha_\text{em}} \, s^2_\text{w} \, M_2, \;\; M_1 = \frac{5}{3} \frac{s^2_\text{w}}{c^2_\text{w}} \, M_2 \; . \tag{2.62}$$

2.3.6 Scalar fermion sector with flavor mixing

In Sect. 1.7 we saw how quarks are rotated from the EW interaction eigenstate basis to the mass eigenstate basis. Since squarks belong to the same supermultiplet, they need to be rotated parallel to the quarks. The rotation is performed via same matrix i.e.

the CKM matrix and the relavent terms in the SSB Lagrangian given in Eq. (2.17) get rotated from the interaction eigenstate basis to what is known as the Super-CKM basis

$$\begin{aligned}\mathcal{L}_{\rm soft} &= -\tilde{U}^*_{Ri} m^2_{\tilde{U}_R ij} \tilde{U}_{Rj} - \tilde{D}^*_{Ri} m^2_{\tilde{D}_R ij} \tilde{D}_{Rj} - \tilde{U}^*_{Li} m^2_{\tilde{U}_L ij} \tilde{U}_{Lj} - \tilde{D}^*_{Li} m^2_{\tilde{D}_L ij} \tilde{D}_{Lj} \\ &\quad -\tilde{U}_{Li} \mathcal{A}^u_{ij} \tilde{U}^*_{Rj} \mathcal{H}^0_2 - \tilde{D}_{Li} (V_{\rm CKM})_{ki} \mathcal{A}^u_{kj} \tilde{U}^*_{Rj} \mathcal{H}^+_2 - \tilde{U}_{Li} (V^*_{\rm CKM})_{ik} \mathcal{A}^d_{kj} \tilde{D}^*_{Rj} \mathcal{H}^-_1 \\ &\quad +\tilde{D}_{Li} \mathcal{A}^d_{ij} \tilde{D}^*_{Rj} \mathcal{H}^0_1 + \text{h.c.}, \end{aligned} \tag{2.63}$$

where $\tilde{U}_{L,R}$ with $U = u, c, t$ represents up-type squarks, $\tilde{D}_{L,R}$ with $D = d, s, b$ represents down-type squarks in Super-CKM basis. The soft masses $m_{\tilde{U}_L}$, $m_{\tilde{U}_R}$, $m_{\tilde{D}_L}$, $m_{\tilde{D}_R}$ and trilinear couplings $\mathcal{A}^q$ with $q = u, d$ in Super-CKM basis are related to the EW interaction eigenstate basis by

$$\begin{aligned} \mathcal{A}^q &= V^q_L \bar{A}^q V^{q\dagger}_R, \quad m^2_{\tilde{U}_R} = V^u_R m^2_{\tilde{U}} V^{u\dagger}_R, \\ m^2_{\tilde{D}_R} &= V^d_R m^2_{\tilde{D}} V^{d\dagger}_R, \quad m^2_{\tilde{U}_L} = V^u_L m^2_{\tilde{Q}} V^{u\dagger}_L, \\ m^2_{\tilde{D}_L} &= V^d_L m^2_{\tilde{Q}} V^{d\dagger}_L. \end{aligned} \tag{2.64}$$

In the Super-CKM basis, not only squarks with different flavor can mix among themselves but we will have left-right mixing also. This will results in 6×6 mass matrices for up-type and down-type squarks. The same arguments hold for the sleptons but in this case flavor mixing will be induced by the PMNS matrix of the neutrino sector and transmitted by the (tiny) neutrino Yukawa couplings. Thus we will have 6×6 mass matrix for the charged sleptons in the so called Super-PMNS basis, however for the sneutrinos we have a 3×3 mass matrix, since within the MSSM even with type I seesaw (to be defined below), we have only three EW interaction eigenstates, $\tilde{\nu}_L$ with $\nu = \nu_e, \nu_\mu, \nu_\tau$ (right handed neutrinos decouple below their respective mass scale).

The non-diagonal entries in this 6×6 general matrix for sfermions can be described in terms of a set of dimensionless parameters δ^{FAB}_{ij} ($F = Q, U, D, L, E; A, B = L, R$; $i, j = 1, 2, 3$, $i \neq j$) where F identifies the sfermion type, L, R refer to the "left-" and "right-handed" SUSY partners of the corresponding fermionic degrees of freedom, and i, j indices run over the three generations. (Non-zero values for the δ^{FAB}_{ij} are generated via the processes discussed in the introduction.)

One usually writes the 6×6 non-diagonal mass matrices, $\mathcal{M}^2_{\tilde{u}}$ and $\mathcal{M}^2_{\tilde{d}}$ being ordered respectively as $(\tilde{u}_L, \tilde{c}_L, \tilde{t}_L, \tilde{u}_R, \tilde{c}_R, \tilde{t}_R)$, $(\tilde{d}_L, \tilde{s}_L, \tilde{b}_L, \tilde{d}_R, \tilde{s}_R, \tilde{b}_R)$ in the Super-CKM basis, $\mathcal{M}^2_{\tilde{l}}$ being ordered as $(\tilde{e}_L, \tilde{\mu}_L, \tilde{\tau}_L, \tilde{e}_R, \tilde{\mu}_R, \tilde{\tau}_R)$ in the Super-PMNS basis and write them in terms of left- and right-handed blocks $M^2_{\tilde{q}\,AB}$, $M^2_{\tilde{l}\,AB}$ ($q = u, d$, $A, B = L, R$), which are non-diagonal 3×3 matrices,

$$\mathcal{M}^2_{\tilde{q}} = \begin{pmatrix} M^2_{\tilde{q}\,LL} & M^2_{\tilde{q}\,LR} \\ M^{2\,\dagger}_{\tilde{q}\,LR} & M^2_{\tilde{q}\,RR} \end{pmatrix}, \qquad \tilde{q} = \tilde{u}, \tilde{d}\ , \tag{2.65}$$

where:

$$
\begin{aligned}
M^2_{\tilde{u}\,LL\,ij} =& m^2_{\tilde{U}_L\,ij} + \left(m^2_{u_i} + (T^u_3 - Q_u s^2_{\rm w}) M^2_Z \cos 2\beta\right) \delta_{ij}, \\
M^2_{\tilde{u}\,RR\,ij} =& m^2_{\tilde{U}_R\,ij} + \left(m^2_{u_i} + Q_u s^2_{\rm w} M^2_Z \cos 2\beta\right) \delta_{ij}, \\
M^2_{\tilde{u}\,LR\,ij} =& \left\langle \mathcal{H}^0_2 \right\rangle \mathcal{A}^u_{ij} - m_{u_i} \mu \cot\beta\, \delta_{ij}, , \\
M^2_{\tilde{d}\,LL\,ij} =& m^2_{\tilde{D}_L\,ij} + \left(m^2_{d_i} + (T^d_3 - Q_d s^2_{\rm w}) M^2_Z \cos 2\beta\right) \delta_{ij}, \\
M^2_{\tilde{d}\,RR\,ij} =& m^2_{\tilde{D}_R\,ij} + \left(m^2_{d_i} + Q_d s^2_{\rm w} M^2_Z \cos 2\beta\right) \delta_{ij}, \\
M^2_{\tilde{d}\,LR\,ij} =& \left\langle \mathcal{H}^0_1 \right\rangle \mathcal{A}^d_{ij} - m_{d_i} \mu \tan\beta\, \delta_{ij} \ ,
\end{aligned}
\tag{2.66}
$$

and

$$
\mathcal{M}^2_{\tilde{l}} = \begin{pmatrix} M^2_{\tilde{l}\,LL} & M^2_{\tilde{l}\,LR} \\ M^{2\,\dagger}_{\tilde{l}\,LR} & M^2_{\tilde{l}\,RR} \end{pmatrix}, \tag{2.67}
$$

where:

$$
\begin{aligned}
M^2_{\tilde{l}\,LL\,ij} =& m^2_{\tilde{L}\,ij} + \left(m^2_{l_i} + (-\frac{1}{2} + s^2_{\rm w}) M^2_Z \cos 2\beta\right) \delta_{ij}, \\
M^2_{\tilde{l}\,RR\,ij} =& m^2_{\tilde{E}\,ij} + \left(m^2_{l_i} - s^2_{\rm w} M^2_Z \cos 2\beta\right) \delta_{ij}, \\
M^2_{\tilde{l}\,LR\,ij} =& \left\langle \mathcal{H}^0_1 \right\rangle \mathcal{A}^e_{ij} - m_{l_i} \mu \tan\beta\, \delta_{ij},
\end{aligned}
\tag{2.68}
$$

with, $i, j = 1, 2, 3$, $Q_u = 2/3$, $Q_d = -1/3$, $T^u_3 = 1/2$ and $T^d_3 = -1/2$. $(m_{u_1}, m_{u_2}, m_{u_3}) = (m_u, m_c, m_t)$, $(m_{d_1}, m_{d_2}, m_{d_3}) = (m_d, m_s, m_b)$ are the quark masses and $(m_{l_1}, m_{l_2}, m_{l_3}) = (m_e, m_\mu, m_\tau)$ are the lepton masses.

It should be noted that the non-diagonality in flavor comes exclusively from the SSB parameters, that could be non-vanishing for $i \neq j$, namely: the masses $m^2_{\tilde{U}_L\,ij}$, $m^2_{\tilde{U}_R\,ij}$, $m^2_{\tilde{D}_L\,ij}$, $m^2_{\tilde{D}_R\,ij}$, $m_{\tilde{L}\,ij}$, $m_{\tilde{E}\,ij}$ and the trilinear couplings, $\mathcal{A}^f_{ij}$.

In the sneutrino sector there is, correspondingly, a one-block 3×3 mass matrix, that is referred to the $(\tilde{\nu}_{eL}, \tilde{\nu}_{\mu L}, \tilde{\nu}_{\tau L})$ Super-PMNS basis:

$$
\mathcal{M}^2_{\tilde{\nu}} = \left(\ M^2_{\tilde{\nu}\,LL} \ \right), \tag{2.69}
$$

where:

$$
M^2_{\tilde{\nu}\,LL\,ij} = m^2_{\tilde{L}\,ij} + \left(\frac{1}{2} M^2_Z \cos 2\beta\right) \delta_{ij}, \tag{2.70}
$$

It is important to note that due to $SU(2)_{\rm L}$ gauge invariance the same soft masses $m_{\tilde{Q}\,ij}$ enter in both up-type and down-type squarks mass matrices similarly $m_{\tilde{L}\,ij}$ enter in both the slepton and sneutrino LL mass matrices. The SSB parameters for the up-type squarks differ from corresponding ones for down-type squarks by a rotation with CKM matrix. The same would hold for sleptons i.e. the soft SUSY-breaking parameters of the sneutrinos would differ from the corresponding ones for charged sleptons by a rotation with the PMNS matrix. However, taking the neutrino masses and oscillations

into account in the SM leads to LFV effects that are extremely small. For instance, in $\mu \to e\gamma$ they are of $\mathcal{O}(10^{-47})$ in case of Dirac neutrinos with mass around 1 eV and maximal mixing [41–43], and of $\mathcal{O}(10^{-40})$ in case of Majorana neutrinos [41, 43]. Consequently we do not expect large effects from the inclusion of neutrino mass effects here and neglect a rotation with the PMNS matrix. The sfermion mass matrices in terms of the δ_{ij}^{FAB} are given as

$$m^2_{\tilde{U}_L} = \begin{pmatrix} m^2_{\tilde{Q}_1} & \delta^{QLL}_{12} m_{\tilde{Q}_1} m_{\tilde{Q}_2} & \delta^{QLL}_{13} m_{\tilde{Q}_1} m_{\tilde{Q}_3} \\ \delta^{QLL}_{21} m_{\tilde{Q}_2} m_{\tilde{Q}_1} & m^2_{\tilde{Q}_2} & \delta^{QLL}_{23} m_{\tilde{Q}_2} m_{\tilde{Q}_3} \\ \delta^{QLL}_{31} m_{\tilde{Q}_3} m_{\tilde{Q}_1} & \delta^{QLL}_{32} m_{\tilde{Q}_3} m_{\tilde{Q}_2} & m^2_{\tilde{Q}_3} \end{pmatrix} , \tag{2.71}$$

$$m^2_{\tilde{D}_L} = V^\dagger_{\rm CKM}\, m^2_{\tilde{U}_L}\, V_{\rm CKM} , \tag{2.72}$$

$$m^2_{\tilde{U}_R} = \begin{pmatrix} m^2_{\tilde{U}_1} & \delta^{URR}_{12} m_{\tilde{U}_1} m_{\tilde{U}_2} & \delta^{URR}_{13} m_{\tilde{U}_1} m_{\tilde{U}_3} \\ \delta^{URR}_{21} m_{\tilde{U}_2} m_{\tilde{U}_1} & m^2_{\tilde{U}_2} & \delta^{URR}_{23} m_{\tilde{U}_2} m_{\tilde{U}_3} \\ \delta^{URR}_{31} m_{\tilde{U}_3} m_{\tilde{U}_1} & \delta^{URR}_{32} m_{\tilde{U}_3} m_{\tilde{U}_2} & m^2_{\tilde{U}_3} \end{pmatrix} , \tag{2.73}$$

$$m^2_{\tilde{D}_R} = \begin{pmatrix} m^2_{\tilde{D}_1} & \delta^{DRR}_{12} m_{\tilde{D}_1} m_{\tilde{D}_2} & \delta^{DRR}_{13} m_{\tilde{D}_1} m_{\tilde{D}_3} \\ \delta^{DRR}_{21} m_{\tilde{D}_2} m_{\tilde{D}_1} & m^2_{\tilde{D}_2} & \delta^{DRR}_{23} m_{\tilde{D}_2} m_{\tilde{D}_3} \\ \delta^{DRR}_{31} m_{\tilde{D}_3} m_{\tilde{D}_1} & \delta^{DRR}_{32} m_{\tilde{D}_3} m_{\tilde{D}_2} & m^2_{\tilde{D}_3} \end{pmatrix} , \tag{2.74}$$

$$v_2 \mathcal{A}^u = \begin{pmatrix} m_u A_u & \delta^{ULR}_{12} m_{\tilde{Q}_1} m_{\tilde{U}_2} & \delta^{ULR}_{13} m_{\tilde{Q}_1} m_{\tilde{U}_3} \\ \delta^{ULR}_{21} m_{\tilde{Q}_2} m_{\tilde{U}_1} & m_c A_c & \delta^{ULR}_{23} m_{\tilde{Q}_2} m_{\tilde{U}_3} \\ \delta^{ULR}_{31} m_{\tilde{Q}_3} m_{\tilde{U}_1} & \delta^{ULR}_{32} m_{\tilde{Q}_3} m_{\tilde{U}_2} & m_t A_t \end{pmatrix} , \tag{2.75}$$

$$v_1 \mathcal{A}^d = \begin{pmatrix} m_d A_d & \delta^{DLR}_{12} m_{\tilde{Q}_1} m_{\tilde{D}_2} & \delta^{DLR}_{13} m_{\tilde{Q}_1} m_{\tilde{D}_3} \\ \delta^{DLR}_{21} m_{\tilde{Q}_2} m_{\tilde{D}_1} & m_s A_s & \delta^{DLR}_{23} m_{\tilde{Q}_2} m_{\tilde{D}_3} \\ \delta^{DLR}_{31} m_{\tilde{Q}_3} m_{\tilde{D}_1} & \delta^{DLR}_{32} m_{\tilde{Q}_3} m_{\tilde{D}_2} & m_b A_b \end{pmatrix} . \tag{2.76}$$

$$m^2_{\tilde{L}} = \begin{pmatrix} m^2_{\tilde{L}_1} & \delta^{LLL}_{12} m_{\tilde{L}_1} m_{\tilde{L}_2} & \delta^{LLL}_{13} m_{\tilde{L}_1} m_{\tilde{L}_3} \\ \delta^{LLL}_{21} m_{\tilde{L}_2} m_{\tilde{L}_1} & m^2_{\tilde{L}_2} & \delta^{LLL}_{23} m_{\tilde{L}_2} m_{\tilde{L}_3} \\ \delta^{LLL}_{31} m_{\tilde{L}_3} m_{\tilde{L}_1} & \delta^{LLL}_{32} m_{\tilde{L}_3} m_{\tilde{L}_2} & m^2_{\tilde{L}_3} \end{pmatrix} \tag{2.77}$$

$$v_1 \mathcal{A}^e = \begin{pmatrix} m_e A_e & \delta^{ELR}_{12} m_{\tilde{L}_1} m_{\tilde{E}_2} & \delta^{ELR}_{13} m_{\tilde{L}_1} m_{\tilde{E}_3} \\ \delta^{ELR}_{21} m_{\tilde{L}_2} m_{\tilde{E}_1} & m_\mu A_\mu & \delta^{ELR}_{23} m_{\tilde{L}_2} m_{\tilde{E}_3} \\ \delta^{ELR}_{31} m_{\tilde{L}_3} m_{\tilde{E}_1} & \delta^{ELR}_{32} m_{\tilde{L}_3} m_{\tilde{E}_2} & m_\tau A_\tau \end{pmatrix} \tag{2.78}$$

$$m^2_{\tilde{E}} = \begin{pmatrix} m^2_{\tilde{E}_1} & \delta^{ERR}_{12} m_{\tilde{E}_1} m_{\tilde{E}_2} & \delta^{ERR}_{13} m_{\tilde{E}_1} m_{\tilde{E}_3} \\ \delta^{ERR}_{21} m_{\tilde{E}_2} m_{\tilde{E}_1} & m^2_{\tilde{E}_2} & \delta^{ERR}_{23} m_{\tilde{E}_2} m_{\tilde{E}_3} \\ \delta^{ERR}_{31} m_{\tilde{E}_3} m_{\tilde{E}_1} & \delta^{ERR}_{32} m_{\tilde{E}_3} m_{\tilde{E}_2} & m^2_{\tilde{E}_3} \end{pmatrix} \tag{2.79}$$

In this thesis, for simplicity, we are assuming that all δ^{FAB}_{ij} parameters are real, therefore, hermiticity of $\mathcal{M}^2_{\tilde{q}}$, $\mathcal{M}^2_{\tilde{l}}$ and $\mathcal{M}^2_{\tilde{\nu}}$ implies $\delta^{FAB}_{ij} = \delta^{FBA}_{ji}$.

The next step is to rotate the squark states from the Super-CKM basis, $\tilde{q}_{L,R}$, to the physical basis. If we set the order in the Super-CKM basis as above, $(\tilde{u}_L, \tilde{c}_L, \tilde{t}_L, \tilde{u}_R, \tilde{c}_R, \tilde{t}_R)$ and $(\tilde{d}_L, \tilde{s}_L, \tilde{b}_L, \tilde{d}_R, \tilde{s}_R, \tilde{b}_R)$, and in the physical basis as $\tilde{u}_{1,..6}$ and $\tilde{d}_{1,..6}$, respectively, these last rotations are given by two 6×6 matrices, $R^{\tilde{u}}$ and $R^{\tilde{d}}$,

$$\begin{pmatrix} \tilde{u}_1 \\ \tilde{u}_2 \\ \tilde{u}_3 \\ \tilde{u}_4 \\ \tilde{u}_5 \\ \tilde{u}_6 \end{pmatrix} = R^{\tilde{u}} \begin{pmatrix} \tilde{u}_L \\ \tilde{c}_L \\ \tilde{t}_L \\ \tilde{u}_R \\ \tilde{c}_R \\ \tilde{t}_R \end{pmatrix}, \quad \begin{pmatrix} \tilde{d}_1 \\ \tilde{d}_2 \\ \tilde{d}_3 \\ \tilde{d}_4 \\ \tilde{d}_5 \\ \tilde{d}_6 \end{pmatrix} = R^{\tilde{d}} \begin{pmatrix} \tilde{d}_L \\ \tilde{s}_L \\ \tilde{b}_L \\ \tilde{d}_R \\ \tilde{s}_R \\ \tilde{b}_R \end{pmatrix}, \tag{2.80}$$

yielding the diagonal mass-squared matrices for squarks as follows,

$$\mathrm{diag}\{m^2_{\tilde{u}_1}, m^2_{\tilde{u}_2}, m^2_{\tilde{u}_3}, m^2_{\tilde{u}_4}, m^2_{\tilde{u}_5}, m^2_{\tilde{u}_6}\} = R^{\tilde{u}}\, \mathcal{M}^2_{\tilde{u}}\, R^{\tilde{u}\dagger}, \tag{2.81}$$

$$\mathrm{diag}\{m^2_{\tilde{d}_1}, m^2_{\tilde{d}_2}, m^2_{\tilde{d}_3}, m^2_{\tilde{d}_4}, m^2_{\tilde{d}_5}, m^2_{\tilde{d}_6}\} = R^{\tilde{d}}\, \mathcal{M}^2_{\tilde{d}}\, R^{\tilde{d}\dagger}. \tag{2.82}$$

Similarly we need to rotate the sleptons and sneutrinos from the Super-PMNS basis to the physical mass eigenstate basis,

$$\begin{pmatrix} \tilde{l}_1 \\ \tilde{l}_2 \\ \tilde{l}_3 \\ \tilde{l}_4 \\ \tilde{l}_5 \\ \tilde{l}_6 \end{pmatrix} = R^{\tilde{l}} \begin{pmatrix} \tilde{e}_L \\ \tilde{\mu}_L \\ \tilde{\tau}_L \\ \tilde{e}_R \\ \tilde{\mu}_R \\ \tilde{\tau}_R \end{pmatrix}, \quad \begin{pmatrix} \tilde{\nu}_1 \\ \tilde{\nu}_2 \\ \tilde{\nu}_3 \end{pmatrix} = R^{\tilde{\nu}} \begin{pmatrix} \tilde{\nu}_{eL} \\ \tilde{\nu}_{\mu L} \\ \tilde{\nu}_{\tau L} \end{pmatrix}, \tag{2.83}$$

with $R^{\tilde{l}}$ and $R^{\tilde{\nu}}$ being the respective 6×6 and 3×3 unitary rotating matrices that yield the diagonal mass-squared matrices as follows,

$$\mathrm{diag}\{m^2_{\tilde{l}_1}, m^2_{\tilde{l}_2}, m^2_{\tilde{l}_3}, m^2_{\tilde{l}_4}, m^2_{\tilde{l}_5}, m^2_{\tilde{l}_6}\} = R^{\tilde{l}}\, \mathcal{M}^2_{\tilde{l}}\, R^{\tilde{l}\dagger}, \tag{2.84}$$

$$\mathrm{diag}\{m^2_{\tilde{\nu}_1}, m^2_{\tilde{\nu}_2}, m^2_{\tilde{\nu}_3}\} = R^{\tilde{\nu}}\, \mathcal{M}^2_{\tilde{\nu}}\, R^{\tilde{\nu}\dagger}. \tag{2.85}$$

2.4 Minimal Flavor Violation

The SM has been very successfully tested by low-energy flavor observables both from the kaon and B_d sectors. In particular, the two B factories have established that B_d flavor and $\mathcal{CP}$-violating processes are well described by the SM up to an accuracy of the $\sim 10\%$ level [17]. This immediately implies a tension between the solution of the hierarchy problem, calling for a New Physics (NP) scale at or below the TeV scale, and the explanation of the Flavor Physics data require a multi-TeV NP scale, if the new flavor-violating couplings are of generic size.

An elegant way to simultaneously solve the above problems is provided by the MFV hypothesis [15, 16], where flavor and $\mathcal{CP}$-violation in quark sector is assumed to entirely originate from the CKM matrix, even in theories beyond the SM. For example in the MSSM the off-diagonality in the sfermion mass matrix reflects the misalignment (in flavor space) between fermions and sfermions mass matrices, that cannot be diagonalized simultaneously. This misalignment can be produced from various origins. For instance, off-diagonal sfermion mass matrix entries can be generated by RGE running. Going from a high energy scale, where no flavor violation is assumed, down to the EW scale, such entries can be generated due to presence of non diagonal Yukawa matrices in RGE's. For instance, in the CMSSM (see Ref. [18] and references therein), the RGE effects on non-diagonal sfermion SSB parameters are affected only by non-diagonal elements on the Yukawa couplings and the trilinear terms which are taken as proportional to the Yukawas at the GUT scale. We choose the following form of the Yukawa matrices (working in the Super-CKM basis [44]),

$$Y^d = \mathrm{diag}(y_d, y_s, y_b), \quad Y^u = V_{\mathrm{CKM}}^{\dagger}\mathrm{diag}(y_u, y_c, y_t)\ . \tag{2.86}$$

Hence, all flavor violation in the quark and squark sector is generated by the RGE's and controlled by the CKM matrix, i.e. the Yukawa couplings have a strong impact on the size of the induced off-diagonal entries in the squark mass matrices.

The situation is somewhat different in the slepton sector where neutrinos are strictly massless (in the SM and the MSSM). Consequently, there is no slepton mixing, which would induce LFV in the charged sector, allowing not yet observed processes like $l_i \to l_j\gamma$ $(i > j;\ l_{3,2,1} = \tau, \mu, e)$ [45]. However in the neutral sector, we have strong experimental evidence that shows that the neutrinos are massive and mix among themselves [6]. In order to incorporate this, a seesaw mechanism (to be defined below) is used to generate neutrino masses, and the PMNS matrix plays the role of the CKM matrix in the lepton sector. Extending the MFV hypothesis for leptons [46] we can assume that the flavor mixing in the lepton and slepton sector is induced and controlled by the seesaw mechanism.

2.5 The Constrained MSSM

Within the CMSSM the SSB parameters are assumed to be universal at the Grand Unification scale $M_{\rm GUT} \sim 2 \times 10^{16}$ GeV,

$$\begin{gathered}(m_Q^2)_{ij} = (m_U^2)_{ij} = (m_D^2)_{ij} = (m_L^2)_{ij} = (m_E^2)_{ij} = m_0^2\ \delta_{ij}, \\ m_{H_1}^2 = m_{H_2}^2 = m_0^2, \\ m_{\tilde{g}} \ = \ m_{\tilde{W}} \ = \ m_{\tilde{B}} \ = \ m_{1/2}, \\ (\bar{A}^u)_{ij} = A_0 e^{i\phi_A}(Y^u)_{ij}, \quad (\bar{A}^d)_{ij} = A_0 e^{i\phi_A}(Y^d)_{ij}, \quad (\bar{A}^e)_{ij} = A_0 e^{i\phi_A}(Y^e)_{ij}.\end{gathered} \tag{2.87}$$

There is a common mass (square) for all the scalars, m_0^2, a single gaugino mass, $m_{1/2}$, and all the trilinear SSB terms are directly proportional to the corresponding Yukawa couplings in the superpotential with a proportionality constant $A_0 e^{i\phi_A}$, containing a potential non-trivial complex phase.

With the use of the RGE of the MSSM, one can obtain the SUSY spectrum at the EW scale. All the SUSY masses and mixings are then given as a function of m_0^2, $m_{1/2}$, A_0, and $\tan\beta$. We require radiative symmetry breaking to fix $|\mu|$ and $|B\mu|$ [47, 48] with the tree–level Higgs potential.

By definition, this model fulfills the MFV hypothesis, since the only flavor violating terms stem from the CKM matrix. The important point is that, even in a model with universal SSB terms at some high energy scale as the CMSSM, some off-diagonality in the squark mass matrices appears at the EW scale. Working in the basis where the squarks are rotated parallel to the quarks i.e. the Super-CKM basis, the squark mass matrices are not flavor diagonal at the EW scale. This is due to the fact that at $M_{\rm GUT}$ there exist two non-trivial flavor structures, namely the two Yukawa matrices for the up and down quarks, which are not simultaneously diagonalizable. This implies that through RGE evolution some flavor mixing leaks into the sfermion mass matrices. In a general SUSY model the presence of new flavor structures in the SSB terms would generate large flavor mixing in the sfermion mass matrices. However, in the CMSSM, the two Yukawa matrices are the only source of flavor change. As always in the Super-CKM basis, any off-diagonal entry in the sfermion mass matrices at the EW scale will be necessarily proportional to a product of Yukawa couplings. This will play a crucial role in the analysis in chapter 6.

2.6 Seesaw extensions of the MSSM

As already mentioned in the introduction, the neutrino masses can be generated through dimension 5 operator. There are many possible ways to form a dimension-5 gauge singlet term at low energy through the tree-level exchange of a heavy particle at the high energy: (i) each L_L-ϕ pair forms a fermion singlet, (ii) each of the L_L-L_L and ϕ-ϕ pair forms a scalar triplet, (iii) each L_L-ϕ pair forms a fermion triplet, and (iv) each of the L_L-L_L and ϕ-ϕ pair forms a scalar singlet. Case (i) can arise from the tree-level exchange of a right handed fermion singlet and this corresponds to the Type-I seesaw mechanism [7]. Case

(ii) arises when the heavy particle is a Higgs triplet giving rise to the Type-II seesaw mechanism [49,50]. For case (iii) the exchanged particle should be a right-handed fermion triplet, which corresponds to the Type-III seesaw mechanism [51, 52]. The last scenario gives terms only of the form $\overline{\nu_L^C} e_L$, which cannot generate a neutrino mass. We describe Type-I seesaw mechanisms in Sect. 2.6.1 in detail.

2.6.1 Supersymmetric Type-I seesaw model

In order to provide an explanation for the (small) neutrino masses, the MSSM can be extended by the type-I seesaw mechanism [7]. The superpotential for MSSM-seesaw I can be written as

$$W_{\rm SI} \;=\; W_{\rm MSSM} + Y_\nu^{ij} \epsilon_{\alpha\beta} \hat{H}_2^\alpha \hat{N}_i^c \hat{L}_j^\beta + \frac{1}{2} M_N^{ij} \hat{N}_i^c \hat{N}_j^c, \tag{2.88}$$

where $W_{\rm MSSM}$ is given in Eq. (2.16) and $\hat{N}_i^c$ is the additional superfield that contains the three right-handed neutrinos, ν_{Ri}, and their scalar partners, $\tilde{\nu}_{Ri}$. M_N^{ij} denotes the 3×3 Majorana mass matrix for heavy right handed neutrino. The full set of SSB terms is given by,

$$-\mathcal{L}_{\rm soft,SI} \;=\; -\mathcal{L}_{\rm soft} + (m_{\tilde{\nu}}^2)_j^i \tilde{\nu}_{Ri}^* \tilde{\nu}_R^j + (\frac{1}{2} B_\nu^{ij} M_N^{ij} \tilde{\nu}_{Ri}^* \tilde{\nu}_{Rj}^* + A_\nu^{ij} h_2 \tilde{\nu}_{Ri}^* \tilde{l}_{Lj} + \text{h.c.}), \tag{2.89}$$

with $\mathcal{L}_{\rm soft}$ given by Eq. (2.17), $(m_{\tilde{\nu}}^2)_j^i$, A_ν^{ij} and B_ν^{ij} are the new SSB parameters.

By the seesaw mechanism three of the neutral fields acquire heavy masses and decouple at high energy scale that we will denote as M_N, below this scale the effective theory contains the MSSM plus an operator that provides masses to the neutrinos.

$$W_{\rm EW,SI} = W_{\rm MSSM} + \frac{1}{2} (Y_\nu L H_2)^T M_N^{-1} (Y_\nu L H_2), \tag{2.90}$$

where $W_{\rm EW,SI}$ represent the MSSM seesaw I superpotential at EW scale. This framework naturally explains neutrino oscillations in agreement with experimental data [6]. At the electroweak scale an effective Majorana mass matrix for light neutrinos,

$$m_{\rm eff} = -\frac{1}{2} v_u^2 Y_\nu \cdot M_N^{-1} \cdot Y_\nu^T, \tag{2.91}$$

arises from Dirac neutrino Yukawa Y_ν (that can be assumed of the same order as the charged-lepton and quark Yukawas), and heavy Majorana masses M_N. The smallness of the neutrino masses implies that the scale M_N is very high, $\mathcal{O}(10^{14}$ GeV).

From Eqs. (2.88) and (2.89) we can observe that one can choose a basis such that the Yukawa coupling matrix, Y_{ij}^e, and the mass matrix of the right-handed neutrinos, M_N^{ij}, are diagonalized as Y_δ^e and M_R^δ, respectively. In this case the neutrino Yukawa couplings Y_ν^{ij} are not generally diagonal, giving rise to LFV. Here it is important to note that the lepton-flavor conservation is not a consequence of the SM gauge symmetry, even in the

absence of the right-handed neutrinos. Consequently, slepton mass terms can violate the lepton-flavor conservation in a manner consistent with the gauge symmetry. Thus the scale of LFV can be identified with the EW scale, much lower than the right-handed neutrino scale M_N, leading to potentially observable rates.

In the SM augmented by right-handed neutrinos, the flavor violating processes such as $\mu \to e\gamma$, $\tau \to \mu\gamma$ etc., whose rates are proportional to inverse powers of M_R^δ, would be highly suppressed with such a large M_N scale, and hence are far beyond current experimental bounds. However, in SUSY theories, the neutrino Dirac couplings Y_ν enter in the RGE's of the SSB sneutrino and slepton masses, generating LFV. In the basis where the charged-lepton Yukawa couplings matrix Y^e is diagonal, the soft slepton-mass matrix acquires corrections that contain off-diagonal contributions from the RGE running from $M_{\rm GUT}$ down to the Majorana mass scale M_N, of the following form (in the leading-log approximation) [53]:

$$\begin{aligned}
(m^2_{\tilde{L}})_{ij} &\sim \frac{1}{16\pi^2}(6m_0^2 + 2A_0^2)\left({Y_\nu}^\dagger Y_\nu\right)_{ij} \log\left(\frac{M_{\rm GUT}}{M_N}\right) \\
(m^2_{\tilde{E}})_{ij} &\sim 0 \\
(\bar{A}^e)_{ij} &\sim \frac{3}{8\pi^2} A_0 {Y^e}_i \left({Y_\nu}^\dagger Y_\nu\right)_{ij} \log\left(\frac{M_{\rm GUT}}{M_N}\right)
\end{aligned} \tag{2.92}$$

Consequently, even if the soft scalar masses were universal at the unification scale, quantum corrections between the GUT scale and the seesaw scale M_N would modify this structure via renormalization-group running, which generates off-diagonal contributions [54–59] at M_N in a basis such that Y^e is diagonal. Below this scale, the off-diagonal contributions remain almost unchanged.

Therefore the seesaw mechanism induces non trivial values for slepton δ_{ij}^{FAB} resulting in a prediction for LFV decays $l_i \to l_j\gamma$, $(i > j)$ that can be much larger than the non-SUSY case. These rates depend on the structure of Y_ν at a seesaw scale M_N in a basis where Y^e and M_N are diagonal. By using the approach of Ref. [59] a general form of Y_ν containing all neutrino experimental information can be written as:

$$Y_\nu = \frac{\sqrt{2}}{v_2}\sqrt{M_R^\delta} R \sqrt{m_\nu^\delta} U^\dagger \ , \tag{2.93}$$

where R is a general orthogonal matrix and m_ν^δ denotes the diagonalized neutrino mass matrix. In this basis the matrix U can be identified with the $U_{\rm PMNS}$ matrix obtained as:

$$m_\nu^\delta = U^T m_{\rm eff} U \ . \tag{2.94}$$

In order to find values for the slepton generation mixing parameters we need a specific form of the product $Y_\nu^\dagger Y_\nu$ as shown in Eq. (2.92). The simple consideration of direct hierarchical neutrinos with a common scale for right handed neutrinos provides a representative reference value. In this case using Eq. (2.93) we find

$$Y_\nu^\dagger Y_\nu = \frac{2}{v_u^2} M_R U m_\nu^\delta U^\dagger \ . \tag{2.95}$$

Here M_R is the common mass assigned to the ν_R's. In the conditions considered here, LFV effects are independent of the matrix R.

For the forthcoming numerical analysis the values of the Yukawa couplings etc. have to be set to yield values in agreement with the experimental data for neutrino masses and mixings. In our computation, by considering a normal hierarchy among the neutrino masses, we fix $m_{\nu_3} \sim \sqrt{\Delta m^2_{\rm atm}} \sim 0.05$ eV and require $m_{\nu_2}/m_{\nu_3} = 0.17$, $m_{\nu_2} \sim 100 \cdot m_{\nu_1}$ consistent with the measured values of $\Delta m^2_{\rm sol}$ and $\Delta m^2_{\rm atm}$ [60]. The matrix U is identified with $U_{\rm PMNS}$ with the $\mathcal{CP}$-phases set to zero and neutrino mixing angles set to the center of their experimental values.

One can observe that $m_{\rm eff}$ remains unchanged by consistent changes on the scales of M_N and Y_ν. This is no longer correct for the off-diagonal entries in the slepton mass matrices (parameterized by slepton δ^{FAB}_{ij}). These quantities have quadratic dependence on Y_ν and logarithmic dependence on M_N, see Eq. (2.92). Therefore larger values of M_N imply larger LFV effects. By setting $M_N = 10^{14}$ GeV, the largest values of Y_ν are of about 0.29, this implies an important restriction on the parameters space arising from the BR($\mu \to e\gamma$). An example of models with almost degenerate ν_R can be found in [54]. For our numerical analysis we tested several scenarios and we found that the one defined here is the simplest and also the one with larger LFV prediction.

Chapter 3

Precision Observables

In this chapter we will present the calculational details and experimetal status of the various low energy observables considered in this thesis.

3.1 Higher order corrections to EWPO

EWPO that are known with an accuracy at the per-mille level or better have the potential to allow a discrimination between quantum effects of the SM and SUSY models, see Ref. [14] for a review. Examples are the W-boson mass M_W and the Z-boson observables, such as the effective leptonic weak missxing angle $\sin^2\theta_{\rm eff}$.

The W-boson mass can be evaluated from

$$M_W^2\left(1-\frac{M_W^2}{M_Z^2}\right)=\frac{\pi\alpha}{\sqrt{2}G_\mu}(1+\Delta r) \tag{3.1}$$

where α is the fine-structure constant and G_μ the Fermi constant. This relation arises from comparing the prediction for muon decay with the experimentally precisely known Fermi constant. The one-loop contributions to Δr can be written as

$$\Delta r=\Delta\alpha-\frac{c_{\rm w}^2}{s_{\rm w}^2}\Delta\rho+(\Delta r)_{\rm rem}, \tag{3.2}$$

where $\Delta\alpha$ is the shift in the fine-structure constant due to the light fermions of the SM, $\Delta\alpha\propto\log(M_Z/m_f)$, and $\Delta\rho$ is the leading contribution to the ρ parameter [61] from (certain) fermion and sfermion loops (see below). The remainder part $(\Delta r)_{\rm rem}$ contains in particular the contributions from the Higgs sector. The effective leptonic weak mixing angle at the Z-boson resonance, $\sin^2\theta_{\rm eff}$, is defined through the vector and axial-vector couplings ($g_{\rm V}^\ell$ and $g_{\rm A}^\ell$) of leptons (ℓ) to the Z boson, measured at the Z-boson pole. If this vertex is written as $i\bar{\ell}\gamma^\mu(g_{\rm V}^\ell-g_{\rm A}^\ell\gamma_5)\ell Z_\mu$ then

$$\sin^2\theta_{\rm eff}=\frac{1}{4}\left(1-{\rm Re}\,\frac{g_{\rm V}^\ell}{g_{\rm A}^\ell}\right). \tag{3.3}$$

Loop corrections enter through higher-order contributions to $g_{\rm V}^{\ell}$ and $g_{\rm A}^{\ell}$. Both of these (pseudo-)observables are affected by shifts in the quantity $\Delta\rho$ according to

$$\Delta M_W \approx \frac{M_W}{2}\frac{c_{\rm w}^2}{c_{\rm w}^2 - s_{\rm w}^2}\Delta\rho\,, \quad \Delta \sin^2\theta_{\rm eff} \approx -\frac{c_{\rm w}^2 s_{\rm w}^2}{c_{\rm w}^2 - s_{\rm w}^2}\Delta\rho\,. \tag{3.4}$$

The quantity $\Delta\rho$ is defined by the relation

$$\Delta\rho = \frac{\Sigma_Z^{\rm T}(0)}{M_Z^2} - \frac{\Sigma_W^{\rm T}(0)}{M_W^2} \tag{3.5}$$

with the unrenormalized transverse parts of the Z- and W-boson self-energies at zero momentum, $\Sigma_{Z,W}^{\rm T}(0)$. It represents the leading universal corrections to the EWPO induced by mass splitting between partners in isospin doublets [61]. Consequently, it is sensitive to the mass-splitting effects induced by flavor mixing.

Within the SM the corrections to $\Delta\rho$ stem from the splitting in one $SU(2)$ doublet. Due to the mixing of various scalar fermion states the picture is slightly more involved in the MSSM. In MSSM without flavor violation the well known results for the third generation squark contribution to $\Delta\rho$ (without flavor mixing) can be written as

$$\begin{aligned}\Delta\rho = \frac{3G_\mu}{8\sqrt{2}\pi^2}\big[&- \sin^2\theta_{\tilde t}\cos^2\theta_{\tilde t}F_0(m^2_{\tilde t_1}, m^2_{\tilde t_2}) - \sin^2\theta_{\tilde b}\cos^2\theta_{\tilde b}F_0(m^2_{\tilde b_1}, m^2_{\tilde b_2}) \\ &+ \cos^2\theta_{\tilde t}\cos^2\theta_{\tilde b}F_0(m^2_{\tilde t_1}, m^2_{\tilde b_1}) + \sin^2\theta_{\tilde b}\cos^2\theta_{\tilde t}F_0(m^2_{\tilde t_1}, m^2_{\tilde b_2}) \\ &+ \sin^2\theta_{\tilde t}\cos^2\theta_{\tilde b}F_0(m^2_{\tilde t_2}, m^2_{\tilde b_1}) + \sin^2\theta_{\tilde t}\sin^2\theta_{\tilde b}F_0(m^2_{\tilde t_2}, m^2_{\tilde b_2})\big]\end{aligned} \tag{3.6}$$

with

$$F_0(m_1^2, m_2^2) = m_1^2 + m_2^2 - \frac{2m_1^2 m_2^2}{m_1^2 - m_2^2}\ln\left(\frac{m_1^2}{m_2^2}\right)\,. \tag{3.7}$$

In the absence of intergenerational mixing there are only 2×2 mixing matrices to be taken into account, here parametrized by $\theta_{\tilde t}$ ($\theta_{\tilde b}$) in the scalar top (bottom) case. Here one can see that squarks do not need to be the $SU(2)$ partners to give contribution to $\Delta\rho$. In particular the first two terms of Eq. (3.6) describe contributions from the same type (up type or down type) of scalar quarks. Going from this simple case to the one with generation mixing one finds contribution from all three generations, including two 6×6 mixing matrices (which are difficult to analyze analytically). The two gauge boson

self-energies are then given by (see also Ref. [62]),

$$\begin{aligned}
\Sigma_{ZZ}(0) = \frac{e^2}{288\pi^2 s_{\rm w}^2 c_{\rm w}^2}(&-\sum_{s,t=1}^{6}\sum_{i,j=1}^{3} 2[\frac{1}{8}F_0(m^2_{\tilde{u}_s}, m^2_{\tilde{u}_t}) + \frac{1}{4}(A_0^{\rm fin}(m^2_{\tilde{u}_s}) + A_0^{\rm fin}(m^2_{\tilde{u}_t}))] \\
&\{3R^{\tilde{u}}_{t,j}R^{\tilde{u}^*}_{t,j} - 4s_{\rm w}^2(R^{\tilde{u}}_{t,j}R^{\tilde{u}^*}_{t,j} + R^{\tilde{u}}_{t,3+j}R^{\tilde{u}^*}_{t,3+j})\} \\
&\{3R^{\tilde{u}}_{s,i}R^{\tilde{u}^*}_{s,i} - 4s_{\rm w}^2(R^{\tilde{u}}_{s,i}R^{\tilde{u}^*}_{s,i} + R^{\tilde{u}}_{s,3+i}R^{\tilde{u}^*}_{s,3+i})\} \\
&- \sum_{s,t=1}^{6}\sum_{i,j=1}^{3} 2[\frac{1}{8}F_0(m^2_{\tilde{d}_s}, m^2_{\tilde{d}_t}) + \frac{1}{4}(A_0^{\rm fin}(m^2_{\tilde{d}_s}) + A_0^{\rm fin}(m^2_{\tilde{d}_t}))] \\
&\{3R^{\tilde{d}}_{t,j}R^{\tilde{d}^*}_{t,j} - 2s_{\rm w}^2(R^{\tilde{d}}_{t,j}R^{\tilde{d}^*}_{t,j} + R^{\tilde{d}}_{t,3+j}R^{\tilde{d}^*}_{t,3+j})\} \\
&\{3R^{\tilde{u}}_{s,i}R^{\tilde{u}^*}_{s,i} - 2s_{\rm w}^2(R^{\tilde{d}}_{s,i}R^{\tilde{d}^*}_{s,i} + R^{\tilde{d}}_{s,3+i}R^{\tilde{d}^*}_{s,3+i}\} \\
&+ \sum_{s=1}^{6}\sum_{i=1}^{3} A_0^{\rm fin}(m^2_{\tilde{u}_s})[(3-4s_{\rm w}^2)^2 R^{\tilde{u}}_{s,i}R^{\tilde{u}^*}_{s,i} + 16 s_{\rm w}^4 R^{\tilde{u}}_{s,3+i}R^{\tilde{u}^*}_{s,3+i}] \\
&+ \sum_{s=1}^{6}\sum_{i=1}^{3} A_0^{\rm fin}(m^2_{\tilde{d}_s})[(3-2s_{\rm w}^2)^2 R^{\tilde{d}}_{s,i}R^{\tilde{d}^*}_{s,i} + 4 s_{\rm w}^4 R^{\tilde{d}}_{s,3+i}R^{\tilde{d}^*}_{s,3+i}])
\end{aligned}$$

$$\begin{aligned}
\Sigma_{WW}(0) = \frac{e^2}{32\pi^2 s_{\rm w}^2}(&-\sum_{s,t=1}^{6}\sum_{i,j=1}^{3} 4[\frac{1}{8}F_0(m^2_{\tilde{u}_s}, m^2_{\tilde{d}_t}) + \frac{1}{4}(A_0^{\rm fin}(m^2_{\tilde{u}_s}) + A_0^{\rm fin}(m^2_{\tilde{d}_t}))] \\
&R^{\tilde{u}}_{s,i}R^{\tilde{d}}_{t,j}R^{\tilde{u}^*}_{s,j}R^{\tilde{d}^*}_{t,i} \\
&+ \sum_{s=1}^{6}\sum_{i=1}^{3} A_0^{\rm fin}(m^2_{\tilde{u}_s})R^{\tilde{u}}_{s,i}R^{\tilde{u}^*}_{s,i} + \sum_{s=1}^{6}\sum_{i=1}^{3} A_0^{\rm fin}(m^2_{\tilde{d}_s})R^{\tilde{d}}_{s,i}R^{\tilde{d}^*}_{s,i}
\end{aligned}$$

Here $R^{\tilde{u}}$ and $R^{\tilde{d}}$ are the 6×6 rotation matrices for the up and down-type squarks respectively, see Eq. (2.80). The finite part of the one point integral function is given by

$$A_0^{\rm fin}(m^2) = m^2(1 - \log\frac{m^2}{\mu^2}) \; . \tag{3.8}$$

Here it is important to note that the corrections will come, as in Eq. (3.6), from states connected via $SU(2)$ as well as from "same flavor" contributions stemming from the Z boson self-energy, see Eq. (3.5). Larger splitting between "same flavor" states due to the intergenerational mixing thus leads to the expectation of increasing contributions to $\Delta\rho$ from flavor violation effects.

The effects from flavor violation in the squark entering via $\Delta\rho$ were already evaluated in Ref. [62] and included in `FeynHiggs`. We have calculated the effects of slepton flavor mixing to $\Delta\rho$ via `FeynArts`/`FormCalc` setup and added the results to `FeynHiggs` for our numerical evaluation. The details about the changes made to `FeynArts`, `FormCalc` and `FeynHiggs` will be discussed in Sect. 3.7. In Fig. 3.1 and Fig. 3.2, we show the generic

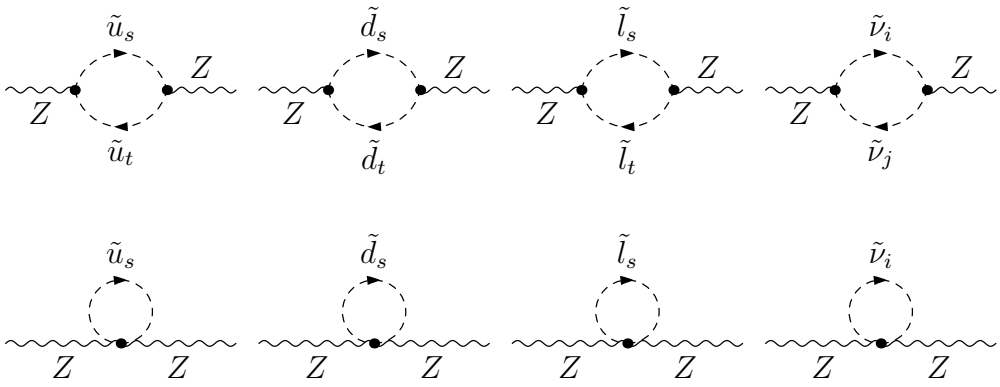

Figure 3.1: Generic Feynman diagrams for Z boson self-energies containing squarks and sleptons in loops. $\tilde{u}_{s,t}$,$\tilde{d}_{s,t}$ and $\tilde{l}_{s,t}$ denote the six mass eigenstates of up-type, down-type and charged sleptons respectively. $\tilde{\nu}_{i,j}$ are the three sneutrinos states $\tilde{\nu}_e$, $\tilde{\nu}_\mu$ and $\tilde{\nu}_\tau$.

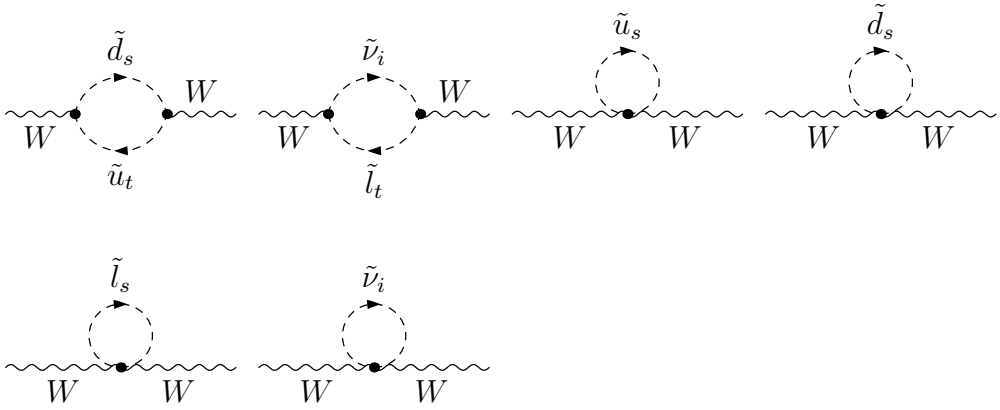

Figure 3.2: Generic Feynman diagrams for W boson self-energies containing squarks and sleptons in loops. $\tilde{u}_{s,t}$,$\tilde{d}_{s,t}$ and $\tilde{l}_{s,t}$ denote the six mass eigenstates of up-type, down-type and charged sleptons respectively. $\tilde{\nu}_{i,j}$ are the three sneutrinos states $\tilde{\nu}_e$, $\tilde{\nu}_\mu$ and $\tilde{\nu}_\tau$.

Feynman diagrams for Z and W boson self energies that enter in the calculation of $\Delta\rho$.

The present experimental uncertainties for the EWPO are [63]

$$\delta M_W^{\rm exp,today} \sim 15 \text{ MeV}, \quad \delta \sin^2\theta_{\rm eff}^{\rm exp,today} \sim 15 \times 10^{-5}\,, \tag{3.9}$$

which will further be reduced [64] to

$$\delta M_W^{\rm exp,future} \sim 4 \text{ MeV}, \quad \delta \sin^2\theta_{\rm eff}^{\rm exp,future} \sim 1.3 \times 10^{-5}\,, \tag{3.10}$$

at the ILC and at the GigaZ option of the ILC, respectively. Even higher precision could be expected from the FCC-ee, see, e.g., Ref. [65].

The prediction of M_W also suffers from various kinds of theoretical uncertainties, parametric and intrinsic. Starting with the parametric uncertainties, an experimental error of 1 GeV on m_t yields a parametric uncertainty on M_W of about 6 MeV, while the parametric uncertainties induced by the current experimental error of the hadronic contribution to the shift in the fine-structure constant, $\Delta\alpha_{\rm had}$, and by the experimental error of M_Z amount to about 2 MeV and 2.5 MeV, respectively. The uncertainty of the M_W prediction caused by the experimental uncertainty of the Higgs mass $\delta M_h^{\rm exp} \lesssim 0.3$ GeV is signifcantly smaller (≈ 0.2 MeV). The intrinsic uncertainties from unknown higher-order corrections in the case of no flavor mixing have been estimated to be around (4.7-9.4) MeV in the MSSM [66, 67] depending on the SUSY mass scale. For our forthcoming numerical analysis, we have added the parameteric uncertainties in quadrature and add the result linearly to the uncertainty from the unknown higher order corrections in the case of no flavor mixing. We assume an additional 10% uncertainty from the flavor mixing contribution to $\Delta\rho^{\rm MSSM}$ and (via Eq. (3.4)) add it linearly to the other uncertainties.

3.2 Higher-order corrections in the Higgs sector

In order to calculate one-loop corrections to the Higgs boson masses, the renormalized Higgs boson self-energies are needed. Here we follow the procedure used in Refs. [68, 69] (and references therein). The parameters appearing in the Higgs potential, see Eq. (2.29), are renormalized as follows:

$$\begin{aligned} M_Z^2 &\to M_Z^2 + \delta M_Z^2, & T_h &\to T_h + \delta T_h, \\ M_W^2 &\to M_W^2 + \delta M_W^2, & T_H &\to T_H + \delta T_H, \\ M^2_{\rm Higgs} &\to M^2_{\rm Higgs} + \delta M^2_{\rm Higgs}, & \tan\beta\ &\to \tan\beta\,(1 + \delta\tan\beta\,). \end{aligned} \tag{3.11}$$

$M^2_{\rm Higgs}$ denotes the tree-level Higgs boson mass matrix given in Eq. (2.37). T_h and T_H are the tree-level tadpoles, i.e. the terms linear in h and H in the Higgs potential.

The field renormalization matrices of both Higgs multiplets can be set up symmetrically,

$$\begin{pmatrix} h \\ H \end{pmatrix} \to \begin{pmatrix} 1 + \frac{1}{2}\delta Z_{hh} & \frac{1}{2}\delta Z_{hH} \\ \frac{1}{2}\delta Z_{hH} & 1 + \frac{1}{2}\delta Z_{HH} \end{pmatrix} \cdot \begin{pmatrix} h \\ H \end{pmatrix} . \tag{3.12}$$

For the mass counter term matrices we use the definitions

$$\delta M^2_{\text{Higgs}} = \begin{pmatrix} \delta m_h^2 & \delta m_{hH}^2 \\ \delta m_{hH}^2 & \delta m_H^2 \end{pmatrix} . \tag{3.13}$$

The renormalized self-energies, $\hat{\Sigma}(p^2)$, can now be expressed through the unrenormalized self-energies, $\Sigma(p^2)$, the field renormalization constants and the mass counter terms. This reads for the $\mathcal{CP}$-even part,

$$\hat{\Sigma}_{hh}(p^2) = \Sigma_{hh}(p^2) + \delta Z_{hh}(p^2 - m^2_{h,\text{tree}}) - \delta m_h^2, \tag{3.14a}$$
$$\hat{\Sigma}_{hH}(p^2) = \Sigma_{hH}(p^2) + \delta Z_{hH}(p^2 - \tfrac{1}{2}(m^2_{h,\text{tree}} + m^2_{H,\text{tree}})) - \delta m_{hH}^2, \tag{3.14b}$$
$$\hat{\Sigma}_{HH}(p^2) = \Sigma_{HH}(p^2) + \delta Z_{HH}(p^2 - m^2_{H,\text{tree}}) - \delta m_H^2 \ . \tag{3.14c}$$

Inserting the renormalization transformation into the Higgs mass terms leads to expressions for their counter terms which consequently depend on the other counter terms introduced in (3.11).

For the $\mathcal{CP}$-even part of the Higgs sectors, these counter terms are:

$$\begin{aligned} \delta m_h^2 = {} & \delta M_A^2 \cos^2(\alpha-\beta) + \delta M_Z^2 \sin^2(\alpha+\beta) \\ & + \tfrac{e}{2M_Z s_\text{w} c_\text{w}}(\delta T_H \cos(\alpha-\beta)\sin^2(\alpha-\beta) + \delta T_h \sin(\alpha-\beta)(1+\cos^2(\alpha-\beta))) \\ & + \delta\tan\!\beta\ \sin\beta\ \cos\beta\,(M_A^2 \sin 2(\alpha-\beta) + M_Z^2 \sin 2(\alpha+\beta)), \end{aligned} \tag{3.15a}$$

$$\begin{aligned} \delta m_{hH}^2 = {} & \tfrac{1}{2}(\delta M_A^2 \sin 2(\alpha-\beta) - \delta M_Z^2 \sin 2(\alpha+\beta)) \\ & + \tfrac{e}{2M_Z s_\text{w} c_\text{w}}(\delta T_H \sin^3(\alpha-\beta) - \delta T_h \cos^3(\alpha-\beta)) \\ & - \delta\tan\!\beta\ \sin\beta\ \cos\beta\,(M_A^2 \cos 2(\alpha-\beta) + M_Z^2 \cos 2(\alpha+\beta)), \end{aligned} \tag{3.15b}$$

$$\begin{aligned} \delta m_H^2 = {} & \delta M_A^2 \sin^2(\alpha-\beta) + \delta M_Z^2 \cos^2(\alpha+\beta) \\ & - \tfrac{e}{2M_Z s_\text{w} c_\text{w}}(\delta T_H \cos(\alpha-\beta)(1+\sin^2(\alpha-\beta)) + \delta T_h \sin(\alpha-\beta)\cos^2(\alpha-\beta)) \\ & - \delta\tan\!\beta\ \sin\beta\ \cos\beta\,(M_A^2 \sin 2(\alpha-\beta) + M_Z^2 \sin 2(\alpha+\beta)) \ . \end{aligned} \tag{3.15c}$$

For the field renormalization we chose to give each Higgs doublet one renormalization constant,

$$\mathcal{H}_1 \to (1 + \tfrac{1}{2}\delta Z_{\mathcal{H}_1})\mathcal{H}_1, \quad \mathcal{H}_2 \to (1 + \tfrac{1}{2}\delta Z_{\mathcal{H}_2})\mathcal{H}_2 \ . \tag{3.16}$$

This leads to the following expressions for the various field renormalization constants in Eq. (3.12):

$$\delta Z_{hh} = \sin^2\!\alpha\, \delta Z_{\mathcal{H}_1} + \cos^2\!\alpha\, \delta Z_{\mathcal{H}_2}, \tag{3.17a}$$
$$\delta Z_{hH} = \sin\alpha\ \cos\alpha\,(\delta Z_{\mathcal{H}_2} - \delta Z_{\mathcal{H}_1}), \tag{3.17b}$$
$$\delta Z_{HH} = \cos^2\!\alpha\, \delta Z_{\mathcal{H}_1} + \sin^2\!\alpha\, \delta Z_{\mathcal{H}_2} \ . \tag{3.17c}$$

The counter term for $\tan\beta$ can be expressed in terms of the vacuum expectation values as

$$\delta\tan\beta = \frac{1}{2}\left(\delta Z_{\mathcal{H}_2} - \delta Z_{\mathcal{H}_1}\right) + \frac{\delta v_2}{v_2} - \frac{\delta v_1}{v_1}\ , \tag{3.18}$$

where the δv_i are the renormalization constants of the v_i:

$$v_1 \to (1+\delta Z_{\mathcal{H}_1})\,(v_1+\delta v_1)\,, \quad v_2 \to (1+\delta Z_{\mathcal{H}_2})\,(v_2+\delta v_2)\ . \tag{3.19}$$

It can be shown that the divergent parts of $\delta v_1/v_1$ and $\delta v_2/v_2$ are equal [69, 70]. Consequently, one can set $\delta v_2/v_2 - \delta v_1/v_1$ to zero.

Similarly for the charged Higgs sector, the renormalized self-energy is expressed in terms of the unrenormalized one and the corresponding counter-terms as:

$$\hat{\Sigma}_{H^-H^+}\left(p^2\right) = \Sigma_{H^-H^+}\left(p^2\right) + \delta Z_{H^-H^+}\left(p^2 - m^2_{H^\pm,\text{tree}}\right) - \delta m^2_{H^\pm}, \tag{3.20}$$

where,

$$\delta m^2_{H^\pm} = \delta M_A^2 + \delta M_W^2 \tag{3.21}$$

and,

$$\delta Z_{H^-H^+} = \sin^2\beta\ \delta Z_{\mathcal{H}_1} + \cos^2\beta\ \delta Z_{\mathcal{H}_2}. \tag{3.22}$$

The renormalization conditions are fixed by an appropriate renormalization scheme. For the mass counter terms on-shell conditions are used, resulting in:

$$\delta M_Z^2 = \mathrm{Re}\,\Sigma_{ZZ}(M_Z^2), \quad \delta M_W^2 = \mathrm{Re}\,\Sigma_{WW}(M_W^2), \quad \delta M_A^2 = \mathrm{Re}\,\Sigma_{AA}(M_A^2). \tag{3.23}$$

For the gauge bosons Σ denotes the transverse part of the self-energy. Since the tadpole coefficients are chosen to vanish in all orders, their counter terms follow from $T_{\{h,H\}} + \delta T_{\{h,H\}} = 0$:

$$\delta T_h = -T_h, \quad \delta T_H = -T_H\ . \tag{3.24}$$

For the remaining renormalization constants for $\delta\tan\beta$, $\delta Z_{\mathcal{H}_1}$ and $\delta Z_{\mathcal{H}_2}$ the most convenient choice is a $\overline{\text{DR}}$ renormalization of $\delta\tan\beta$, $\delta Z_{\mathcal{H}_1}$ and $\delta Z_{\mathcal{H}_2}$,

$$\delta Z_{\mathcal{H}_1} = \delta Z_{\mathcal{H}_1}^{\overline{\text{DR}}} \ = \ -\left[\mathrm{Re}\,\Sigma'_{HH\,|\alpha=0}\right]^{\text{div}}, \tag{3.25a}$$

$$\delta Z_{\mathcal{H}_2} = \delta Z_{\mathcal{H}_2}^{\overline{\text{DR}}} \ = \ -\left[\mathrm{Re}\,\Sigma'_{hh\,|\alpha=0}\right]^{\text{div}}, \tag{3.25b}$$

$$\delta\tan\beta \ = \frac{1}{2}(\delta Z_{\mathcal{H}_2} - \delta Z_{\mathcal{H}_1}) = \delta\tan\beta^{\,\overline{\text{DR}}}\ . \tag{3.25c}$$

The corresponding renormalization scale, $\mu_{\overline{\text{DR}}}$, is set to $\mu_{\overline{\text{DR}}} = m_t$ in all numerical evaluations.

Finally, in the Feynman diagrammatic (FD) approach that we are following here, the higher-order corrected $\mathcal{CP}$-even Higgs boson masses are derived by finding the poles of the (h,H)-propagator matrix. The inverse of this matrix is given by

$$\left(\Delta_{\text{Higgs}}\right)^{-1} = -i\begin{pmatrix} p^2 - m^2_{H,\text{tree}} + \hat{\Sigma}_{HH}(p^2) & \hat{\Sigma}_{hH}(p^2) \\ \hat{\Sigma}_{hH}(p^2) & p^2 - m^2_{h,\text{tree}} + \hat{\Sigma}_{hh}(p^2) \end{pmatrix}\ . \tag{3.26}$$

Determining the poles of the matrix Δ_{Higgs} in Eq. (3.26) is equivalent to solving the equation

$$\left[p^2 - m^2_{h,\text{tree}} + \hat{\Sigma}_{hh}(p^2)\right]\left[p^2 - m^2_{H,\text{tree}} + \hat{\Sigma}_{HH}(p^2)\right] - \left[\hat{\Sigma}_{hH}(p^2)\right]^2 = 0\,. \tag{3.27}$$

Similarly, in the case of the charged Higgs sector, the corrected Higgs mass is derived by the position of the pole in the charged Higgs propagator, which is defined by:

$$p^2 - m^2_{H^\pm,\text{tree}} + \hat{\Sigma}_{H^-H^+}\left(p^2\right) = 0. \tag{3.28}$$

The present experimental uncertainty at the LHC for the mass of light neutral higgs M_h is $\leq$ 300 MeV [4, 5]. This can possibly be reduced by about 50% at the LHC and below the level of $\sim$ 50 MeV at the ILC [71]. Similarly, for the mass of heavy neutral higgs M_H and charged higgs boson $M_{H^\pm}$ an uncertainity at the 1% level could be expected at the LHC [72]. This sets the goal for the theoretical uncertainty, which should be reduced to the same (or higher) level of accuracy.

Higher order corrections to the masses and mixing angles of the Higgs bosons in the MSSM have already been calculated in the literature. For the light and heavy $\mathcal{CP}$-even Higgs boson masses, complete one-loop contributions exist [69, 73–75]. Almost all the dominant contributions at two-loop level are also known [76–90]. For example, with the assumption of vanishing external momenta, the $\mathcal{O}(\alpha_t\alpha_s)$ contributions have been calculated in the Feynman diagrammatic (FD) approach and effective potential (EP) approach and the $\mathcal{O}(\alpha_t^2)$, $\mathcal{O}(\alpha_b\alpha_s)$, $\mathcal{O}(\alpha_t\alpha_b)$ and $\mathcal{O}(\alpha_b^2)$ contributions are calculated in the EP approach. The momentum dependence at two-loop level was evaluated in Refs. [91–94] and in Ref. [95], a nearly full two-loop calculation in EP approach that also include the leading three-loop contributions has been presented. The code `H3m` [96] adds the leading three-loop corrections of $\mathcal{O}(\alpha_t\alpha_s^2)$ to the `FeynHiggs` results. In the very recent work [97], a combination of full one-loop results supplimented with leading and subleading two-loop contributions and a resummation of the leading and subleading logarithmic contributions from scalar-top sector is presented. This combination reduce the theoretical uncertainty from about 3 GeV to about 2 GeV, for scalar-top masses at or below the TeV scale, for the light $\mathcal{CP}$-even Higgs boson mass. Flavor violation effects for the case of squarks in MI approach were calculated in [98, 99]. We have calculated the effects of slepton mixing to the Higgs boson masses in `FeynArts`/`FormCalc` setup and added the result to the `FeynHiggs`. The details about the changes in `FeynArts`, `FormCalc` and `FeynHiggs` can be found in Sect. 3.7. We also calculate the effects of squark mixing in MFV CMSSM and MFV CMSSM-seesaw I. In Fig. 3.3, we show generic Feynman diagrams for Higg self energy while Feynman diagrams for tadpoles are shown in Fig. 3.4.

3.3 *B*-physics observables

In this thesis, we also consider several B-physics observables (BPO): BR($B \to X_s\gamma$), BR($B_s \to \mu^+\mu^-$) and ΔM_{B_s}. Concerning BR($B \to X_s\gamma$) included in the calculation

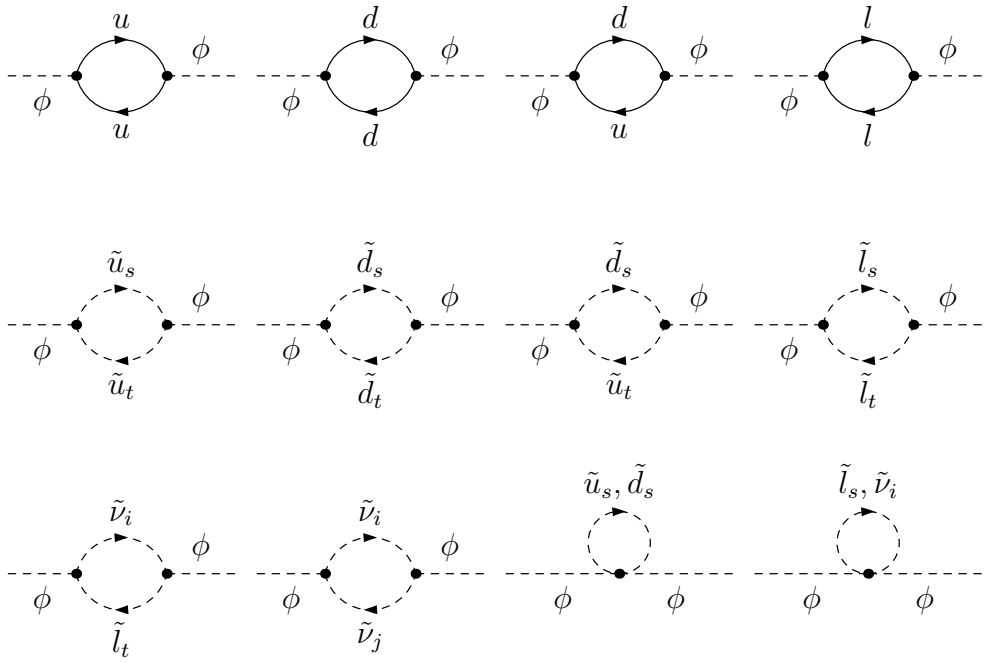

Figure 3.3: Generic Feynman diagrams for the Higgs boson self-energies. ϕ denotes any of the Higgs bosons, h, H, A or $H^{\pm}$; u stand for u, c, t; d stand for d, s, b; l stand for e, μ, τ; $\tilde{u}_{s,t}$, $\tilde{d}_{s,t}$ and $\tilde{l}_{s,t}$ are the six mass eigenstates of up-type, down-type squarks and charged sleptons respectively and $\tilde{\nu}_{i,j}$ are the three sneutrinos states $\tilde{\nu}_e$, $\tilde{\nu}_\mu$ and $\tilde{\nu}_\tau$.

are the most relevant loop contributions to the Wilson coefficients: (i) loops with Higgs bosons (including the resummation of large $\tan\beta$ effects [100]), (ii) loops with charginos and (iii) loops with gluinos. For BR($B_s \to \mu^+\mu^-$) there are three types of relevant one-loop corrections contributing to the relevant Wilson coefficients: (i) Box diagrams, (ii) Z-penguin diagrams and (iii) neutral Higgs boson ϕ-penguin diagrams, where ϕ denotes the three neutral MSSM Higgs bosons, $\phi = h, H, A$ (again large resummed $\tan\beta$ effects have been taken into account). In our numerical evaluation there are included what are known to be the dominant contributions to these three types of diagrams [101]: chargino contributions to box and Z-penguin diagrams and chargino and gluino contributions to ϕ-penguin diagrams. Concerning ΔM_{B_s}, in the MSSM there are in general three types of one-loop diagrams that contribute: (i) Box diagrams, (ii) Z-penguin diagrams and (iii) double Higgs-penguin diagrams (again including the resummation of large $\tan\beta$ enhanced effects). In our numerical evaluation there are included again what are known to be the dominant contributions to these three types of diagrams in scenarios with non-minimal flavor violation (for a review see, for instance, [102]): gluino contributions to box diagrams, chargino contributions to box and Z-penguin diagrams, and chargino and gluino contributions to double ϕ-penguin diagrams. More details about the calculations

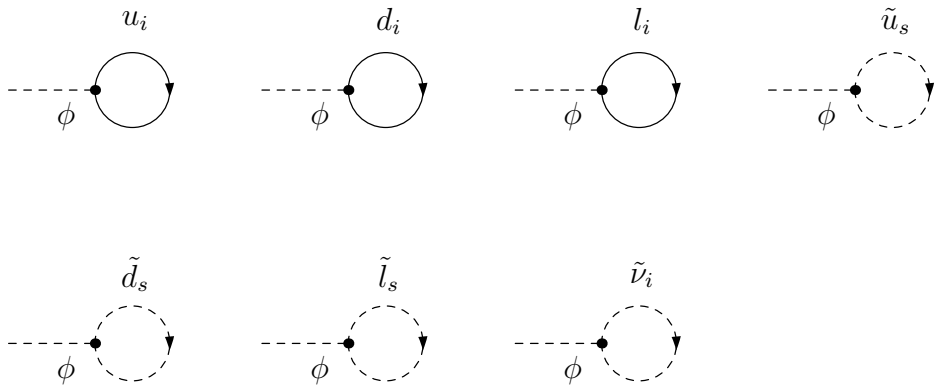

Figure 3.4: Generic Feynman diagrams for the Higgs boson tadpoles. ϕ denotes any of the Higgs bosons, h or H; u stand for u, c, t; d stand for d, s, b; l stand for e, μ, τ; $\tilde{u}_{s,t}$, $\tilde{d}_{s,t}$ and $\tilde{l}_{s,t}$ are the six mass eigenstates of up-type, down-type squarks and charged sleptons respectively and $\tilde{\nu}_{i,j}$ are the three sneutrinos states $\tilde{\nu}_e$, $\tilde{\nu}_\mu$ and $\tilde{\nu}_\tau$.

employed can be found in Refs. [98, 99]. We perform our numerical calculation with the `BPHYSICS` subroutine taken from the `SuFla` code [103] (with some additions and improvements as detailed in Refs. [98, 99]), which has been implemented as a subroutine into (a private version of) `FeynHiggs`. The experimental values used in the numerical analysis[1] and SM prediction of these observables is given in the Tab. 3.1 [105–112].

Observable	Experimental Value	SM Prediction
$\mathrm{BR}(B \to X_s\gamma)$	$3.43 \pm 0.22 \times 10^{-4}$	$3.15 \pm 0.23 \times 10^{-4}$
$\mathrm{BR}(B_s \to \mu^+\mu^-)$	$(3.0)^{+1.0}_{-0.9} \times 10^{-9}$	$3.23 \pm 0.27 \times 10^{-9}$
ΔM_{B_s}	$116.4 \pm 0.5 \times 10^{-10}$ MeV	$(117.1)^{+17.2}_{-16.4} \times 10^{-10}$ MeV

Table 3.1: Experimental values (used in our numerical analysis) of B-physics observables with their SM prediction.

[1] Using the most up-to-date value of $\mathrm{BR}(B_s \to \mu^+\mu^-) = 2.9 \pm 0.7 \times 10^{-9}$ [104] would have had a minor impact on our analysis.

3.4 $h \to \bar{b}s + b\bar{s}$

In SM the branching ratio BR($h \to \bar{b}s + b\bar{s}$) can be at most of $\mathcal{O}(10^{-7})$ [113], too small to have a chance of detection at the LHC. But because of the strong FCNC gluino couplings and the $\tan\beta$-enhancement inherent to the MSSM Yukawa couplings, we may expect several orders of magnitude increase of the branching ratio as compared to the SM result, see Ref. [113, 114] . This decay in the framework of the MSSM has been analyzed in the literature: the SUSY-QCD contributions for this decay were calculated in [113, 114], and the SUSY-EW contributions using the mass insertion approximation were calculated in [115]. Later in [116] the SUSY-EW contributions and their interference effects with the SUSY-QCD contribution were calculated using exact diagonalization of the squark mass matrices. In all these analysis, only LL mixing in the squarks mass matrix was considered, and experimental constraints were imposed only from BR($B \to X_s\gamma$). Most recently in [117] also RR mixing has been included. However mixing of the LR or RL elements of the mass matrix and constraints from other BPO or potential other constraints were not taken into account (except in the most recent analysis in [117]). We (re-)calculate full one-loop contributions from SUSY-QCD as well as SUSY-EW loops with the help of the `FeynArts` [118,119] and `FormCalc` [120] packages. The lengthy analytical results are not shown here. We take into account the experimental constraints not only from BPO but also from the EWPO. In the scalar quark sector we not only consider the LL mixing, but also include the LR-RL and RR mixing for our analysis of BR($h \to \bar{b}s + b\bar{s}$). For our numerical analysis we define

$$\mathrm{BR}(h \to \bar{b}s + b\bar{s}) = \frac{\Gamma(h \to \bar{b}s + b\bar{s})}{\Gamma^{\mathrm{MSSM}}_{h,\mathrm{tot}}} \tag{3.29}$$

where $\Gamma^{\mathrm{MSSM}}_{h,\mathrm{tot}}$ is the total decay width of the light Higgs boson h of the MSSM, as evaluated with `FeynHiggs` [68, 77, 97, 121, 122]. The contributing Feynman diagrams for the decay $h \to \bar{b}s + b\bar{s}$ are shown in Fig. 3.7-3.5. Which BR might be detectable at the LHC or an e^+e^- collider such as the ILC can only be established by means of specific experimental analyses, which, to our knowledge, do not exist yet. However, in the literature it is expected to measure BR's at the level of 10^{-3} at the LHC [113]. In the clean ILC environment in general Higgs boson branching ratios below the level of 10^{-4} can be observed, see e.g. Ref. [123] for a recent review. We will take this as a rough guideline down to which level the decay $h \to \bar{b}s + b\bar{s}$ could be observable. Feynman diagram for SUSY-EW contributions to the decay $h \to \bar{b}s + b\bar{s}$ are shown in Fig. 3.5 and Fig. 3.6, and SUSY-QCD contributions are shown in Fig. 3.7.

3.5 $l_i \to l_j\gamma$

Neutrino oscillation experiments [6] have established the existence of lepton flavor violation. So, as a natural consequence of neutrino oscillations, one would expect flavour mixing in the charged lepton sector as well. This mixing can be manifested in rare decay

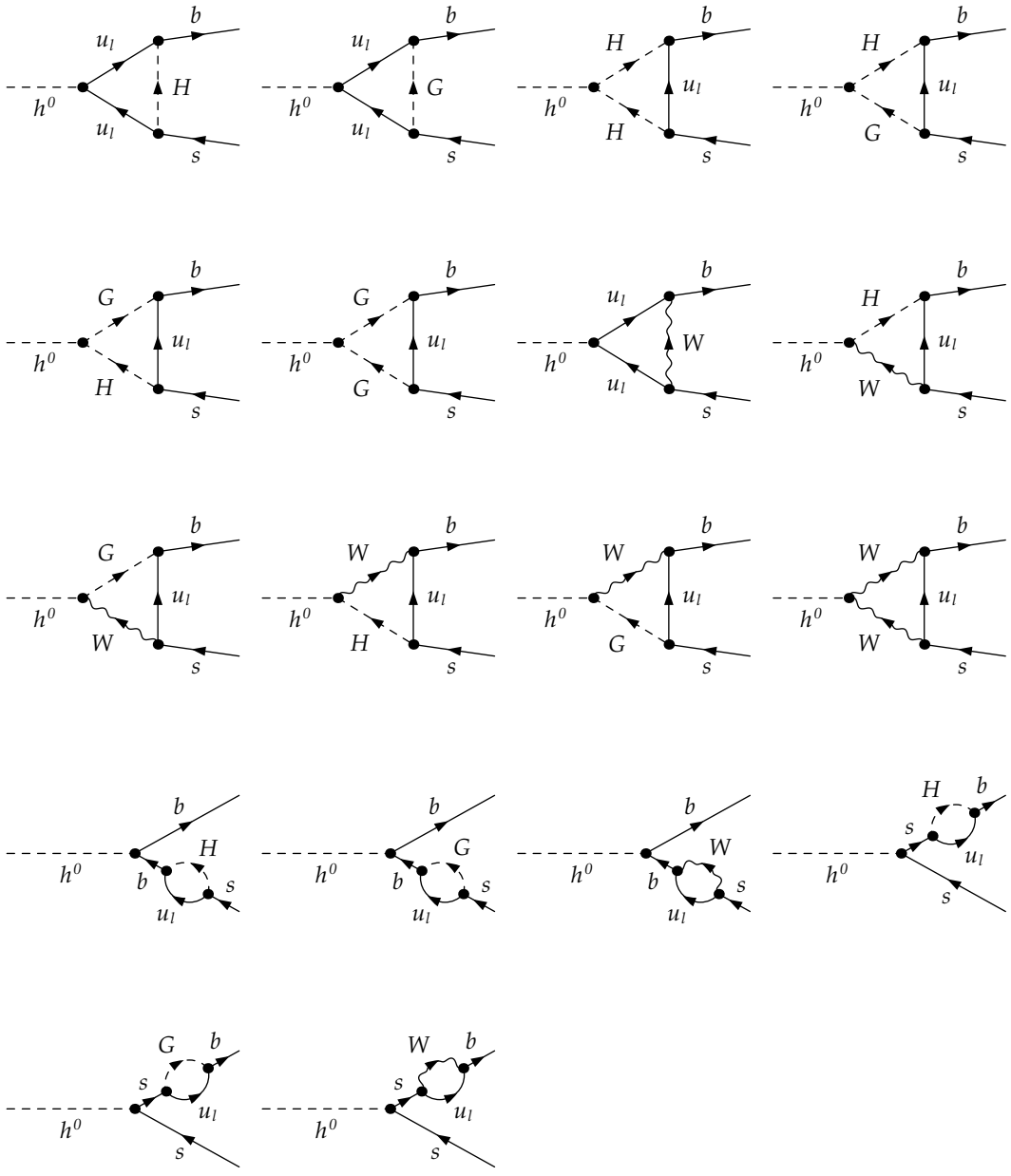

Figure 3.5: Feynman diagrams showing SUSY-EW contributions (except neutralino-chargino) to the decay process $h \to b\bar{s} + \bar{b}s$.

processes such as $\mu \to e\gamma$, $\tau \to e\gamma$, and $\tau \to \mu\gamma$. However, if only the lepton Yukawa couplings carry this information on flavour mixing, as in the SM with massive neutrinos, the expected rates of these processes are extremely tiny [41–43] being proportional to the ratio of masses of neutrinos over the masses of the W bosons. These values are very far from the present experimental upper bounds [124, 125] that can be read from Tab. 3.2. The situation in the MSSM (extended by the seesaw mechanism) is completely different.

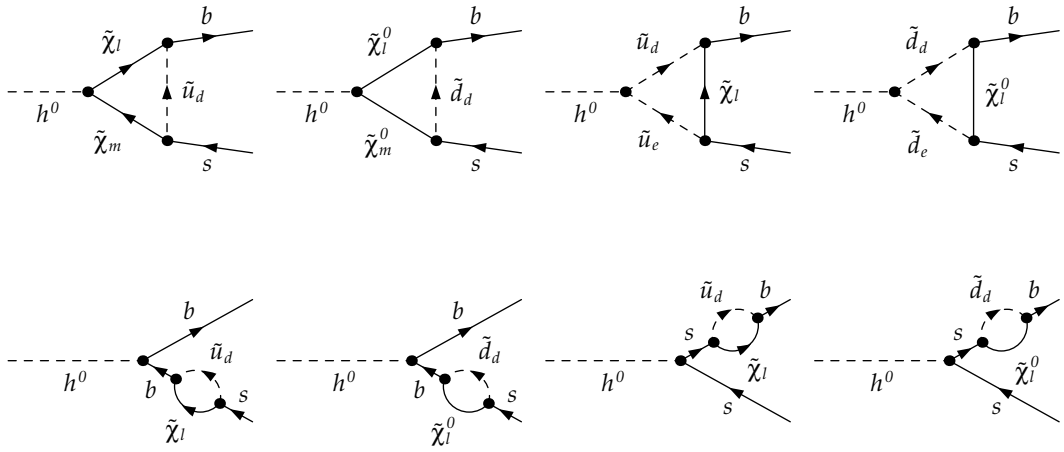

Figure 3.6: Feynman diagrams showing neutralino-chargino contributions to the decay process $h \to b\bar{s} + \bar{b}s$.

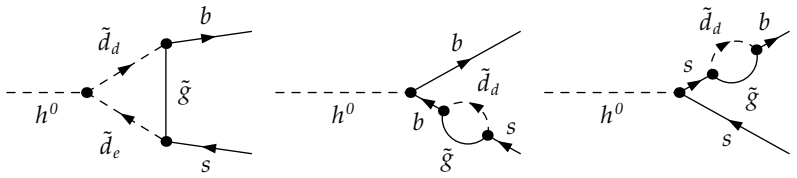

Figure 3.7: Feynman diagrams showing SUSY-QCD contributions to the decay process $h \to b\bar{s} + \bar{b}s$.

Here lepton-slepton misallignment (generated by the presence of seesaw parameters in the RGE's) can dominate the SM contribution by several orders of magnitude. Thus making the study of rare LFV processes very attractive.

We analyze these processes in the framework of CMSSM (extended by Type I seesaw mechanism). MSSM contributions to these decays originate from lepton-slepton-neutralino and lepton-slepton-chargino couplings. The predictions for $\mathrm{BR}(l_i \to l_j\gamma)$ are obtained with `SPheno 3.2.4`. We checked that the use of this code produces results similar to the ones obtained by our private codes used in Ref. [54].

Observable	Experimental value
$\mathrm{BR}(\mu \to e\gamma)$	$< 5.7 \times 10^{-13}$
$\mathrm{BR}(\tau \to e\gamma)$	$< 3.3 \times 10^{-8}$
$\mathrm{BR}(\tau \to \mu\gamma)$	$< 4.4 \times 10^{-8}$

Table 3.2: Present experimental status of LFV processes; their SM prediction is zero.

3.6 $h \to l_i^{\pm} l_j^{\mp}$

Since the discovery of Higgs boson, special effort has been made to determine its properties. The motivation for such an effort resides on understanding the mechanism for EWSB. At present, several aspects of the Higgs boson are to some extent well known, in particular those related with some of its expected "standard" decay modes, namely: WW^*, ZZ^*, $\gamma\gamma$, $b\bar{b}$ and $\tau\bar{\tau}$. Currently, measurements of these decay modes have shown compatibility with the SM expectations, although with large associated uncertainties [126]. Indeed, it is due to these large uncertainties that there is still room for nonstandard decay properties, something that has encouraged such searches at the LHC as well. Searches for invisible Higgs decays have been published in [127, 128]. Recently CMS collaboration using the 2012 dataset taken at $\sqrt{s} = 8$TeV with an integrated luminosity of 19.7 fb^{-1}, has found a 2.5 σ excess in the $h \to \mu\tau$ channel, which translates into BR$(h \to \mu\tau) \approx 0.89^{+40}_{-37}\%$ [129]. However there is no statistically significant excess in the ATLAS results [130].

One needs to find the theoretical framework which can accomodate larger rates for LFVHD to explain CMS excess while still respecting the upper bounds on cLFV's. Efforts in such direction have been done in different contexts, with pioneer works in Refs. [131, 132]. More recenty, Ref. [133] studied the problem in the MSSM, while [134] in the R-parity violating MSSM. These decays have been considered as well in the inverse seesaw model in [135]. Possible effects due to vectorlike leptons have been investigated in [136]. Extended scalar sectors involving several Higgs doublets and flavor symmetries (Yukawa textures) have been examined too [137–140]. Finally, the Type-III Two Higgs Doublet Model has been considered in Refs. [141, 142]. Basically, the bottom line of these analyses is that unless one deals with extra Higgs doublets, LFVHD are below the LHC reach.

In this thesis we calculate the LFVHD in SUSY using FD approach. We study the lepton-slepton misalignment effects to LFVHD, both in the MI approach and in MFV CMSSM-seesaw I. We do not use mass insertion approximation and exact diagonalization of the slepton mass matrix is performed. Feynman diagrams entering our calculation are shown in Fig. 3.8 where first two rows correspond to the decay $h \to e^{\pm}\mu^{\mp}$, middle two rows correspond to $h \to e^{\pm}\tau^{\mp}$ and last two rows correspond to $h \to \mu^{\pm}\tau^{\mp}$. For the analytical calculation we used `FeynArts`/`FormCalc` setup. For this purpose, we implimented LFV Feynman rules for the MSSM in these packages (see Sect. 3.7 for details).

For numerical analysis we define the branching ratios of LFVHD as

$$\mathrm{BR}(h \to l_i^{\pm} l_j^{\mp}) = \frac{\Gamma(h \to l_i^{\pm} l_j^{\mp})}{\Gamma(h \to l_i^{\pm} l_j^{\mp}) + \Gamma_h^{\mathrm{MSSM}}} \tag{3.30}$$

where $i, j = e, \mu, \tau$ and Γ_h^{MSSM} is total decay width of $\mathcal{CP}$-even light Higgs boson h.

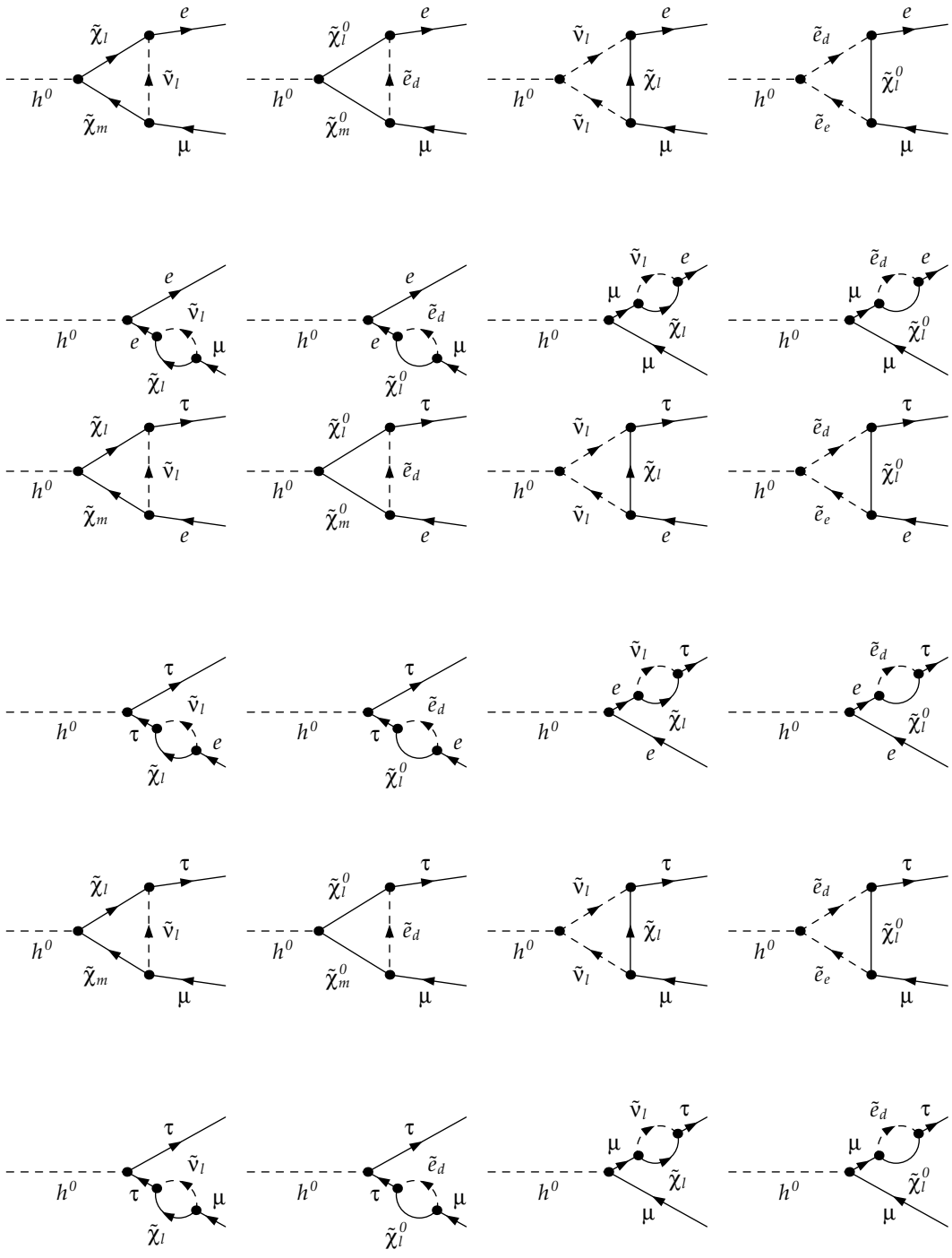

Figure 3.8: Feynman diagrams for LFV decays $h \to l_i^{\pm} l_j^{\mp}$.

3.7 Changes in FeynArts, FormCalc and FeynHiggs

FeynArts [118] and FormCalc [120] provide a high level of automation for perturbative calculations up to one loop. This is particularly important for models with a large particle content such as the MSSM [119]. Here we briefly describe the recent extension of the implementation of the MSSM in these packages to include LFV. Details on the previous inclusion of NMFV can be found in Refs. [118, 143]. This involves firstly the modification of the slepton couplings in the existing FeynArts model file for the MSSM and secondly the corresponding initialization routines for the slepton masses and mixings, i.e. the 6×6 and 3×3 diagonalization of the mass matrices in FormCalc.

3.7.1 FeynArts Model File

FeynArts' add-on model file FV.mod applies algebraic substitutions to the Feynman rules of MSSM.mod to upgrade minimal to non-minimal flavor mixing in the sfermion sector. The original version modified only the squark sector, i.e. NMFV, and needed to be generalized to include LFV. We solved this by allowing the user to choose which sfermion types to introduce non-minimal mixing for through the variable $FV (set before model initialization, of course). For example,

```
$FV = {11, 12, 13, 14};
InsertFields[..., Model -> {MSSM, FV}]
```

sets non-minimal mixing for all four sfermion types, with $11 = \tilde{\nu}$, $12 = \tilde{l}$, $13 = \tilde{u}$, and $14 = \tilde{d}$ as usual in MSSM.mod. For compatibility with the old NMFV-only version, the default is `$FV = {13, 14}`.

FV.mod introduces the following new quantities:

UASf[s_1,s_2,t]	the slepton mixing matrix R, where $s_1, s_2 = 1 \ldots 6$, $t = 1\,(\tilde{\nu}), 2\,(\tilde{l}), 3\,(\tilde{u}), 4\,(\tilde{d})$,
MASf[s,t]	the slepton masses, where $s = 1 \ldots 6$, $t = 1\,(\tilde{\nu}), 2\,(\tilde{l}), 3\,(\tilde{u}), 4\,(\tilde{d})$.

Entries $4 \ldots 6$ are unused for the sneutrino.

3.7.2 Model initialization in FormCalc

The initialization of the generalized slepton-mixing parameters MASf and UASf is already built into FormCalc's regular MSSM model-initialization file model_mssm.F but not turned on by default. It must be enabled by adjusting the FV preprocessor flag in run.F:

```
#define FV 2
```

where 2 is the lowest sfermion type t for which flavor violation is enabled, i.e. $\tilde{l}$.

The flavor-violating parameters δ_{ij}^{FAB} are represented in `FormCalc` by the `deltaSf` matrix:

`double complex deltaSf(`s_1`,`s_2`,`t`)`	the matrix $(\delta_t)_{s_1 s_2}$, where
	$s_1, s_2 = 1 \ldots 6$ ($1 \ldots 3$ for $\tilde{\nu}$),
	$t = 2\,(\tilde{l}), 3\,(\tilde{u}), 4\,(\tilde{d})$.

Since δ is an Hermitian matrix, only the entries above the diagonal are considered. The δ_{ij}^{FAB} are located at the following places in the matrix δ:

$$\left(\begin{array}{ccc|ccc} \cdot & \delta_{12}^{LLL} & \delta_{13}^{LLL} & \cdot & \delta_{12}^{ELR} & \delta_{13}^{ELR} \\ \cdot & \cdot & \delta_{23}^{LLL} & \delta_{12}^{ERL*} & \cdot & \delta_{23}^{ELR} \\ \cdot & \cdot & \cdot & \delta_{13}^{ERL*} & \delta_{23}^{ERL*} & \cdot \\ \hline \cdot & \cdot & \cdot & \cdot & \delta_{12}^{ERR} & \delta_{13}^{ERR} \\ \cdot & \cdot & \cdot & \cdot & \cdot & \delta_{23}^{ERR} \\ \cdot & \cdot & \cdot & \cdot & \cdot & \cdot \end{array}\right)$$

The trilinear couplings A_f acquire non-zero off-diagonal entries in the presence of LFV through the relations

$$m_{f,i}(A_f)_{ij} = (M^2_{\tilde{f},LR})_{ij}\,, \quad i,j = 1 \ldots 3\,, \tag{3.31}$$

see Eq. (2.68). These off-diagonal trilinear couplings (and hence the δ's) appear directly in the Higgs–slepton–slepton couplings, whereas all other effects are mediated through the masses and mixings.

The described changes are contained in the `FeynArts` 3.9 and `FormCalc` 8.4 packages which are publicly available from `www.feynarts.de`.

3.7.3 Inclusion of LFV into `FeynHiggs`

As discussed above, the new corrections to the (renormalized) Higgs-boson self-energies (and thus to the Higgs-boson masses), as well as to $\Delta\rho$ (and thus to M_W and $\sin^2\theta_{\text{eff}}$) have been included in `FeynHiggs` [68, 77, 97, 121, 122].

The corrections are activated by setting one or more of the δ_{ij}^{FAB} to non-zero values. All δ_{ij}^{FAB} that are not set are assumed to be zero. The non-zero value can be set in three ways:

- by including them in the input file, e.g.

  `deltaLLL23  0.1`

  where the general format of the identifier is

  `delta`$FXYij$, F `= L,E,Q,U,D,` XY `= LL,LR,RL,RR,` ij `= 12,23,13`

- by calling the subroutine `FHSetLFV(...)` from your Fortran/C/C++ code.

- by calling the routine `FHSetLFV[...]` from your Mathematica code.

The detailed invocation of `FHSetLFV` is given in the corresponding man page included in the `FeynHiggs` distribution. The LFV corrections are included starting from `FeynHiggs` version 2.10.2, available from `feynhiggs.de`.

Chapter 4

Quark Flavor Mixing Effects in the Model Independent Approach

MFV sceneraios put tight constraints on the possible value of the FCNC couplings, especially for the first and second generation squarks which are sensitive to the data on $K^0 - \bar{K}^0$ and $D^0 - \bar{D}^0$ mixing. However, the third generation is less constrained, since present data on $B^0 - \bar{B}^0$ mixing still leaves some room for FCNCs. This allows some parameter space for the more general scenerios focusing on the mixing between second and third generation (s)quarks. One such example is the neutral higgs decay $h \to \bar{b}s + b\bar{s}$. The SM contribution is highly suppressed for this process but the SUSY-QCD quark-squark-gluino loop contribution can enhance the MSSM contribuion by several orders of magnitude. Also the SUSY-EW one loop contribution from quark-squark-chargino and quark-squark-neutralino loop even though subdominent, can have sizable effects on the BR($h \to \bar{b}s + b\bar{s}$), where in particular the interfrence effects of SUSY-QCD and SUSY-EW loop corrections can be relevant.

This decay in the framework of the MSSM has been analyzed in the literature: the SUSY-QCD contributions for this decay were calculated in [113, 114], and the SUSY-EW contributions using the mass insertion approximation were calculated in [115]. Later in [116] the SUSY-EW contributions and their interference effects with the SUSY-QCD contribution were calculated using exact diagonalization of the squark mass matrices. In all these analysis, only LL mixing in the squarks mass matrix was considered, and experimental constraints were imposed only from BR($B \to X_s\gamma$). Most recently in [117] also RR mixing has been included. However mixing of the LR or RL elements of the mass matrix and constraints from other BPO or potential other constraints were not taken into account (except in the most recent analysis in [117]).

In this chapter we will analyze the decay $h \to \bar{b}s + b\bar{s}$, evaluated at the full one-loop level, by taking into account the experimental constraints not only from BPO but also from the EWPO. In the scalar quark sector we will not only consider the LL mixing, but also include the LR-RL and RR mixing for our analysis of BR($h \to \bar{b}s + b\bar{s}$). We will analyze this decay in the model independent approach where flavor mixing parameters are put in by hand without any emphasis on the origin of this mixing (but respecting the experimental bounds from BPO and EWPO). The results presented in this chapter

were published in [144]. In the next section we enlist the input parameters for our MI analysis.

4.1 Input parameters

Regarding our choice of MSSM parameters for our forthcoming numerical analysis, we have chosen the framework of [145], This framework is well compatible with present data.

In this framework, six specific points in the MSSM parameter space, have been selected. These points are allowed by present data, including recent LHC searches and the measurements of the muon anomalous magnetic moment. In Tab. 4.1 the values of the various MSSM parameters as well as the values of the predicted MSSM mass spectra are summarized. They were evaluated with the program `FeynHiggs` [68, 77, 97, 121, 122]. For simplicity, and to reduce the number of independent MSSM input parameters we have assumed equal soft masses for the sleptons of the first and second generations (similarly for the squarks), equal soft masses for the left and right slepton sectors (similarly for the squarks, where $\tilde{Q}$ denotes the the "left-handed" squark sector, whereas $\tilde{U}$ and $\tilde{D}$ denote the up- and down-type parts of the "right-handed" squark sector) and also equal trilinear couplings for the stop, A_t, and sbottom squarks, A_b. In the slepton sector we just consider the stau trilinear coupling, A_τ. The other trilinear sfermion couplings are set to zero. Regarding the SSB parameters for the gaugino masses, M_i $(i = 1, 2, 3)$, we assume an approximate GUT relation. The pseudoscalar Higgs mass M_A, and the μ parameter are also taken as independent input parameters. In summary, the six points S1, ..., S6 are defined in terms of the following subset of ten input MSSM parameters:

$$\begin{aligned} m_{\tilde{L}_1} &= m_{\tilde{L}_2} \; ; \; m_{\tilde{L}_3} \text{ (with } m_{\tilde{L}_i} = m_{\tilde{E}_i} \; , \; i = 1, 2, 3) \\ m_{\tilde{Q}_1} &= m_{\tilde{Q}_2} \; ; \; m_{\tilde{Q}_3} \text{ (with } m_{\tilde{Q}_i} = m_{\tilde{U}_i} = m_{\tilde{D}_i} \; , \; i = 1, 2, 3) \\ A_t &= A_b \; ; \; A_\tau \\ M_2 &= 2M_1 \, = \, M_3/4 \; ; \; \mu \\ M_A \quad &; \quad \tan\beta \end{aligned} \tag{4.1}$$

The specific values of these ten MSSM parameters in Tab. 4.1, to be used in the forthcoming analysis, are chosen to provide different patterns in the various sparticle masses, but all leading to rather heavy spectra, thus they are naturally in agreement with the absence of SUSY signals at LHC. In particular all points lead to rather heavy squarks and gluinos above 1200 GeV and heavy sleptons above 500 GeV (where the LHC limits would also permit substantially lighter scalar leptons). The values of M_A within the interval $(500, 1500)$ GeV, $\tan\beta$ within the interval $(10, 50)$ and a large A_t within $(1000, 2500)$ GeV are fixed such that a light Higgs boson h within the LHC-favoured range $(123, 127)$ GeV is obtained. It should also be noted that the large chosen values of $M_A \geq 500$ GeV place the Higgs sector of our scenarios in the so called decoupling

	S1	S2	S3	S4	S5	S6
$m_{\tilde{L}_{1,2}}$	500	750	1000	800	500	1500
$m_{\tilde{L}_3}$	500	750	1000	500	500	1500
M_2	500	500	500	500	750	300
A_τ	500	750	1000	500	0	1500
μ	400	400	400	400	800	300
$\tan\beta$	20	30	50	40	10	40
M_A	500	1000	1000	1000	1000	1500
$m_{\tilde{Q}_{1,2}}$	2000	2000	2000	2000	2500	1500
$m_{\tilde{Q}_3}$	2000	2000	2000	500	2500	1500
A_t	2300	2300	2300	1000	2500	1500
$m_{\tilde{l}_1} - m_{\tilde{l}_6}$	489-515	738-765	984-1018	474-802	488-516	1494-1507
$m_{\tilde{\nu}_1} - m_{\tilde{\nu}_3}$	496	747	998	496-797	496	1499
$m_{\tilde{\chi}_1^\pm} - m_{\tilde{\chi}_2^\pm}$	375-531	376-530	377-530	377-530	710-844	247-363
$m_{\tilde{\chi}_1^0} - m_{\tilde{\chi}_4^0}$	244-531	245-531	245-530	245-530	373-844	145-363
M_h	126.6	127.0	127.3	123.1	123.8	125.1
M_H	500	1000	999	1001	1000	1499
M_A	500	1000	1000	1000	1000	1500
$M_{H^\pm}$	507	1003	1003	1005	1003	1502
$m_{\tilde{u}_1} - m_{\tilde{u}_6}$	1909-2100	1909-2100	1908-2100	336-2000	2423-2585	1423-1589
$m_{\tilde{d}_1} - m_{\tilde{d}_6}$	1997-2004	1994-2007	1990-2011	474-2001	2498-2503	1492-1509
$m_{\tilde{g}}$	2000	2000	2000	2000	3000	1200

Table 4.1: Selected points in the MSSM parameter space (upper part) and their corresponding spectra (lower part). All mass parameters and trilinear couplings are given in GeV.

regime [146], where the couplings of h to gauge bosons and fermions are close to the SM Higgs couplings, and the heavy H couples like the pseudoscalar A, and all heavy Higgs bosons are close in mass. Increasing M_A the heavy Higgs bosons tend to decouple from low energy physics and the light h behaves like $H_{\rm SM}$. This type of MSSM Higgs sector

seems to be in good agreement with recent LHC data [147]. We have checked with the code `HiggsBounds` [148] (but not yet taking into account the most recent update [149]) that the Higgs sector is in agreement with the LHC searches (where S3 is right "at the border"). Particularly, the so far absence of gluinos at LHC, forbids too low M_3 and, therefore, given the assumed GUT relation, forbids also a too low M_2. Consequently, the values of M_2 and μ are fixed as to get gaugino masses compatible with present LHC bounds. Finally, we have also required that all our points lead to a prediction of the anomalous magnetic moment of the muon in the MSSM that can fill the present discrepancy between the SM prediction and the experimental value (see [145] for more details).

4.2 Experimental constraints on δ_{ij}^{FAB}

In this section we will present the present experimental constraints on the squark mixing parameters δ_{ij}^{FAB} for the above mentioned MSSM points S1...S6 defined in Tab. 4.1. The experimental constraints from BPO for the same set of parameters that we are using were already calculated in [99] for one $\delta_{ij}^{FAB} \neq 0$, which we reproduce here for completeness in the Tab. 4.2.

We now turn our attention to the constraints from M_W. In Fig. 4.1 we show the M_W as a function of δ_{23}^{QLL}, δ_{23}^{ULR} and δ_{23}^{DLR} in the scenarios S1 ... S6. The area between the orange lines shows the allowed value of M_W with 3σ experimental uncertainty. The corresponding constraints from M_W on δ_{ij}^{FAB}, also taking into account the theoretical uncertainties as described at the end of Sect. 3.1, are shown in Tab. 4.3. No constraints can be found on the δ_{ij}^{RR}, as their contribution to M_W does not reach the MeV level, and consequently we do not show them here. Furtheremore, the constraints for the δ_{23}^{URL} and δ_{23}^{DRL} are similar to those for δ_{23}^{ULR} and δ_{23}^{DLR}, respectively, and not shown here.

On the other hand, the constraints on δ_{23}^{QLL} are modified by the EWPO specially the region (-0.83:-0.78) for the point S5, which was allowed by the BPO, is now excluded. The allowed intervals for the points S1-S3 have also shrunk. However the point S4 was already excluded by BPO, similarly the allowed interval for S6 do not get modified by EWPO. The constraints on δ_{23}^{ULR} and δ_{23}^{DLR} are less restrictive then the ones from BPO except for the point S4 where the region (0.076:0.12) is excluded for δ_{23}^{DLR} by EWPO.

4.3 BR($h \to \bar{b}s + b\bar{s}$)

In order to illustrate the contributions from different diagrams we show in Fig. 4.2 the SUSY-EW, SUSY-QCD and total SUSY contribution to $\Gamma(h \to \bar{b}s + b\bar{s})$ as a function of δ_{23}^{QLL} (upper left), δ_{23}^{DLR} (upper right), δ_{23}^{DRL} (lower left) and δ_{23}^{DRR} (lower right). These four δ_{ij}^{FAB} are the only relevant ones, since we are mainly concerned with the down-type sector, and mixing with the first generation does not play a role.

In order to compare our results with the literature, we have used the same set of

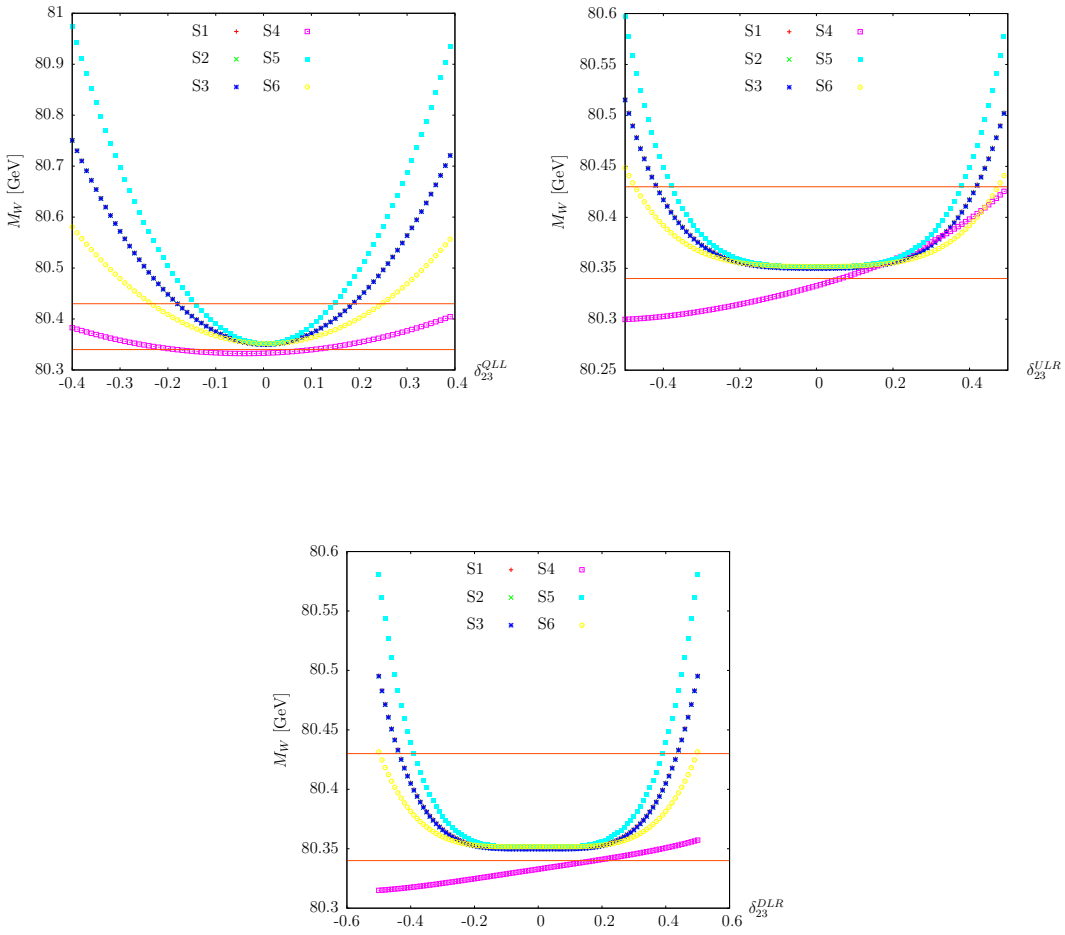

Figure 4.1: M_W as a function of δ_{23}^{QLL} (upper left), δ_{23}^{ULR} (upper right) and δ_{23}^{DLR} (lower).

input parameters as in [116]:

$$\mu = 800 \text{ GeV}, \; m_{\text{SUSY}} = 800 \text{ GeV}, \; A_f = 500 \text{ GeV},$$
$$M_A = 400 \text{ GeV}, \; M_2 = 300 \text{ GeV}, \; \tan\beta = 35\,, \tag{4.2}$$

where we have chosen, for simplicity, m_{SUSY} as a common value for the soft SUSY-breaking squark mass parameters, $m_{\text{SUSY}} = M_{\tilde{Q}} = M_{\tilde{U}} = M_{\tilde{D}}$, and all the various trilinear parameters to be universal, $A_f = A_t = A_b = A_c = A_s$. The value of the δ_{ij}^{FAB}'s are varied from -0.9 to 0.9, and GUT relations are used to calculate M_1 and M_3. In Ref. [116], only LL mixing was considered. In this limit we find results in qualitative agreement with Ref. [116]. This analysis has been done just to illustrate the different contributions and we do not take into account any experimental constraints. A detailed analysis for realisitic SUSY scenerios (defined in Tab. 4.1) constrained by BPO and EWPO can be found below.

As can be seen in Fig. 4.2, for the decay width $\Gamma(h \to \bar{b}s + b\bar{s})$ the SUSY-QCD contribution is dominant in all the cases. For LL mixing shown in the upper left plot,

		Total allowed intervals
δ_{23}^{QLL}	S1	(-0.27:0.28)
	S2	(-0.23:0.23)
	S3	(-0.12:0.06) (0.17:0.19)
	S4	excluded
	S5	(-0.83:-0.78) (-0.14:0.14)
	S6	(-0.076:0.14)
δ_{23}^{ULR}	S1	(-0.27:0.27)
	S2	(-0.27:0.27)
	S3	(-0.27:0.27)
	S4	excluded
	S5	(-0.22:0.22)
	S6	(-0.37:0.37)
δ_{23}^{DLR}	S1	(-0.0069:0.014) (0.12:0.13)
	S2	(-0.0069:0.014) (0.11:0.13)
	S3	(-0.0069:0.014) (0.11:0.13)
	S4	(0.076:0.12) (0.26:0.30)
	S5	(-0.014:0.021) (0.17:0.19)
	S6	(0:0.0069) (0.069:0.076)
δ_{23}^{URL}	S1	(-0.27:0.27)
	S2	(-0.27:0.27)
	S3	(-0.27:0.27)
	S4	excluded
	S5	(-0.22:0.22)
	S6	(-0.37:0.37)
δ_{23}^{DRL}	S1	(-0.034:0.034)
	S2	(-0.034:0.034)
	S3	(-0.034:0.034)
	S4	excluded
	S5	(-0.062:0.062)
	S6	(-0.021:0.021)
δ_{23}^{URR}	S1	(-0.99:0.99)
	S2	(-0.99:0.99)
	S3	(-0.98:0.97)
	S4	excluded
	S5	(-0.99:0.99)
	S6	(-0.96:0.94)
δ_{23}^{DRR}	S1	(-0.96:0.96)
	S2	(-0.96:0.96)
	S3	(-0.96:0.94)
	S4	excluded
	S5	(-0.97:0.97)
	S6	(-0.97:-0.94) (-0.63:0.64) (0.93:0.97)

Table 4.2: Present allowed (by BPO) intervals for the δ_{ij}^{FAB} for the MSSM points defined in Tab. 4.1 [99].

		Total allowed intervals
δ_{23}^{QLL}	S1	(-0.18:0.18)
	S2	(-0.18:0.18)
	S3	(-0.18:0.18)
	S4	(-0.53:-0.17)(0.10:0.45)
	S5	(-0.14:0.14)
	S6	(-0.23:0.23)
$\delta_{23}^{ULR}, \delta_{23}^{URL}$	S1	(-0.41:0.41)
	S2	(-0.41:0.41)
	S3	(-0.41:0.41)
	S4	(0.10:0.50)
	S5	(-0.39:0.39)
	S6	(-0.47:0.47)
$\delta_{23}^{DLR}, \delta_{23}^{DRL}$	S1	(-0.43:0.43)
	S2	(-0.43:0.43)
	S3	(-0.43:0.43)
	S4	(0.16:0.99)
	S5	(-0.39:0.39)
	S6	(-0.49:0.49)

Table 4.3: Present allowed (by M_W) intervals for the squark mixing parameters δ_{ij}^{FAB} for the selected S1-S6 MSSM points defined in Tab. 4.1.

the SUSY-QCD contribution reaches up to $\mathcal{O}(10^{-6})$, while the SUSY-EW contribution reach up to $\mathcal{O}(10^{-7})$, resulting in a total contribution "in between", due to the negative interference between SUSY-EW and SUSY-QCD contribution. For LR and RL mixing, shown in the upper right and lower left plot, respectively, the SUSY-QCD contribution reach up to the maximum value of $\mathcal{O}(10^{-2})$, while the SUSY-EW contribution reach only up to $\mathcal{O}(10^{-7})$. In this case total contriution is almost equal to SUSY-QCD contribution as SUSY-EW contibution (and thus the interference) is relatively neglible. For RR mixing, shown in the lower right plot, the SUSY-EW contribution of $\mathcal{O}(10^{-10})$ is again neglible compared to SUSY-QCD contribution of $\mathcal{O}(10^{-7})$.

Now we turn to realistic scenarios that are in agreement with experimental data from BPO and EWPO. Starting point are the scenarios S1...S6 defined in Tab. 4.1, where we vary the flavor violating δ_{ij}^{FAB} within the experimentally allowed ranges following the results given in Tabs. 4.2, 4.3. We start with the scenarios in which we allow one of the δ_{ij}^{FAB} to be varied, while the others are set to zero. In Fig. 4.3 we show BR($h \to \bar{b}s + b\bar{s}$) as a function of δ_{23}^{QLL} (upper left), δ_{23}^{DLR} (upper right), δ_{23}^{DRL} (lower left) and δ_{23}^{DRR} (lower right), i.e. for the same set of δ_{ij}^{FAB} that has been analyzed in Fig. 4.2. It can be seen that allowing only one $\delta_{ij}^{FAB} \neq 0$ results in rather small values of BR($h \to \bar{b}s + b\bar{s}$). LL (upper

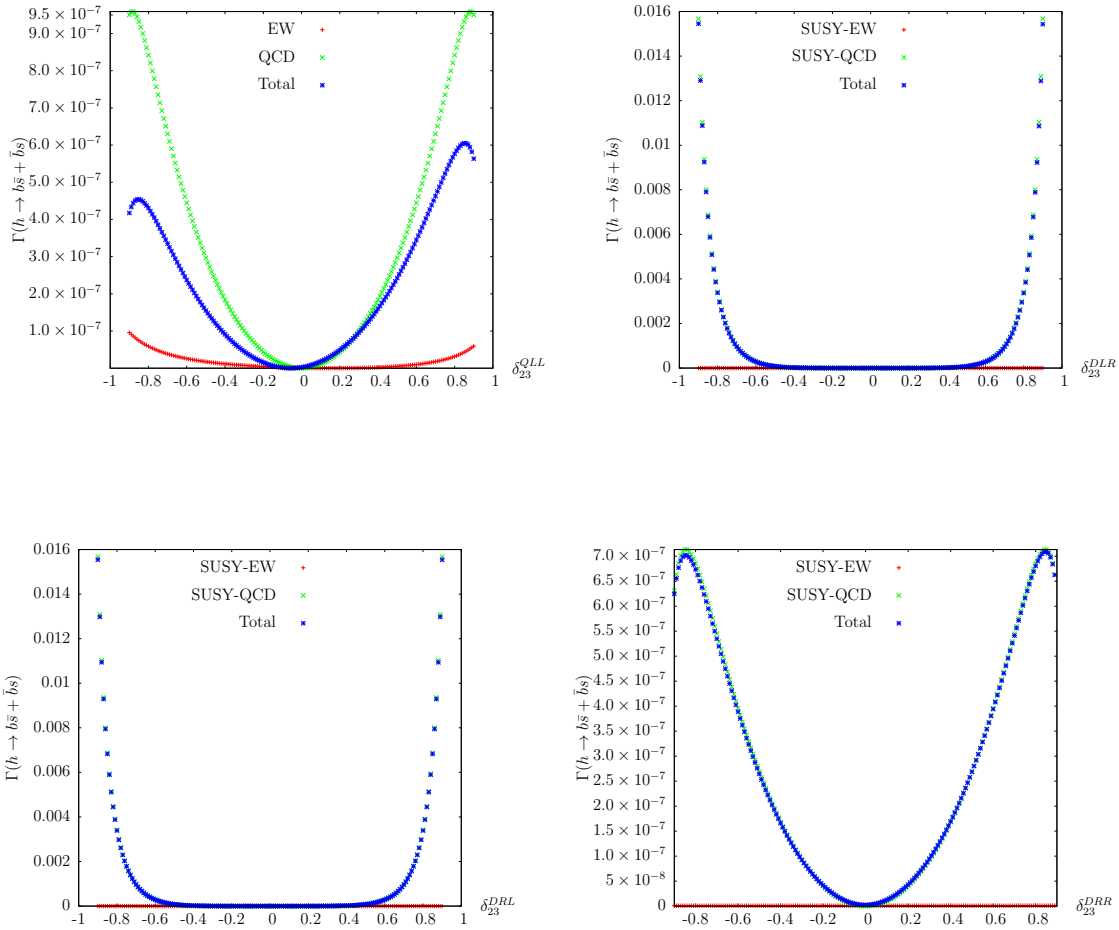

Figure 4.2: $\Gamma(h \to \bar{b}s + b\bar{s})$ as a function of δ_{23}^{QLL} (upper left), δ_{23}^{DLR} (upper right), δ_{23}^{DRL} (lower left) and δ_{23}^{DRR} (lower right).

left) and RL (lower left plot) mixing results in $\mathcal{O}(10^{-7})$ values for BR$(h \to \bar{b}s + b\bar{s})$. One order of magnitude can be gained in the RR mixing case (lower right). The largest values of BR$(h \to \bar{b}s + b\bar{s})$ are obtained in the case of $\delta_{23}^{DLR} \neq 0$ (upper right plot). Here in S4 and S5 values of BR$(h \to \bar{b}s + b\bar{s}) \sim 2 \times 10^{-4}$ can be found, possibly in the reach of future e^+e^- colliders, see Sect. 3.4.

So far we have shown the effects of independent variations of one δ_{ij}^{FAB}. Obviously, a realistic model would include several $\delta_{ij}^{FAB} \neq 0$ that may interfere, increasing or decreasing the results obtained with just the addition of independent contributions. GUT based MFV models that induce the flavor violation via RGE running automatically generate several $\delta_{ij}^{FAB} \neq 0$ at the EW scale. In the following we will present results with two or three $\delta_{ij}^{FAB} \neq 0$, where we combined the ones that showed the largest effects.

In Figs. 4.4-4.7, in the left columns we show the $3\,\sigma$ contours (with experimental and theory uncertainties added linearly) of BR$(B \to X_s\gamma)$ (Black), BR$(B_s \to \mu^+\mu^-)$ (Green), ΔM_{B_s} (Blue) and M_W (Red). For non-visible contours the whole plane is

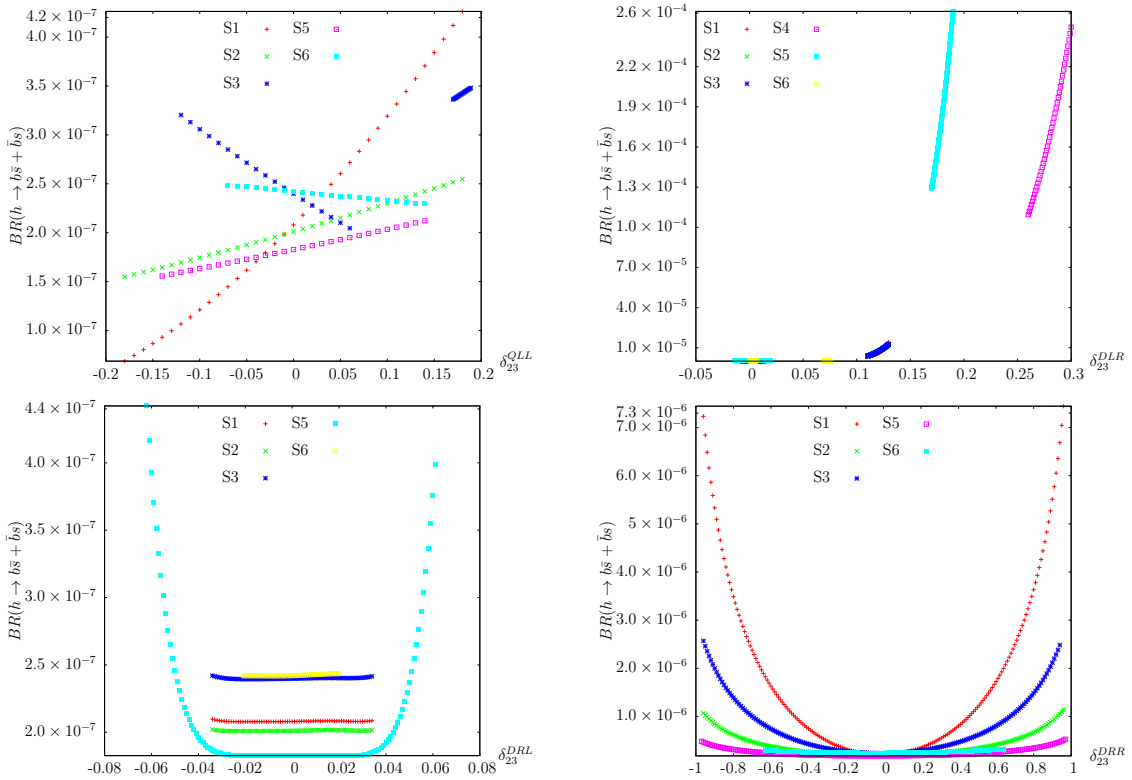

Figure 4.3: BR($h \to \bar{b}s + b\bar{s}$) as a function of δ_{23}^{QLL} (upper left), δ_{23}^{DLR} (upper right), δ_{23}^{DRL} (lower left) and δ_{23}^{DRR} (lower right).

allowed by that constraint. The right columns show, for the same parameters, the results for BR($h \to \bar{b}s + b\bar{s}$). In Figs. 4.4 and 4.5 we present the results for the plane (δ_{23}^{QLL},δ_{23}^{DLR}) for S1...S3 and for S4...S6, respectively. Similarly, in Figs. 4.6 and 4.7 we show the (δ_{23}^{DRR}, δ_{23}^{DLR}) plane. The shaded area in the left columns indicates the area that is allowed by all experimental constraints. In the (δ_{23}^{QLL}, δ_{23}^{DLR}) planes one can see that the large values for δ_{23}^{QLL} are not allowed by M_W, on the other hand, BR($B \to X_s\gamma$) mostly restricts the value of δ_{23}^{DLR}. The largest values for BR($h \to \bar{b}s + b\bar{s}$) in each plane in the arrea allowed by the BPO and the EWPO are summarized in the upper part of Tab. 4.4. One can see that in most cases we find BR($h \to \bar{b}s + b\bar{s}$) $\sim \mathcal{O}(10^{-5})$, which would render the observation difficult at current and future colliders. However, in the (δ_{23}^{QLL}, δ_{23}^{DLR}) plane in the scenarios S4 and S5 maximum values of $\mathcal{O}(3 \times 10^{-4})$ can be observed, which could be detectable at future ILC measurements. In the (δ_{23}^{DRR}, δ_{23}^{DLR}) plane for these two scenarios even values of $\mathcal{O}(10^{-3})$ are reached, which would make a measurement of the flavor violating Higgs decay relatively easy at the ILC.

As a last step in model independent analysis, we consider the case of three $\delta_{ij}^{FAB} \neq 0$ at a time. For this purpose we scan the parameters in the (δ_{23}^{QLL}, δ_{23}^{DLR}) plane and set $\delta_{23}^{DRR} = 0.5$. For reasons of practicability we choose *one* intermediate value for δ_{23}^{DRR}; a very small value will have no additional effect, and a very large value of δ_{23}^{DRR} leads to

Plane	MSSM point	Maximum possible value	Figure
$(\delta_{23}^{QLL}, \delta_{23}^{DLR})$	S1	1.38×10^{-5}	Fig. 4.4
	S2	1.39×10^{-5}	Fig. 4.4
	S3	1.43×10^{-5}	Fig. 4.4
	S4	3.34×10^{-4}	Fig. 4.5
	S5	2.74×10^{-4}	Fig. 4.5
	S6	1.36×10^{-8}	Fig. 4.5
$(\delta_{23}^{DRR}, \delta_{23}^{DLR})$	S1	4.41×10^{-6}	Fig. 4.6
	S2	3.32×10^{-6}	Fig. 4.6
	S3	3.07×10^{-5}	Fig. 4.6
	S4	1.66×10^{-3}	Fig. 4.7
	S5	1.97×10^{-3}	Fig. 4.7
	S6	6.03×10^{-8}	Fig. 4.7
$(\delta_{23}^{QLL}, \delta_{23}^{DLR})$ with $\delta_{23}^{DRR} = 0.5$	S1	7.49×10^{-6}	Fig. 4.8
	S2	7.33×10^{-6}	Fig. 4.8
	S3	3.50×10^{-6}	Fig. 4.8
	S4	Excluded	Fig. 4.9
	S5	Excluded	Fig. 4.9
	S6	Excluded	Fig. 4.9

Table 4.4: Maximum possible value for BR($h \to \bar{b}s + b\bar{s}$) for two and three $\delta_{ij}^{FAB} \neq 0$ case for the selected S1-S6 MSSM points defined in Tab. 4.1.

large excluded areas in the (δ_{23}^{QLL}, δ_{23}^{DLR}) plane. We show our results in Figs. 4.8 and 4.9 in the scenarios S1-S3 and S4-S6, respectively. Colors and shadings are chosen as in the previous analysis. Here it should be noted that in S4 the whole plane is excluded by M_W, and in S5 by BR($B_s \to \mu^+\mu^-$) (both contours are not visible). In S6 no overlap between the four constraints is found, and again this scenario is excluded. We have checked that also a smaller value of $\delta_{23}^{DRR} = 0.2$ does not qualitatively change the picture for S4, S5 and S6. The highest values that can be reached for BR($h \to \bar{b}s + b\bar{s}$) in the three remaining scenarios in the experimentally allowed regions are shown in the lower part of Tab. 4.4. One can see only very small valus or $\mathcal{O}(5 \times 10^{-6})$ are found, i.e. choosing $\delta_{23}^{DRR} \neq 0$ did not lead to observable values of BR($h \to \bar{b}s + b\bar{s}$).

To summarize, in our model independent analysis, allowing for more than one $\delta_{ij}^{FAB} \neq 0$ we find that the additional freedom resulted in somewhat larger values of BR($h \to \bar{b}s + b\bar{s}$) as compared to the case of only one non-zero δ_{ij}^{FAB}. In particular in the two scenarios S4 and S5 values of BR($h \to \bar{b}s + b\bar{s}$) $\sim 10^{-3} - 10^{-4}$ can be reached, allowing the detection of the flavor violating Higgs decay at the ILC. The other scenarios always yield values that are presumably too low for current and future colliders.

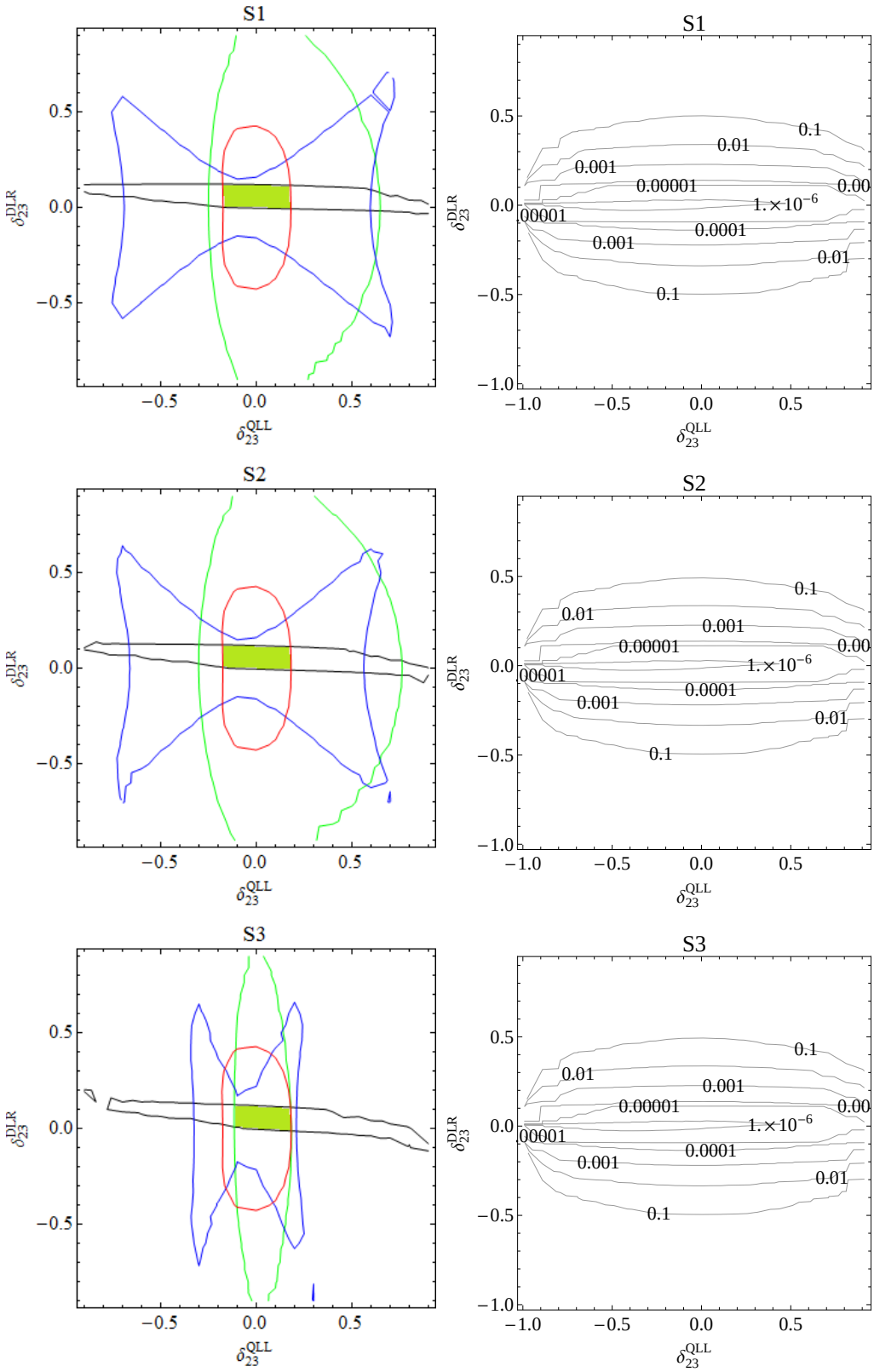

Figure 4.4: Left: Contours of BR($B \to X_s\gamma$) (Black), BR($B_s \to \mu^+\mu^-$) (Green), ΔM_{B_s}(Blue) and M_W (Red) in (δ_{23}^{QLL} , δ_{23}^{DLR}) plane for points S1-S3. The shaded area shows the range of values allowed by all constraints. Right: corresponding contours for BR($h \to \bar{b}s + b\bar{s}$).

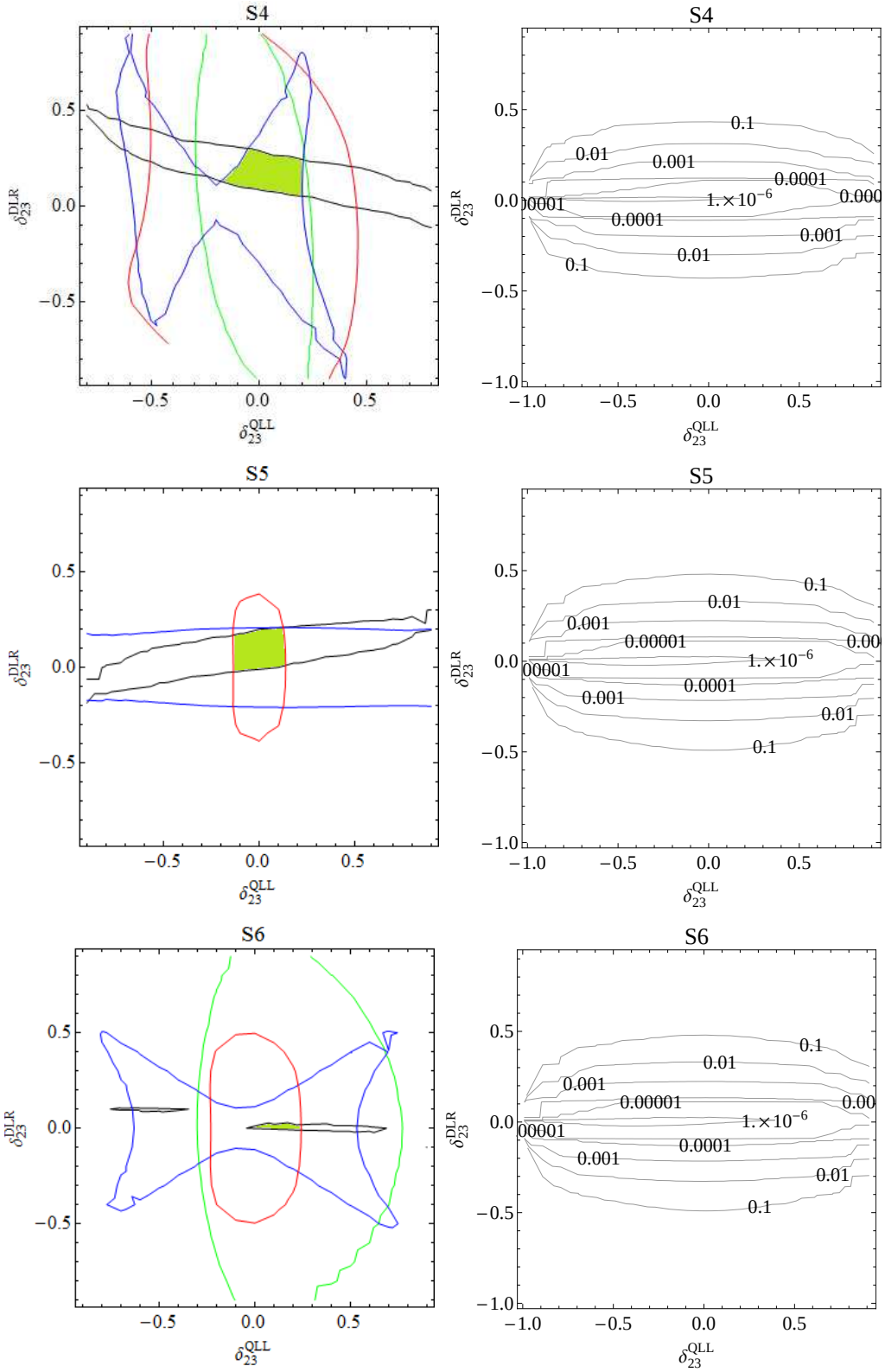

Figure 4.5: Left: Contours of BR($B \to X_s\gamma$) (Black), BR($B_s \to \mu^+\mu^-$) (Green), ΔM_{B_s} (Blue) and M_W (Red) in (δ_{23}^{QLL} , δ_{23}^{DLR}) plane for points S4-S6. The shaded area shows the range of values allowed by all constraints. Right: corresponding contours for BR($h \to \bar{b}s + b\bar{s}$).

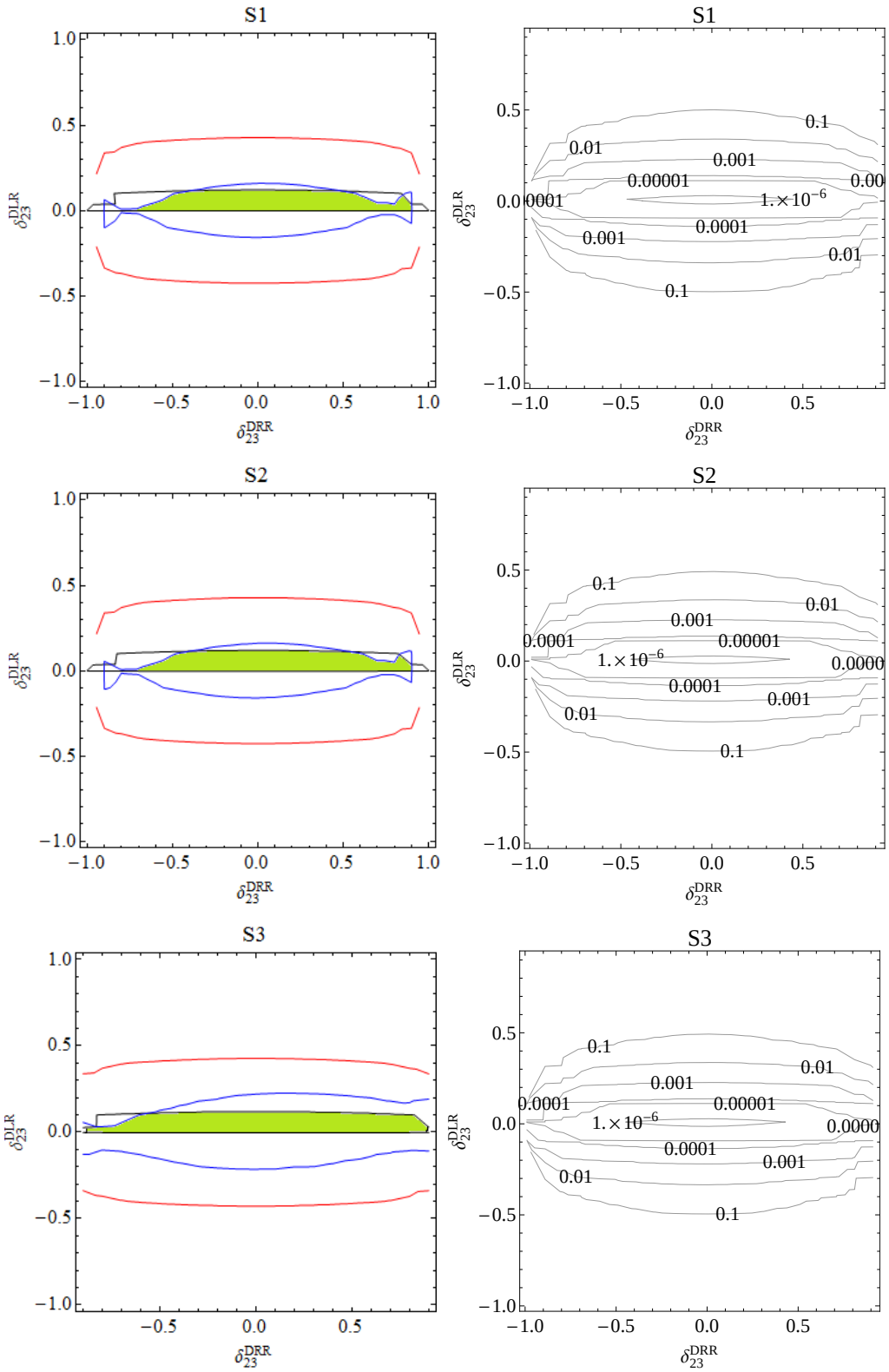

Figure 4.6: Left: Contours of BR($B \to X_s\gamma$) (Black), BR($B_s \to \mu^+\mu^-$) (Green), ΔM_{B_s} (Blue) and M_W (Red) in (δ_{23}^{DRR} , δ_{23}^{DLR}) plane for points S1-S3. The shaded area shows the range of values allowed by all constraints. Right: corresponding contours for BR($h \to \bar{b}s + b\bar{s}$).

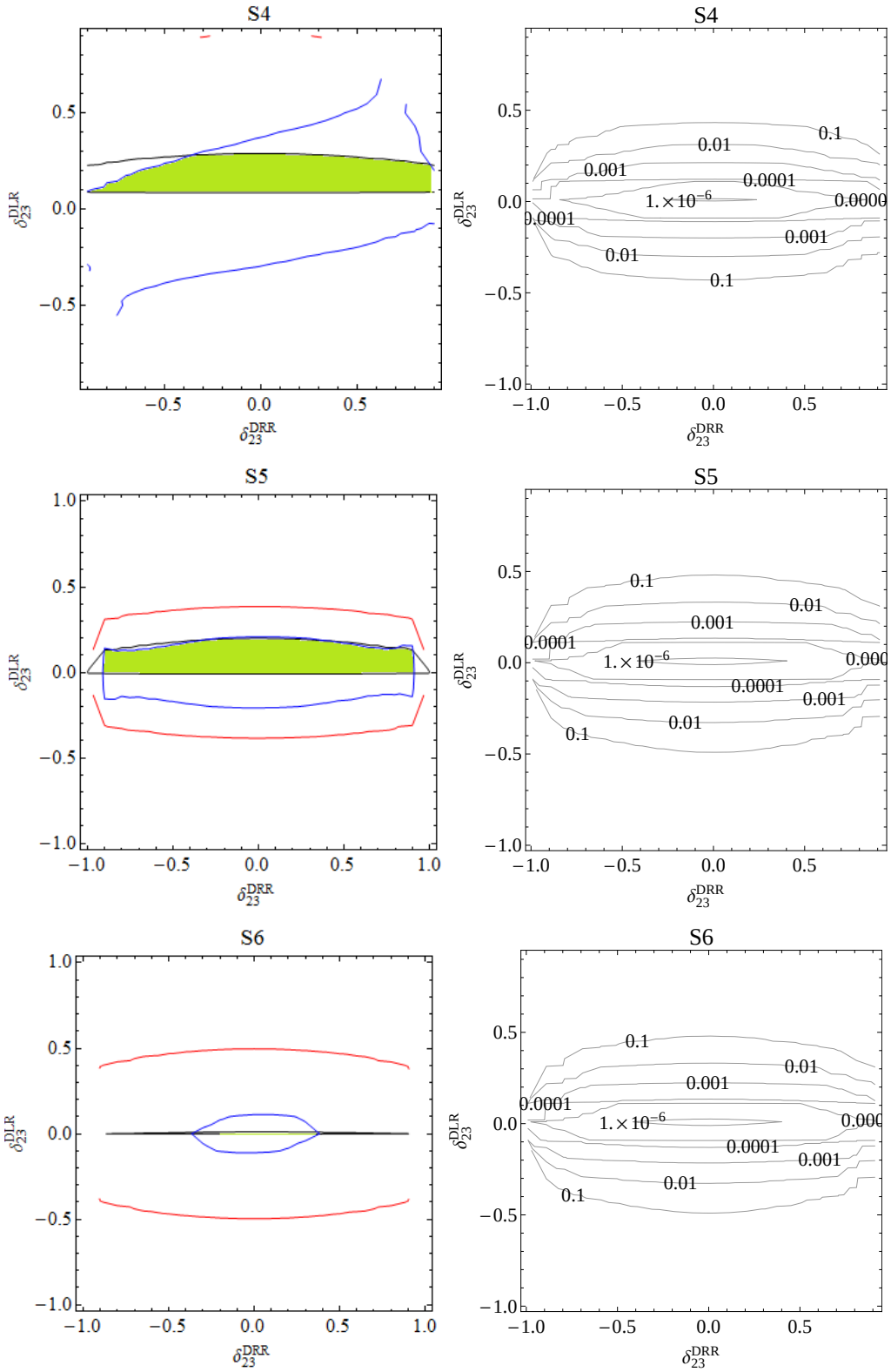

Figure 4.7: Left: Contours of BR($B \to X_s\gamma$) (Black), BR($B_s \to \mu^+\mu^-$) (Green), ΔM_{B_s} (Blue) and M_W (Red) in (δ_{23}^{DRR} , δ_{23}^{DLR}) plane for points S4-S6. The shaded area shows the range of values allowed by all constraints. Right: corresponding contours for BR($h \to \bar{b}s + b\bar{s}$).

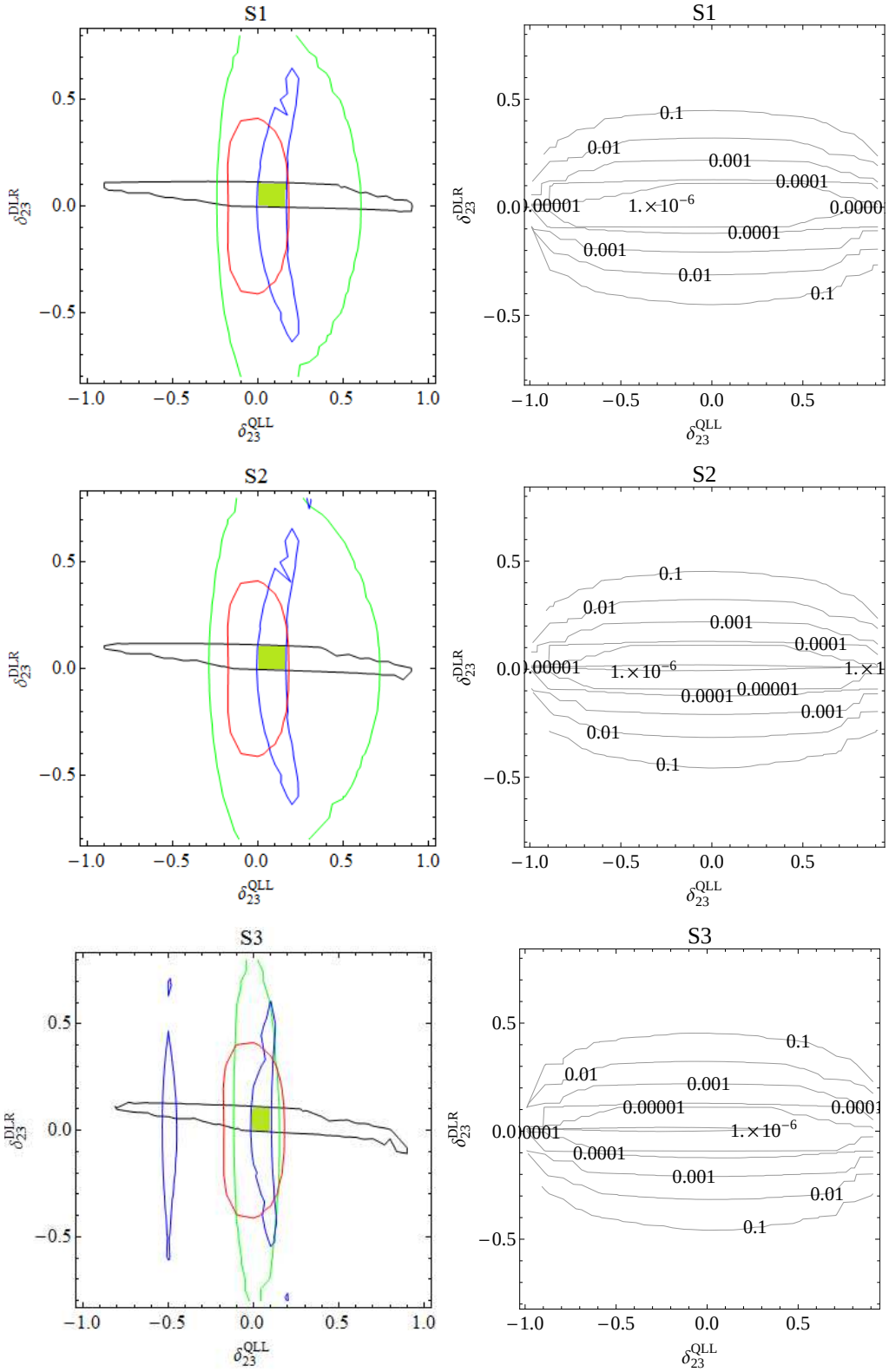

Figure 4.8: Left: Contours of BR($B \to X_s\gamma$) (Black), BR($B_s \to \mu^+\mu^-$) (Green), ΔM_{B_s} (Blue) and M_W (Red) in the (δ_{23}^{QLL} , δ_{23}^{DLR}) plane with $\delta_{23}^{DRR} = 0.5$ for points S1-S3. The shaded area shows the range of values allowed by all constraints. Right: corresponding contours for BR($h \to \bar{b}s + b\bar{s}$).

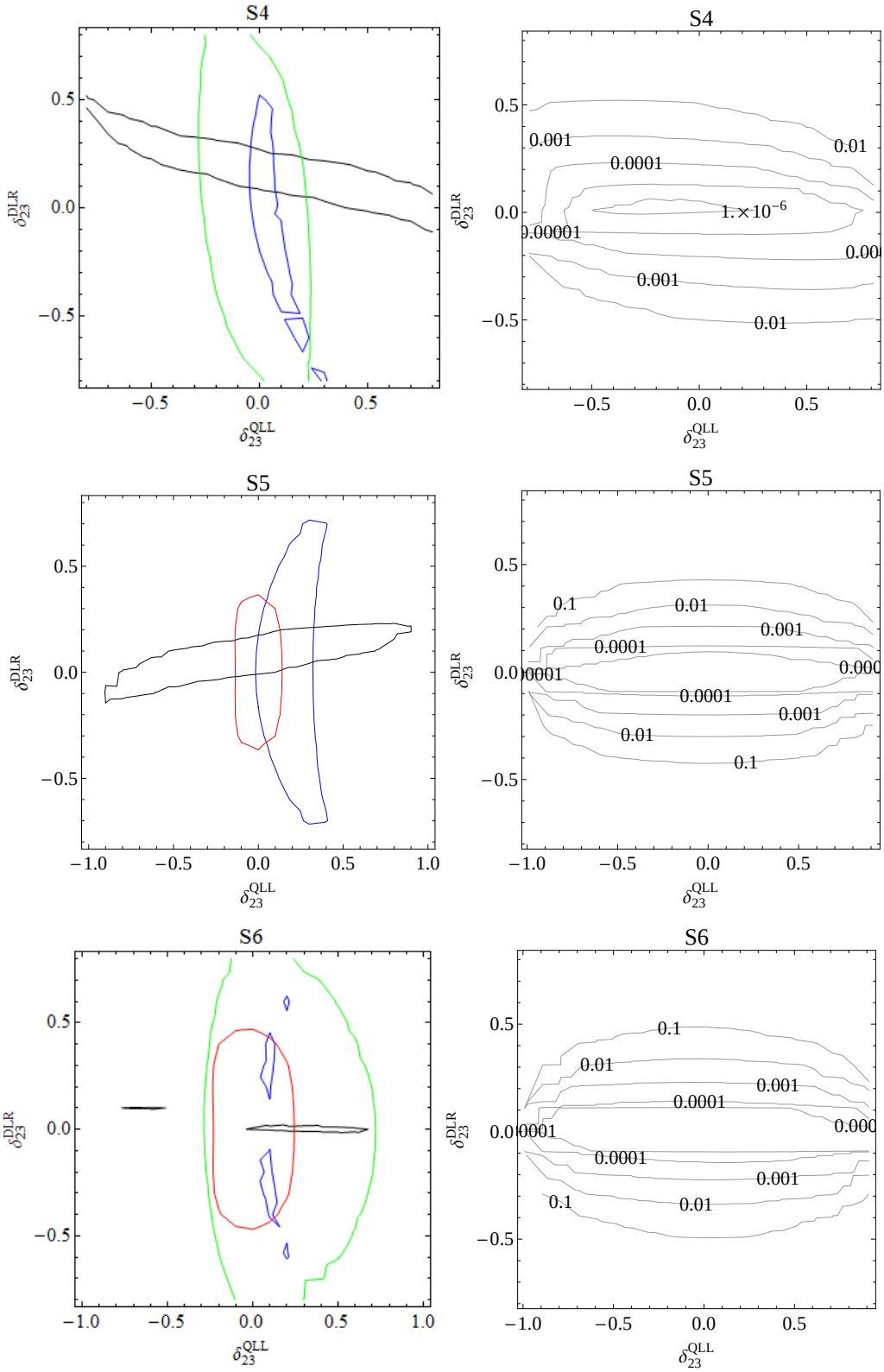

Figure 4.9: Left: Contours of BR($B \to X_s\gamma$) (Black), BR($B_s \to \mu^+\mu^-$) (Green), ΔM_{B_s} (Blue) and M_W (Red) in the (δ_{23}^{QLL} , δ_{23}^{DLR}) plane with $\delta_{23}^{DRR} = 0.5$ for points S4-S6. The shaded area shows the range of values allowed by all constraints. Right: corresponding contours for BR($h \to \bar{b}s + b\bar{s}$).

Chapter 5

Lepton Flavor Mixing Effects in the Model Independent Approach

In this chapter we analyse the lepton flavor mixing in MI approach. We use the same set of input parameter (Tab. 4.1) that was used in the previous chater. As a first step, we have calculated the sensitivity of EWPO like the W-boson mass or the effective weak leptonic mixing angle to the δ_{ij}^{FAB}'s in slepton sector entering in the Z and W boson self energies at one-loop level through the ρ parameter. Besides EWPO we also explore the effects of LFV on the MSSM Higgs sector. We evaluate the effects of LFV on the predictions of the masses of the light and heavy $\mathcal{CP}$-even Higgs bosons, M_h and M_H, as well as on the charged Higgs-boson mass $M_{H^\pm}$. Here we do not calculate predictions for cLFV decays in the MI approach as they were already explored in [145] for the same set of input parameters that we are using. They calculated the constraints on slepton δ_{ij}^{FAB}'s from cLFV decays (mentioned in the following section). We have also calculated the predictions for LFVHD which will be presented in the last section. The results presented in this chapter were published in [150].

5.1 Constraints on δ_{ij}^{FAB} from cLFV decays

We need to set the range of values for the explored δ_{ij}^{FAB}'s. We use the constraints (shown in Tab. 5.1) as taken from Ref. [145], calculated from the following LFV processes.

1.- Radiative LFV decays: $\mu \to e\gamma$, $\tau \to e\gamma$ and $\tau \to \mu\gamma$. These are sensitive to the δ_{ij}^{FAB}'s via the $(l_i l_j \gamma)_{1-\text{loop}}$ vertices with a real photon.

2.- Leptonic LFV decays: $\mu \to 3e$, $\tau \to 3e$ and $\tau \to 3\mu$. These are sensitive to the δ_{ij}^{FAB}'s via the $(l_i l_j \gamma)_{1-\text{loop}}$ vertices with a virtual photon, via the $(l_i l_j Z)_{1-\text{loop}}$ vertices with a virtual Z, and via the $(l_i l_j h)_{1-\text{loop}}$, $(l_i l_j H)_{1-\text{loop}}$ and $(l_i l_j A)_{1-\text{loop}}$ vertices with virtual Higgs bosons.

3.- Semileptonic LFV tau decays: $\tau \to \mu\eta$ and $\tau \to e\eta$. These are sensitive to the δ_{ij}^{FAB}'s via $(\tau\mu A)_{1-\text{loop}}$ and $(\tau e A)_{1-\text{loop}}$ vertices, respectively, with a virtual A, and

via $(\tau\mu Z)_{1-\text{loop}}$ and $(\tau eZ)_{1-\text{loop}}$ vertices, respectively with a virtual Z.

4.- Conversion of μ into e in heavy nuclei: These are sensitive to the δ_{ij}^{FAB}'s via the $(\mu e\gamma)_{1-\text{loop}}$ vertex with a virtual photon, via the $(\mu eZ)_{1-\text{loop}}$ vertex with a virtual Z, and via the $(\mu eh)_{1-\text{loop}}$ and $(\mu eH)_{1-\text{loop}}$ vertices with a virtual h and H Higgs boson, respectively.

	S1	S2	S3	S4	S5	S6
$\lvert\delta_{12}^{LLL}\rvert_{\max}$	10×10^{-5}	7.5×10^{-5}	5×10^{-5}	6×10^{-5}	42×10^{-5}	8×10^{-5}
$\lvert\delta_{12}^{ELR}\rvert_{\max}$	2×10^{-6}	3×10^{-6}	4×10^{-6}	3×10^{-6}	2×10^{-6}	1.2×10^{-5}
$\lvert\delta_{12}^{ERR}\rvert_{\max}$	1.5×10^{-3}	1.2×10^{-3}	1.1×10^{-3}	1×10^{-3}	2×10^{-3}	5.2×10^{-3}
$\lvert\delta_{13}^{LLL}\rvert_{\max}$	5×10^{-2}	5×10^{-2}	3×10^{-2}	3×10^{-2}	23×10^{-2}	5×10^{-2}
$\lvert\delta_{13}^{ELR}\rvert_{\max}$	2×10^{-2}	3×10^{-2}	4×10^{-2}	2.5×10^{-2}	2×10^{-2}	11×10^{-2}
$\lvert\delta_{13}^{ERR}\rvert_{\max}$	5.4×10^{-1}	5×10^{-1}	4.8×10^{-1}	5.3×10^{-1}	7.7×10^{-1}	7.7×10^{-1}
$\lvert\delta_{23}^{LLL}\rvert_{\max}$	6×10^{-2}	6×10^{-2}	4×10^{-2}	4×10^{-2}	27×10^{-2}	6×10^{-2}
$\lvert\delta_{23}^{ELR}\rvert_{\max}$	2×10^{-2}	3×10^{-2}	4×10^{-2}	3×10^{-2}	2×10^{-2}	12×10^{-2}
$\lvert\delta_{23}^{ERR}\rvert_{\max}$	5.7×10^{-1}	5.2×10^{-1}	5×10^{-1}	5.6×10^{-1}	8.3×10^{-1}	8×10^{-1}

Table 5.1: Present upper bounds on the slepton mixing parameters $|\delta_{ij}^{FAB}|$ for the selected S1-S6 MSSM points defined in Tab. 4.1. The bounds for $|\delta_{ij}^{ERL}|$ are similar to those of $|\delta_{ij}^{ELR}|$.

5.2 Numerical results

We have implemented the full one-loop results for the W and Z boson and the Higgs boson self-energies in `FeynHiggs`, including all LFV mixing terms (see Sect. 3.7 for details). The analytical results are lenghty and are not shown here. They can, however, be found in the latest version of our code, `FeynHiggs 2.10.2`. For the numerical investigation we have analyzed all 12 slepton δ_{ij}^{FAB}'s for the MSSM scenarios defined in Tab. 4.1. In order to get a good understanding of the LFV effects to $\Delta\rho$ and consequently M_W and $\sin^2\theta_{\rm eff}$ we define

$$\Delta\rho^{\rm LFV} = \Delta\rho - \Delta\rho^{\rm MSSM}, \tag{5.1}$$

$$\delta M_W^{\rm LFV} = M_W - M_W^{\rm MSSM}, \tag{5.2}$$

$$\delta \sin^2\theta_{\rm eff}^{\rm LFV} = \sin^2\theta_{\rm eff} - \sin^2\theta_{\rm eff}^{\rm MSSM}, \tag{5.3}$$

where $\Delta\rho^{\rm MSSM}$, $M_W^{\rm MSSM}$ and $\sin^2\theta_{\rm eff}^{\rm MSSM}$ are the values of the relevant observables with all $\delta_{ij}^{FAB} = 0$ (and the latter two evaluated with the help of Eq. (3.4)). Furthermore we define

$$\Delta M_h^{\rm LFV} = M_h - M_h^{\rm MSSM}, \tag{5.4}$$

$$\Delta M_H^{\rm LFV} = M_H - M_H^{\rm MSSM}, \tag{5.5}$$

$$\Delta M_{H^\pm}^{\rm LFV} = M_{H^\pm} - M_{H^\pm}^{\rm MSSM}, \tag{5.6}$$

where $M_h^{\rm MSSM}$, $M_H^{\rm MSSM}$ and $M_{H^\pm}^{\rm MSSM}$ corresponds to the Higgs masses with all $\delta_{ij}^{FAB} = 0$. The SM results for M_W and $\sin^2\theta_{\rm eff}$ are $M_W = 80.361$ GeV and $\sin^2\theta_{\rm eff} = 0.23152$ as evaluated with `FeynHiggs` (using the approximation formulas given in Refs. [151, 152]). The numerical values of $\Delta\rho$, M_W, $\sin^2\theta_{\rm eff}$, M_h, M_H and $M_{H^\pm}$ in the MSSM with all $\delta_{ij}^{FAB} = 0$ are summarized in Tab. 5.2.

Our numerical results are shown in Fig. 5.1 to Fig. 5.8. The six plots in each figure are ordered as follows. Upper left: $\Delta\rho^{\rm LFV}$, upper right: $\delta M_W^{\rm LFV}$, middle left: $\delta\sin^2\theta_{\rm eff}^{\rm LFV}$, middle right: $\Delta M_h^{\rm LFV}$, lower left: $\Delta M_H^{\rm LFV}$, and lower right: $\Delta M_{H^\pm}^{\rm LFV}$, as a function of δ_{13}^{LL} (Fig.5.1), δ_{23}^{LLL} (Fig.5.2), δ_{13}^{ELR} (Fig.5.3), δ_{23}^{ELR} (Fig.5.4), δ_{13}^{ERL} (Fig.5.5), δ_{23}^{ERL} (Fig.5.6), δ_{13}^{ERR} (Fig.5.7) and δ_{23}^{ERR} (Fig.5.8). The legends are shown only in the first plot of each figure. We do not show results for LFV effects involving only the first and second generation. While they are included for completeness in our analytical results, they are expected to have a negligible effect on the observables considered here. The latter is confirmed by the numerical analysis presented in the next subsections.

Applying the most recent limits from the above listed LFV process yield up-to-date limits on the δ_{ij}^{FAB} [145]. Using the these upper bounds on δ_{ij}^{FAB}, as given in the Tab. 5.1, we calculate the corrections to the Higgs boson masses and the EWPO. For each explored non-vanishing delta, δ_{ij}^{FAB}, the corresponding sfermion physical masses and the sfermion rotation matrices, as well as the EWPO and Higgs masses were numerically computed with `FeynHiggs 2.10.2`, where we have included the analytical results of our calculations.

	S1	S2	S3	S4	S5	S6
$\Delta\rho$	2.66×10^{-5}	1.72×10^{-5}	1.39×10^{-5}	2.35×10^{-4}	2.36×10^{-5}	2.14×10^{-5}
M_W	80.362	80.362	80.361	80.375	80.364	80.363
$\sin^2\theta_{\text{eff}}$	0.23151	0.23152	0.23152	0.23143	0.23150	0.23151
M_h	126.257	126.629	126.916	123.205	123.220	124.695
M_H	500.187	999.580	999.206	1001.428	1000.239	1499.365
$M_{H^\pm}$	506.888	1003.182	1003.005	1005.605	1003.454	1501.553

Table 5.2: The values of $\Delta\rho$, M_W, $\sin^2\theta_{\text{eff}}$, M_h, M_H and $M_{H^\pm}$ for the selected S1-S6 MSSM points defined in Tab. 4.1 (i.e. with all $\delta_{ij}^{FAB} = 0$). Mass values are in GeV.

5.2.1 EWPO

We start with the investigation of the LFV effects on the EWPO. The experimental bounds on δ_{12}^{FAB} where $A, B = L, R$ are very strict (as discussed above, see Tab. 5.1) and does not yield sizable contribution. The bounds on the other δ_{ij}^{FAB}'s are relatively less strict but still in most cases we do not get sizable contributions for EWPO (but now can quantify their corresponding sizes). The only sizable contribution that we get comes from δ_{23}^{LLL}. The upper left plot in Fig. 5.2 shows our results for $\Delta\rho$ as functions of δ_{23}^{LLL}, under the presently allowed experimental range given in 5.1, where, depending on the choice of the scenario (S1 ... S6) values of up to $\mathcal{O}(10^{-3})$ can be reached. The largest values are found in S5, where the largest values of δ_{23}^{LLL} of up to ± 0.3 are permitted. For the same value of δ_{23}^{LLL} we find the largest contributions in S6, which possesses the relatively largest values of SSB parameters in the slepton sector. This indicates that in general large contributions to the EWPO are possible as soon as heavy sleptons are involved. Consequently, while such heavy sleptons are in general difficult to detect directly at the LHC or the ILC, their presence could be visible in case of large LFV contributions via a shift in the EWPO.

Turning to the (pseudo-)observables M_W and $\sin^2\theta_{\text{eff}}$, which are shown in the upper right and middle left plot of Fig. 5.2, respectively, we can compare the size of the LFV

contributions to the current and future anticipated accuracies in these observables. The black line in both plots indicates the result for $\delta_{23}^{LLL} = 0$. The red line shows the current level of accuracy, see Eq. (3.9), while the blue line indicates the future ILC/GigaZ precision, see Eq. (3.10). We refrain from putting the absolute values of these observables, since their values strongly depend on the choice of the stop/sbottom sector (see Ref. [14] and references therein), which is independent on the slepton sector under investigation here. While the current level of accurcay only has the potential to restrict δ_{23}^{LLL} in S5 and S6, the future accuracy, in particular for $\sin^2\theta_{\rm eff}$, can set stringent bounds in all six scenarios.

The overall conclusion for the EWPO is that while δ_{23}^{LLL} is most difficult to restrict from "conventional" LFV observables, see Sect. 5.1, it has (by far) the strongest impact on EWPO. Even with the current precision, and even better with the (anticipated) future accuracies, depending on the values of the scalar top/bottom sector new bounds beyond the "conventional" LFV observables can be obtained.

5.2.2 Higgs masses

We now turn to the effects of the LFV contribtions on the prediction of the neutral $\mathcal{CP}$-even and the charged MSSM Higgs boson masses. As discussed in Sect. 3.2, the theoretical accuracy should reach a precision of ~ 50 MeV in the case of M_h and about $\sim 1\%$ in the case of the heavy Higgs bosons. The calculation of M_h in the presence of NMFV in the scalar quark sector, as obtained in Ref. [98], indicated that from the colored sector corrections of $\mathcal{O}(10$ GeV) are possible (i.e. for NMFV δ_{ij}^{FAB} in agreement with all other precision data). Similar or even larger corrections where found for the heavy Higgs bosons, in particular for the mass of the charged Higgs boson. Large corrections were connected especially to non-zero values of $\delta_{23}^{ULR,URL}$. While the corrections from the scalar lepton sector are naturally much smaller than from the scalar quark sector, it could be expected that the LFV contributions can exceed future and possibly even current experimental uncertainties. In the absence of the knowledge of the exact LFV contributions a theoretical uncertainty had to be assigned at least at the level of $\mathcal{O}(100$ MeV) for M_h and $\mathcal{O}(10$ GeV) for $M_{H^\pm}$. Both uncertainties are at the level (or exceeding) the future anticipated accuracies for these Higgs-boson masses. Consequently, the LFV have to be evaluated and analyzed in order to reach the required level of precision.

As described above, the Higgs-boson masses are shown in the middle right plot (M_h), the lower left (M_H) and the lower right plot ($M_{H^\pm}$) in each figure. As expected from the NMFV analysis in the scalar quark sector [98], the largest effects are found for $\delta_{23}^{ELR,ERL}$, but similarly for $\delta_{13}^{ELR,ERL}$, indicating that only the electroweak, but not the Yukawa couplings, play a relevant role in these corrections. Contrary to the expectations, the corrections to M_h *always* stay below the level of a few MeV. While this result eliminates the above menioned uncertainty of $\mathcal{O}(100$ MeV), these contributions are too small to yield a sizable numerical effect.

Turning to the heavy Higgs bosons, the contributions to M_H, most sizable again for $\delta_{23,13}^{ELR,ERL}$, do not exceed $\mathcal{O}(100$ MeV) and are thus effectively negligible. Substantially

larger corrections are found, in agreement with the expectations from Ref. [98] for the charged Higgs-boson mass. They can reach the level of nearly -2 GeV, see Figs. 5.3 - 5.6. For the chosen values of M_A (or $M_{H^\pm}$) this stays below the level of 1%. However, the absolute size of the corrections is not connected to the value of $M_{H^\pm}$ in S1-S6. Choosing starting values of M_A somewhat smaller (requiering a new evaluation of the corresponding bounds on the LFV δ_{ij}^{FAB}), could yield relative corrections to $M_{H^\pm}$ at the level of 1%. Furthremore, as in the case of the light Higgs-boson mass, the explicit calculation of the LFV effects eliminates the theory uncertainty associated to these effects, thus improving the theoretical accuracy.

5.2.3 BR($h \to l_i^\pm l_j^\mp$)

As a last step in MI analysis, we present here the slepton mixing effects to the LFVHD. These decays were calculated using newly modified (see Sect. 3.7) `FeynArts/FormCalc` setup. The constraints from cLFV decays on slepton δ_{ij}^{FAB}'s are very tight and we do not expect large values for the BR's. In Fig. 5.9 we present our numerical results for BR($h \to e^\pm\tau^\mp$) and BR($h \to \mu^\pm\tau^\mp$) as a function of slepton mixing δ_{ij}^{FAB}'s for the six points defined in the Tab. 4.1. BR($h \to e^\pm\mu^\mp$) can only reach $\mathcal{O}(10^{-17})$ at maximum and we do not show them here. BR($h \to e^\pm\tau^\mp$) and BR($h \to \mu^\pm\tau^\mp$) can reach at most to $\mathcal{O}(10^{-9})$ for some parameter points, which is very small compared to the CMS excess [129]. The reason for such a small value in the experimentally allowed parameter range is the following. The same couplings namely chargino-lepton-slepton and neutralino-lepton-slepton are responsible for the cLFV decays and LFVHD, making it very difficult to find any larger values for LFVHD BR's. Our results show that if the excess shown in the CMS results [129] persists, we will need to find some other sources of LFV to explain CMS result. Lepton-slepton misalignment is not sufficient to explain this excess. On the other hand our results are in agreement with the ATLAS results [130] which do not see any excess over SM background.

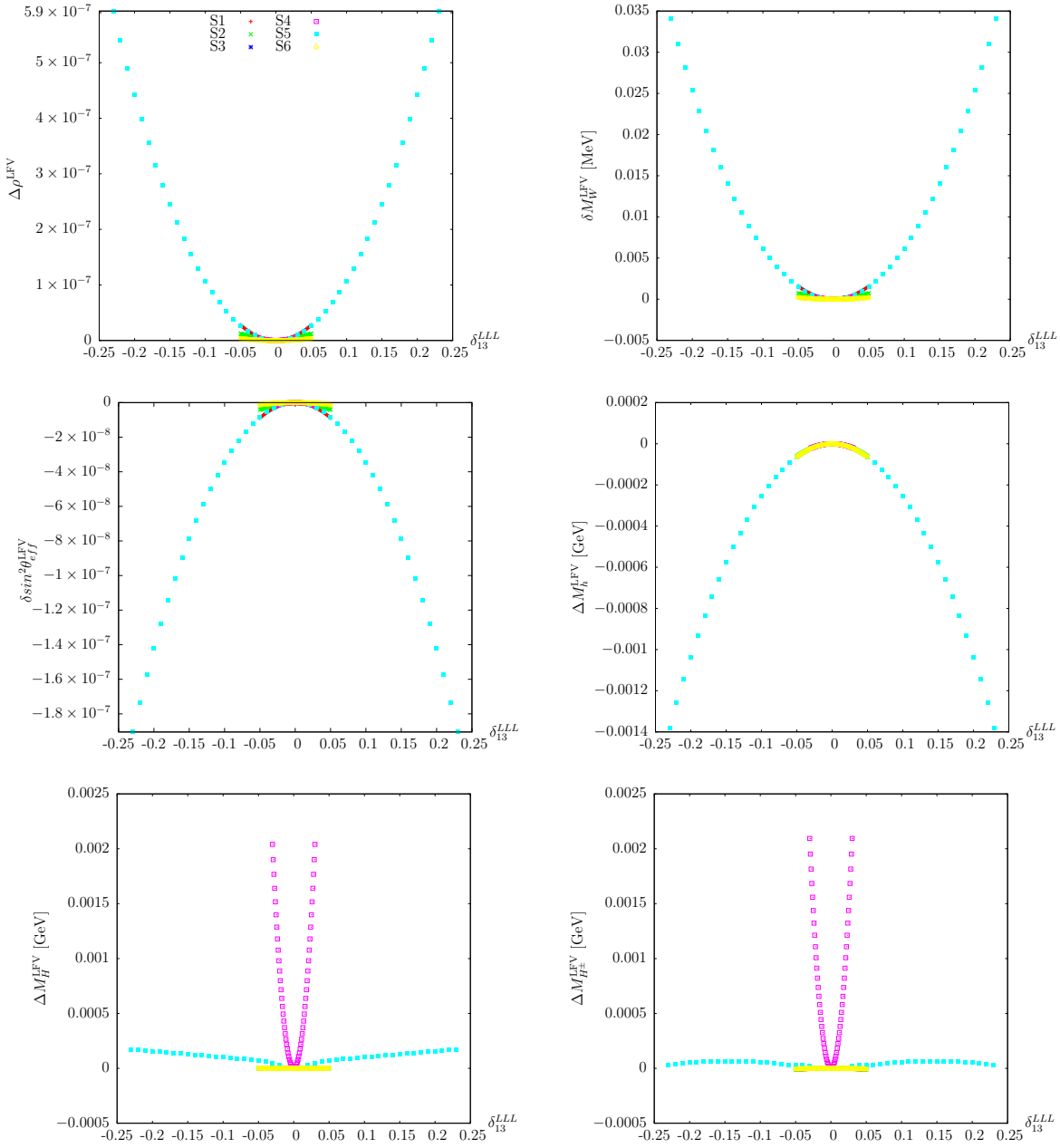

Figure 5.1: EWPO and Higgs masses as a function of δ_{13}^{LLL}.

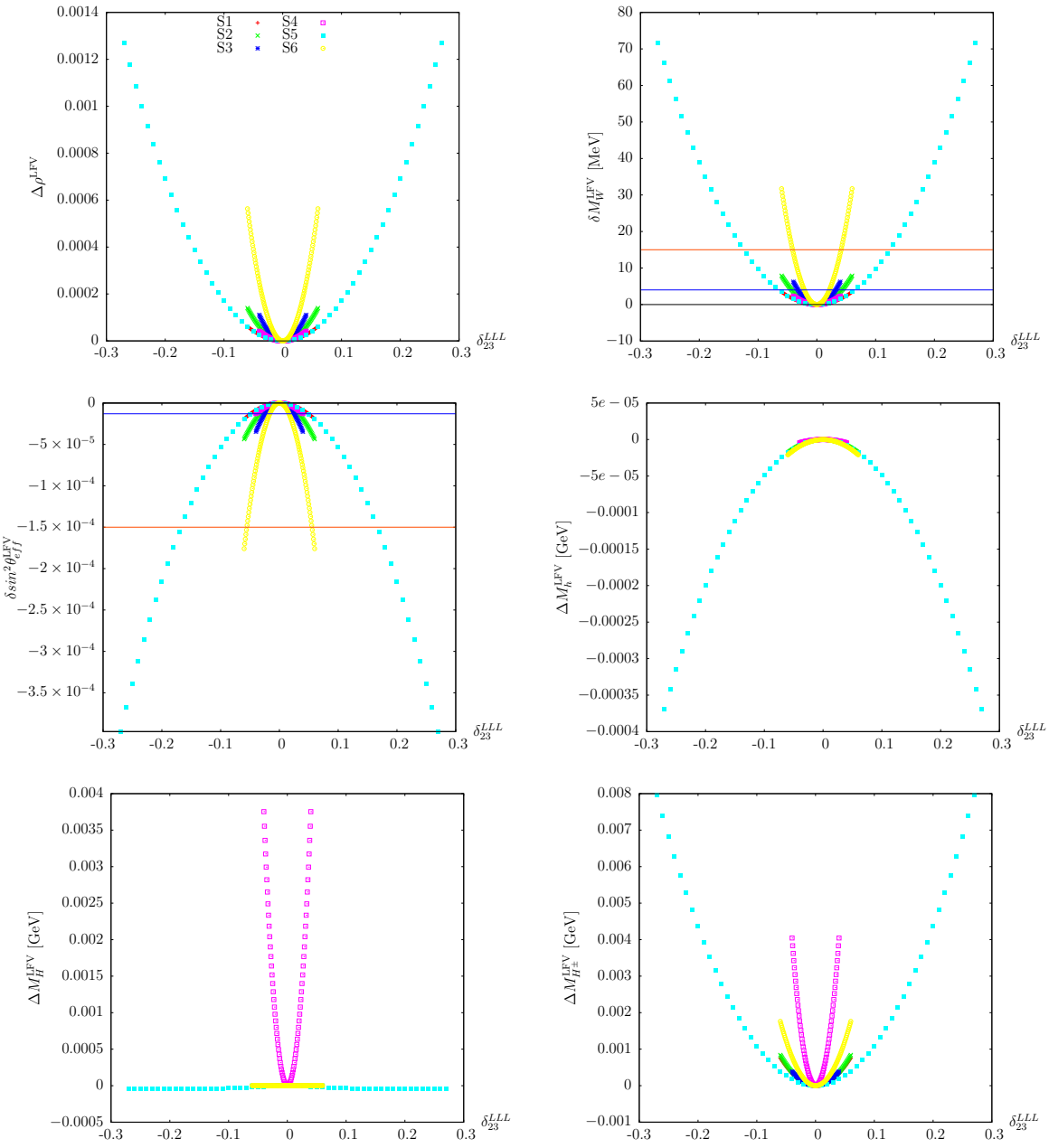

Figure 5.2: EWPO and Higgs masses as a function of δ_{23}^{LLL}. Solid red (blue) line shows the present (future) experimental uncertainty.

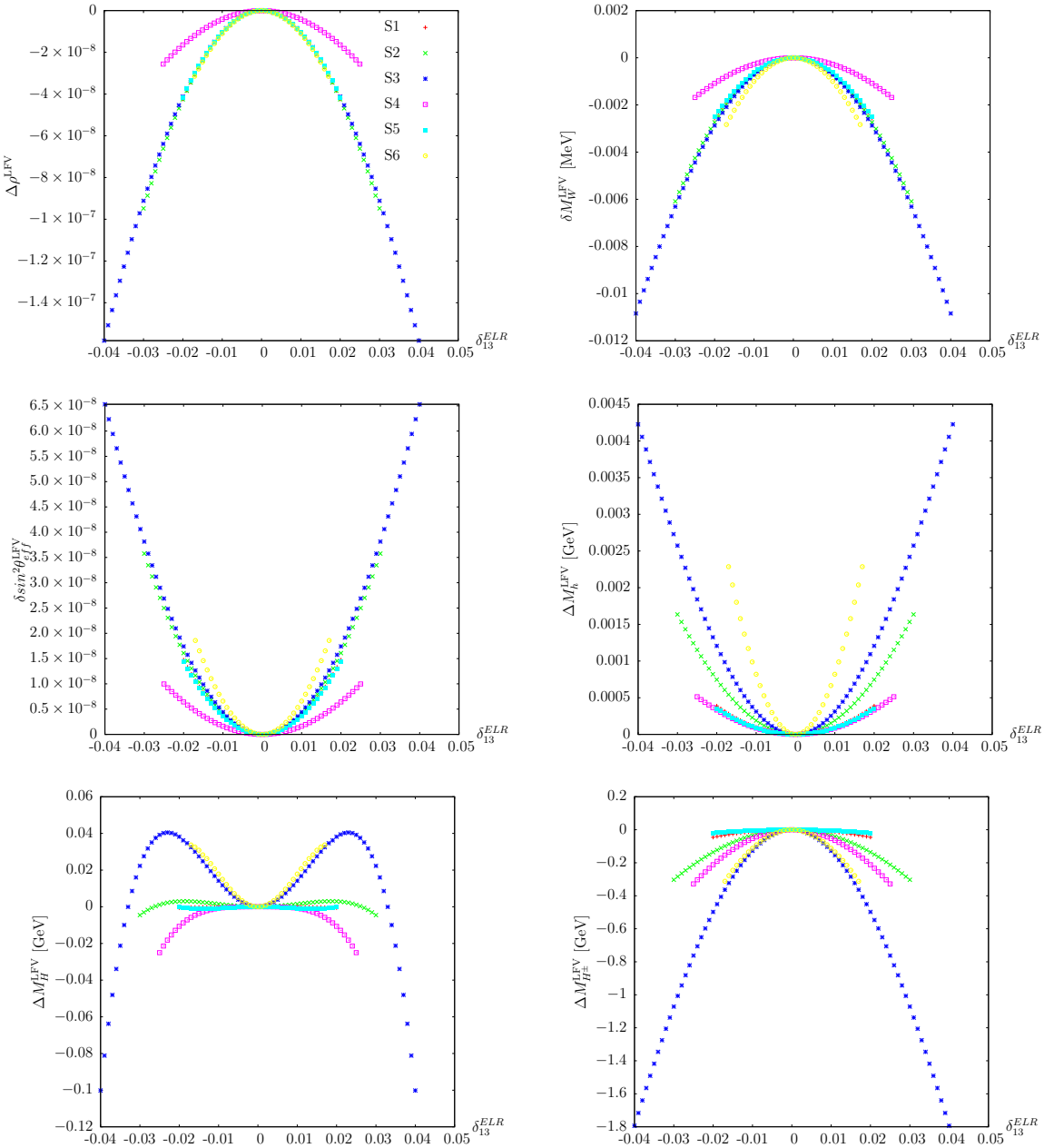

Figure 5.3: EWPO and Higgs masses as a function of δ_{13}^{ELR}.

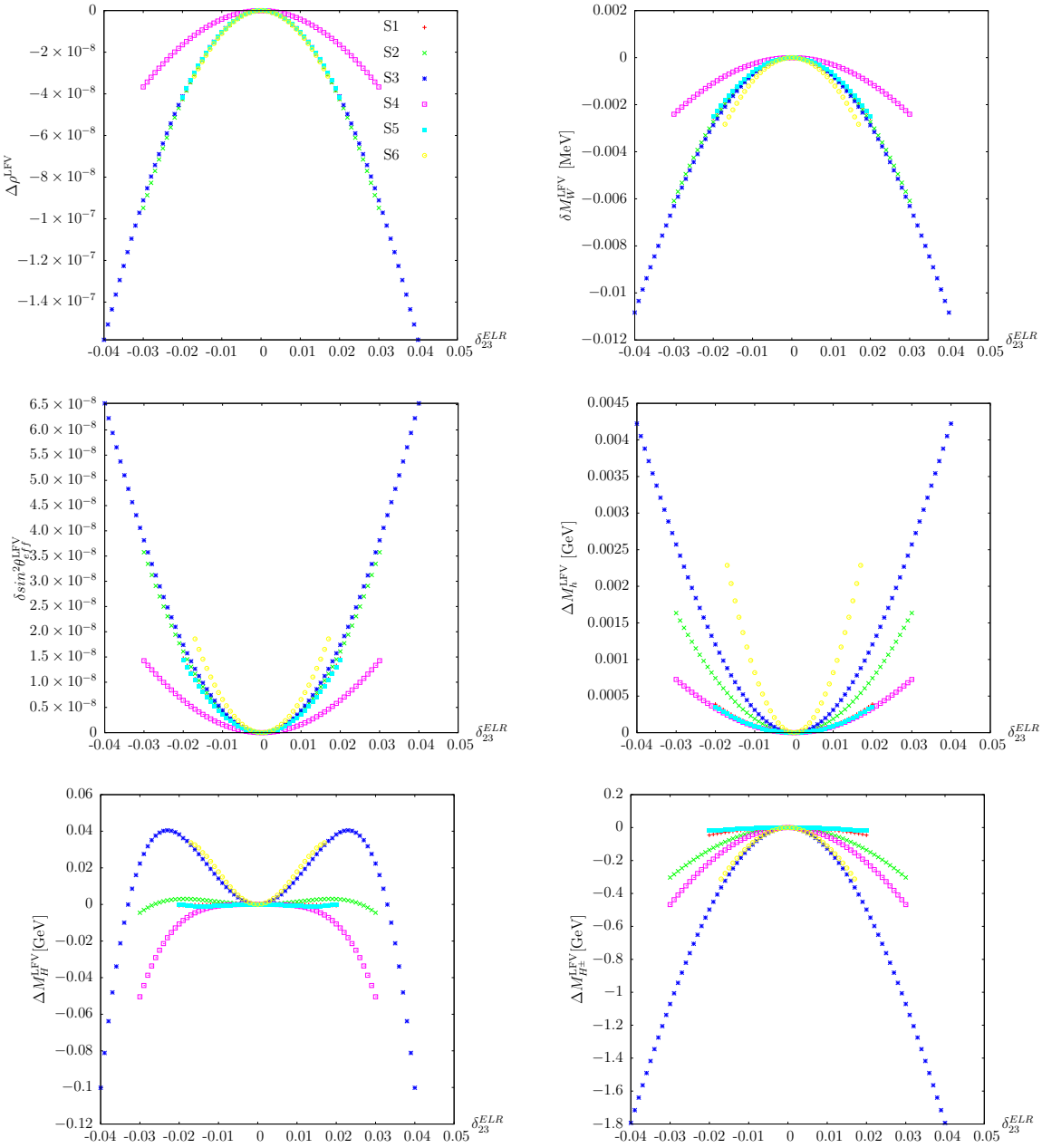

Figure 5.4: EWPO and Higgs masses as a function of δ_{23}^{ELR}.

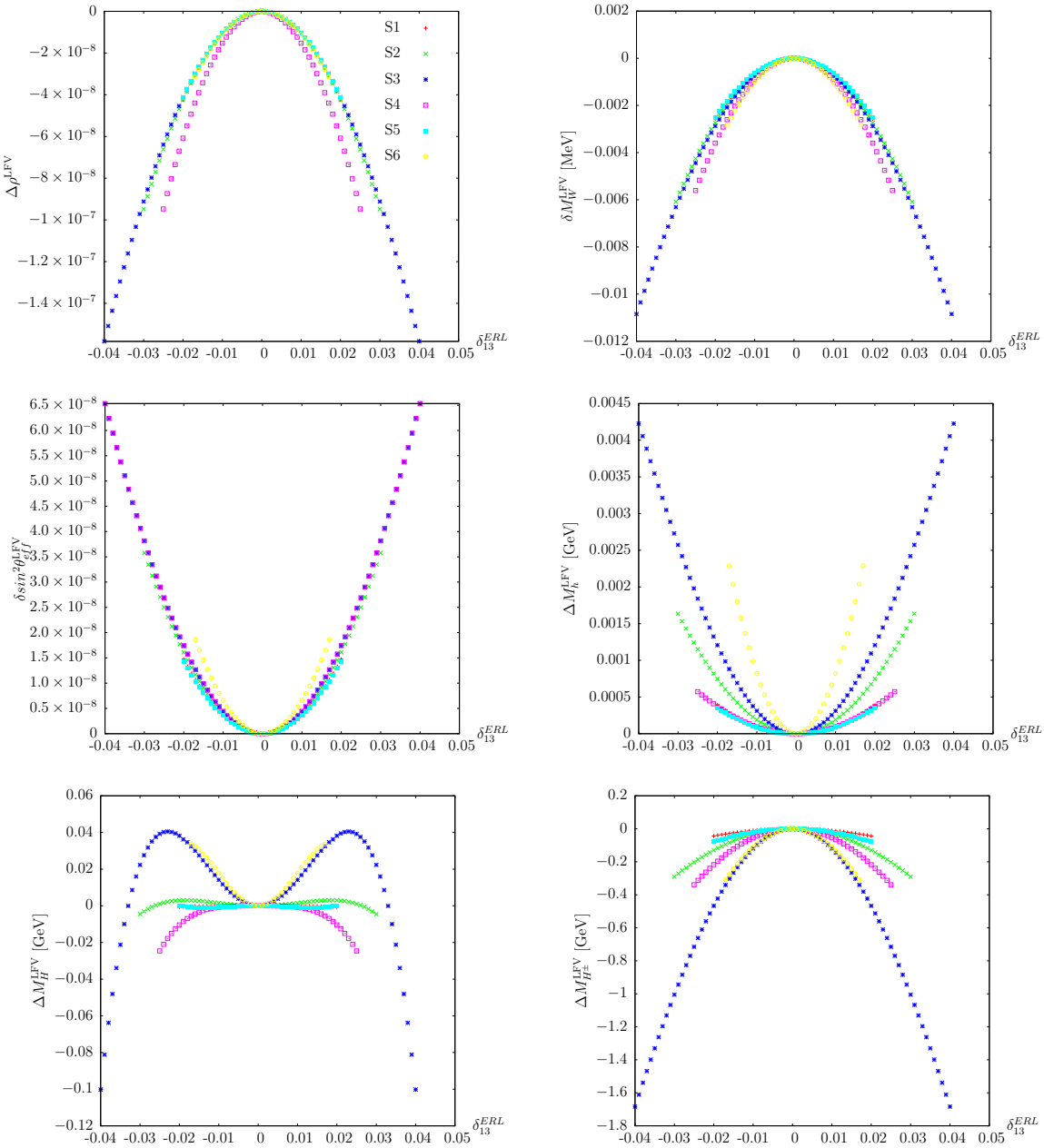

Figure 5.5: EWPO and Higgs masses as a function of δ_{13}^{ERL}.

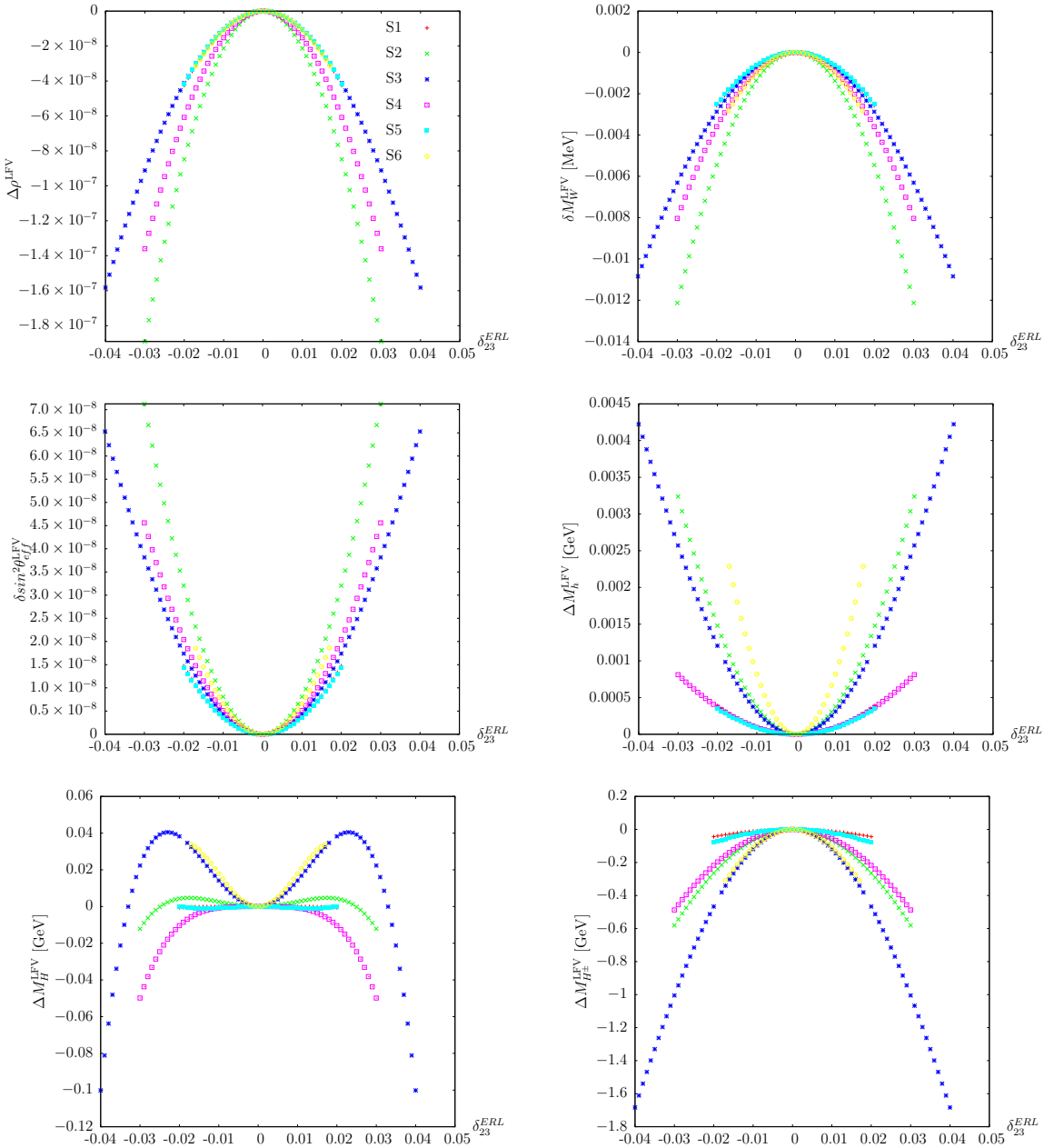

Figure 5.6: EWPO and Higgs masses as a function of δ_{23}^{ERL}.

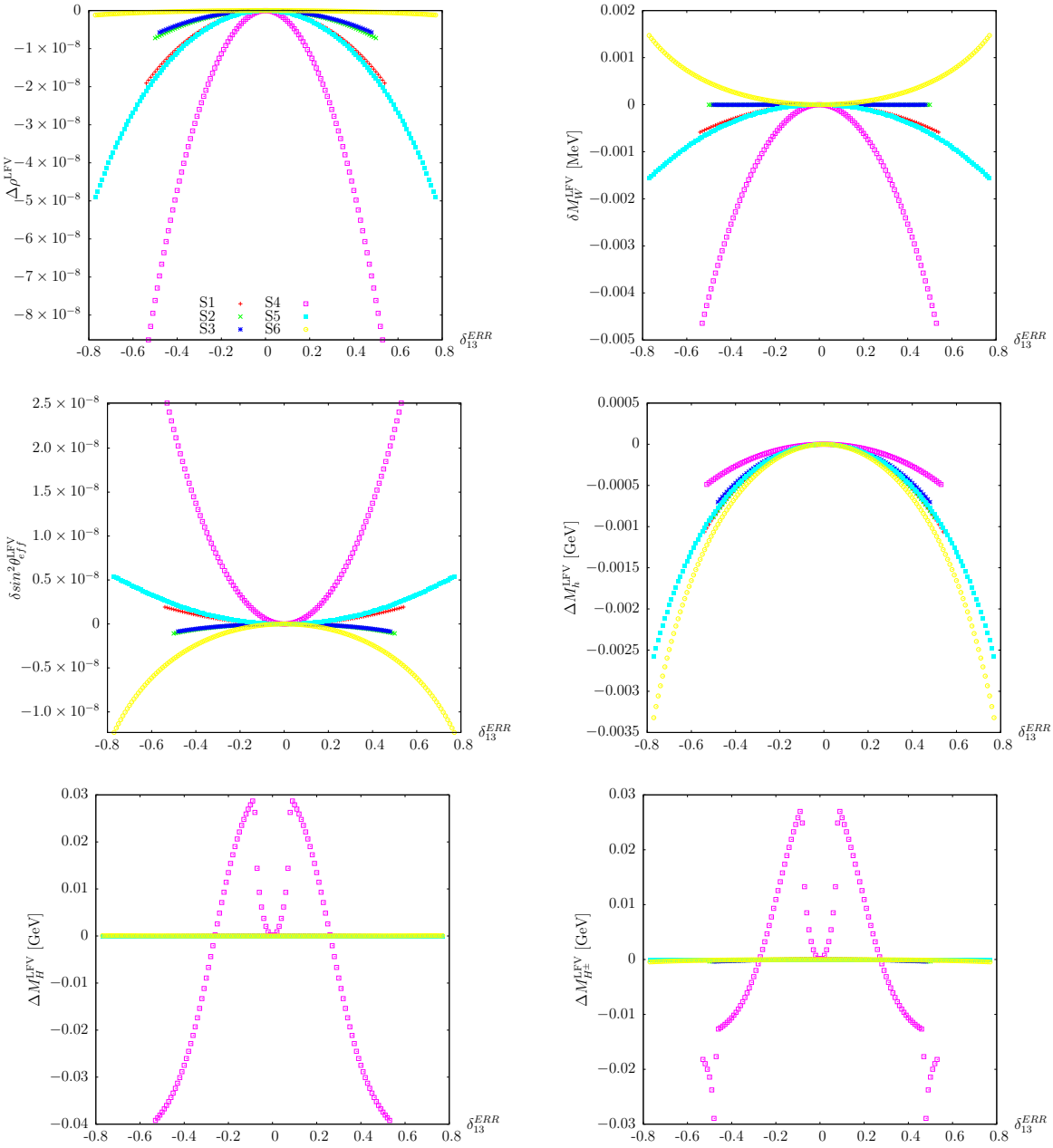

Figure 5.7: EWPO and Higgs masses as a function of δ_{13}^{ERR}.

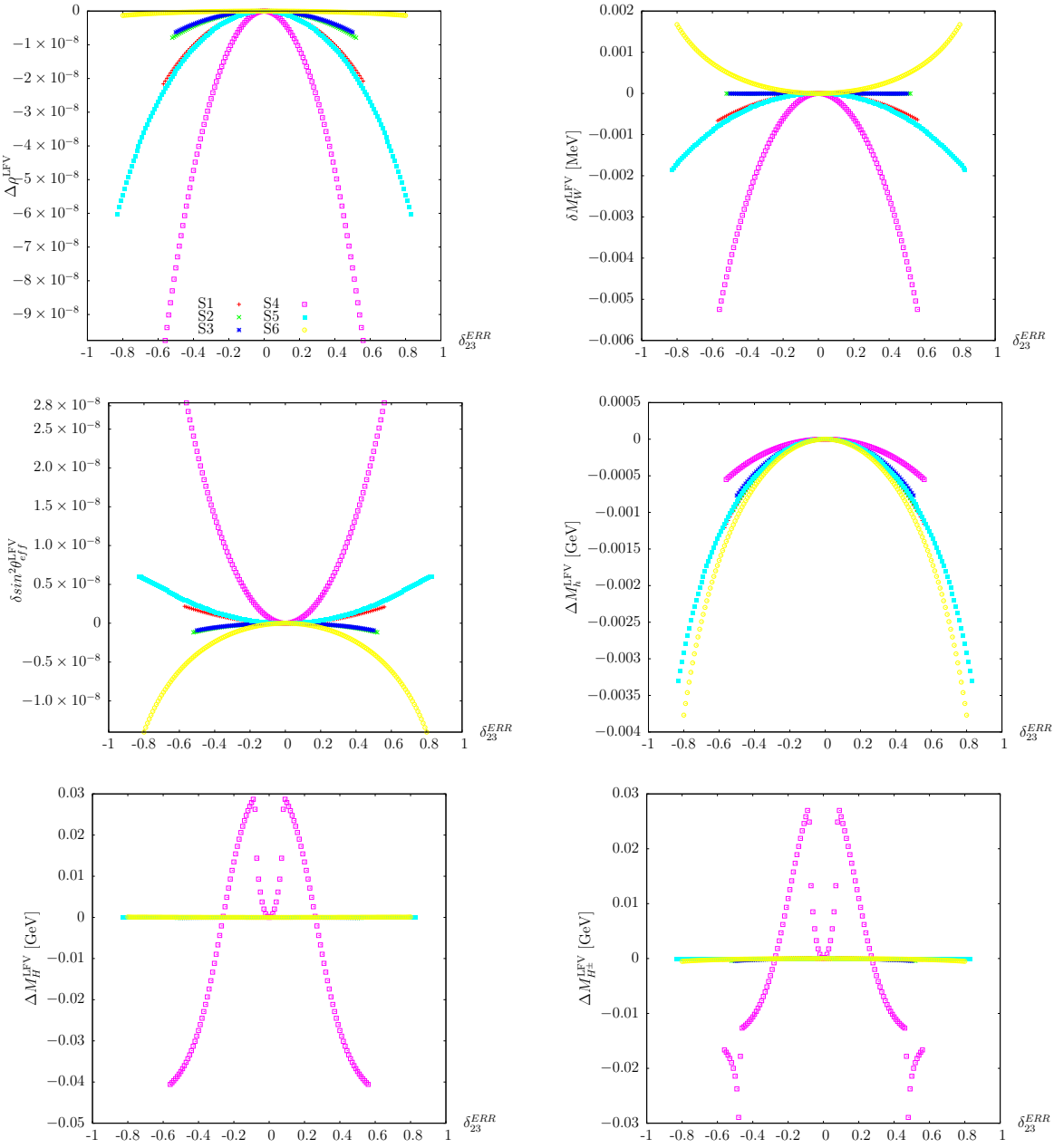

Figure 5.8: EWPO and Higgs masses as a function of δ_{23}^{ERR}.

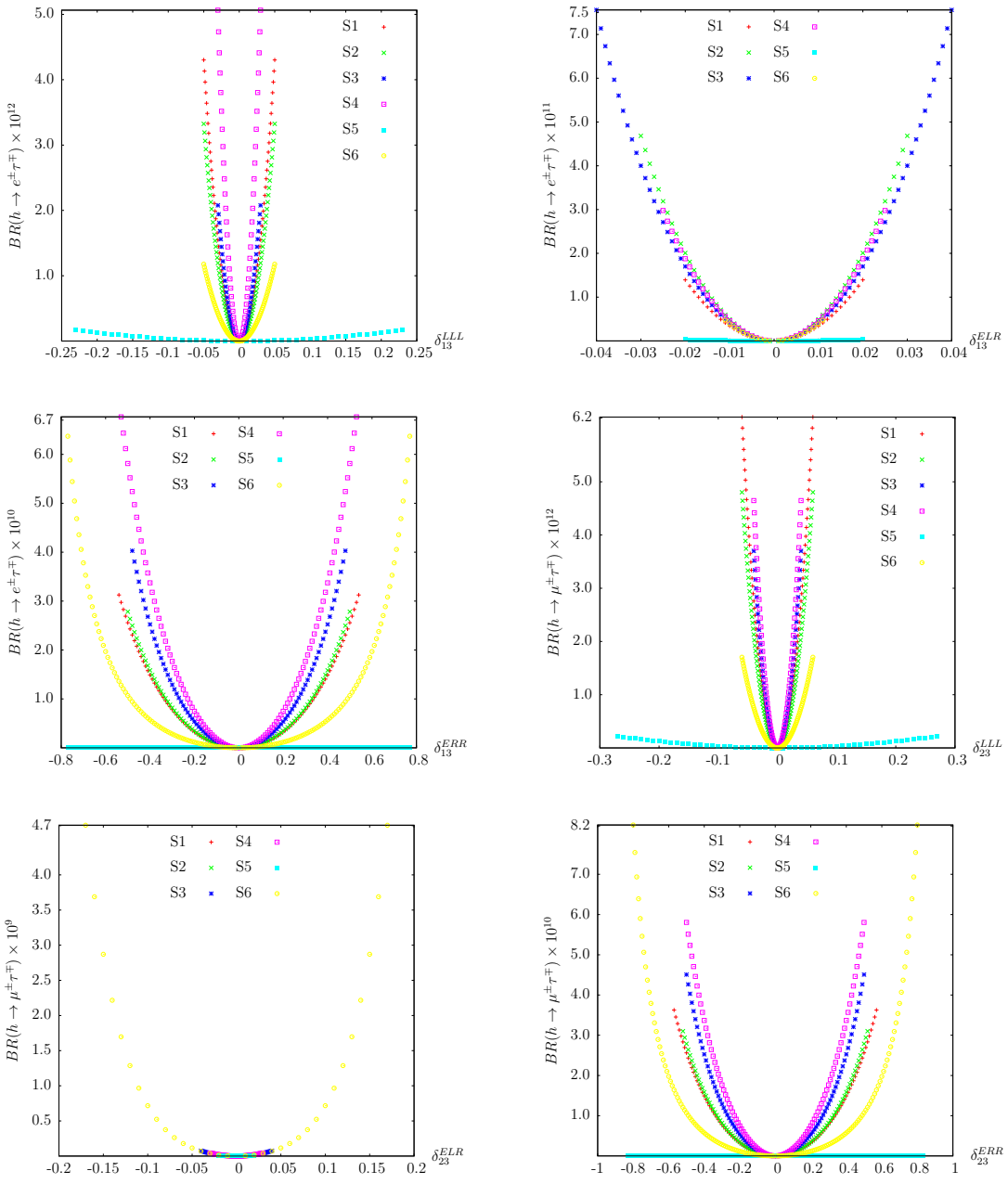

Figure 5.9: Lepton flavor violating decays $h \to e\tau$ and $h \to \mu\tau$ as a function of slepton mixing δ_{ij}^{AB} for the six points defined in the Tab. 4.1.

Chapter 6

Flavor Mixing Effects in MFV CMSSM & its Seesaw Extension

After presenting the MI analysis in the previous chapters, here we will investigate the predictions for off-diagonal sfermion SSB mass terms and flavor mixing effects in the CMSSM and CMSSM-seesaw I.

This work is motivated by the fact that in many analyses of the CMSSM, or extensions such as the NUHM1 or NUHM2 (see Ref. [18] and references therein), the hypothesis of MFV has been used, and it has been assumed that the contributions coming from MFV are negligible not only for FCNC processes but for other observables like EWPO and Higgs masses as well, see, e.g., Ref. [19]. In this chapter we will analyze whether this assumption is justified, and whether including these MFV effects could lead to additional constraints on the CMSSM parameter space. In this respect we evaluate in the CMSSM and in the CMSSM-seesaw I the following set of observables:

- BPO, in particular BR($B \to X_s\gamma$), BR($B_s \to \mu^+\mu^-$) and ΔM_{B_s},
- EWPO, in particular M_W and the effective weak leptonic mixing angle, $\sin^2\theta_{\text{eff}}$,
- the masses of the neutral and charged Higgs bosons in the MSSM,
- QFVHD in particular $h \to \bar{b}s + b\bar{s}$,
- cLFV decays in particular $\mu \to e\gamma$, $\tau \to e\gamma$, $\tau \to \mu\gamma$ as well as
- LFVHD in particular $h \to e^\pm\mu^\mp$, $h \to e^\pm\tau^\mp$ and $h \to \mu^\pm\tau^\mp$.

In order to perform our calculations, we used `SPheno` [153] to generate the CMSSM (containing also the type I seesaw) particle spectrum by running RGE from the GUT down to the EW scale. The particle spectrum was handed over in the form of an SLHA file [154] to `FeynHiggs` [68, 77, 97, 121, 122] to calculate EWPO and Higgs boson masses. The BPO were calculated by the `BPHYSICS` subroutine included in the SuFla code [103] (see also Refs. [98, 99] for the improved version used here). QFVHD and LFVHD were calculated using `FeynArts`/`FormCalc` setup whereas cLFV decays were calculated with

SPheno 3.2.4. The following section describes the details of our computational setup. The results presented in this chapter were published in [155].

6.1 Computational setup

The SUSY spectra have been generated with the code SPheno 3.2.4 [153] (for the CMSSM and the CMSSM-seesaw I). We defined the SLHA [154] file at the GUT scale. In a first step within SPheno, gauge and Yukawa couplings at M_Z scale are calculated using tree-level formulas. Fermion masses, the Z boson pole mass, the fine structure constant α, the Fermi constant G_F and the strong coupling constant $\alpha_s(M_Z)$ are used as input parameters. The gauge and Yukawa couplings, calculated at M_Z, are then used as input for the one-loop RGE's to obtain the corresponding values at the GUT scale which is calculated from the requirement that $g_1 = g_2$. The CMSSM boundary conditions are then applied to the complete set of two-loop RGE's and are evolved to the EW scale. At this point the SM and SUSY radiative corrections are applied to the gauge and Yukawa couplings, and the two-loop RGE's are again evolved to GUT scale. After applying the CMSSM boundary conditions again the two-loop RGE's are run down to EW scale to get SUSY spectrum. This procedure is iterated until the required precision is achieved. The output is then written in the form of an SLHA, file which is used as input to calculate low energy observables discussed below.

For our scans of the CMSSM-seesaw I parameter space we use SPheno 3.2.4 [153] with the model "see-saw type-I" and apply a similar procedure to that in the CMSSM case. The neutrino related input parameters are included in the respective SLHA input blocks (see Ref. [154] for details). The predictions for BR($l_i \to l_j \gamma$) are also obtained with SPheno 3.2.4, see the discussion in Sect. 6.4. We checked that the use of this code produces results similar to the ones obtained by our private codes used in Ref. [54].

6.2 Input parameters

In order to get an overview about the size of the effects in the CMSSM parameter space, the relevant parameters m_0, $m_{1/2}$ have been scanned as, or in case of A_0 and $\tan\beta$ have been set to all combinations of

$$m_0 = 500 \text{ GeV} \ldots 5000 \text{ GeV} , \tag{6.1}$$

$$m_{1/2} = 1000 \text{ GeV} \ldots 3000 \text{ GeV} , \tag{6.2}$$

$$A_0 = -3000, -2000, -1000, 0 \text{ GeV} , \tag{6.3}$$

$$\tan\beta = 10, 20, 35, 45 , \tag{6.4}$$

with $\mu > 0$. Primarily we are not interested in the absolute values for EWPO BPO and Higgs masses but the effects that comes from flavor violation within the MFV framework, i.e. the effect from the off-diagonal entries in the sfermion mass matrices. We first calculate the low-energy observables by setting all $\delta_{ij}^{FAB} = 0$ by hand. In a

second step we evaluate the observables with the values of δ_{ij}^{FAB} obtained through RGE running. We then evaluate the "pure MFV effects",

$$\Delta\mathrm{BR}^{\mathrm{MFV}}(B \to X_s\gamma) = \mathrm{BR}(B \to X_s\gamma) - \mathrm{BR}^{\mathrm{MSSM}}(B \to X_s\gamma) \,, \tag{6.5}$$

$$\Delta\mathrm{BR}^{\mathrm{MFV}}(B_s \to \mu^+\mu^-) = \mathrm{BR}(B_s \to \mu^+\mu^-) - \mathrm{BR}^{\mathrm{MSSM}}(B_s \to \mu^+\mu^-) \,, \tag{6.6}$$

$$\Delta M_{B_s}^{\mathrm{MFV}} = \Delta M_{B_s} - \Delta M_{B_s}^{\mathrm{MSSM}} \,, \tag{6.7}$$

where $\mathrm{BR}^{\mathrm{MSSM}}(B \to X_s\gamma)$, $\mathrm{BR}^{\mathrm{MSSM}}(B_s \to \mu^+\mu^-)$ and $\Delta M_{B_S}^{\mathrm{MSSM}}$ corresponds to the values of relevant observables with all $\delta_{ij}^{FAB} = 0$. Furthermore we define

$$\Delta M_h^{\mathrm{MFV}} = M_h - M_h^{\mathrm{MSSM}} \tag{6.8}$$

$$\Delta M_H^{\mathrm{MFV}} = M_H - M_H^{\mathrm{MSSM}} \tag{6.9}$$

$$\Delta M_{H^\pm}^{\mathrm{MFV}} = M_{H^\pm} - M_{H^\pm}^{\mathrm{MSSM}} \tag{6.10}$$

where M_h^{MSSM}, M_H^{MSSM} and $M_{H^\pm}^{\mathrm{MSSM}}$ corresponds to the Higgs masses with all $\delta_{ij}^{FAB} = 0$. Similarly we define for the EWPO

$$\Delta\rho^{\mathrm{MFV}} = \Delta\rho - \Delta\rho^{\mathrm{MSSM}} \tag{6.11}$$

$$\Delta M_W^{\mathrm{MFV}} = M_W - M_W^{\mathrm{MSSM}} \tag{6.12}$$

$$\Delta \sin^2\theta_{\mathrm{eff}}^{\mathrm{MFV}} = \sin^2\theta_{\mathrm{eff}} - \sin^2\theta_{\mathrm{eff}}^{\mathrm{MSSM}} \tag{6.13}$$

where $\Delta\rho^{\mathrm{MSSM}}$, M_W^{MSSM} and $\sin^2\theta_{\mathrm{eff}}^{\mathrm{MSSM}}$ are the values of the relavant observables with all $\delta_{ij}^{FAB} = 0$.

6.3 Effects of squark mixing in the CMSSM

In this section we analyze the effects from RGE induced flavor violating mixing in the scalar quark sector in the CMSSM (i.e. with no mixing in the slepton sector). The RGE running from the GUT scale to the EW has been performed as described in Sect. 6.1, with the subsequent evaluation of the low-energy observables as discussed in Chap: 3.

In Figs. 6.1-6.8 we show the results of our CMSSM analysis in the m_0–$m_{1/2}$ plane for four different combinations of $\tan\beta = 10, 45$ (left and right column) and $A_0 = 0, -3000$ GeV (upper and lower row). This set represents four "extreme" cases of the parameter space and give an overview about the possible sizes of the effects and their dependences on $\tan\beta$ and A_0 (which we verified with other, not shown, combinations).

6.3.1 Squark δ_{ij}^{FAB}'s

We start with the three most relevant δ_{ij}^{FAB}'s. In Figs. 6.1-6.3 we show the results for δ_{13}^{QLL}, δ_{23}^{QLL} and δ_{23}^{ULR}, respectively, which are expected to yield the largest results. The values show the expected pattern of their size with $\delta_{23}^{QLL} \sim \mathcal{O}(10^{-2})$ being the largest one, and δ_{13}^{QLL} and δ_{23}^{ULR} about one or two orders of magnitude smaller. All other δ_{ij}^{FAB}

which are not shown reach only values of $\mathcal{O}(10^{-5})$. One can observe an interesting pattern in these figures: the values of δ_{ij}^{FAB} increase with larger values of either $\tan\beta$ or A_0. The values for δ^{QLL} increase with m_0, whereas the δ^{ULR} and δ^{DLR} decrease with m_0. This behavior can be understood for the RGE's of the non diagonal SUSY breaking parameters (see, e.g., Ref. [156]), δ^{QLL}'s are defined as ratios of off-diagonal soft terms that grow with m_0^2 over diagonal soft masses that also grow with m_0. However, δ^{ULR}'s and δ^{DLR}'s arises from the ratio of the RGE generated off-diagonal trilinear terms which depend on the value of A_0, that is considered fixed in our case, over m_0 growing diagonal soft masses. As discussed above, these $\delta_{ij}^{FAB} \neq 0$ are often neglected in phenomenological analyses of the CMSSM (see, e.g., Ref. [19]). We also emphasize that these effects are purely due to the presenece of the CKM matrix on the RGE's, their contribution will vanish when the mixing of the two first generation with the third generation is neglected (as we have checked numerically).

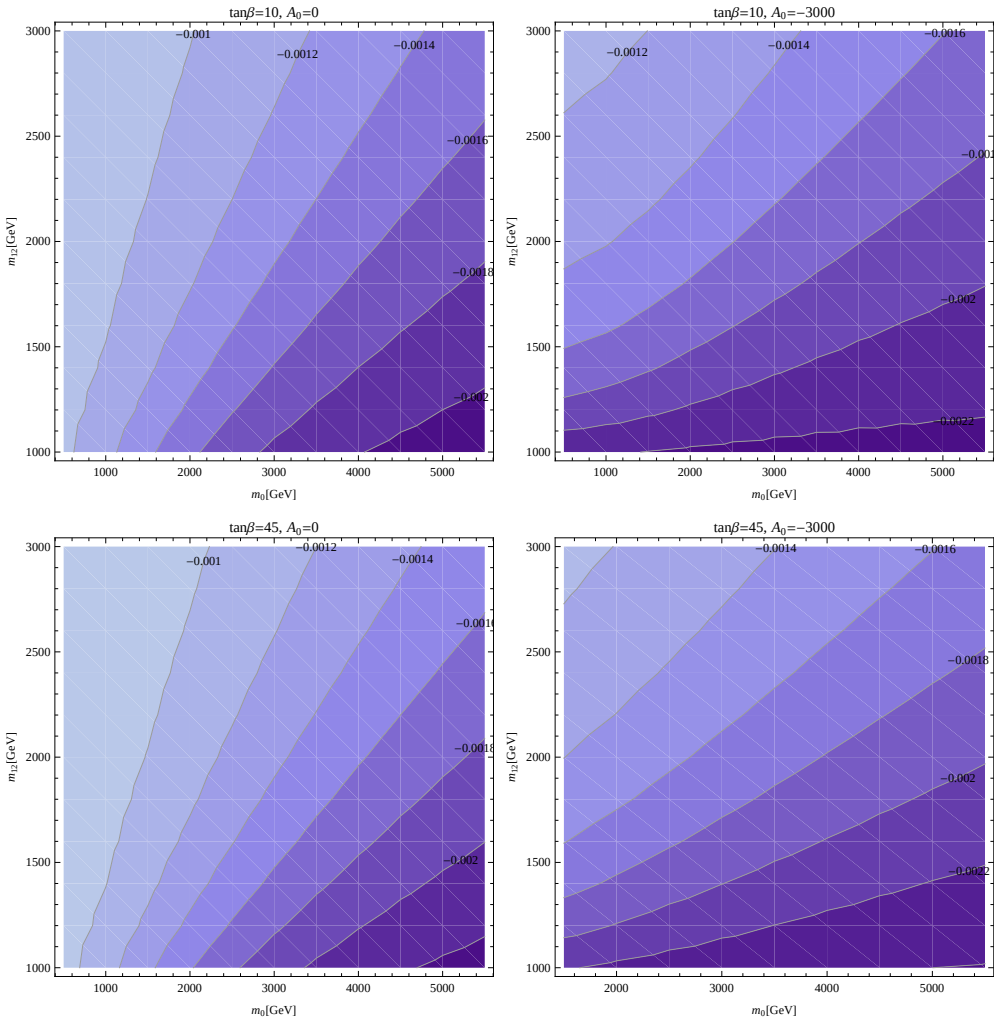

Figure 6.1: Contours of δ_{13}^{QLL} in the m_0–$m_{1/2}$ plane for different values of $\tan\beta$ and A_0 in the CMSSM.

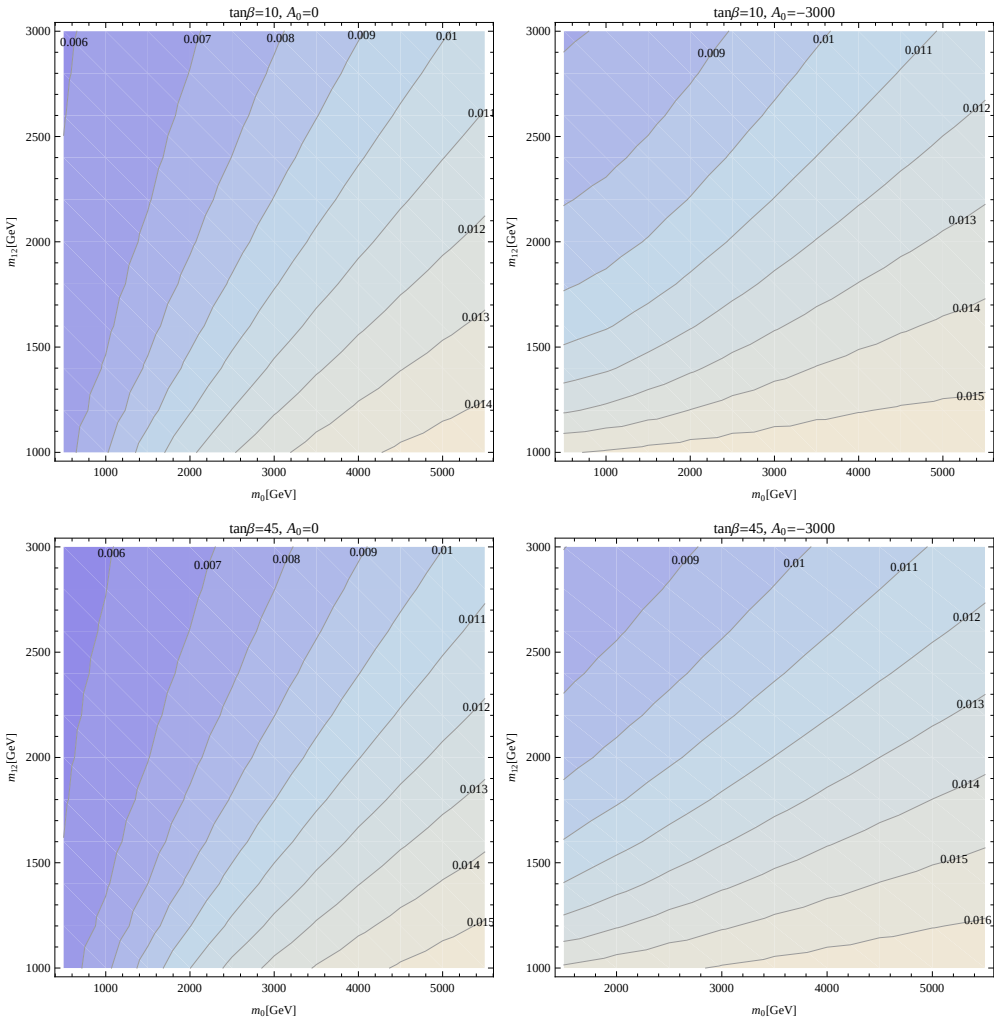

Figure 6.2: Contours of δ_{23}^{QLL} in the m_0–$m_{1/2}$ plane for different values of $\tan\beta$ and A_0 in the CMSSM.

6.3.2 EWPO

In Figs. 6.4-6.6 we analyze the effects of the non-zero δ_{ij}^{FAB} on the EWPO $\Delta\rho^{\rm MFV}$, $\Delta M_W^{\rm MFV}$ and $\Delta\sin^2\theta_{\rm eff}^{\rm MFV}$, respectively. Here the same pattern is reflected for the EWPO, i.e. by increasing the value of $\tan\beta$ or A_0, we find larger contributions to the EWPO. In particular one can observe a non-decoupling effect for large values of m_0. Larger soft SUSY-breaking parameters with the non-zero values in particular of δ_{23}^{QLL}, see above, lead to an enhanced splitting in masses belonging to an $SU(2)$ doublet, and thus to an enhanced contribution to the ρ-parameter. The corresponding effects on M_W and $\sin^2\theta_{\rm eff}$, for $m_0 \gtrsim 3$ TeV, exhibit corrections that are several times larger than the current experimental accuracy (whereas the SUSY corrections with all $\delta_{ij}^{FAB} = 0$ decouple and go to zero). Consequently, including the non-zero values of the δ_{ij}^{FAB} and correctly taking

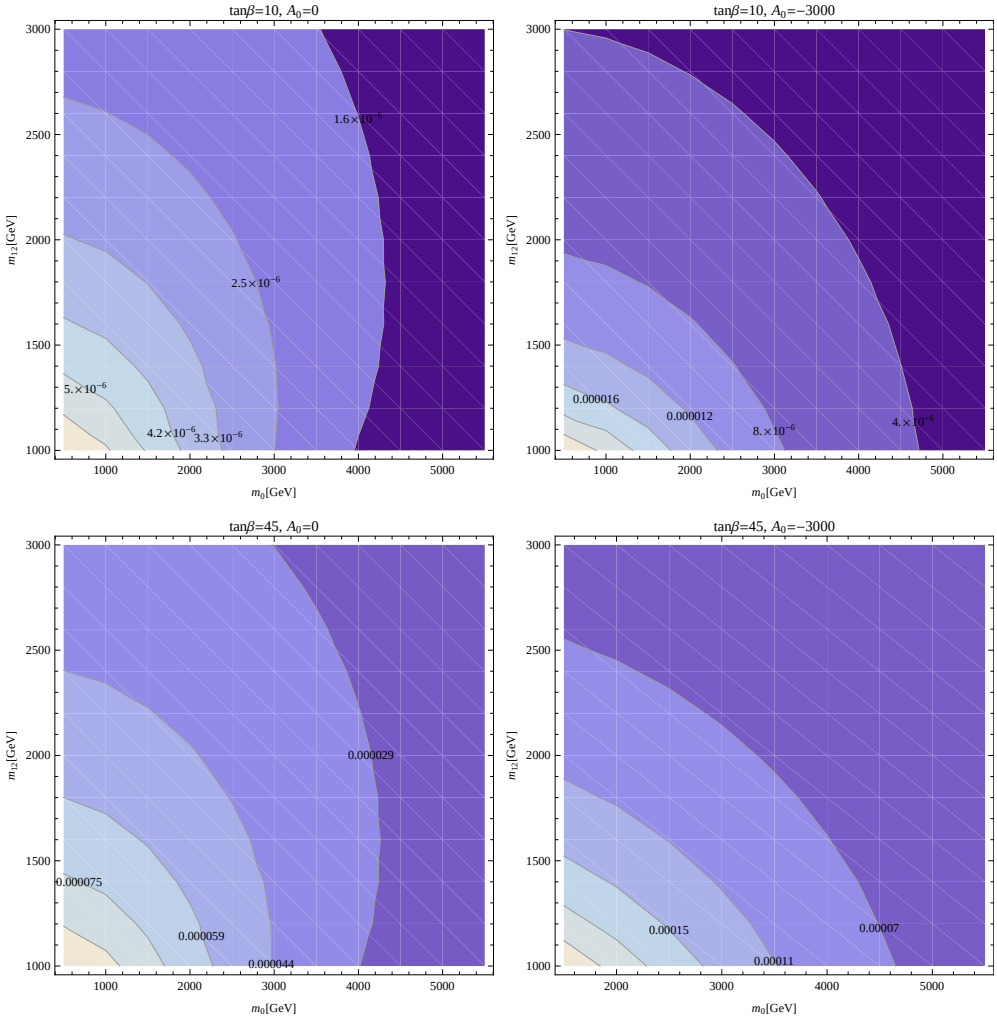

Figure 6.3: Contours of δ_{23}^{ULR} in the m_0–$m_{1/2}$ plane for different values of $\tan\beta$ and A_0 in the CMSSM.

these corrections into account, would yield an *upper* limit on m_0, which in the known analyses so far is unconstrained from above [19]. A more detailed analysis within the CMSSM will be needed to determine the real upper bound on m_0, which, however, is beyond the scope of this thesis.

In order to gain more insight about the source of the large corrections to $\Delta\rho$ (and thus to the EWPO), we show in Fig. 6.7 several relative mass (square) differences, $(m_2^2 - m_1^2)/(m_2^2 + m_1^2)$ in the m_0–$m_{1/2}$ plane for fixed $A_0 = 0$ and $\tan\beta = 45$. The left plot shows the mass difference for the two most stop-like squarks (i.e. in the limit of zero inter-generational mixing they coincide with the two scalar tops). The right plot shows the relative mass difference for the lightest most stop-like and most sbottom-like squark. (These results are simply the `Spheno` output in our scenario.) In both cases one can see that the relative mass differences increase (controlled by the non-zero δ_{ij}^{FAB} induced by the CKM matrix in the RGE running) in a fashion similar as the δ^{QLL} discussed

above, i.e. in particular for $m_0 > m_{1/2} > 1$ TeV. These increasing mass differences lead (together with contributions from the mixing matrices) to the observed increase of $\Delta\rho$ as in Fig. 6.4.

Our findings can be briefly compared to the existing literature. The EWPO in the context of flavor violation were evaluated first in Ref. [62], where correspondingly large corrections were found for large δ_{23}^{QLL} (in fact, that was the only parameter dependence analyzed in that paper, and only the mixing between the second and third generation of squarks was taken into account). Subsequently, the EWPO were also evaluated for the full three-generation mixing in Ref. [157]. The numerical analysis, however, was restricted to a degenerate and fixed SUSY mass scale. Correspondingly, no large effects with increasing SUSY mass scales were analyzed and only relative small corrections were found. Due to the different numerical set-up, however, there is no contradiction with our results for $\Delta\rho$.

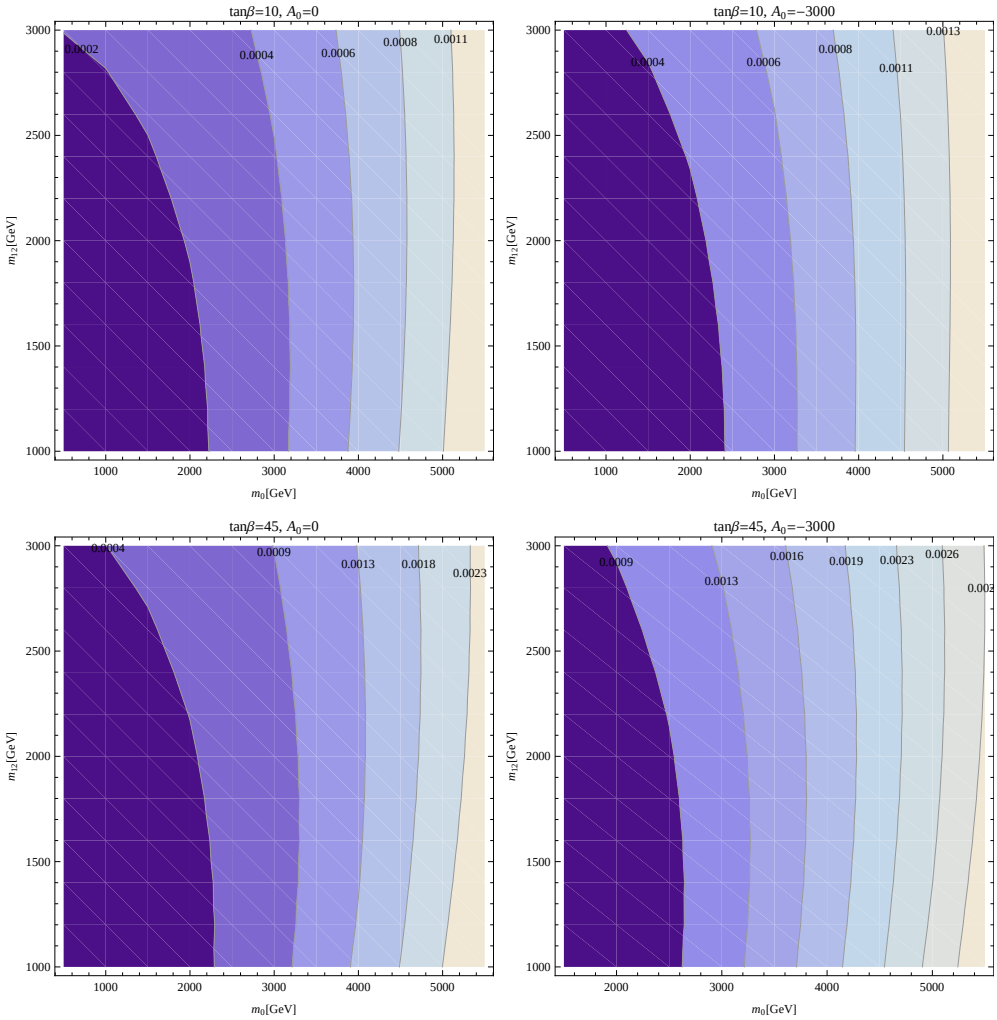

Figure 6.4: Contours of $\Delta\rho^{\mathrm{MFV}}$ in the m_0–$m_{1/2}$ plane for different values of $\tan\beta$ and A_0 in the CMSSM.

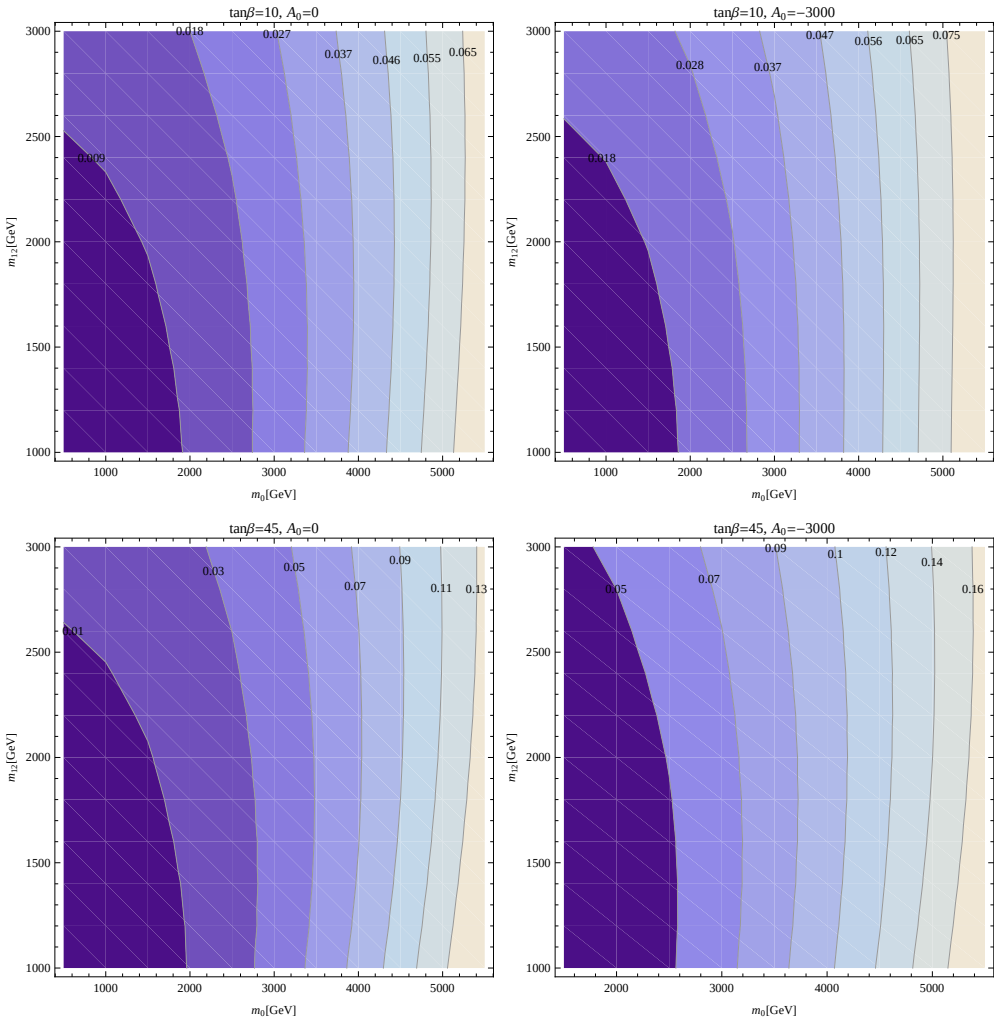

Figure 6.5: Contours of $\Delta M_W^{\rm MFV}$ in GeV in the m_0–$m_{1/2}$ plane for different values of $\tan\beta$ and A_0 in the CMSSM.

6.3.3 Higgs masses and the BPO

In Fig. 6.8 we show the results of our CMSSM analysis with the effects of the non-zero δ_{ij}^{FAB} on the Higgs mass calculations and on the BPO in the m_0–$m_{1/2}$ plane for $\tan\beta = 45$ and $A_0 = -3000$. We only show this "extreme" case, where smaller values of $\tan\beta$ and A_0 would lead to smaller effects. In the upper left, upper right and middle left plot we show $\Delta M_h^{\rm MFV}$, $\Delta M_H^{\rm MFV}$ and $\Delta M_{H^\pm}^{\rm MFV}$, respectively. It can be seen that the effects on the neutral Higgs boson masses are negligible w.r.t. the experimental accuracy. The effects on $M_{H^\pm}$ can reach $\mathcal{O}(100$ MeV), where largest effects are found for both very small values of m_0 and $m_{1/2}$ (dominated by δ_{23}^{ULR}) or very large values of m_0 and $m_{1/2}$ (dominated by $\delta_{13,23}^{QLL}$). Corrections of up to -300 MeV are found, but still remaining below the foreseeable future precision. Consequently, also in the Higgs mass evaluation

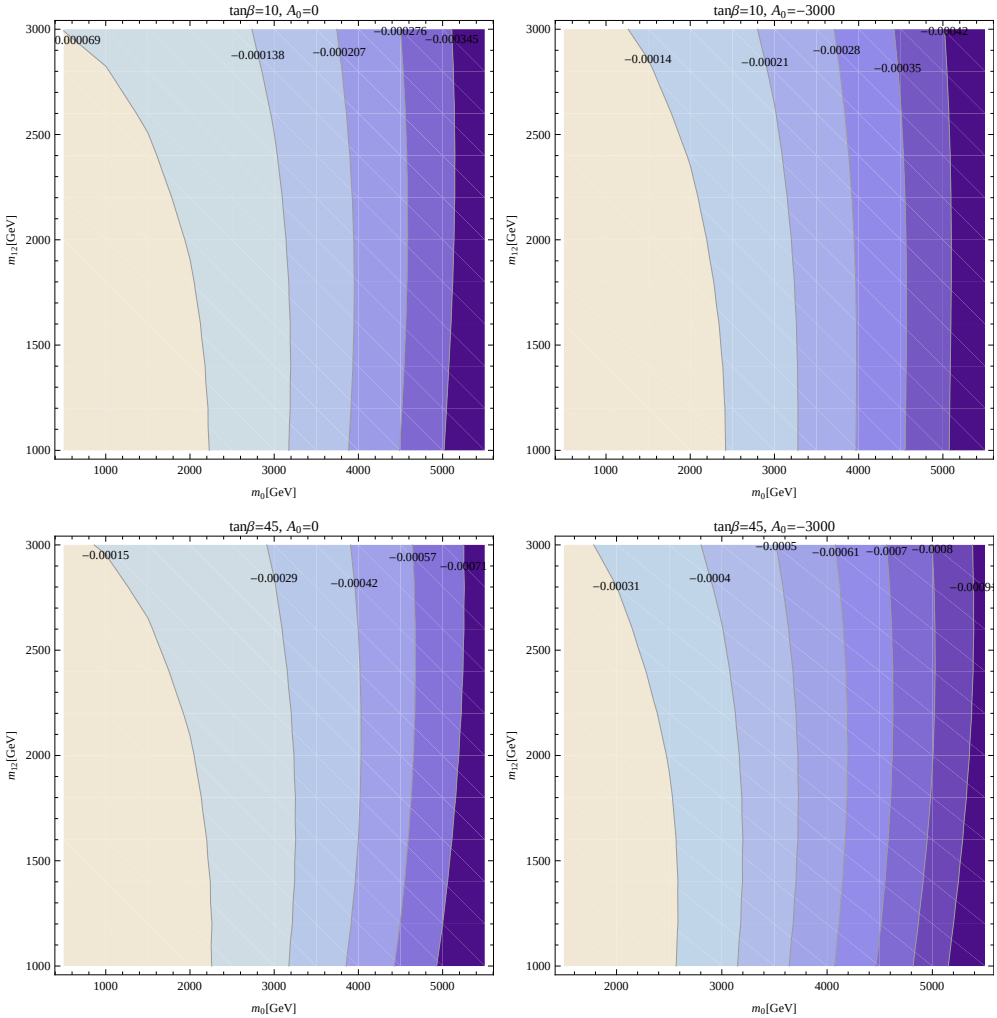

Figure 6.6: Contours of $\Delta \sin^2 \theta_{\text{eff}}^{\text{MFV}}$ in the m_0–$m_{1/2}$ plane for different values of $\tan\beta$ and A_0 in the CMSSM.

not taking into account the non-zero values of the δ_{ij}^{FAB} is a good approximation. In the middle right, lower left and lower right plot of Fig. 6.8 we show the results for the BPO $\Delta\text{BR}^{\text{MFV}}(B \to X_s\gamma)$, $\Delta\text{BR}^{\text{MFV}}(B_s \to \mu^+\mu^-)$ and $\Delta M_{B_s}^{\text{MFV}}$, respectively. The effects in $\Delta\text{BR}^{\text{MFV}}(B \to X_s\gamma)$ are of $\mathcal{O}(-10^{-5})$ and thus one order of magnitude smaller than the experimenal accuracay. Similarly, we find $\Delta\text{BR}^{\text{MFV}}(B_s \to \mu^+\mu^-) \sim \mathcal{O}(10^{-10})$ and $\Delta M_{B_s}^{\text{MFV}} \sim \mathcal{O}(10^{-15}\text{ GeV})$, i.e. one or several orders of magnitude below the experimental precision. This shows that for the BPO neglecting the effects of non-zero δ_{ij}^{FAB} in the CMSSM is a good approximation.

6.3.4 $\text{BR}(h \to \bar{b}s + b\bar{s})$

The results are shown in Fig. 6.9, where we display the contours of $\text{BR}(h \to \bar{b}s + b\bar{s})$ in the $(m_0, m_{1/2})$ plane for $\tan\beta = 10$, $A_0 = 0$ (upper left), $\tan\beta = 10$, $A_0 = -3000$ GeV (upper right), $\tan\beta = 45$, $A_0 = 0$ (lower left) and $\tan\beta = 45$, $A_0 = -3000$ GeV (lower

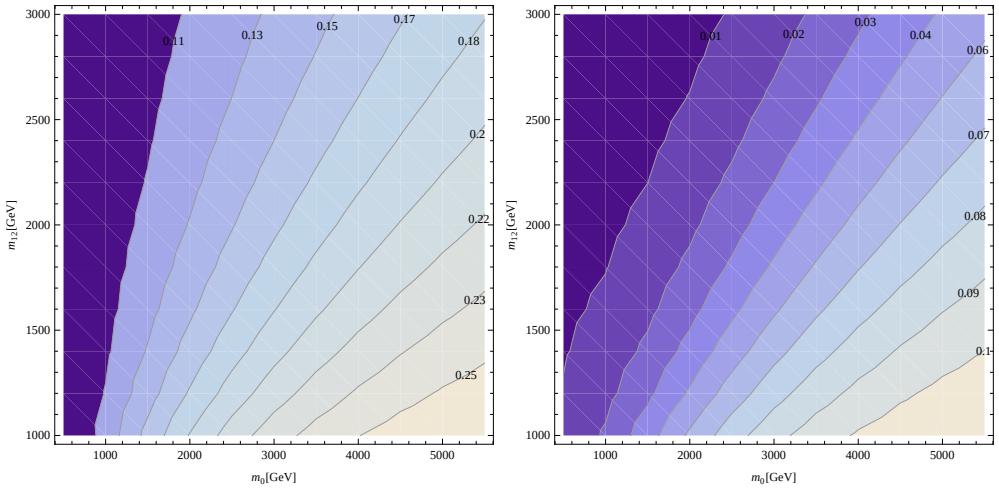

Figure 6.7: Contours of $(m_2^2 - m_1^2)/(m_2^2 + m_1^2)$ in the m_0–$m_{1/2}$ plane for fixed values of $A_0 = 0$ and $\tan\beta = 45$. Left: the two most stop-like squarks (i.e. in the limit of zero inter-generational mixing they coincide with the two scalar tops), right: the lightest most stop-like and most sbottom-like squarks (see text).

right). By comparison with planes for other $\tan\beta$-A_0 combinations we have varyfied that these four planes constitute a representative example. The allowed parameter space can be deduced by comparing to the results presented above and in Refs. [158]. While not all the planes are in agreement with current constraints, large parts, in particular for larger values of m_0 and $m_{1/2}$ are compatible with a combination of direct searches, flavor and electroweak precision observables as well as astrophysical data. Upper bounds on m_0 at the few TeV level could possibly be set by including the findings of Sect. 6.3.2 into a global CMSSM analysis.

In Fig. 6.9 one can see that for most of parameter space values of $\mathcal{O}(10^{-7})$ are found for $\mathrm{BR}(h \to \bar{b}s + b\bar{s})$, i.e. outside the reach of current or future collider experiments. Even for the "most extreme" set of parameters we have analyzed, $\tan\beta = 45$ and $A_0 = -3000$ GeV, no detectable rate has been found. Turning the argument around, any observation of the decay $h \to \bar{b}s + b\bar{s}$ at the (discussed) future experiments would exclude the CMSSM as a possible model.

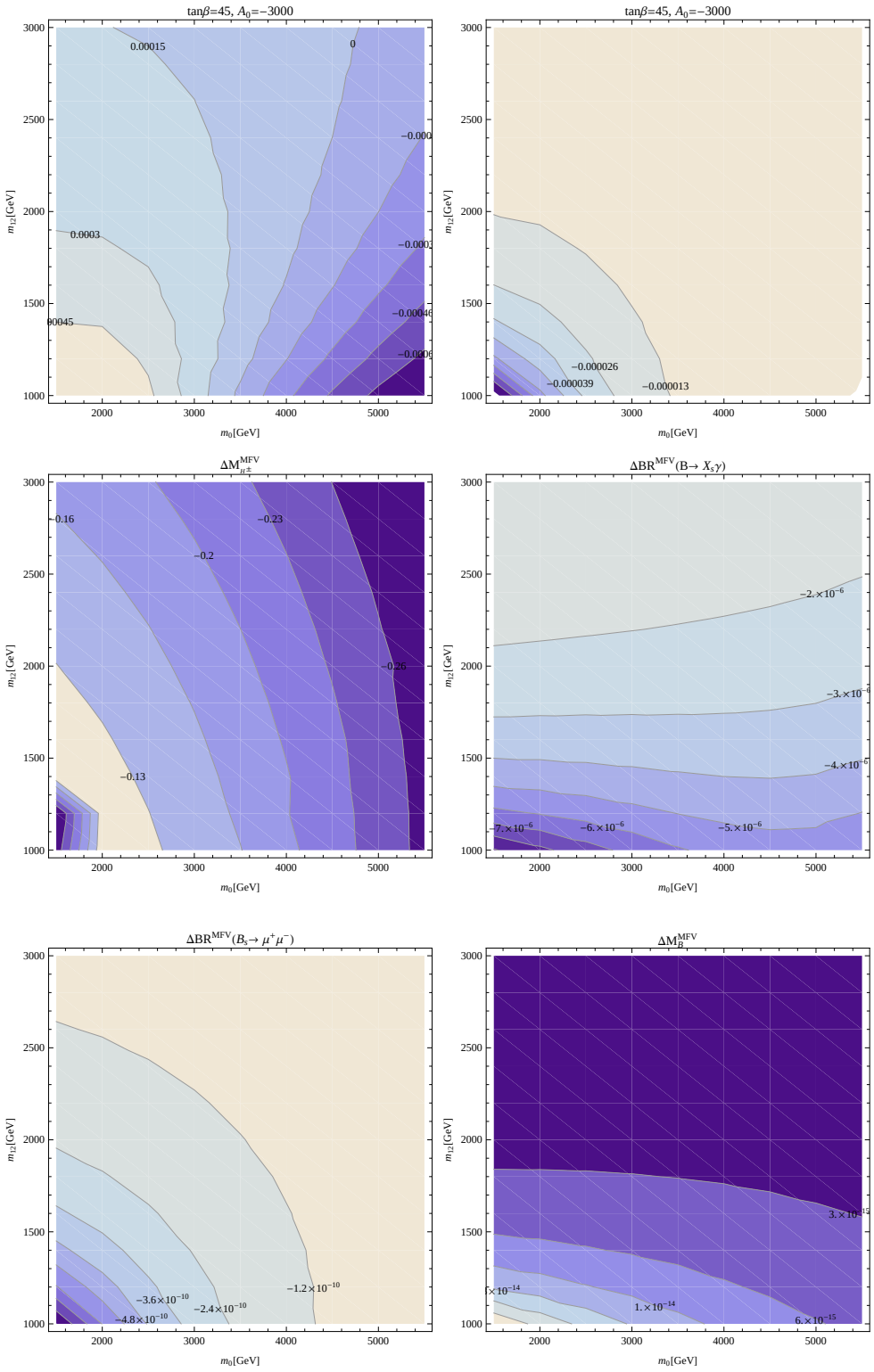

Figure 6.8: Contours of Higgs mass corrections ($\Delta M_h^{\rm MFV}$, $\Delta M_H^{\rm MFV}$ and $\Delta M_{H^\pm}^{\rm MFV}$ in GeV) and BPO ($\Delta{\rm BR}^{\rm MFV}(B \to X_s\gamma)$, $\Delta{\rm BR}^{\rm MFV}(B_s \to \mu^+\mu^-)$ and $\Delta M_{B_s}^{\rm MFV}$) in the m_0–$m_{1/2}$ plane for $\tan\beta = 45$ and $A_0 = -3000$ GeV in the CMSSM.

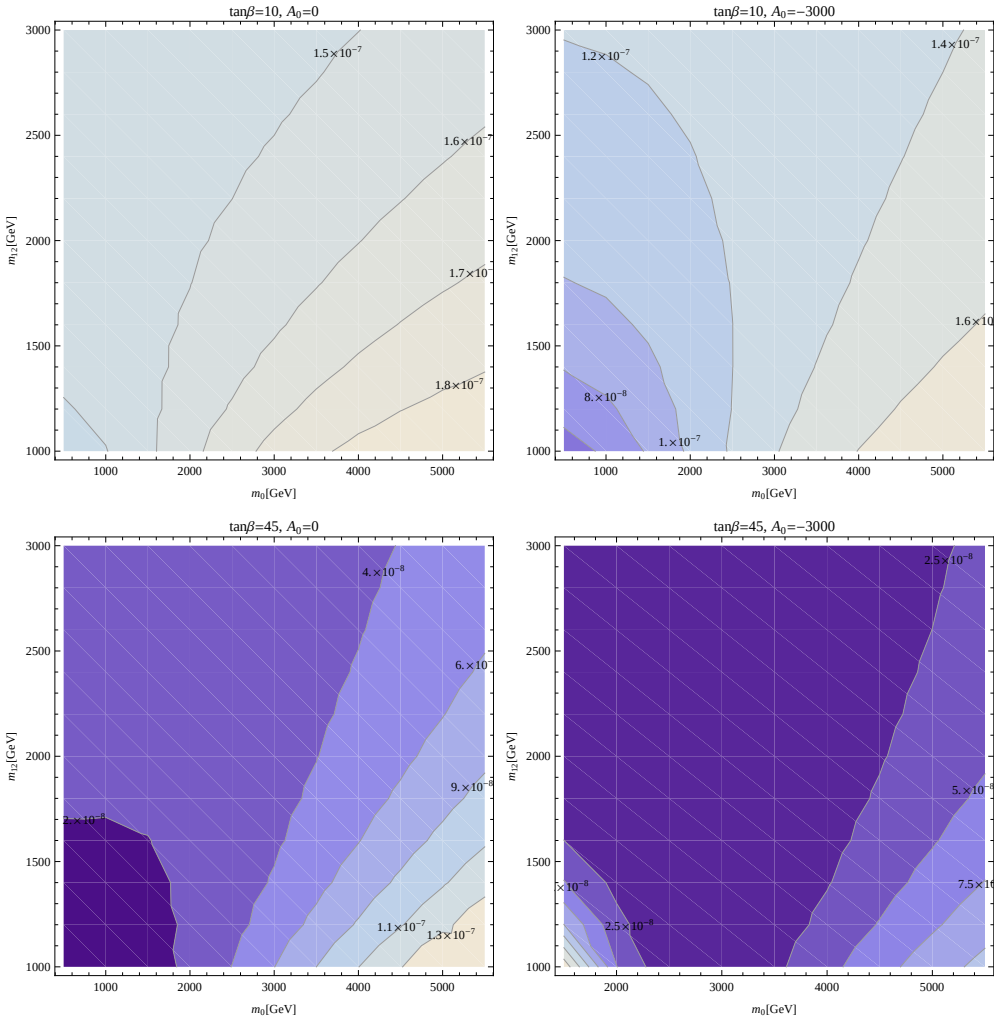

Figure 6.9: Contours of BR($h \to b\bar{s} + \bar{b}s$) in the m_0–$m_{1/2}$ plane for different values of $\tan\beta$ and A_0 in the CMSSM.

6.4 Effects of slepton mixing in CMSSM-seesaw I.

In this section we analyze the effects of non-zero δ_{ij}^{FAB} values in the CMSSM-seesaw I. In order to investigate the effects induced just by the mixings in the slepton sector, such that we can compare their contribution from the one produced by the mixings in the squak sector (and to discriminate it from effects from mixings in the squark sector) we present here the results with only δ_{ij}^{FAB} in the slepton sector non-zero, i.e. after the RGE running with both CKM and seesaw parameters non-zero, the δ_{ij}^{FAB} from the squark sector are set to zero by hand at the EW scale. The effects of the squark mixing in the CMSSM-seesaw I are nearly indistinguishable from the ones analyzed in the previous subsection.

As mentioned in Sect. 2.6.1, the calculations in this section are done by using the values of Y_ν constructed from Eq. (2.93) with degenerate M_R's. The matrix R is set to the identity since it does not enter in Eq. (2.95) and therefore the slepton δ_{ij}^{FAB}'s do not depend on it. The matrix m_ν^δ is a diagonal mass matrix adjusted to reproduce neutrino masses at low energy compatible with the experimental observations and with hierarchical neutrino masses. We performed our computation by using the seesaw scale $M_N = 10^{14}$ GeV. With this choice the bound $\mathrm{BR}(\mu \to e\gamma) < 5.7 \times 10^{-13}$ [124] imposes severe restrictions on the m_0–$m_{1/2}$ plane, excluding values of m_0 below 2–3 TeV (depending on $\tan\beta$ and A_0). The values of the slepton δ_{ij}^{FAB} will increase as the scale M_N increases but also does the parameter space excluded by the $\mathrm{BR}(\mu \to e\gamma)$ bound. For example, by increasing M_N by an order of magnitude, the largest entries in the matrix Y_ν will become of $\mathcal{O}(1)$ and the bound on $\mathrm{BR}(\mu \to e\gamma)$ will only be satisfied if $m_0 \approx 5$ TeV (see more details below).

6.4.1 Slepton δ_{ij}^{FAB}'s

Our numerical results in the CMSSM-seesaw I are shown in Figs. 6.10 - 6.16. As in the CMSSM we present the results in the m_0–$m_{1/2}$ plane for four combinations of $\tan\beta = 10, 45$ (upper and lower row) and $A_0 = 0, -3000$ GeV (left and right column), again capturing the "extreme" cases. We start presenting the three most relevant δ_{ij}^{FAB}. Figs. 6.10-6.12 show δ_{12}^{LLL}, δ_{13}^{LLL} and δ_{23}^{LLL}, respectively. As expected, δ_{23}^{LLL} turns out to be largest of $\mathcal{O}(0.01)$, while the other two are about one order of magnitude smaller. The dependence on $\tan\beta$ is not very prominent, but going from $A_0 = 0$ to -3000 GeV has a strong impact on the δ_{ij}^{FAB}. For small A_0 the size of the δ_{ij}^{FAB} is increasing with larger m_0 and $m_{1/2}$, for $A_0 = -3000$ GeV the largest values are found for small m_0 and $m_{1/2}$.

6.4.2 EWPO

In Figs. 6.13-6.15 we show the results for the EWPO. The same pattern and non-decoupling behavior for EWPO as in the case of CMSSM (squark δ_{ij}^{FAB}) can be observed. However, the corrections induced by slepton flavor violation are relatively small compared to squark case. For the most extreme cases, i.e. the largest values of m_0, the

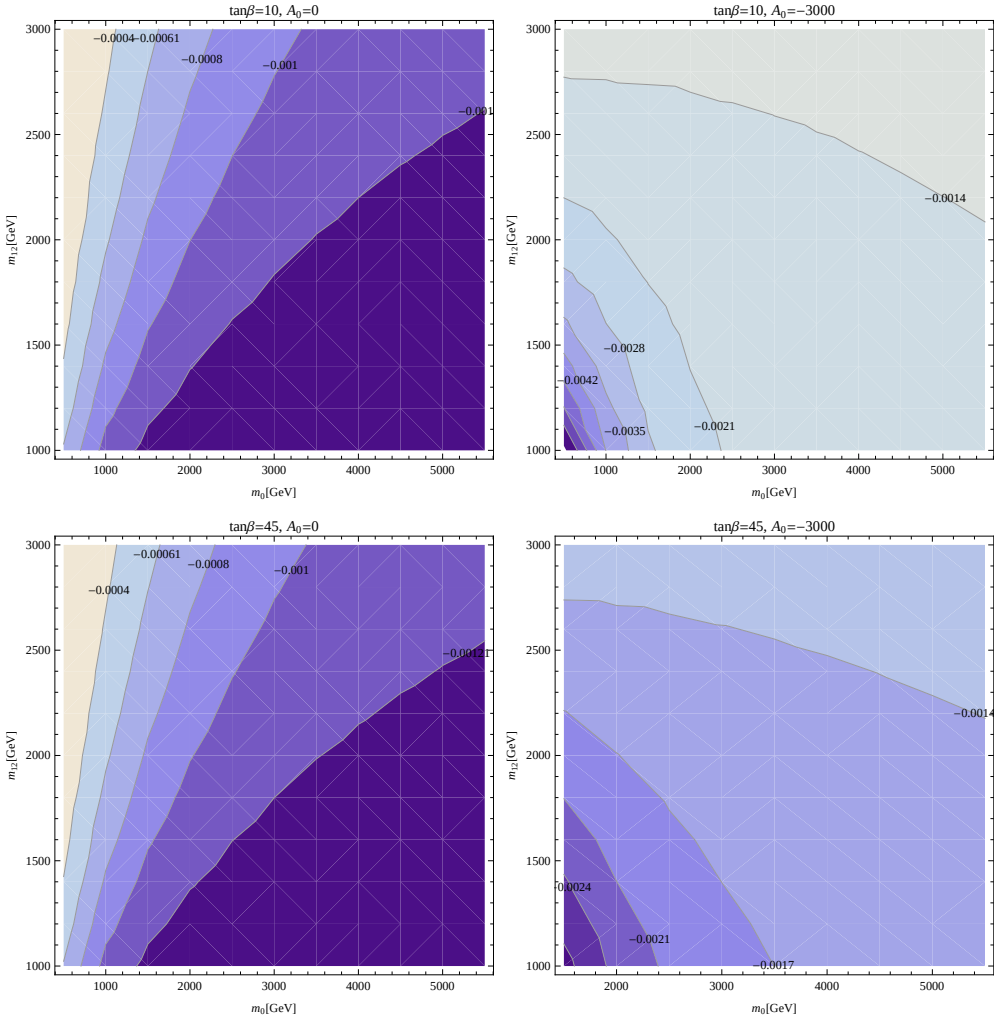

Figure 6.10: Contours of δ_{12}^{LLL} in the m_0–$m_{1/2}$ plane for different values of $\tan\beta$ and A_0 in the CMSSM-seesaw I.

corrections to M_W turn out to be of the same order of the experimental uncertainty. For those parts of the parameter space neglecting the effects of LFV to the EWPO could turn out to be an insufficient approximation, in particular in view of future improved experimental accuracies.

6.4.3 Higgs masses

Finally, in Fig. 6.16 we present the corrections to the Higgs boson masses induced by slepton flavor violation. Here we only show $\Delta M_h^{\rm MFV}$ (left) and $\Delta M_{H^\pm}^{\rm MFV}$(right) for $\tan\beta = 10$ and $A_0 = 0$. They turn out to be negligibly small in both cases. Corrections to $\Delta M_H^{\rm MFV}$, which are not shown, are even smaller. We have checked that these results hold also for other combinations of $\tan\beta$ and A_0. Consequently, within the Higgs sector the approximation of neglecting the effects of the δ_{ij}^{FAB} is fully justified.

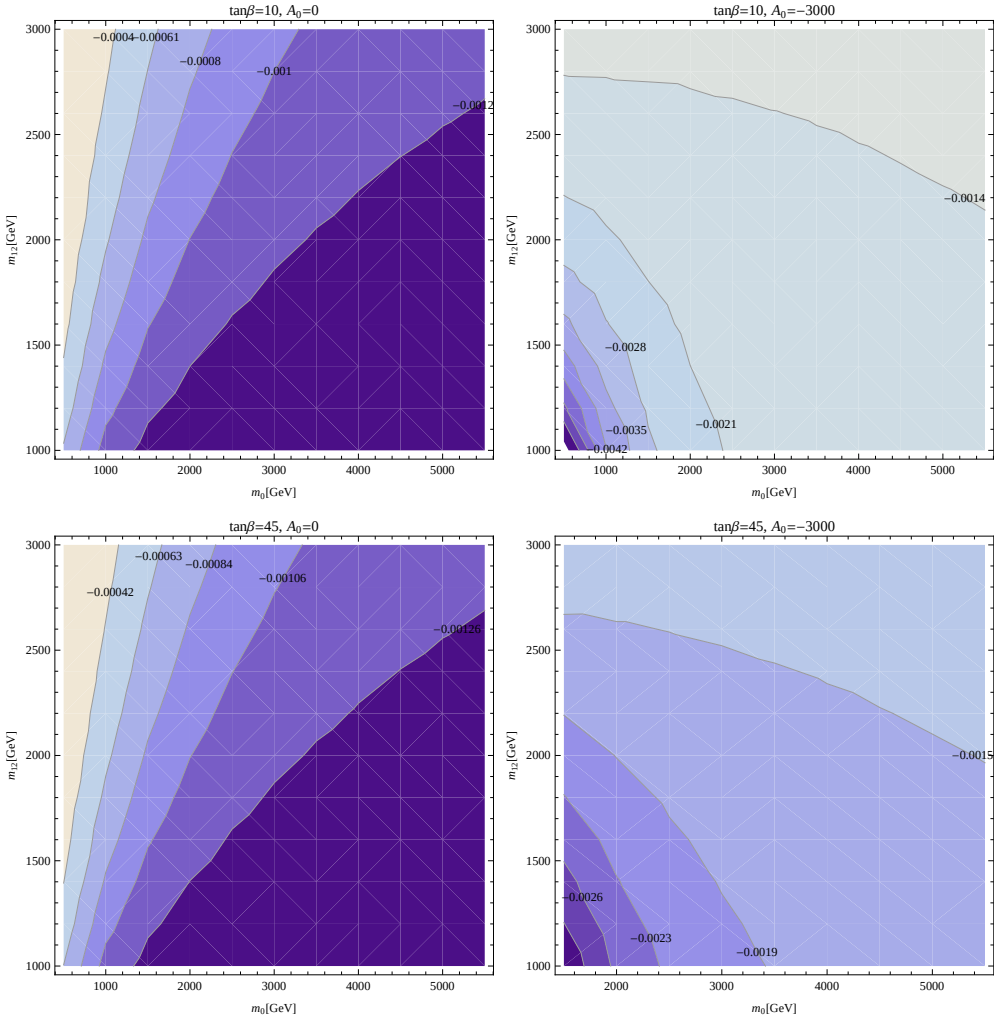

Figure 6.11: Contours of δ_{13}^{LLL} in the m_0–$m_{1/2}$ plane for different values of $\tan\beta$ and A_0 in the CMSSM-seesaw I.

6.4.4 BR($l_i \to l_j\gamma$)

The experimental limit $\mathrm{BR}(\mu \to e\gamma) < 5.7 \times 10^{-13}$ put severe constraints on slepton δ_{ij}^{FAB}'s as discussed before. In Fig. 6.17, we show the predictions for $\mathrm{BR}(\mu \to e\gamma)$ in m_0–$m_{1/2}$ for different values of A_0 and $\tan\beta$ in CMSSM-seesaw I. The selected values of Y_ν result in a large prediction for, e.g., $\mathrm{BR}(\mu \to e\gamma)$ that can eliminate some of the m_0–$m_{1/2}$ parameter plane, in particular combinations of low values of m_0 and $m_{1/2}$. For $\tan\beta = 10$ and $A_0 = 0$, $\mathrm{BR}(\mu \to e\gamma)$ (upper left plot of Fig. 6.17) do not exclude any region in m_0–$m_{1/2}$ plane, whereas with $\tan\beta = 10$ and $A_0 = -3000$ lower left region below $m_0, m_{1/2} = 2000$ is excluded (see upper right plot of Fig. 6.17). For combinations like $\tan\beta = 45$, $A_0 = 0$ and $\tan\beta = 45$, $A_0 = -3000$ even larger parts of the plane are excluded by $\mathrm{BR}(\mu \to e\gamma)$. In Fig. 6.18 and Fig. 6.19, we show the predictions for $\mathrm{BR}(\tau \to e\gamma)$ and $\mathrm{BR}(\tau \to \mu\gamma)$ respectively. It can be seen that these processes do not

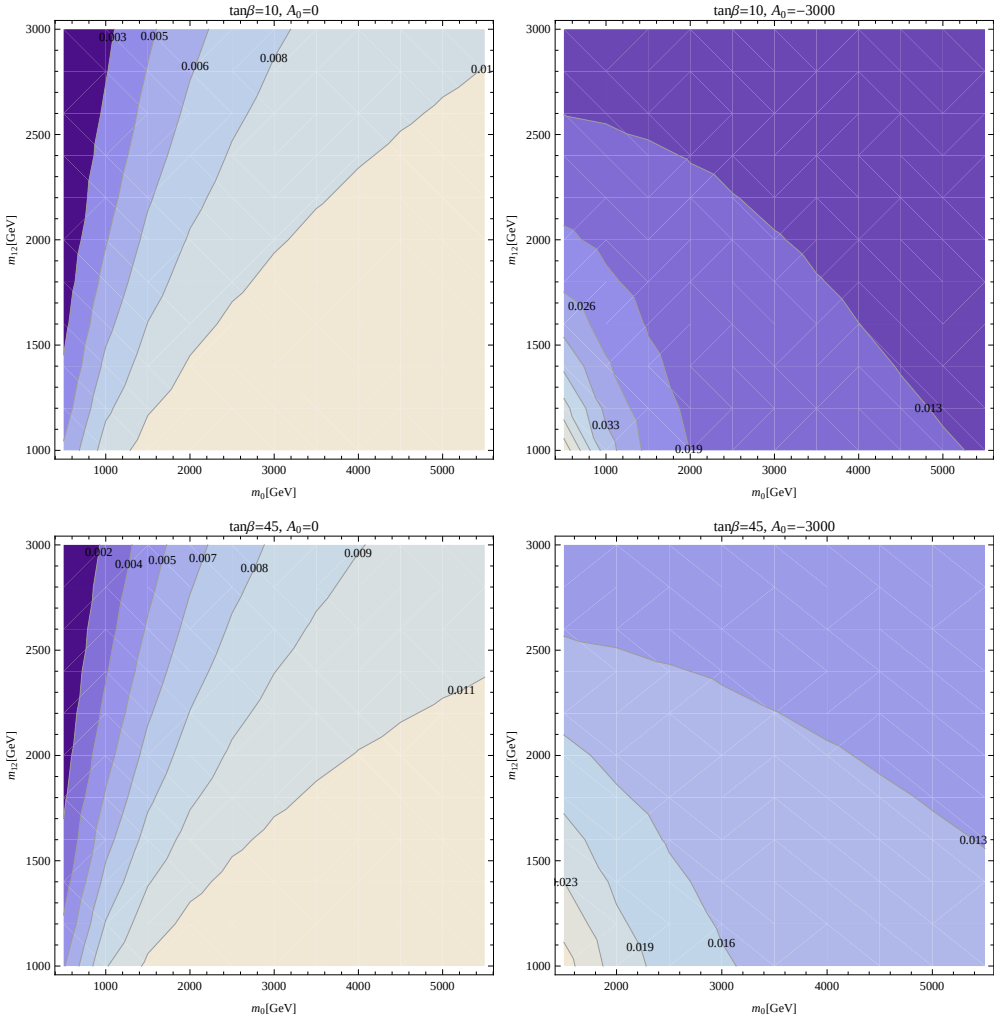

Figure 6.12: Contours of δ_{23}^{LLL} in the m_0–$m_{1/2}$ plane for different values of $\tan\beta$ and A_0 in the CMSSM-seesaw I.

reach their respective experimental bounds $\mathrm{BR}(\tau \to e\gamma) < 3.3 \times 10^{-8}$, $\mathrm{BR}(\tau \to \mu\gamma) < 4.4 \times 10^{-8}$. Consequently they do not exclude any parameter space.

6.4.5 $\mathrm{BR}(h \to l_i^{\pm} l_j^{\mp})$

Fig. 6.20 shows the results for $\mathrm{BR}(h \to e\mu)$. The largest value is of the $\mathcal{O}(10^{-16})$ for low m_0 and $m_{1/2}$ values but is excluded from $\mathrm{BR}(\mu \to e\gamma)$. In the allowed range they are typically $\mathcal{O}(10^{-18})$. Similarly Fig. 6.21 and Fig. 6.22 shows the predictions for $\mathrm{BR}(h \to e\tau)$ and $\mathrm{BR}(h \to \tau\mu)$ respectively. Predictions of the $\mathcal{O}(10^{-14})$ and $\mathcal{O}(10^{-12})$ are possible for $\mathrm{BR}(h \to e\tau)$ and $\mathrm{BR}(h \to \tau\mu)$ in the lower left region of the m_0–$m_{1/2}$ plane respectively but are excluded from $\mathrm{BR}(\mu \to e\gamma)$ bound. In the allowed region they are of the $\mathcal{O}(10^{-16})$ or less. These results are in a clear contradiction to the recently

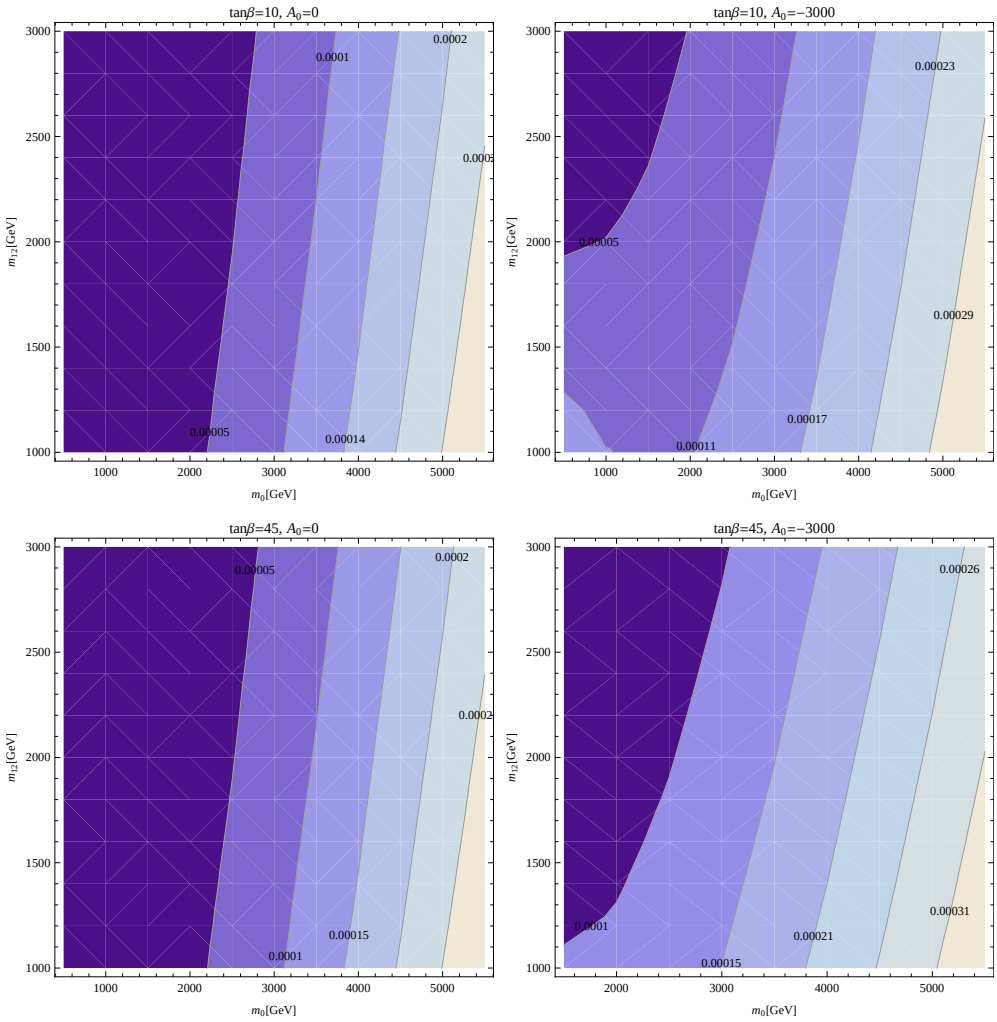

Figure 6.13: Contours of $\Delta\rho^{\rm MFV}$ in the m_0–$m_{1/2}$ plane for different values of $\tan\beta$ and A_0 in the CMSSM-seesaw I.

reported CMS excess [129]. If this excess seen in the CMS is confirmed in the future analysis, we will need models other than the CMSSM-seesaw I to explain this excess. However our findings are in agreement with the ATLAS reports [130], where they do not see any significant excess over background. It remains to be seen how these results will develop with the LHC Run II.

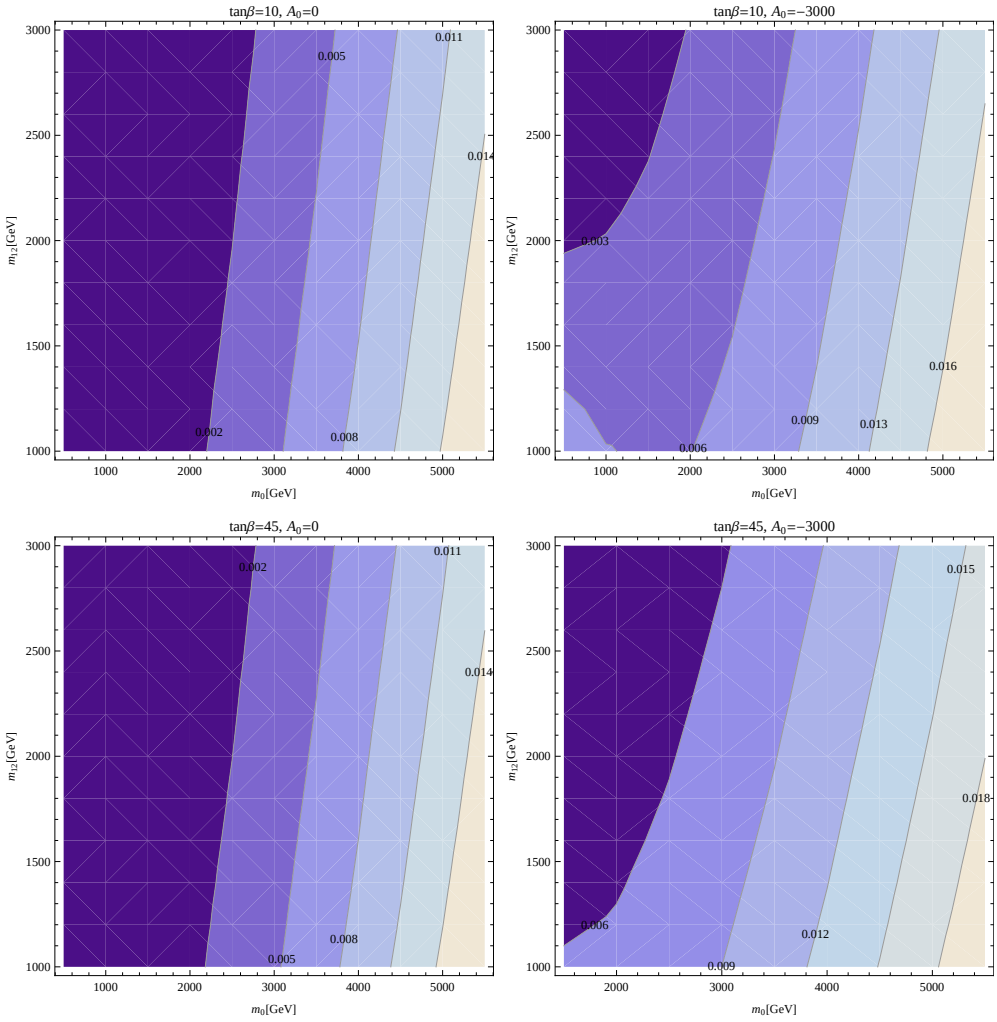

Figure 6.14: Contours of $\Delta M_W^{\rm MFV}$ in GeV in the m_0–$m_{1/2}$ plane for different values of $\tan\beta$ and A_0 in the CMSSM-seesaw I.

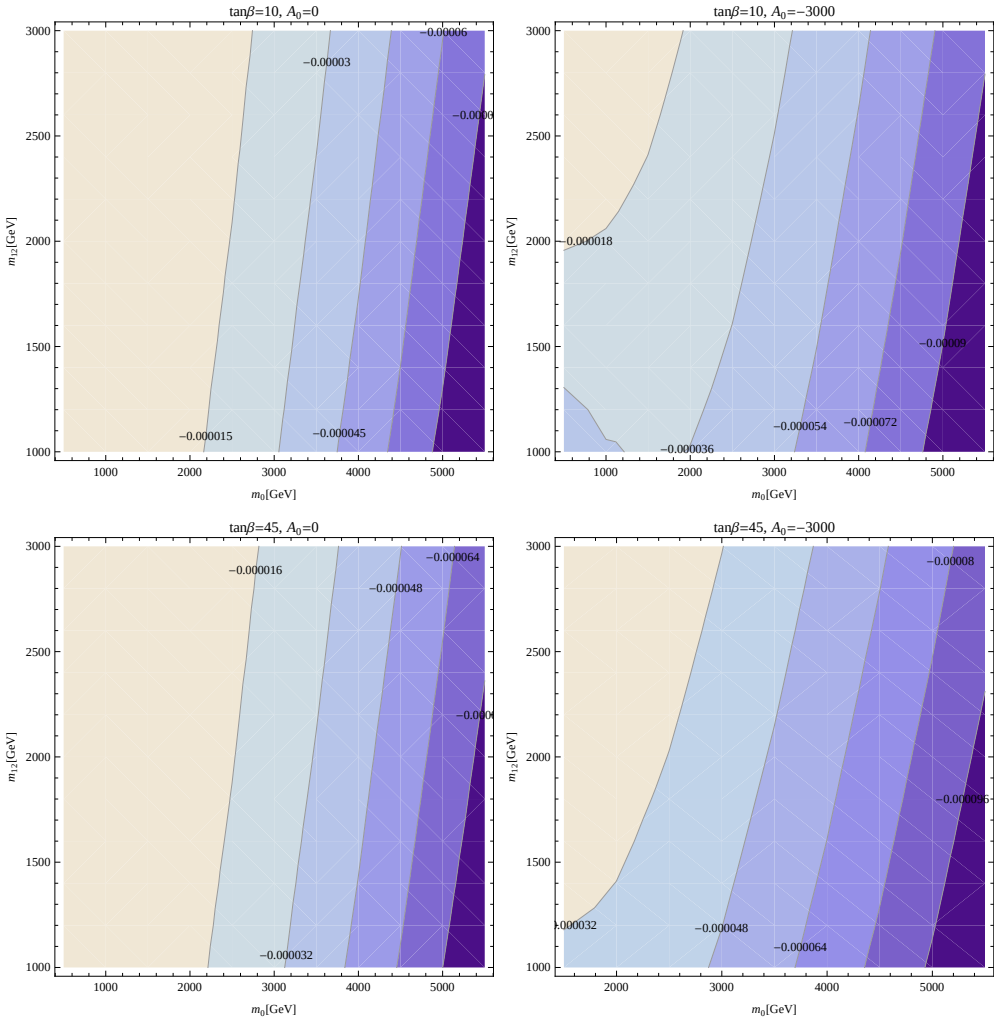

Figure 6.15: Contours of $\Delta \sin^2 \theta_{\rm eff}^{\rm MFV}$ in the m_0–$m_{1/2}$ plane for different values of $\tan\beta$ and A_0 in the CMSSM-seesaw I.

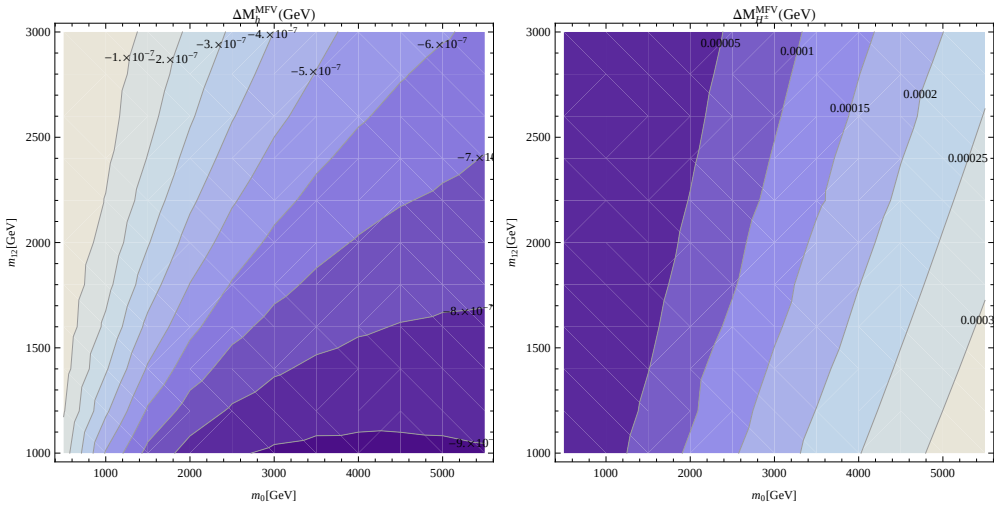

Figure 6.16: Contours of $\Delta M_h^{\rm MFV}$ (left) and $\Delta M_{H^\pm}^{\rm MFV}$ (right) in the m_0–$m_{1/2}$ plane for $\tan\beta = 10$ and $A_0 = 0$ in the CMSSM-seesaw I.

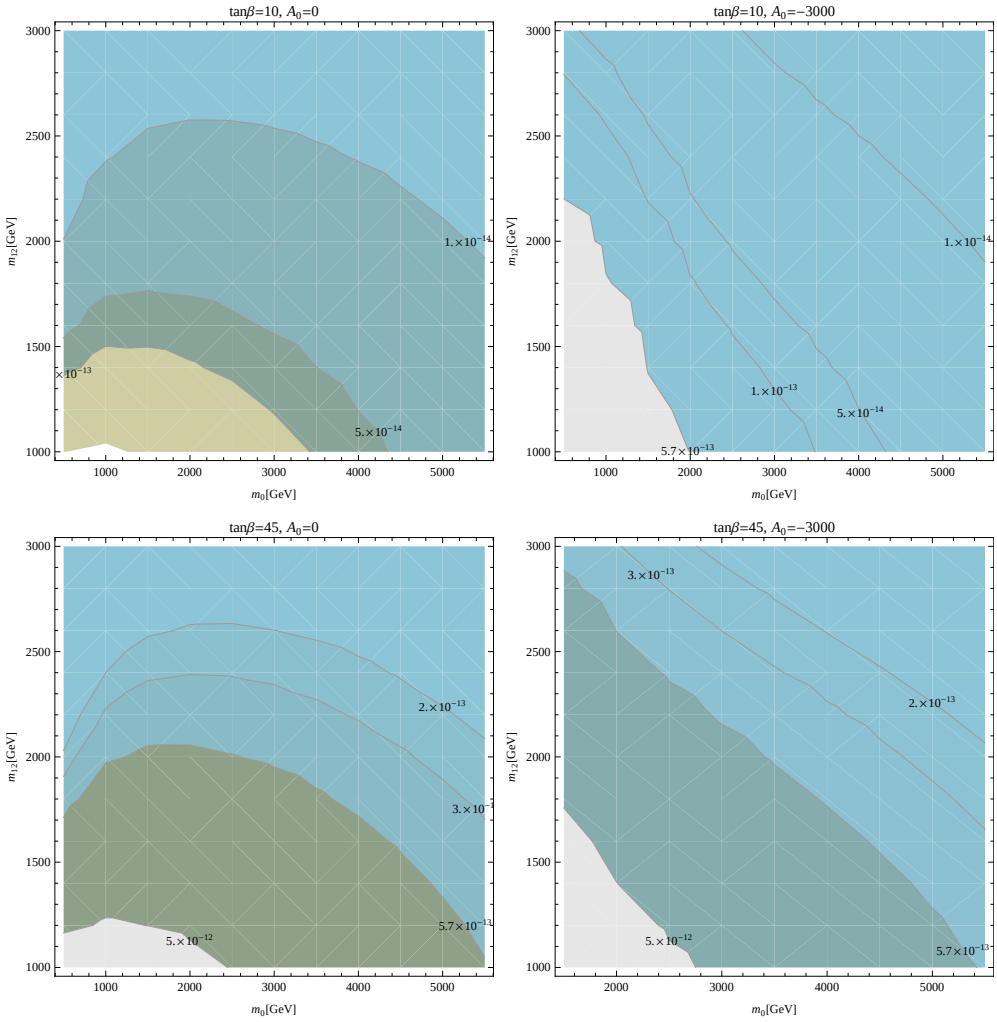

Figure 6.17: Contours of BR($\mu \to e\gamma$) in the m_0–$m_{1/2}$ plane for different values of $\tan\beta$ and A_0 in the CMSSM-seesaw I.

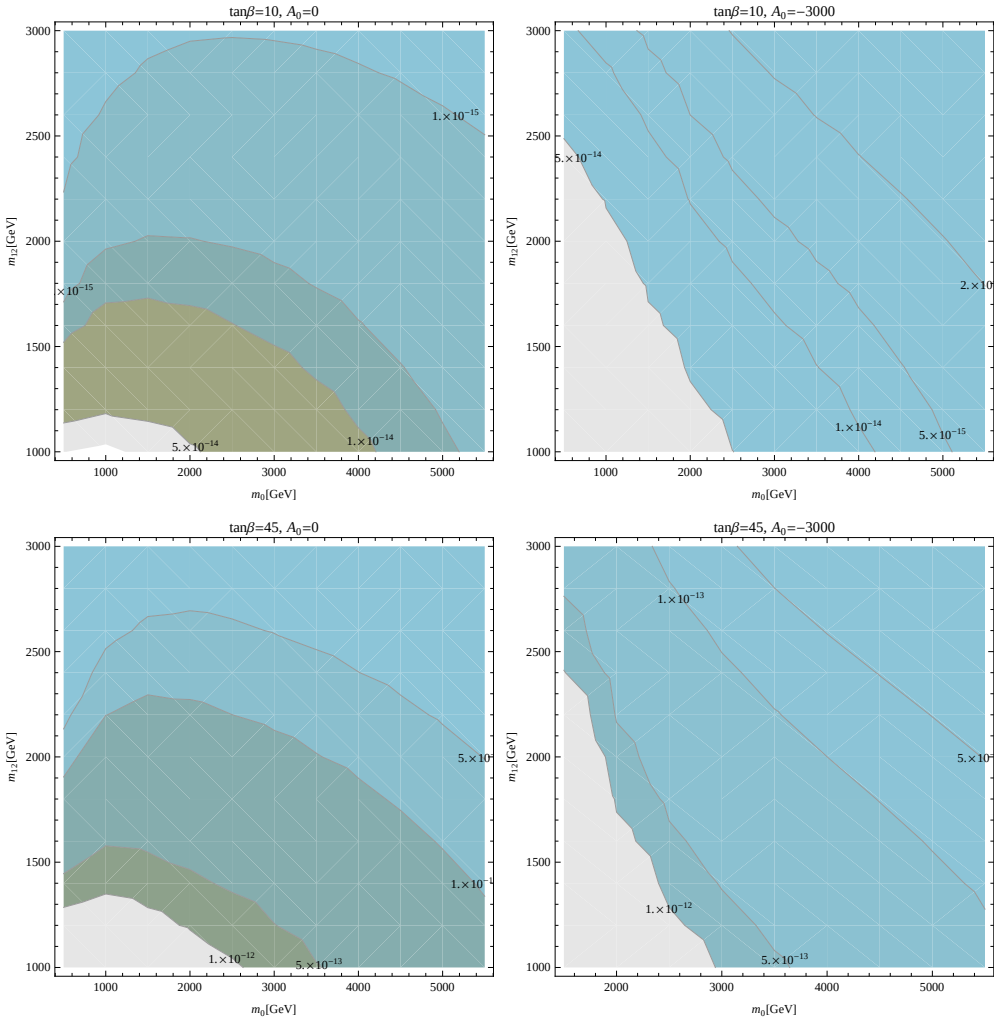

Figure 6.18: Contours of BR($\tau \to e\gamma$) in the m_0–$m_{1/2}$ plane for different values of $\tan\beta$ and A_0 in the CMSSM-seesaw I.

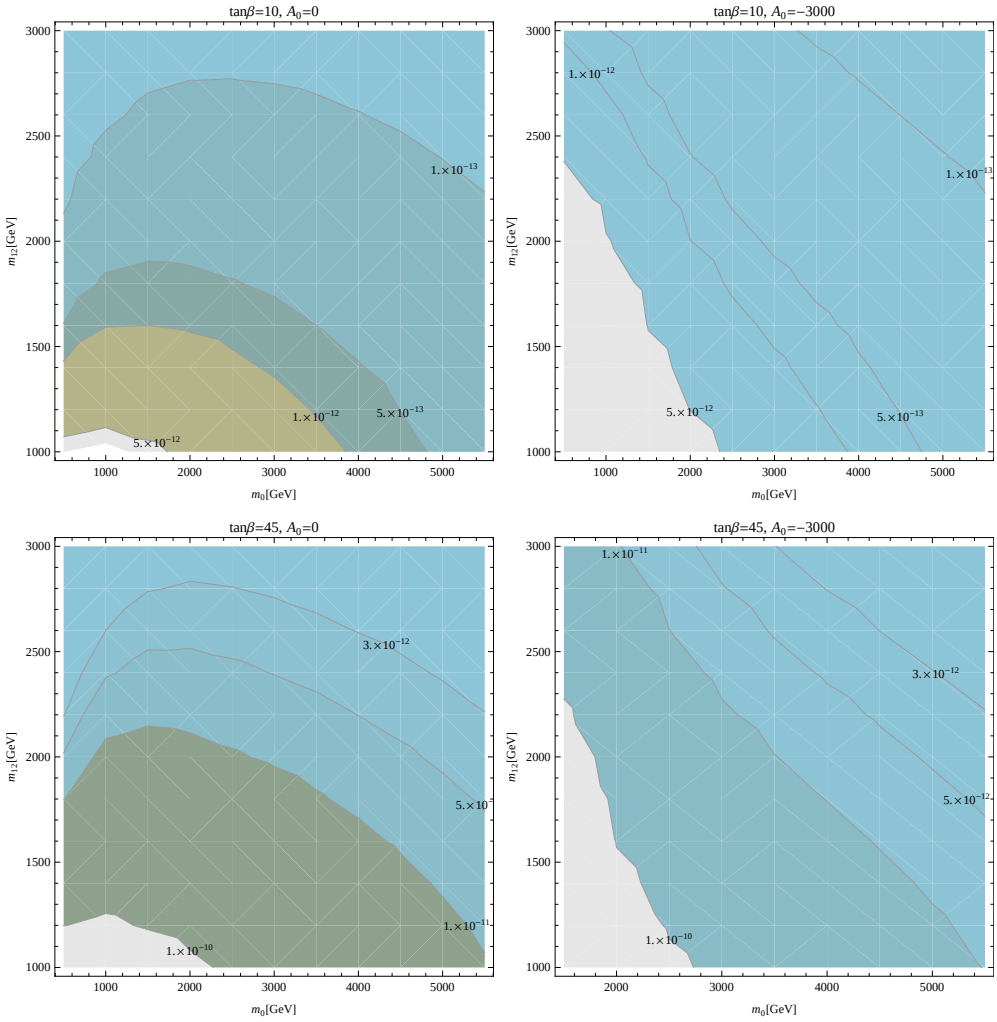

Figure 6.19: Contours of BR($\tau \to \mu\gamma$) in the m_0–$m_{1/2}$ plane for different values of $\tan\beta$ and A_0 in the CMSSM-seesaw I.

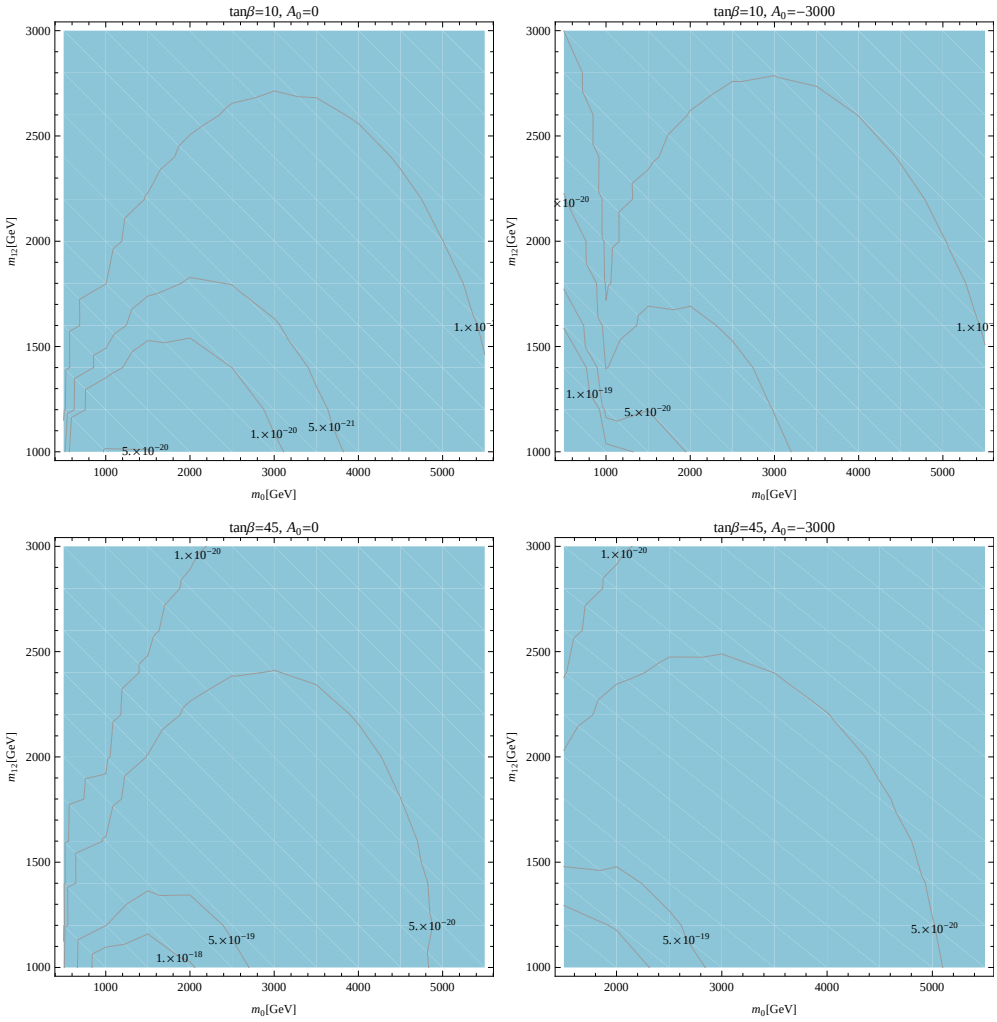

Figure 6.20: Contours of BR($h \to e\mu$) in the m_0–$m_{1/2}$ plane for different values of $\tan\beta$ and A_0 in the CMSSM-seesaw I.

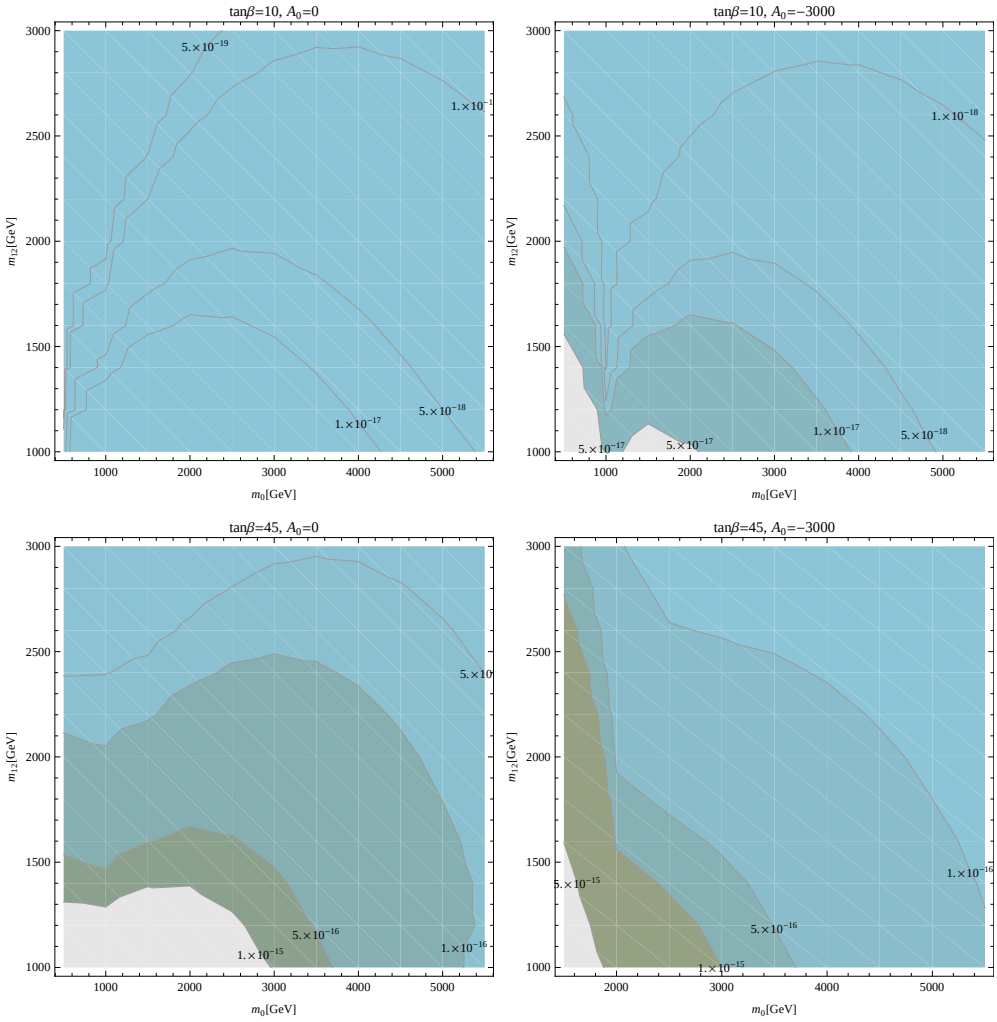

Figure 6.21: Contours of BR($h \to e\tau$) in the m_0–$m_{1/2}$ plane for different values of $\tan\beta$ and A_0 in the CMSSM-seesaw I.

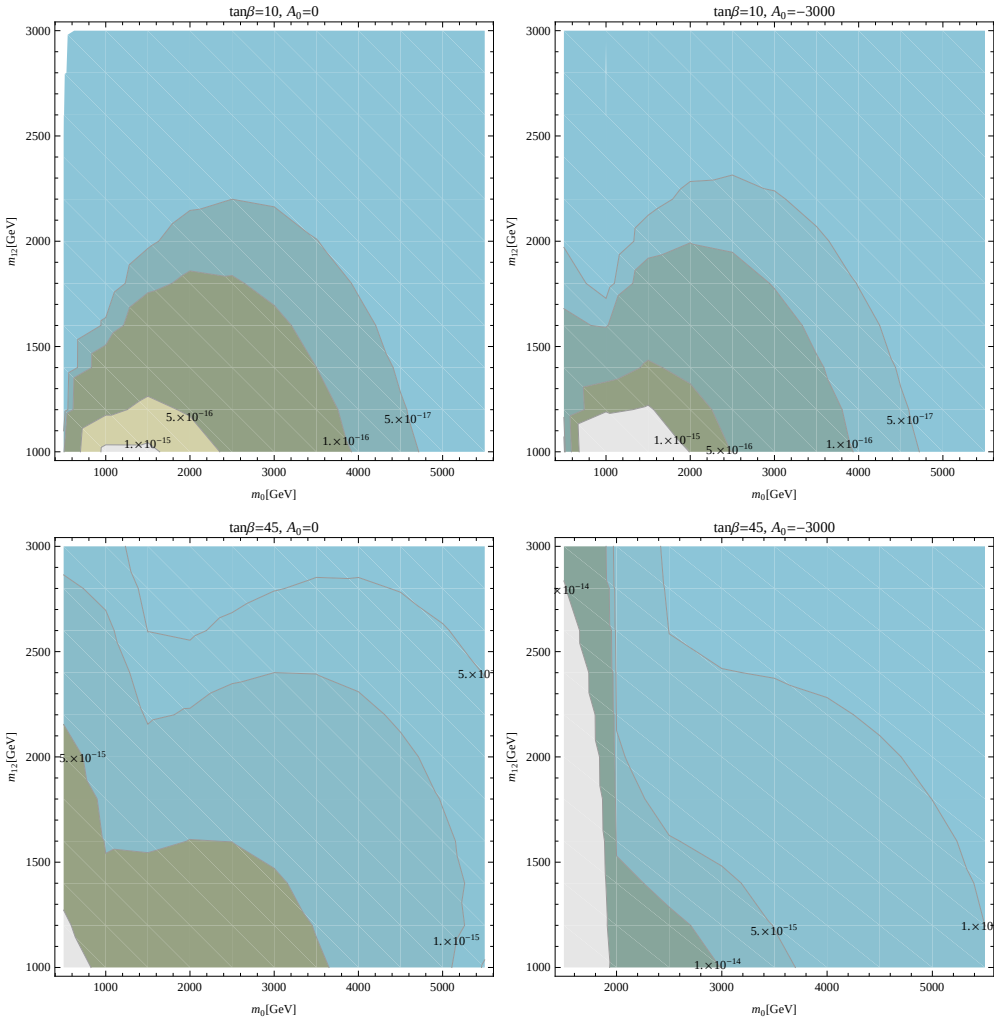

Figure 6.22: Contours of BR($h \to \tau\mu$) in the m_0–$m_{1/2}$ plane for different values of $\tan\beta$ and A_0 in the CMSSM-seesaw I.

Chapter 7

Summary & Conclusions

SUSY proves to be a very powerful and technically well equiped theory as it successfully explains some of the major deficiencies of the SM, but still lacks experimental endorsement. Direct searches for sparticles at LHC did not succeed so far. The other way around is to probe SUSY via virtual effects of additional particles to the precision observables. For example, in the MSSM, the fermion-sfermion misallignment can generate flavor changing effects that can dominate the SM effects by several orders of magnitude. Any possible experimental deviation from the SM results for the precision observales could be a hint of SUSY. Also, as this misallignment arises from the soft SUSY-breaking terms, this may provide guidlines for the SUSY model building. In this thesis, keeping the above mentioned points in mind, we studied the possible phenomenological consequences of flavor mixing to various observables.

The flavor mixing was parameterized in terms of a set of dimensionless parameters δ_{ij}^{FAB} ($F = Q, U, D, L, E; A, B = L, R;\ i, j = 1, 2, 3$). In chapter 1, we reviewed some aspacts of the SM, similarly in chapter 2, a general introduction to MSSM and its seesaw extension was discussed. Calculational details for the considered observables were given in chapter 3 where we presented the higher order corrections to the electroweak precision observables (EWPO), higher order corrections to Higgs boson masses, calculational details of the B-physics observables (BPO), quark flavor violating Higgs decays (QFVHD) and lepton flavor violating Higgs decays (LFVHD). In order to calculate slepton mixing effects (squark mixing was already present), we prepared an add-on model file for `FeynArts` to include lepton flavor violation in the already existing MSSM model file of the `FeynArts`. `FormCalc` drivers were also modified accordingly. The inclusion of lepton flavor violation (LFV) into `FeynArts`/`FormCalc` allowed us to calculate the one-loop LFV effects on EWPO (via the calculation of gauge-boson self-energies) as well on the Higgs-boson masses of the MSSM (via the calculation of the Higgs-boson self-energies). The corresponding results have been included in the code `FeynHiggs` and are publicly available from version 2.10.2 on. We have (re-)caculated the decay $h \to \bar{b}s + b\bar{s}$ in the `FeynArts` and `FormCalc` setup. The BPO and EWPO constraints have been evalated with the help of (a private version of) `FeynHiggs`, taking into account the full flavor violating one-loop corrections to M_W and to the relevant BPO (supplemented with further MSSM higher-order corrections).

The effects of squarks mixing to EWPO, BPO and QFVHD such as $h \to \bar{b}s + b\bar{s}$ in the Model Independent (MI) approach were presented in chapter 4. This evaluation improved on existing analyses in various ways. We took into account the full set of SUSY QCD and SUSY EW corrections, allowing for LL, RL, LR and RR mixing simultaneously. The parameter space was restricted not only by BPO, but also by EWPO, in particular the mass of the W boson. We have shown that M_W can yield non-trivial, additional restrictions on the parameter space of the squark flavor violating δ_{ij}^{FAB}.

In six representative scenarios, which are allowed by current searches for SUSY particles and heavy Higgs bosons, we have evaluated the allowed parameter space for the various δ_{ij}^{FAB} by applying BPO and EWPO constraints. Within these allowed ranges we have then evaluated $\mathrm{BR}(h \to \bar{b}s + b\bar{s})$. In the case of only one $\delta_{ij}^{FAB} \neq 0$ we have found that only relatively large values of δ_{23}^{DLR} could lead to rates of $\mathrm{BR}(h \to \bar{b}s + b\bar{s}) \sim 10^{-4}$, which could be in the detectable range of future e^+e^- colliders. Allowing two $\delta_{ij}^{FAB} \neq 0$ simultaneously lead to larger values up to $\mathrm{BR}(h \to \bar{b}s + b\bar{s}) \sim 10^{-3}$, which would make the observation at the ILC relatively easy. Allowing for a third $\delta_{ij}^{FAB} \neq 0$, on the other hand, did not lead to larger values of the flavor violating branching ratio.

The effects of slepton mixing to EWPO, Higgs boson masses and LFVHD in the MI approach were presented in chapter 5. The numerical analysis was performed on the basis of same six benchmark points as in the previous chapter. These benchmark points represent different combinations of parameters in the sfermion sector. The restrictions on the various slepton δ_{ij}^{FAB} in these six scenarios, provided by experimental limits on LFV processes (such as $\mu \to e\gamma$) were taken from Ref. [145], and the effects on EWPO and Higgs-boson masses were evaluated in the experimentally allowed ranges. In this way we were able to provide a general overview about the possible size of LFV effects and potential new restrictions on the slepton δ_{ij}^{FAB} from EWPO and Higgs-boson masses.

The LFV effects in the EWPO turned out to be sizable for δ_{23}^{LLL} but (at least in the scenarios under investigation) negligible for the other δ_{ij}^{FAB}. The effects of varying δ_{23}^{LLL} in the experimentally allowed ranges turned out to exceed the current experimental uncertainties of M_W and $\sin^2\theta_{\mathrm{eff}}$ in the case of heavy sleptons. No new general bounds could be set on δ_{23}^{LLL}, however, since the absolute values of M_W and $\sin^2\theta_{\mathrm{eff}}$ strongly depend on the choices in the stop/sbottom sector, which is disconnected from the slepton sector presently under investigation. Such bounds could be set on a point-by-point basis in the LFV MSSM parameter space, however. Looking at the future anticipated accuracies, also lighter sleptons yielded contributions exceeding that precision. It may therefore be possible in the future to set bounds on δ_{23}^{LLL} from EWPO that are stronger than from direct LFV processes.

In the Higgs sector, based on evaluations for flavor violation in the squark sector, non-negligible corrections to the light $\mathcal{CP}$-even Higgs mass as well as to the charged Higgs-boson mass could be expected. The associated theoretical uncertainties exceeded the anticipated future precision for M_h and $M_{H^\pm}$. Taking the existing limits on the δ_{ij}^{FAB} from LFV processes into account, however, the corrections mostly turned out to be small. For the light $\mathcal{CP}$-even Higgs mass they stay at the few-MeV level. For the charged Higgs boson mass they can reach $\mathcal{O}(2\ \mathrm{GeV})$, which, depending on the choice of the heavy

Higgs-boson mass scale, could be at the level of the future experimental precision. More importantly, the theoretical uncertainty from LFV effects that previously existed for the evaluation of the MSSM Higgs-boson masses, has been reduced below the level of future experimental accuracy.

The predictions for the LFVHD in the MI approach were also presented in chapter 5. However due to very tight constraints on the slepton δ_{ij}^{FAB}'s from cLFV decays, the BR's for these processes turned out to be very small.

Effects of squark mixing in the the CMSSM and slepton mixing in CMSSM extended by type I Seesaw under the Minimal Flavor Violation (MFV) hypothesis were presented in chaptor 6. This work was motivated by the fact that in many phenomenological analyses of the CMSSM the effects of intergenerational mixing in the squark and/or slepton sector are neglected. However, such mixings are naturally induced, assuming no flavor violation at the GUT scale, by the RGE running from the GUT to the EW scale exactly due to the presence of the CKM and/or the PMNS matrix. In this sense the CMSSM and the CMSSM-seesaw I represent two simple "realistic" GUT based models, in which flavor violation in induced solely by RGE running. The spectra of the CMSSM and CMSSM-seesaw I have been numerically evaluated with the help of the program `SPheno` by taking the GUT scale input run down via the appropriate RGEs to the EW scale.

We have evaluated the predictions for BPO, MSSM Higgs boson masses, EWPO in the CMSSM and CMSSM-seesaw I. In order to numerically analyze the effects of neglecting intergenerational mixing these observables have been evaluated with the full spectrum at the EW scale, as well as with the spectrum, but with all intergenerational mixing set artificially to zero (as it has been done in many phenomenological analyses).

The difference in the various observables indicates the possible size of the effects neglected in those analyses. In this way it can be checked whether neglecting those mixing effects is a justified approximation.

Within the CMSSM we have taken a fixed grid of A_0 and $\tan\beta$, while scanning the m_0–$m_{1/2}$ plane. We found that the value of δ_{ij}^{FAB} increases with the increase of the A_0 or $\tan\beta$ values. The Higgs boson masses receive corrections below current and future experimental uncertainties, where the shifts in $M_{H^\pm}$ were found largest at the level of $\mathcal{O}(100\text{ MeV})$. Similarly for the BPO the induced effects are at least one order of magnitude smaller than the current experimental uncertainty. For those two groups of observables the approximation of neglecting intergenerational mixing explicitly is a viable option.

The picture changes for the EWPO. We find that the masses of the squarks grow with m_0, and thus do the mixing terms, inducing a splitting between masses in an $SU(2)$ doublet, leading to a non-decoupling effect. For $m_0 \gtrsim 3$ TeV the effects induced in M_W and $\sin^2\theta_{\text{eff}}$ are found to be several times larger than the current experimental uncertainties and could shift the CMSSM prediction outside the allowed experimental range. In this way, taking the intergenerational mixing into account could in principle set bounds on m_0 that are not present in recent phenomenological analyses. By investigating numerically squark mass differences, we have shown that this behavior can be traced

back to the non-decoupling effects in the scalar quark mass matrices, provided by `Spheno` when taking into account the CKM matrix in the RGE running. However, we would like to point out that this bound only holds because of the particularly simple structure of the CMSSM and cannot be extended easily to other, more complicated model frameworks.

In the final step of the numerical analysis within the CMSSM we have evaluated $\mathrm{BR}(h \to \bar{b}s + b\bar{s})$. Here we have found that for most of parameter space values of $\mathcal{O}(10^{-7})$ are found for $\mathrm{BR}(h \to \bar{b}s + b\bar{s})$, i.e. outside the reach of current or future collider experiments.

Going to the CMSSM-seesaw I the numerical results depend on the concrete model definition. We have chosen a set of parameter that reproduces correctly the observed neutrino data and simultaneously induces large LFV effects and induces *relatively* large corrections to the calculated observables. Consequently, parts of the parameter space are excluded by the experimental bounds on $\mathrm{BR}(\mu \to e\gamma)$. However $\mathrm{BR}(\tau \to e\gamma)$ and $\mathrm{BR}(\tau \to \mu\gamma)$ do not reach to their respective experimental limits. Again predictions for the BR of LFVHD turned out very small in CMSSM-seesaw I. We can conclude that we will need models other than the CMSSM-seesaw I to explain the CMS excess (if it persists) for the channel $\mathrm{BR}(h \to \mu\tau)$. Concerning the precision observables we find that BPO are not affected, we also find that the additional effects induced by slepton flavor violation on Higgs boson masses are negligible. Again the EWPO are found to show the largest impact, where for M_W effects at the same level as the current experimental accuracy have been observed for very large values of m_0. As above, we would like to point out that these effects are due to the relatively simple structure of the CMSSM-seesaw I.

To summarize our MFV analysis: we have analyzed two "realistic" GUT based models in which flavor violation is solely induced by the CKM matrix via RGE running (as evaluated using the `Spheno code`). We find that artificially setting all flavor violating terms to zero in the CMSSM and CMSSM-seesaw I is an acceptable approximation for BPO, Higgs boson masses (evaluated using a private version of `FeynHiggs`). However, in the EWPO (also evaluated with `FeynHiggs`) in our numerical analysis we find larger effects in the CMSSM and CMSSM-seesaw I. The numerical contributions are larger than the current experimental accuracy in M_W and $\sin^2\theta_{\mathrm{eff}}$. Taking those effects correctly into account could in principle place new bounds on m_0 that are not present in recent phenomenological analyses.

Resumen y Conclusiones

La teoría supersimétrica ha demostrado un enorme potencial para explicar algunas de los mayores problemas del Modelo Estánder (ME), aunque hasta la fecha no se haya encontrado ninguna evidencia experimental de sus predicciones. Por ejemplo, la búsqueda directa de partículas supersimétricas no ha tenido éxito por el momento. Sin embargo, es posible detectar la presencia de las nuevas partículas en los cambios que éstas producen en algunos parámetros medidos con gran precisión. En particular, el modelo supersimétrico mínimo (MSSM) predice nuevas contribuciones al cambio de sabor (FC) de los fermiones debido a mezclas entre las masas de sus correspondientes parejas supersimétricas. Esta mezcla está originada por los parámetros responsables de la rotura de la Supersimetría, lo cual tiene un gran interés desde el punto de vista del diseño de modelos supersimétricos concretos. El cambio de sabor derivado de la no alineación entre fermiones y sus parejas escalares no se manifiesta en la aproximación a nivel más bajo ("tree level") de los cálculos, pero sí en el primer orden ("one-loop" level) cuya contribución puede ser importante para ciertos valores de los parámetros del MSSM.

En esta tesis, se ha estudiado la posible contribución de la mezcla de sabor fermiónico a varias observaciones. La mezcla de sabor se ha introducido por medio de un conjunto de parámetros adimensionales denominados δ_{ij}^{FAB} ($F = Q, U, D, L, E; A, B = L, R; i, j = 1, 2, 3$). En el capítulo 1, se revisaron algunos aspectos del ME; en el capítulo 2, se introdujo el MSSM y la extensión de éste que incluye un mecanismo del tipo "see-saw" para explicar las oscilaciones de sabor de los neutrinos. Los detalles de la contribución SUSY a algunos observables de interés se presenta en el capítulo 3, en concreto se consideran: observables de la teoría electro-débil medidos con gran precisión (EWPO), correcciones a la masa del bosón de Higgs, detalles en el cómputo de la física relacionada con el quark b (B-physics observables (BPO)), desintegraciones del bosón de Higgs con violación de sabor de quark (QFVHD) y finalmente, desintegraciones del bosón de Higgs con violación de sabor leptónico (LFVHD). Para calcular los efectos de la mezcla del sector leptónico se elaboró un algoritmo adicional para `FeynArts`, con él se incluye LFV en el modelo del MSSM que el paquete ya tiene definido. Con ello ampliamos la capacidad de los programas incluidos en `FeynArts`/`FormCalc` para computar el efecto del LFV en observables como EWPO (a partir del cómputo de las auto-energías de los bosones gauge) y también sobre la masa de los bosones de Higgs del MSSM. Los resultados correspondientes han sido incluidos en el el código `FeynHiggs` y están disponibles para su libre distribución a partir de la versión 2.10.2. Se revisó el cálculo de la desintegración $h \to \bar{b}s + b\bar{s}$ utilizando los códigos actualizados de `FeynArts` y `FormCalc`. Los cálculos

para evaluar los observables BPO y EWPO se realizaron con la ayuda de `FeynHiggs` (utilizando una versión no pública), teniendo en cuenta la contribución a la de todos los términos que violan sabor, en el caso de M_W y de los más relevantes en el caso de BPO.

En el capítulo 4 se han estudiado los efectos de la mezcla de sabor de los squarks en la observación de EWPO, BPO y QFVHD (por ejemplo en $h \to \bar{b}s + b\bar{s}$) de una manera independiente del modelo (MI) que produce la mezcla de sabor. Nuestro cálculo mejora otros previos en varios aspectos: se ha tenido en cuenta el total de las correcciones supersimétricas del tipo fuerte y electro-débil y, además, se permitió la mezcla simultánea de contribuciones del tipo LL, RL, LR y RR. También se consideró la limitación del valor de los parámetros impuesta no solo por los BPO, sino también por los EWPO, en particular la masa del bosón M_W. Se mostró que la contribución a M_W produce restricciones adicionales al espacio de los parámetros δ_{ij}^{FAB} que mezclan el sabor de los squarks.

En la evaluación de los posibles valores de los parámetros δ_{ij}^{FAB} se han teniendo en cuenta las limitaciones procedentes de los valores de los BPO y EWPO. Para ello, se consideraron seis escenarios representativos no excluidos ni por la búsqueda de partículas SUSY ni por el valor experimental de la masa del bosón de Higgs. Los valores de δ_{ij}^{FAB} obtenidos se usaron para calcular $\mathrm{BR}(h \to \bar{b}s + b\bar{s})$. En el caso de tomar sólo uno de los $\delta_{ij}^{FAB} \neq 0$ se encontró que únicamente valores relativamente grandes de δ_{23}^{DLR} predicen valores de $\mathrm{BR}(h \to \bar{b}s + b\bar{s}) \sim 10^{-4}$, detectables en futuros colisionadores e^+e^- . Permitiendo dos $\delta_{ij}^{FAB} \neq 0$ simultáneamente se obtiene un valor $\mathrm{BR}(h \to \bar{b}s + b\bar{s}) \sim 10^{-3}$, que podría observarse en el ILC. En cambio, si se permite un tercer $\delta_{ij}^{FAB} \neq 0$, no incrementa más el valor de esas predicciones.

En el capítulo 5 se estudiaron los efectos de la mezcla de sabor de los sleptones en los EWPO, las masas de los bosones de Higgs de una manera independiente del modelo que origina la mezcla del sabor. Nuestro análisis numérico toma como referencia seis modelos supersimétricos a los que se atribuyen determinados valores de los parámetros de modo que las propiedades de los fermiones sean diferentes en cada uno de los casos. Los valores de los δ_{ij}^{FAB} en los seis escenarios están limitados por la no observación de la violación del sabor leptónico (LFV) en procesos como $\mu \to e\gamma$ [145], lo que se ha tenido en cuenta en la evaluación del los EWPO y las masas de los bosones de Higgs. De este modo hemos podido computar, de una manera general, el posible impacto de las restricciones en el valor de los δ_{ij}^{FAB} debido a éstos observables en la predicción de procesos con LFV. Encontramos que éstas son considerables para δ_{23}^{LLL} e insignificantes para el resto de los δ_{ij}^{FAB}, al menos en los escenarios considerados en nuestra investigación. El efecto de variar los valores de δ_{23}^{LLL} dentro de los intervalos permitidos experimentalmente implica contribuciones para M_W y $\sin^2\theta_{\mathrm{eff}}$ que pueden exceder el margen de error con el que están medidos. Sin embargo, esto no implica nuevas restricciones en los valores de δ_{23}^{LLL}, ya que los valores absolutos de M_W y $\sin^2\theta_{\mathrm{eff}}$ dependen en gran medida del s-top y el s-bottom. Este sector está desconectado del de los sleptones, objeto de nuestra investigación. Sin embargo, en algunos casos, los limites que resultan de los EWPO pueden ser más restrictivos que los procedentes de la medida directa de procesos con LFV. En el sector de los bosones de Higgs, la introducción de violación de sabor de

los s-quarks implica contribuciones no triviales a las masas del bosón de Higgs neutro más ligero M_h y a la del cargado $M_{H^\pm}$. En ambos casos, la incertidumbre teórica en su determinación es superior a la experimental. Si consideramos los valores para δ_{ij}^{FAB} permitidos por los límites de procesos con LFV , la contribución a ambas masas es pequeña. Para M_h es del orden de unos pocos MeVs mientras para $M_{H^\pm}$ puede llegar hasta 2 GeV. Esta última puede alcanzar el valor de la futura precisión experimental, dependiendo de la masa del bosón de Higgs neutro más pesado. Pero lo más relevante, es el hecho de que la incertidumbre derivada de los efectos de LFV en la evaluación de las masas de los bosones de Higgs neutros se ha reducido hasta hacerse del mismo orden que la que se prevé alacanzar en experimentos futuros. En el capítulo 5 tambien se presentaron las predicciones para LFVHD siguiendo la técnica MI. Sin embargo, las severas restricciones impuestas por los procesos con cLFV hacen que las predicciones para esos procesos sean muy pequeñas.

En el capítulo 6 se estudiaron los efectos de la mezcla de squarks en el CMSSM y de sleptones en la extensión de éste con un mecanismo "see-saw" de tipo I. En ambos casos se utilizó la hipótesis de violación de sabor mínima (MFV). Este trabajo fue motivado por el hecho de que muchos análisis fenomenológicos del CMSSM no incluyen estos efectos. Sin embargo, aparecen de manera natural en la evolución de los parámetros del modelo entre las escalas de energía de gran unficiación (GUT) y electro-débil (EW) debido a la presencia de las matrices CKM y PMNS en las RGE´s. En este sentido, los modelos CMSSM y CMSSM-seesaw I constituyen dos ejemplos sencillos de modelos con gran unificación en los que la violación de sabor procede únicamente de las RGE. El espectro de masas de las partículas supersimétricas en ambos casos se ha evaluado numéricamente mediante el programa `Spheno`, a partir de los valores a la escala GUT. Se calcularon las predicciones para BPO, y la masa de los bosones de Higgs en el CMSSM y el CMSSM-seesaw I. Se evaluó el impacto de incluir la mezcla de sabor comparando el cómputo con el caso simple en el que ésta se desprecia, como ocurre en otros análisis previos al nuestro. Los resultados indican en qué casos pueden ignorarse las mezclas de sabor.

En el caso del CMSSM se ha hecho un recorrido a través de una red de valores en el plano m_0–$m_{1/2}$ para valores fijos de A_0 y $\tan\beta$. Se encontró que el valor de δ_{ij}^{FAB} aumenta al incrementar los valores de éstos últimos valores. Los valores de las correcciones a las masas de los bosones de Higgs son inferiores a la precisión en su valor experimental (presente y futuro) . De manera análoga el impacto sobre los BPO está por debajo de la incertidumbre en su medida experimental. Por tanto, encontramos que para estos dos grupos de observables está justificado el ignorar los efectos de la mezcla. La conclusión es diferente en el caso de los EWPO, aquí encontramos que las masas de los squarks aumentan con m_0, y con ello los parámetros de mezcla, esto genera una diferencia entre las masas del doblete de $SU(2)$ que debe ser tenida en cuenta en el cómputo de estos observables. Para $m_0 \gtrsim 3$ TeV encontramos que induce a valores de M_W y $\sin^2\theta_{\rm eff}$ que superan varias veces la incertidumbre experimental, hasta el punto llevar a las predicciones del CMSSM fuera de los límites experimentales. De esta manera, nuestro análisis permite establecer límites para la masa del m_0 que no aparecían en

trabajos anteriores. El origen de la diferencia en las masas de los squarks responsable de ésta contribución fue corroborado numéricamente utilizando `Spheno`, con el que se compararon los efectos de incluir o ignorar la matriz CKM en la integración de las RGE. Sin embargo, debemos señalar que nuestras conclusiones son difíciles de extrapolar a modelos más complejos que los aquí utilizados.

El último eslabón de nuestro análisis con el CMSSM ha sido la evaluación del $\mathrm{BR}(h \to \bar{b}s + b\bar{s})$. En este caso, encontramos valores del orden de 10^{-7}. Esto es, fuera del alcance de su detección en los experimentos proyectados para un futuro próximo. En el caso del CMSSM-seesaw I los resultados numéricos dependen de cómo esté definido el modelo. Se eligió un conjunto de parámetros que reproduce correctamente las observaciones referentes a los neutrinos y a su vez induce a contribuciones apreciables de LFV en los observables que estudiamos. En consecuencia, algunas regiones del espacio de parámetros están exluídas por su predicción a $\mathrm{BR}(\mu \to e\gamma)$. En cambio, las de los $\mathrm{BR}(\tau \to e\gamma)$ y $\mathrm{BR}(\tau \to \mu\gamma)$ no alcanzan sus respectivos límites experimentales. Las predicciones para los BR de LFVHD son muy pequeñas también en el CMSSM-seesaw I. Con ello concluimos que precisamos de modelos diferentes del CMSSM-seesaw I para explicar la observación de $\mathrm{BR}(h \to \mu\tau)$ en el detector CMS del CERN. En lo tocante a los observables medidos con gran precisión, encontramos que los BPO no están afectados. Tampoco las predicciones de las masas de los bosones de Higgs. El mayor impacto aparece una vez más en los EWPO, en el caso de la M_W pueden ser del orden de la incertidumbre experimental.

En resumen, en nuestro estudio de MFV hemos utilizado dos modelos con gran unificación "realistas" en los que la violación de sabor es introducida al tener en cuenta la presencia de las matrices CKM y PMNS en las RGE's. Se encontró que el desestimar los efectos de violación de sabor es adecuado para los BPO y las masas de los bosones de Higgs. Sin embargo, para los EWPO se encontraron efectos grandes. El valor de la contribución a M_W y $\sin^2\theta_{\mathrm{eff}}$ es superior a la incertidumbre de su valor experimental. Por tanto, los efectos de violación de sabor, objeto de nuestro estudio imponen un nuevo límite superior a m_0 que no se ha tenido en cuenta en otros análisis fenomenológicos recientes.

Bibliography

[1] S.L. Glashow, Nucl. Phys. B **22**, 579 (1961)

[2] S. Weinberg, Phys. Rev. Lett. **19**, 1264 (1967)

[3] A. Salam, in: Proceedings of the 8th Nobel Symposium, p. 367, ed. N. Svartholm, Almqvist and Wiksell, Stockholm 1968; S.L. Glashow, I. Iliopoulos, L. Maiani, Phys. Rev. D **2**, 1285 (1970); N. Cabibbo, Phys. Rev. Lett. **10**, 531 (1963); M. Kobayashi, K. Maskawa, Prog. Theor. Phys. **49**, 652 (1973)

[4] G. Aad *et al.* [ATLAS Collaboration], ATLAS-CONF-2013-014, ATLAS-CONF-2013-025

[5] S. Chatrchyan *et al.* [CMS Collaboration], CMS-PAS-HIG-13-005

[6] S. Fukuda *et al.* [Super-Kamiokande Collaboration], Phys. Rev. Lett. **86**, 5656 (2001). `arXiv:hep-ex/0103033`; S. Fukuda *et al.* [Super-Kamiokande Collaboration], Phys. Rev. Lett. **86**, 5651 (2001). `arXiv:hep-ex/0103032`; S. Fukuda *et al.* [Super-Kamiokande Collaboration], Phys. Lett. B **539**, 179 (2002). `arXiv:hep-ex/0205075`; M. Apollonio *et al.* [CHOOZ Collaboration], Phys. Lett. B **466**, 415 (1999). `arXiv:hep-ex/9907037`; Q. Ahmad *et al.* [SNO Collaboration], Phys. Rev. Lett. **87**, 071301 (2001). `arXiv:nucl-ex/0106015`; Q. Ahmad *et al.* [SNO Collaboration], Phys. Rev. Lett. **89**, 011301 (2002). `arXiv:nucl-ex/0204008`; M. Ambrosio et al. [MACRO Collaboration], Phys. Lett. B **517**, 59 (2001); G. Giacomelli and M. Giorgini [MACRO Collaboration], `arXiv:hep-ex/0110021`; K. Eguchi *et al.* [KamLAND Collaboration], `arXiv:hep-ex/0212021`

[7] P. Minkowski, Phys. Lett. B **67**, 421 (1977); M. Gell-Mann, P. Ramond and R. Slansky, in *Complex Spinors and Unified Theories* eds. P. Van. Nieuwenhuizen and D. Freedman, *Supergravity* (North-Holland, Amsterdam, 1979), p.315 [Print-80-0576 (CERN)]; T. Yanagida, in *Proceedings of the Workshop on the Unified Theory and the Baryon Number in the Universe*, eds. O. Sawada and A. Sugamoto (KEK, Tsukuba, 1979), p.95; S. Glashow, in *Quarks and Leptons*, eds. M. Lévy *et al.* (Plenum Press, New York, 1980), p.687; R. Mohapatra and G. Senjanović, Phys. Rev. Lett. **44**, 912 (1980)

[8] F. Zwicky, Helv. Phys. Acta **6**, 110–127 (1933); Ap.J. **86**, 217-246 (1937)

[9] G.Hinshaw *et al.*, Astrophys. J. Suppl. **180**, 225 (2009). `arXiv:1212.5226`; E. Komatsu *et al.*, Astrophys. J. Suppl. **180**, 330 (2009). `arXiv:0803.0547`

[10] P. Ade *et al.* (Planck Collaboration), Astron. Astrophys. **571**, A16 (2014). `arXiv:1303.5076`; Astron. Astrophys. **571**, A22 (2014). `arXiv:1303.5082`

[11] H. Nilles, Phys. Rept. **110**, 1 (1984); H. Haber and G. Kane, Phys. Rept. **117**, 75 (1985); R. Barbieri, Riv. Nuovo Cim. **11**, 1 (1988)

[12] G. Aad *et al.* [ATLAS Collaboration], JHEP **1409**, 176 (2014). arXiv:1405.7875 [hep-ex]; arXiv:1507.05525 [hep-ex]; full ATLAS Run 1 results can be found at https://twiki.cern.ch/twiki/bin/view/AtlasPublic/SupersymmetryPublicResults.

[13] S. Chatrchyan *et al.* [CMS Collaboration], JHEP **1406**, 055 (2014). arXiv:1402.4770 [hep-ex]; full CMS Run 1 results can be found at https://twiki.cern.ch/twiki/bin/view/CMSPublic/PhysicsResultsSUS.

[14] S. Heinemeyer, W. Hollik and G. Weiglein, Phys. Rept. **425**, 265 (2006). arXiv:hep-ph/0412214

[15] R. Chivukula and H. Georgi, Phys. Lett. B **188**, 99 (1987); L. Hall and L. Randall, Phys. Rev. Lett. **65**, 2939 (1990); A. Buras *et al.*, Phys. Lett. B **500**, 161 (2001)

[16] G. D'Ambrosio *et al.*, Nucl. Phys. B **645**, 155 (2002)

[17] Y. Amhis *et al.* [Heavy Flavor Averaging Group], arXiv:1207.1158 [hep-ex] SLAC-R-1002, FERMILAB-PUB-12-871-PPD

[18] S. S. AbdusSalam *et al.*, Eur. Phys. J. C **71**, 1835 (2011). arXiv:1109.3859 [hep-ph]

[19] O. Buchmueller *et al.*, Eur. Phys. J. C **74**, 3212 (2014). arXiv:1408.4060 [hep-ph]; Eur. Phys. J. C **74**, 2922 (2014). arXiv:1312.5250 [hep-ph]; Eur. Phys. J. C **72**, 2243 (2012). arXiv:1207.7315 [hep-ph]; Eur. Phys. J. C **72**, 1878 (2012). arXiv:1110.3568 [hep-ph]

[20] G. Kane, "Modern Elementary Particle Physics" Perseus Books, (1987).

[21] W. Hollik, arXiv:1012.3883 [hep-ph]

[22] G.'t Hooft, Nucl. Phys. B **33**, 173 (1971); G.'t Hooft, Nucl. Phys. B **35**, 167 (1971)

[23] N. Cabibbo, Phys. Rev. Lett. **10** 531 (1963)

[24] S.L. Glashow, J. Iliopoulos and L. Maiani, Phys. Rev. D **2**, 1285 (1970)

[25] M. Kobayashi and K. Maskawa, Prog. Theor. Phys. **49**, 652 (1973)

[26] L.L. Chau and W. Y. Keung, Phys. Rev. Lett. **53**, 1802 (1984)

[27] L. Wolfenstein, Phys. Rev. Lett. **51**, 1945 (1983)

[28] K.A. Olive *et al.* [PDG Collaboration], Chin. Phys. C **38**, 090001 (2014) CKM Review: http://pdg.lbl.gov/2014/reviews/rpp2014-rev-ckm-matrix.pdf

[29] S. Coleman and J. Mandula, Phys. Rev. **159**, 1251 (1967)

[30] S. P. Martin, arXiv:hep-ph/9709356

[31] L. Girardello and M. T. Grisaru, Nucl. Phys. B **194**, 65 (1982)

[32] S. Dimopoulos, S. Raby, and F. Wilczek, Phys. Rev. D **24**, 1681 (1981)

[33] W. J. Marciano and G. Senjanovic, Phys. Rev. D **25**, 3092 (1982)

[34] U. Amaldi, W. de Boer, P. H. Frampton, H. Furstenau, and J. T. Liu, Phys. Lett. B **281**, 374 (1992)

[35] R. N. Mohapatra, `arXiv:hep-ph/9911272`

[36] P. Van Nieuwenhuizen, Phys. Rept. **68**, 189 (1981)

[37] S. L. Glashow und S. Weinberg, Phys. Rev. D **15**, 1958 (1977)

[38] P. Fayet, Phys. Lett. B **64**, 159 (1976); Phys. Lett. B **69**, 489 (1977); Phys. Lett. B **84**, 416 (1979)

[39] G. R. Farrar, P. Fayet, Phys. Lett. B **76**, 575 (1978)

[40] J. Gunion, H. Haber, G. Kane and S. Dawson, The Higgs Hunter's Guide, Addison-Wesley, 1990.

[41] Y. Kuno and Y. Okada, Rev. Mod. Phys. **73**, 151 (2001). `arXiv:hep-ph/9909265`

[42] S. Bilenky, S. Petcov and B. Pontecorvo, Phys. Lett. B **67**, 309 (1977); W. Marciano and A. Sanda, Phys. Lett. B **67**, 303 (1977)

[43] T. Cheng, L.-F. Li, Phys. Rev. Lett. **45**, 1908 (1980)

[44] B. Allanach *et al.*, Comput. Phys. Commun. **180**, 8 (2009). `arXiv:0801.0045 [hep-ph]`

[45] F. Borzumati and A. Masiero, Phys. Rev. Lett. **57**, 961 (1986)

[46] V. Cirigliano et al. Nucl. Phys. B **728**, 121 (2005). `arXiv:hep-ph/0507001`

[47] N. Falck, Z. Phys. C **30**, 247 (1986)

[48] S. Bertolini, F. Borzumati, A. Masiero, and G. Ridolfi, Nucl. Phys. B **353**, 591 (1991)

[49] M. Magg and C. Wetterich, Phys. Lett. B **94**, 61 (1980)

[50] G. Lazarides, Q. Shafi, and C. Wetterich, Nucl. Phys. B **181**, 287 (1981)

[51] Foot, R., Lew, H., He, X. G., and Joshi, G. C. Z. Phys. C **44**, 441 (1989)

[52] E. Ma and D. P. Roy, Nucl. Phys. B **644**, 290–302 (2002)

[53] J. Hisano, T. Moroi, K. Tobe and M. Yamaguchi, Phys. Rev. D **53** 2442 (1996)

[54] M. Cannoni, J. Ellis, M. Gómez and S. Lola, Phys. Rev. D **88**, 075005 (2013). `arXiv:1301.6002 [hep-ph]`

[55] M. Gómez, G. Leontaris, S. Lola and J. Vergados, Phys. Rev. D **59**, 116009 (1999). arXiv:hep-ph/9810291

[56] J. Ellis, M. E. Gómez, G. Leontaris, S. Lola and D. Nanopoulos, Eur. Phys. J. C **14**, 319 (2000). arXiv:hep-ph/9911459

[57] S. Antusch, E. Arganda, M. Herrero and A. Teixeira, JHEP **0611**, 090 (2006). arXiv:hep-ph/0607263

[58] J. Ellis, M. Gómez and S. Lola, JHEP **0707**, 052 (2007). arXiv:hep-ph/0612292

[59] J. Casas and A. Ibarra, Nucl. Phys. B **618**, 171 (2001). arXiv:hep-ph/0103065

[60] G. Fogli, E. Lisi, A. Marrone, D. Montanino, A. Palazzo and A. Rotunno, Phys. Rev. D **86**, 013012 (2012). arXiv:1205.5254 [hep-ph]

[61] M. Veltman, Nucl. Phys. B **123**, 89 (1977)

[62] S. Heinemeyer, W. Hollik, F. Merz, S. Peñaranda, Eur. Phys. J. C **37**, 481 (2004). arXiv:hep-ph/0403228

[63] The LEP Collaborations, the LEP Electroweak Working Group, the Tevatron Electroweak Working Group, the SLD Electroweak and Heavy Flavour Working Groups, Precision electroweak measurements and constraints on the Standard Model, CERN-PH-EP/2009-023; see http://www.cern.ch/LEPEWWG

[64] M. Baak *et al.*, arXiv:1310.6708[hep-ph]

[65] S. Heinemeyer, talk given at the 8^{th} *FCC-ee Physics Workshop*, Paris, France, October 2014, see: https://indico.cern.ch/event/337673/session/3/contribution/41/material/slides .

[66] S. Heinemeyer, W. Hollik, D. Stöckinger, A. M. Weber, and G. Weiglein JHEP **08**, 052 (2006). arXiv:hep-ph/0604147

[67] J. Haestier, S. Heinemeyer, D. Stöckinger, and G. Weiglein JHEP **0512**, 027 (2005). arXiv:hep-ph/0508139

[68] M. Frank, T. Hahn, S. Heinemeyer, W. Hollik, R. Rzehak and G. Weiglein, JHEP **0702**, 047 (2007). arXiv:hep-ph/0611326

[69] A. Dabelstein, Nucl. Phys. B **456**, 25 (1995). arXiv:hep-ph/9503443; Z. Phys. C **67** 495 (1995). arXiv:hep-ph/9409375

[70] A. Brignole, Phys. Lett. B **281**, 284 (1992); P. Chankowski, S. Pokorski and J. Rosiek, Phys. Lett. B **286**, 307 (1992)

[71] H. Baer *et al.*, arXiv:1306.6352 [hep-ph]

[72] S. Gennai *et al.* Eur. Phys. J. C **52**, 383 (2007). arXiv:0704.0619 [hep-ph]

[73] J. Ellis, G. Ridolfi and F. Zwirner, Phys. Lett. B **257**, 83 (1991); Y. Okada, M. Yamaguchi and T. Yanagida, Prog. Theor. Phys. **85**, 1 (1991); H. Haber and R. Hempfling, Phys. Rev. Lett. **66**, 1815 (1991)

[74] A. Brignole, Phys. Lett. B **281**, 284 (1992)

[75] P. Chankowski, S. Pokorski and J. Rosiek, Phys. Lett. B **286**, 307 (1992); Nucl. Phys. B **423**, 437 (1994). arXiv:hep-ph/9303309

[76] S. Heinemeyer, W. Hollik and G. Weiglein, Phys. Rev. D **58**, 091701 (1998). arXiv:hep-ph/9803277; Phys. Lett. B **440**, 296 (1998). arXiv:hep-ph/9807423

[77] S. Heinemeyer, W. Hollik and G. Weiglein, Eur. Phys. J. C **9**, 343 (1999). arXiv:hep-ph/9812472

[78] S. Heinemeyer, W. Hollik and G. Weiglein, Phys. Lett. B **455**, 179 (1999). arXiv:hep-ph/9903404

[79] S. Heinemeyer, W. Hollik, H. Rzehak and G. Weiglein, Eur. Phys. J. C **39**, 465 (2005). arXiv:hep-ph/0411114

[80] M. Carena, H. Haber, S. Heinemeyer, W. Hollik, C. Wagner, and G. Weiglein, Nucl. Phys. B **580**, 29 (2000). arXiv:hep-ph/0001002

[81] R. Zhang, Phys. Lett. B **447**, 89 (1999). arXiv:hep-ph/9808299; J. Espinosa and R. Zhang, JHEP **0003**, 026 (2000). arXiv:hep-ph/9912236

[82] G. Degrassi, P. Slavich and F. Zwirner, Nucl. Phys. B **611**, 403 (2001). arXiv:hep-ph/0105096

[83] R. Hempfling and A. Hoang, Phys. Lett. B **331**, 99 (1994). arXiv:hep-ph/9401219

[84] A. Brignole, G. Degrassi, P. Slavich and F. Zwirner, Nucl. Phys. B **631**, 195 (2002). arXiv:hep-ph/0112177

[85] J. Espinosa and R. Zhang, Nucl. Phys. B **586**, 3 (2000). arXiv:hep-ph/0003246

[86] J. Espinosa and I. Navarro, Nucl. Phys. B **615**, 82 (2001). arXiv:hep-ph/0104047

[87] A. Brignole, G. Degrassi, P. Slavich and F. Zwirner, Nucl. Phys. B **643**, 79 (2002). arXiv:hep-ph/0206101

[88] G. Degrassi, A. Dedes and P. Slavich, Nucl. Phys. B **672**, 144 (2003). arXiv:hep-ph/0305127

[89] M. Carena, J. Espinosa, M. Quirós and C. Wagner, Phys. Lett. B **355**, 209 (1995). arXiv:hep-ph/9504316; M. Carena, M. Quirós and C. Wagner, Nucl. Phys. B **461**, 407 (1996). arXiv:hep-ph/9508343

[90] J. Casas, J. Espinosa, M. Quirós and A. Riotto, Nucl. Phys. B **436**, 3 (1995). [Erratum-ibid. B **439**, 466 (1995)] arXiv:hep-ph/9407389

[91] S. Martin, Phys. Rev. D **71**, 016012 (2005). arXiv:hep-ph/0405022

[92] S. Borowka, T. Hahn, S. Heinemeyer, G. Heinrich and W. Hollik, Eur. Phys. J. C **74**, 2994 (2014). arXiv:1404.7074 [hep-ph]

[93] S. Borowka, T. Hahn, S. Heinemeyer, G. Heinrich, W. Hollik, arXiv:1505.03133 [hep-ph]

[94] G. Degrassi, S. Di Vita and P. Slavich, Eur. Phys. J. C **75**, 61 (2015). arXiv:1410.3432 [hep-ph]

[95] S. Martin, Phys. Rev. D **65**, 116003 (2002). arXiv:hep-ph/0111209; Phys. Rev. D **66**, 096001 (2002). arXiv:hep-ph/0206136; Phys. Rev. D **67**, 095012 (2003). arXiv:hep-ph/0211366; Phys. Rev. D **68**, 075002 (2003). arXiv:hep-ph/0307101; Phys. Rev. D **70**, 016005 (2004). arXiv:hep-ph/0312092; Phys. Rev. D **71**, 116004 (2005). arXiv:hep-ph/0502168; Phys. Rev. D **75**, 055005 (2007). arXiv:hep-ph/0701051; S. Martin and D. Robertson, Comput. Phys. Commun. **174**, 133 (2006). arXiv:hep-ph/0501132

[96] R. Harlander, P. Kant, L. Mihaila and M. Steinhauser, Phys. Rev. Lett. **100**, 191602 (2008). [Phys. Rev. Lett. **101**, 039901 (2008)] [arXiv:0803.0672 [hep-ph]]; JHEP **1008**, 104 (2010). arXiv:1005.5709 [hep-ph]

[97] T. Hahn, S. Heinemeyer, W. Hollik, H. Rzehak and G. Weiglein, Phys. Rev. Lett. **112**, 141801 (2014). arXiv:1312.4937 [hep-ph]

[98] M. Arana-Catania, S. Heinemeyer, M. Herrero and S. Penaranda, JHEP **1205**,015 (2012). arXiv:1109.6232 [hep-ph]; arXiv:1201.6345 [hep-ph]

[99] M. Arana-Catania, S. Heinemeyer and M. J. Herrero, Phys. Rev. D **90**, 075003 (2014). arXiv:1405.6960 [hep-ph]

[100] G. Isidori and A. Retico, JHEP **0209**, 063 (2002). arXiv:hep-ph/0208159

[101] P. Chankowski and L. Slawianowska, Phys. Rev. D **63**, 054012 (2001). arXiv:hep-ph/0008046

[102] J. Foster, K. Okumura and L. Roszkowski, JHEP **0508**, 094 (2005). arXiv:hep-ph/0506146

[103] G. Isidori and P. Paradisi, Phys. Lett. B **639**, 499 (2006). arXiv:hep-ph/0605012; G. Isidori, F. Mescia, P. Paradisi and D. Temes, Phys. Rev. D **75**, 115019 (2007). arXiv:hep-ph/0703035

[104] CMS and LHCb Collaborations, CMS-PAS-BPH-13-007, LHCb-CONF-2013-012, CERN-LHCb-CONF-2013-012.

[105] See: https://www.slac.stanford.edu/xorg/hfag/rare/2013/radll/OUTPUT/TABLES/radll.pdf .

[106] M. Misiak, Acta Phys. Polon. B **40**, 2987 (2009). arXiv:0911.1651 [hep-ph]

[107] S. Chatrchyan et al. [CMS Collaboration], Phys. Rev. Lett. **111**, 101804 (2013). arXiv:1307.5025 [hep-ex]

[108] R. Aaij et al. [LHCb Collaboration], Phys. Rev. Lett. **111**, 101805 (2013). arXiv:1307.5024 [hep-ex]

[109] A. Buras, J. Girrbach, D. Guadagnoli and G. Isidori, Eur. Phys. J. C **72**, 2172 (2012). arXiv:1208.0934 [hep-ph]

[110] See: https://www.slac.stanford.edu/xorg/hfag/osc/PDG_2013/ .

[111] A. Buras, M. Jamin and P. Weisz, Nucl. Phys. B **347**, 491 (1990)

[112] E. Golowich, J. Hewett, S. Pakvasa, A. Petrov and G. Yeghiyan, Phys. Rev. D **83**, 114017 (2011). arXiv:1102.0009 [hep-ph]

[113] S. Bejar, F. Dilme, J. Guasch and J. Sola, arXiv:hep-ph/0402188

[114] A. M. Curiel, M. J. Herrero, D. Temes, Phys. Rev. D **67**, 075008 (2003). arXiv:hep-ph/0210335

[115] D. A. Demir, Phys. Lett. B **571**, 193 (2003). arXiv:hep-ph/0303249

[116] A. Curiel, M. Herrero, W. Hollik, F. Merz and S. Peñaranda, Phys. Rev. D **69**, 075009 (2004). arXiv:hep-ph/0312135

[117] G. Barenboim, C. Bosch, J. Lee, M. López-Ibáñez and O. Vives, arXiv:1507.08304 [hep-ph]

[118] J. Küblbeck, M. Böhm and A. Denner, Comput. Phys. Commun. **60**, 165 (1990); T. Hahn, Comput. Phys. Commun. **140**, 418 (2001). arXiv:hep-ph/0012260

[119] T. Hahn and C. Schappacher, Comput. Phys. Commun. **143**, 54 (2002). arXiv:hep-ph/0105349 The program and the user's guide are available via www.feynarts.de .

[120] T. Hahn and M. Pérez-Victoria, Comput. Phys. Commun. **118**, 153 (1999). arXiv:hep-ph/9807565

[121] S. Heinemeyer, W. Hollik and G. Weiglein, Comput. Phys. Commun. **124**, 76 (2000). arXiv:hep-ph/9812320; T. Hahn, S. Heinemeyer, W. Hollik, H. Rzehak and G. Weiglein, Comput. Phys. Commun. **180**, 1426 (2009) see www.feynhiggs.de

[122] G. Degrassi, S. Heinemeyer, W. Hollik, P. Slavich and G. Weiglein, Eur. Phys. J. C **28**, 133 (2003). arXiv:hep-ph/0212020

[123] G. Moortgat-Pick *et al.*, arXiv:1504.01726 [hep-ph]

[124] J. Adam *et al.* [MEG Collaboration], arXiv:1303.0754 [hep-ex]

[125] B. Aubert *et al.* [BABAR Collaboration], Phys. Rev. Lett. **104**, 021802 (2010). arXiv:0908.2381 [hep-ex]

[126] S. Chatrchyan *et al.* [CMS Collaboration], CMS-PAS-HIG-14-009 (2014), http://cdsweb.cern.ch/record/1728249

[127] G. Aad *et al.* [ATLAS Collaboration], Phys. Rev. Lett. **112**, 201802 (2014). arXiv:1402.3244 [hep-ex]

[128] S. Chatrchyan *et al.* [CMS Collaboration], Eur. Phys. J. C **74**, 2980 (2014). arXiv:1404.1344 [hep-ex]

[129] CMS Collaboration, CERN Report No. CMS-PAS-HIG-14-005, 2014 (unpublished).

[130] G. Aad,*et al.*, [ATLAS Collaboration] arXiv:1508.03372 [hep-ex]

[131] A. Pilaftsis, Phys. Lett. B **285**, 68 (1992)

[132] J. L. Diaz-Cruz and J. J. Toscano, Phys. Rev. D **62**, 116005 (2000). arXiv:hep-ph/9910233

[133] M. Arana-Catania, E. Arganda and M. J. Herrero, JHEP **1309**, 160 (2013). arXiv:1304.3371 [hep-ph]

[134] A. Arhrib, Y. Cheng and O. C. W. Kong, Europhys. Lett. **101**, 31003 (2013). arXiv:1208.4669 [hep-ph]

[135] E. Arganda, M. J. Herrero, X. Marcano and C. Weiland, arXiv:1405.4300 [hep-ph]

[136] A. Falkowski, D. M. Straub and A. Vicente, JHEP **1405**, 092 (2014). arXiv:1312.5329 [hep-ph]

[137] G. Bhattacharyya, P. Leser and H. Päs, Phys. Rev. D **83**, 011701 (2011). arXiv:1006.5597 [hep-ph]

[138] G. Bhattacharyya, P. Leser and H. Päs, Phys. Rev. D **86**, 036009 (2012). arXiv:1206.4202 [hep-ph]

[139] M. Arroyo, J. L. Diaz-Cruz, E. Diaz and J. A. Orduz-Ducuara, arXiv:1306.2343 [hep-ph]

[140] M. D. Campos, A. E. C. Hernández, H. Päs and E. Schumacher, arXiv:1408.1652 [hep-ph]

[141] S. Davidson and G. J. Grenier, Phys. Rev. D **81**, 095016 (2010). arXiv:1001.0434 [hep-ph]

[142] J. Kopp and M. Nardecchia, arXiv:1406.5303 [hep-ph]

[143] T. Hahn, W. Hollik, J.I. Illana, S. Peñaranda, arXiv:hep-ph/0512315

[144] M.E. Gómez, S. Heinemeyer and M. Rehman, arXiv:1511.04342 [hep-ph]

[145] M. Arana-Catania, S. Heinemeyer and M. Herrero, Phys. Rev. D **88**, 015026 (2013). arXiv:1304.2783 [hep-ph]

[146] H. Haber and Y. Nir, Nucl. Phys. B **335**, 363 (1990)

[147] S. Chatrchyan *et al.* [CMS Collaboration], arXiv:1303.4571 [hep-ex];
Pedrame Bargassa, talk given at "Rencontres de Moriond EW 2014",
https://indico.in2p3.fr/getFile.py/access?contribId=189&sessionId=0&resId=1&materialId=slides&confId=9116;
Mike Flowerdew, talk given at "Rencontres de Moriond EW 2014",
https://indico.in2p3.fr/getFile.py/access?contribId=169&sessionId=0&resId=0&materialId=slides&confId=9116;
Paul Thompson, talk given at "Rencontres de Moriond EW 2014",
https://indico.in2p3.fr/getFile.py/access?contribId=220&sessionId=8&resId=0&materialId=slides&confId=9116;
Kevin Einsweiler, talk given at "Rencontres de Moriond EW 2014",
https://indico.in2p3.fr/getFile.py/access?contribId=227&sessionId=1&resId=1&materialId=slides&confId=9116 .

[148] P. Bechtle, O. Brein, S. Heinemeyer, G. Weiglein and K. Williams, Comput. Phys. Commun. **181**, 138 (2010). arXiv:0811.4169 [hep-ph]; Comput. Phys. Commun. **182**, 2605 (2011). arXiv:1102.1898 [hep-ph]; P. Bechtle, O. Brein, S. Heinemeyer, O. Stål, T. Stefaniak, G. Weiglein and K. Williams, Eur. Phys. J. C **74**, 2693 (2014). arXiv:1311.0055 [hep-ph]

[149] P. Bechtle, S. Heinemeyer, O. Stal, T. Stefaniak and G. Weiglein, Eur. Phys. J. C **75**, 421 (2015). arXiv:1507.06706 [hep-ph]

[150] M. Gómez, T. Hahn, S. Heinemeyer, M. Rehman, Phys. Rev. D **90**, 074016 (2014). arXiv:1408.0663 [hep-ph]

[151] M. Awramik, M. Czakon, A. Freitas and G. Weiglein, Phys. Rev. D **69**, 053006 (2004). arXiv:hep-ph/0311148

[152] M. Awramik, M. Czakon, A. Freitas and G. Weiglein, Phys. Rev. Lett. **93**, 201805 (2004). arXiv:hep-ph/0407317

[153] W. Porod, Comput. Phys. Commun. **153**, 275 (2003). arXiv:hep-ph/0301101

[154] P. Skands et al., JHEP **0407**, 036 (2004). arXiv:hep-ph/0311123; B. Allanach et al., Comput. Phys. Commun. **180**, 8 (2009). arXiv:0801.0045 [hep-ph]

[155] M. Gómez, S. Heinemeyer and M. Rehman, Eur. Phys. J. C **75**, 434 (2015). arXiv:1501.02258 [hep-ph]

[156] S. P. Martin and M. T. Vaughn, Phys. Rev. D **50**, 2282 (1994). [Phys. Rev. D **78**, 039903 (2008)] arXiv:hep-ph/9311340

[157] J. Cao, G. Eilam, K. i. Hikasa and J. Yang, Phys. Rev. D **74**, 031701 (2006). arXiv:hep-ph/0604163

[158] O. Buchmueller *et al.*, Eur. Phys. J. C **74**, 2922 (2014). arXiv:1312.5250 [hep-ph]; arXiv:1508.01173 [hep-ph]